ACR No. L5C05

NACA-TR-824 S

INGLEWOOD, CALIFORNIA

NATIONAL ADVISORY COMMITTEE FOR AERONAUTICS

WARTIME REPORT

ORIGINALLY ISSUED

March 1945 as

Advance Confidential Report L5C05

SUMMARY OF AIRFOIL DATA

By Ira H. Abbott, Albert E. von Doenhoff, and Louis S. Stivers, Jr.

Langley Memorial Aeronautical Laboratory
Langley Field, Va.

TECHNICAL LIBRARY

AIRESEARCH MANUFACTURING CO.

9851-9951 SEPULVEDA BLVD.

INGLEWOOD,

CALIFORNIA



WASHINGTON

NACA WARTIME REPORTS are reprints of papers originally issued to provide rapid distribution of advance research results to an authorized group requiring them for the war effort. They were previously held under a security status but are now unclassified. Some of these reports were not technically edited. All have been reproduced without change in order to expedite general distribution.

TABLE OF CONTENTS

SUMMARY	l
INTRODUCTION	
SYMBOLS	3
HISTORICAL DEVELOPMENT	7
DESCRIFTION OF AIRFOILS Method of Combining Mean Lines and Thickness Distributions NACA Four-Digit Series Airfoils Numbering system Thickness distributions Mean lines NACA Five-Digit Series Airfoils Numbering system Thickness distributions Mean lines NACA 1-Series Airfoils Numbering system Thickness distribution Mean lines NACA 6-Series Airfoils Numbering system Thickness distributions Mean lines NACA 7-Series Airfoils Numbering system Thickness distributions Mean lines NACA 7-Series Airfoils Numbering system Thickness distributions Mean lines NACA 7-Series Airfoils Numbering system Thickness distributions	9 11 11 12 12 12 12 12 13 13 13 15 16 16
THEORETICAL CONSIDERATIONS Pressure Distributions Methods of derivation of thickness distributions Rapid estimation of pressure distributions Numerical examples Effect of camber on pressure distribution Critical Mach Number Moment Coefficients Methods of calculation Numerical examples Angle of Zero Lift Methods of calculation Numerical examples Description of Flow around Airfoils	18 21 25 28 29 30 30 31 31 31

	T	age
EXPERIMENTAL CHARACTERISTICS		35
Sources of Data		35
Drag Characteristics of Smooth Airfoils		35
Drag characteristics in low-drag range		35
Drag characteristics outside low-drag range		37
Effects of type of section on drag characteristics		
Effective aspect ratio		38
Effect of Surface Irregularities on Drag		39
Permissible roughness		39
Permissible vaviness		
Drag with fixed transition		42
Drag with practical construction methods		43
Effects of propeller slipstream and airplane vibration		44
Lift Characteristics of Smooth Airfoils		45
Two-dimensional data		
Two-dimensional data		, -
Three-dimensional data		
Lift Characteristics of Adugn Allicets	K	50
Two-dimensional data		
Three-dimensional data	77	
Unconservative Airfoils		-
Pitching Moment		
Position of Aerodynamic Center		-
High-Lift Devices	•	
Lateral-Control Devices	•	57
Leading-Edge Air Intakes		57
Interference		1
		58
APPLICATION TO WING DESIGN		58
Amplication of Section Data		1
Solection of Root Section		00
Selection of Tip Section	•	OI
		62
CONCLUSIONS		02
TABLET TO		
APPENDIX - METHODS OF OBTAINING DATA IN THE LANGLEY		65
TWO-DIMENSIONAL LOW-TURBULENCE TUNNELS		1-
Description of Tunnels		
List of Symbols		65
Measurement of Lift		
Measurement of Drag		10
Tunnol-Wall Corrections		10
Correction for Blocking at High Lifts		
Comparison with Experiment		79

		Page
REFERENCES	 	80
TABLES	 	88
FIGURES (NUMBERED)		
SUPPLEMENTARY DATA I Basic Thickness Forms II Mean Lines III Airfoil Ordinates IV Predicted Critical Mach Numbers V Aerodynamic Characteristics		

the state of the s

NATIONAL ADVISORY COMMITTEE FOR AERONAUTICS

ADVANCE CONFIDENTIAL REPORT

SUMMARY OF AIRFOIL DATA

By Ira H. Abbott, Albert E. von Doenhoff, and Louis S. Stivers, Jr.

SUMMARY

Recent airfoil data for both flight and wind-tunnel tests have been collected and correlated insofar as possible. The flight data consist largely of drag measurements made by the wake-survey method. Most of the data on airfoil section characteristics were obtained in the Langley two-dimensional low-turbulence pressure tunnel. Detail data necessary for the application of NACA 6-series airfoils to wing design are presented in supplementary figures, together with recent data for the NACA 00-, 14-, 24-, 44-, and 230-series airfoils. The general methods used to derive the basic thickness forms for NACA 6- and 7-series airfoils and their corresponding pressure distributions are presented. Data and methods are given for rapidly obtaining the approximate pressure distributions for NACA four-digit, five-digit, 6-, and 7-series airfoils.

The report includes an analysis of the lift, drag, pitchingmoment, and critical-speed characteristics of the airfoils, together with a discussion of the effects of surface conditions. Data on high-lift devices are presented. Problems associated with lateral-control devices, leading-edge air intakes, and interference are briefly discussed. The data indicate that the effects of surface condition on the lift and drag characteristics are at least as large as the effects of the airfoil shape and must be considered in airfoil selection and the prediction of wing characteristics. Airfoils permitting extensive laminar flow, such as the NACA 6-series airfoils, have much lower drag coefficients at high speed and cruising lift coefficients than earlier types of airfoils if, and only if, the wing surfaces are sufficiently smooth and fair. The NACA 6-series airfoils also have favorable critical-speed characteristics, and do not appear to present unusual problems associated with the application of high-lift and lateral-control devices.

INTRODUCTION

A considerable amount of airfoil data has been accumulated from tests in the langley two-dimensional low-turbulence tunnels. Data have also been obtained from tests both in other wind tunnels and in flight and include the effects of high-lift devices, surface irregularities, and interference. Some data are also available on the effects of airfoil section on aileron characteristics. Although a large amount of these data has been published, the scattered nature of the data and the limited objectives of the reports have prevented adequate analysis and interpretation of the results. The purpose of this report is to summarize these data and to correlate and interpret them insofar as possible.

Recent information on the aerodynamic characteristics of NACA airfoils is presented. The historical development of NACA airfoils is briefly reviewed. New data are presented that permit the rapid calculation of the approximate pressure distributions for the older NACA four-digit and five-digit airfoils by the same methods used for the NACA 6-series airfoils. The general methods used to derive the basic thickness forms for NACA 6- and 7-series airfoils together with their corresponding pressure distributions are presented. Detail data necessary for the application of the airfoils to wing design are presented in supplementary figures placed at the end of the paper. The report includes an analysis of the lift, drag, pitching-moment, and critical-speed characteristics of the airfoils, together with a discussion of the effects of surface conditions. Available data on high-lift devices are presented. Problems associated with lateral-control devices, leading-edge air intakes, and interference are briefly discussed, together with aerodynamic problems of application.

Numbered figures are used to illustrate the text and to present miscellaneous data. Supplementery figures and tables are not numbered but are conveniently arranged at the end of the report according to the numerical designation of the airfoil section within the following headings:

I .- Basic thickness forms

II .- Mean lines

III .- Airfoil ordinates

IV .- Predicted critical Mach numbers

V .- Aerodynamic characteristics

These supplementary figures and tables present the basic data for the airfoils.

SYMBOLS

A	aspect ratio
An, Bn	Fourier series coefficients
8.	mean-line designation, fraction of chord from leading edge over which design load is uniform; in derivation of thickness distributions, basic length usually considered unity
Ъ	wing span
bfi	flap span, inboard
bfo	flap span, outboard
CD	drag coefficient
$c^{D^{T=0}}$	drag coefficient at zero lift
CL	lift coefficient
$\Delta C_{L_{f}}$	increment of maximum lift caused by flap deflection
С	chord
ca	aileron chord
c _d	section drag coefficient
cdmin	minimum section drag coefficient
c _{fi}	flap chord, inboard
cfo	flap chord, outboard
$\frac{c_f}{c}$	flap-chord ratio
CH	section aileron hinge-moment coefficient (2)

Δc _H	increment of alleron hinge-moment coefficient at constant lift
$\Delta c_H \delta$	hinge-moment parameter
ci	section lift coefficient
cli	design section lift coefficient
c _m a.c.	moment coefficient about aerodynamic center
cmc/4	moment coefficient about quarter-chord point
c_n	section normal-force coefficient
D	drag
VH	loss of total pressure
H _O	free-stream total pressure
h	section aileron hinge moment
h _e	exit height
k	constant
I	lift
М	Mach number
Mcr	critical Mach number
OU, OL	typical points on upper and lower surfaces of airfoil
Р	pressure coefficient $\left(\frac{p-p_0}{q_0}\right)$
Pcr	critical pressure coefficient
PR	resultant pressure coefficient; difference between local upper- and lower-surface pressure coefficients
p	local static pressure; also, angular velocity in roll in pb/2V
Po	free-stream static pressure

pb/2V	helix angle of wing tip
qo	free-stream dynamic pressure
R	Reynolds number
Rcr	critical Reynolds number
S	pressure coefficient $\left(\frac{H_0 - p}{q_0}\right)$
t _l	first airfoil thickness ratio
t ₂	second airfoil thickness ratio
V	free-stream velocity
Vi	inlet velocity
V	local velocity
Δν	increment of local velocity
Δva	increment of local velocity caused by additional type of load distribution
$\left(\frac{v}{v}\right)_{t_1}$	velocity ratio corresponding to thickness t ₁
$\left(\frac{\Lambda}{\Delta}\right)^{+5}$	velocity ratio corresponding to thickness to
x	distance along chord
× _c	mean-line abscissa
x^{Γ}	abscissa of lower surface
x _U	abscissa of upper surface
$\left(\frac{x}{c}\right)_{tr}$	chordwise position of transition
У	distance perpendicular to chord

Уc	mean-line ordinate
YL	ordinate of lower surface
Уt	ordinate of symmetrical thickness distribution
УU	ordinate of upper surface
Z	complex variable in circle plane
z t	complex variable in near-circle plane
α	angle of attack
$\frac{\Delta \alpha_0}{\Delta \delta}$	section aileron effectiveness parameter, ratio of change in section angle of attack to increment of aileron deflection at a constant value of lift coefficient
a _l o	anglo of zero lift
a ⁰	section angle of attack
Δαο	increment of section angle of attack
$\alpha_{\hat{1}}$	section angle of attack corresponding to design lift coefficient
δ	flap or alleron deflection; down deflection is positive
8fi	flap deflection, inboard
850	flap deflection, outboard
€	airfeil parameter $(\phi - \theta)$
€ TE	value of ε at trailing edge
ζ	complex variable in airfoil plane
θ	angular coordinate of z¹; also, angle whose tangent is slope of mean line
λ	taper ratio (Tip chord) Root chord

T	turbulence factor (Effective Reynolds number Test Reynolds number)
ø	angular coordinate of z
Ψ	airfoil parameter determining radial coordinate of z
Ψ0	average value of ψ , $\left(\frac{1}{2\pi}\int_{0}^{2\pi}\psi\mathrm{d}\phi\right)$

HISTORICAL DEVELOPMENT

The development of types of NACA airfoils now in common use was started in 1929 with a systematic investigation of a family of airfoils in the Langley variable-density tunnel. Airfoils of this family were designated by numbers having four digits, such as the NACA 4412 airfoil. All airfoils of this family had the same basic thickness distribution (reference 1), and the amount and type of camber was systematically varied to produce the family of related airfoils. This investigation of the NACA airfoils of the four-digit series produced airfoil sections having higher maximum lift coefficients and lower minimum drag coefficients than those of sections developed before that time. The investigation also provided information on the changes in aerodynamic characteristics resulting from variations of geometry of the mean line and thickness ratio (reference 1).

The investigation was extended in references 2 and 3 to include airfoils with the same thickness distribution but with positions of the maximum camber far forward on the airfoil. These airfoils were designated by numbers having five digits, such as the NACA 23012 airfoil. Some airfoils of this family showed favorable aerodynamic characteristics except for a large sudden loss in lift at the stall.

Although these investigations were extended to include a limited number of airfoils with varied thickness distributions (references 1 and 3 to 6), no extensive investigations of thickness distribution were made. Comparison of experimental drag data at low lift coefficients with the skin-friction coefficients for flat plates indicated that nearly all of the profile drag under such conditions was attributable to skin friction. It was therefore apparent that any pronounced reduction of the profile drag must be obtained by a reduction of the skin friction through increasing the relative extent of the laminar boundary layer.

Decreasing pressures in the direction of flow and low airstream turbulence were known to be favorable for laminar flow. An attempt was accordingly made to increase the relative extent of laminar flow by the development of airfoils having favorable pressure gradients over a greater proportion of the chord than the airfoils developed in references 1, 2, 3, and 6. The actual attainment of extensive laminar boundary layers at large Reynolds numbers was a previously unsolved experimental problem requiring the development of new test equipment with very low airstream turbulence. This work was greatly encouraged by the experiments of Jones (reference 7), who demonstrated the possibility of obtaining extensive laminar layers in flight at relatively large Reynolds numbers. Uncertainty with regard to factors affecting separation of the turbulent boundary layer required experiments to determine the possibility of making the rather sharp pressure recoveries required over the rear portion of the new type of airfoil.

New wind tunnels were designed specifically for testing airfoils under conditions closely approaching flight conditions of air-stream turbulence and Reynolds number. The resulting wind tunnels, the Langley two-dimensional low-turbulence tunnel (LTT) and the Langley two-dimensional low-turbulence pressure tunnel (TDT), and the methods used for obtaining and correcting data are briefly described in the appendix. In these tunnels the models completely span the comparatively narrow test sections; two-dimensional flow is thus provided, which obviates difficulties previously encountered in obtaining section data from tests of finite-span wings and in correcting adequately for support interference (reference 8).

Difficulty was encountered in attempting to design airfoils having desired pressure distributions because of the lack of adequate theory. The Theodorsen method (reference 9), as ordinarily used for calculating the pressure distributions about airfoils, was not sufficiently accurate near the leading edge for prediction of the local pressure gradients. In the absence of a suitable theoretical method, the 9-percent-thick symmetrical airfoil of the NACA 16-series (reference 10) was obtained by empirical modification of the previously used thickness distributions (reference 4). These NACA 16-series sections represented the first family of the low-drag high-critical-speed sections.

Successive attempts to design airfoils by approximate theoretical methods led to families of airfoils designated NACA 2-to 5-series sections (reference 11). Experience with these sections showed that none of the approximate methods tried was sufficiently accurate to show correctly the effect of changes in profile near the leading edge. Wind-tunnel and flight tests of these airfoils showed that extensive laminar boundary layers could be maintained at

at comparatively large values of the Reynolds number if the airfoil surfaces were sufficiently fair and smooth. These tests also provided qualitative information on the effects of the magnitude of the favorable pressure gradient, leading-edge radius, and other shape variables. The data also showed that separation of the turbulent boundary layer over the rear of the section, especially with rough surfaces, limited the extent of laminar layer for which the airfoils should be designed. The airfoils of these early families generally showed relatively low maximum lift coefficients and, in many cases, were designed for a greater extent of laminar flow than is practical. It was learned that, although sections designed for an excessive extent of laminar flow gave extremely low drag coefficients near the design lift coefficient when smooth, the drag of such sections became unduly large when rough, particularly at lift coefficients higher than the design lift. These families of airfoils are accordingly considered obsolete.

The NACA 6-series basic thickness forms were derived by new and improved methods described herein in the section "Methods of Derivation of Thickness Distributions," in accordance with design criterions established with the objective of obtaining desirable drag, critical Mach number, and maximum-lift characteristics. The present report deals largely with the characteristics of these sections. The development of the NACA 7-series family has also been started. This family of airfoils is characterized by a greater extent of laminar flow on the lower than on the upper surface. These sections permit low pitching-moment coefficients with moderately high design lift coefficients at the expense of some reduction in maximum lift and critical Mach number.

Acknowledgement is gratefully expressed for the expert guidance and many original contributions of Mr. Eastman N. Jacobs, who supervised this work.

DESCRIPTION OF AIRFOILS

Method of Combining Mean Lines and Thickness Distributions

The cambered airfoil sections of all NACA families considered herein are obtained by combining a mean line and a thickness distribution. The necessary geometric data and some theoretical aerodynamic data for the mean lines and thickness distributions may be obtained from the supplementary figures by the methods described for each faimly of airfoils.

The process for combining a mean line and a thickness distribution to obtain the desired cambered airfoil section is illustrated in figure 1. The leading and trailing edges are defined as the forward and rearward extremities, respectively, of the mean line. The chord line is defined as the straight line connecting the leading and trailing edges. Ordinates of the cambered airfoil are obtained by laying off the thickness distribution perpendicular to the mean line. The abscissas, ordinates, and slopes of the mean line are designated as x_c , y_c , and tan θ , respectively. If xu and yu represent, respectively, the abscissa and ordinate of a typical point of the upper surface of the airfoil and yt is the ordinate of the symmetrical thickness distribution at chordwise position x, the upper-surface coordinates are given by the following relations:

$$x_{U} = x - y_{t} \sin \theta \tag{1}$$

$$y_{U} = y_{c} + y_{t} \cos \theta \qquad (2)$$

The corresponding expressions for the lower-surface coordinates are

$$x_L = x + y_t \sin \theta$$
 (3)

$$x_{L} = x + y_{t} \sin \theta \qquad (3)$$

$$y_{L} = y_{c} - y_{t} \cos \theta \qquad (4)$$

The center for the leading-edge radius is found by drawing a line through the end of the chord at the leading edge with the slope equal to the slope of the mean line at that point and laying off a distance from the leading edge along this line equal to the leading-edge radius. This method of construction causes the cambered airfoils to project slightly forward of the leading-edge point. Because the slope at the leading edge is theoretically infinite for the mean lines having a theoretically finite load at the leading edge, the slope of the radius through the end of the chord for such mean lines is usually taken as the slope of the mean line at $\frac{x}{c} = 0.005$. This procedure is justified by the manner in which the slope increases to the theoretically infinite value as x/c approaches 0. The slope increases slowly until very small values of x/c are reached. Large values of the slope are thus limited to values of x/c very close to 0 and may be neglected in practical airfoil design.

Tables of ordinates are included in the supplementary data for all airfoils for which standard characteristics are presented.

NACA Four-Digit-Series Airfoils

Numbering system. The numbering system for the NACA airfoils of the four-digit series (reference 1) is based on the airfoil geometry. The first integer indicates the maximum value of the mean-line ordinate $y_{\rm c}$ in percent of the chord. The second integer indicates the distance from the leading edge to the location of the maximum camber in tenths of the chord. The last two integers indicate the airfoil thickness in percent of the chord. Thus, the NACA 2415 airfoil has 2-percent camber at 0.4 of the chord from the leading edge and is 15 percent thick.

The first two integers taken together define the mean line, for example, the NACA 24 mean line. The symmetrical airfoil sections representing the thickness distribution for a family of airfoils are designated by zeros for the first two integers, as in the case of the NACA 0015 airfoil.

Thickness distributions. - Data for the NACA 0006, 0008, 0009, 0010, 0012, 0015, 0018, 0021, and 0024 thickness distributions are presented in the supplementary figures. Ordinates for intermediate thicknesses may be obtained correctly by scaling the tabulated ordinates in proportion to the thickness ratio (reference 1). The leading-edge radius varies as the square of the thickness ratio. Values of $(v/V)^2$, which is equivalent to the low-speed pressure distribution, and of v/V are also presented. These data were obtained by Theodorsen's method (reference 9). Values of the velocity increments $\Delta v_{\rm e}/V$ induced by changing angle of attack (see section "Rapid Estimation of Pressure Distribution") are also presented for an additional lift coefficient of approximately unity. Values of the velocity ratio v/V for intermediate thickness ratios may be obtained approximately by linear scaling of the velocity increments obtained from the tabulated values of v/V for the nearest thickness ratio; thus,

$$\left(\frac{\mathbf{v}}{\mathbf{v}}\right)_{\mathbf{t}_{2}} = \left[\left(\frac{\mathbf{v}}{\mathbf{v}}\right)_{\mathbf{t}_{1}} - 1\right] \frac{\mathbf{t}_{2}}{\mathbf{t}_{1}} + 1$$
 (5)

Values of the velocity-increment ratio $\Delta v_a/V$ may be obtained for intermediate thicknesses by interpolation.

Mean lines. Data for the NACA 62, 63, 64, 65, 66, and 67 mean lines are presented in the supplementary figures. The data presented include the mean-line ordinates y_c , the slope dy_c/dx , the design lift coefficient $c_{l\,i}$ and the corresponding design angle of attack α_i , the moment coefficient $c_{mc/4}$, the resultant

pressure coefficient P_R , and the velocity ratio $\Delta v/V$. The theoretical aerodynamic characteristics were obtained from thin-airfoil theory. All tabulated values for each mean line, accordingly, vary linearly with the maximum ordinate y_C , and data for similar mean lines with different amounts of camber within the usual range may be obtained simply by scaling the tabulated values. Data for the NACA 22 mean line may thus be obtained by multiplying the data for the NACA 62 mean line by the ratio 2:6, and for the NACA 44 mean line by multiplying the data for the NACA 64 mean line by the ratio 4:6.

NACA Five-Digit-Series Airfoils

Numbering system. The numbering system for airfoils of the NACA five-digit series is based on a combination of theoretical aerodynamic characteristics and geometric characteristics (references 2 and 3). The first integer indicates the amount of camber in terms of the relative magnitude of the design lift coefficient; the design lift coefficient in tenths is thus three-halves of the first integer. The second and third integers together indicate the distance from the leading edge to the location of the maximum camber; this distance in percent of the chord is one-half the number represented by these integers. The last two integers indicate the airfoil thickness in percent of the chord. The NACA 23012 airfoil thus has a design lift coefficient of 0.3, has its maximum camber at 15 percent of the chord, and has a thickness ratio of 12 percent.

Thickness distributions. - The thickness distributions for airfoils of the NACA five-digit series are the same as those for airfoils of the NACA four-digit series.

Mean lines. - Data for the NACA 210, 220, 230, 240, and 250 mean lines are presented in the supplementary figures in the same form as for the mean lines given herein for the four-digit series. All tabulated values for each mean line vary linearly with the maximum ordinate or with the design lift coefficient. Thus, data for the NACA 430 mean line may be obtained by multiplying the data for the NACA 230 mean line by the ratio 4:2 and for the NACA 640 mean line by multiplying the data for the NACA 240 mean line by the ratio 6:2.

NACA 1-Series Airfoils

Numbering system. - The NACA 1-series airfoils are designated by a five-digit number - as, for example, the NACA 16-212 section. The first integer represents the series designation. The second integer indicates the distance in tenths of the chord from the

NACA ACR No. 15005

leading edge to the position of minimum pressure for the symmetrical section at zero lift. The first number following the dash indicates the amount of camber expressed in terms of the design lift coefficient in tenths, and the last two numbers together indicate the thickness in percent of the chord. The commonly used sections of this family have minimum pressure at 0.6 of the chord from the leading edge and are usually referred to as the NACA 16-series sections.

Thickness distributions. - Data for the NACA 16-006, 16-009, 16-012, 16-015, 16-018, and 16-021 thickness distributions (reference 10) are presented in the supplementary figures. These data are similar in form to those airfoils of the NACA four-digit series, and data for intermediate thickness ratios may be obtained in the same manner.

Mean lines. The NACA 16-series airfoils as commonly used are cambered with a mean line of the uniform-load type (a = 1.0), which is described under the section for the NACA 6-series airfoils that follows. If any other type of mean line is used, this fact should be stated in the airfoil designation.

NACA 6-Series Airfoils

Numbering system. The NACA 6-series airfoils are usually designated by a six-digit number together with a statement showing the type of mean line used. For example, in the designation NACA 65,3-218, a = 0.5, the "6" is the series designation. The "5" denotes the chordwise position of minimum pressure in tenths of the chord behind the leading edge for the basic symmetrical section at zero lift. The "3" following the comma gives the range of lift coefficient in tenths above and below the design lift coefficient in which favorable pressure gradients exist on both surfaces. The "2" following the dash gives the design lift coefficient in tenths. The last two digits indicate the airfoil thickness in percent of the chord. The designation "a = 0.5" shows the type of mean line used. When the mean-line designation is not given, it is understood that the uniform-load mean line (a = 1.0) has been used.

When the mean line used is obtained by combining more than one mean line, the design lift coefficient used in the designation is the algebraic sum of the design lift coefficients of the mean lines used, and the mean lines are described in the statement following the number as in the following case:

NACA 65,3-218
$$\begin{cases} a = 0.5, c_{1i} = 0.3 \\ a = 1.0, c_{1i} = -0.1 \end{cases}$$

Airfoils having a thickness distribution obtained by linearly increasing or decreasing the ordinates of one of the originally derived thickness distributions are designated as in the following example:

NACA
$$65(318)-217$$
, $a = 0.5$

The significance of all of the numbers except those in the parentheses is the same as before. The first number and the last two numbers enclosed in the parentheses denote, respectively, the low-drag range and the thickness in percent of the chord of the originally derived thickness distribution.

The more recent NACA 6-series airfoils are derived as members of thickness families having a simple relationship between the conformal transformations for airfoils of different thickness ratios but having minimum pressure at the same chordwise position. These airfoils are distinguished from the earlier individually derived airfoils by writing the number indicating the low-drag range as a subscript; for example,

NACA
$$65_3$$
-218, $a = 0.5$

For NACA 6-series airfoils having a thickness ratio less than 0.12 of the chord the subscript number indicating the low-drag range should be less than unity. Rather than use a fractional number, a subscript of unity was originally employed for these airfoils. Since this usage is not consistent with the previous definition of a number indicating the low-drag range, the designations of airfoil sections having a thickness ratio less than 0.12 of the chord are now given without such a number. As an example, an NACA 6-series airfoil having a thickness ratio of 0.10 of the chord would be designated

NACA 65-210

Ordinates for the basic thickness distributions designated by a subscript are slightly different from those for the corresponding individually derived thickness distributions. As before, if the ordinates of the basic thickness distribution have been changed by a factor, the low-drag range and thickness ratio of the original thickness distribution are enclosed in parentheses as follows:

NACA
$$65(318)-217$$
, $a = 0.5$

If, however, the ordinates of a basic thickness distribution having a thickness ratio less than 0.12 of the chord have been

NACA ACR No. 15005

changed by a factor, the number indicating the low-drag range is eliminated and only the original thickness ratio is enclosed in parentheses as follows:

If the design lift coefficient in tenths or the airfoil thickness in percent of chord are not whole integers, the numbers giving these quantities are usually enclosed in parentheses as in the following designation:

NACA
$$65_{(318)}$$
-(1.5)(16.5), a = 0.5

Some early experimental airfoils are designated by the insertion of the letter x immediately preceding the hyphen as in the designation 66.2x-115.

Thickness distributions. - Data for available NACA 6-series thickness forms are presented in the supplementary figures. These data are comparable with the similar data for airfoils of the NACA four-digit series, except that ordinates for intermediate thicknesses may not be correctly obtained by scaling the tabulated ordinates proportional to the thickness ratio. This method of changing the ordinates by a factor will, however, produce shapes satisfactorily approximating members of the family if the change in thickness ratio is small. Values of v/V and $\Delta v_a/V$ for intermediate thickness ratios may be approximated as described for the NACA four-digit series.

Mean lines. The mean lines commonly used with the NACA 6-series airfoils produce a uniform chordwise loading from the leading edge to the point $\frac{X}{C}$ = a and a linearly decreasing load from this point to the trailing edge. Data for NACA mean lines with values of a equal to 0, 0.1, 0.2, 0.3, 0.4, 0.5, 0.6, 0.7, 0.8, 0.9, and 1.0 are presented in the supplementary figures. The ordinates were computed by the following formula, which represents a simplification of the original expression for mean-line ordinates given in reference 11:

$$\frac{y_{c}}{c} = \frac{c_{l_{\frac{1}{2}}}}{2\pi(a+1)} \left\{ \frac{1}{1-a} \left[\frac{1}{2} \left(a - \frac{x}{c} \right)^{2} \log_{e} \left| a - \frac{x}{c} \right| \right. \\
\left. - \frac{1}{2} \left(1 - \frac{x}{c} \right)^{2} \log_{e} \left(1 - \frac{x}{c} \right) + \frac{1}{4} \left(1 - \frac{x}{c} \right)^{2} - \frac{1}{4} \left(a - \frac{x}{c} \right)^{2} \right] \\
- \frac{x}{c} \log_{e} \frac{x}{c} + g - h\frac{x}{c} \right\}$$
(6)

where

$$g = -\frac{1}{1-a} \left[a^{2} \left(\frac{1}{2} \log_{e} a - \frac{1}{4} \right) + \frac{1}{4} \right]$$

$$h = \frac{1}{1-a} \left[\frac{1}{2} (1-a)^{2} \log_{e} (1-a) - \frac{1}{4} (1-a)^{2} \right] + g$$

The ideal angle of attack α_i corresponding to the design lift coefficient is given by

$$\alpha_i = -h \frac{c_{l_i}}{2\pi(a+1)}$$

The data are presented for a design lift coefficient cliequal to unity. All tabulated values vary directly with the design lift coefficient. Corresponding data for similar mean lines with other design lift coefficients may accordingly be obtained simply by multiplying the tabulated values by the desired design lift coefficient.

In order to camber NACA 6-series airfoils, mean lines are usually used having values of a equal to or greater than the distance from the leading edge to the location of minimum pressure for the selected thickness distribution at zero lift. For special purposes, load distributions other than those corresponding to the simple mean lines may be obtained by combining two or more types of mean line having positive or negative values of the design lift coefficient. The geometric and aerodynamic characteristics of such combinations may be obtained by algebraic addition of the values for the component mean lines.

NACA 7-Series Airfoils

Numbering system. - The NACA 7-series airfoils are designated by a number of the following type (reference 12):

NACA 747A315

The first number "7" indicates the series number. The second number "4" indicates the extent over the upper surface, in tenths of the chord from the leading edge, of the region of favorable pressure gradient at the design lift coefficient. The third number "7" indicates the extent over the lower surface, in tenths of the chord from the leading edge, of the region of favorable pressure gradient at the design lift coefficient. The significance of the last group of three numbers is the same as for the previous NACA 6-series airfoils. The letter "A" which follows the first three numbers is a serial letter to distinguish different airfoils having parameters that would correspond to the same numerical designation. For example, a second airfoil having the same extent of favorable pressure gradient over the upper and lower surfaces, the same design lift coefficient, and the same maximum thickness as the original airfoil but having a different mean-line combination or thickness distribution would have the serial letter "B". Mean lines used for the NACA 7-series airfoils are obtained by combining two or more of the previously described mean lines. A list of the thickness distributions and mean lines used to form these airfoils is presented in table I. The basic thickness distribution is given a designation similar to those of the final cambered airfoils. For example, the basic thickness distribution for the NACA 747A315 and 747A415 airfoils is given the designation NACA 747A015 even though minimum pressure occurs at 0.4c on both upper and lower surfaces at zero lift. Combination of this thickness distribution with the mean lines listed in table I for the NACA 747A315 airfoil changes the pressure distribution to the desired type as shown in figure 2.

Thickness distributions. Data for available NACA 7-series thickness distributions are presented in the supplementary figures. These thickness distributions are individually derived and do not form thickness families. The thickness ratio may, however, be changed a moderate amount - say 1 or 2 percent - by multiplying the tabulated ordinates by a suitable factor without seriously altering their characteristics features. Values of $(v/v)^2$ and of v/v for thinner or thicker thickness distributions may be approximated by the method of equation (5). If the change in thickness ratio is small, tabulated values of $\Delta v_a/v$ may be applied directly with reasonable accuracy.

THEORETICAL CONSIDERATIONS

Pressure Distributions

A knowledge of the pressure distribution over an airfoil is desirable for structural design and for estimation of the critical

NACA ACR No. 15005

Mach number and moment coefficient if tests are not available. The pressure distribution also exerts a strong or predominant influence on the boundary-layer flow and, hence, on the airfoil characteristics. It is therefore usually advisable to relate the airfoil characteristics to the pressure distribution rather than directly to the airfoil geometry.

Methods of derivation of thickness distributions. As mentioned in the section "Historical Development," the basic symmetrical thickness distributions of the NACA 6- and 7-series airfoils, together with their corresponding pressure distributions, are derived by means of conformal transformations. The transformations used to relate the known flow about a circle to that about an airfoil section were developed by Theodorsen in reference 9. Figure 3 shows schematically the significance of the various phases of the process.

The circle about which the flow is originally calculated has its center at the origin and a radius of ae^{ψ_0} . The equation of this circle in complex coordinates is

$$y_0 + i \emptyset$$

$$z = ae \tag{7}$$

where

z complex variable in circle plane

ø angular coordinate of z

a basic length usually considered unity

ψo constant determining radius of circle

This true circle is transformed into an arbitrary, almost circular curve by the relation

$$\frac{z^{\dagger}}{z} = e^{(\psi \cdot \psi_0) + i(\theta - \phi)}$$
 (8)

the equation of the almost circular curve is

$$z' = ae^{\psi + i\theta}$$
 (9)

where

z' complex variable in near-circle plane

aeV radial coordinate of z'

θ angular coordinate of z*

In order for the transformation (8) to be conformal, it is necessary that the quantity $(\theta - \phi)$ (given the symbol $-\epsilon$) be the conjugate function of $(\psi - \psi_0)$; that is, if ϵ is represented by a Fourier series of the form

$$\epsilon = \sum_{n=1}^{\infty} A_n \sin n\emptyset - \sum_{n=1}^{\infty} B_n \cos n\emptyset$$

then $(\psi - \psi_0)$ is given by the relation

$$(\psi - \psi_0) = \sum_{n=1}^{\infty} A_n \cos n\phi + \sum_{n=1}^{\infty} B_n \sin n\phi$$

This relationship, indicates that, if the function $\varepsilon(\emptyset)$ is given, $(\psi - \psi_0)$ can be calculated as a function of \emptyset . Means of performing this calculation are presented in reference 13. The transformation relating the almost circular curve to the airfoil shape is

$$\zeta = z^{\dagger} + \frac{a^2}{z^{\dagger}} \tag{10}$$

where ζ is the complex variable in the airfoil plane. The coordinates of the airfoil x and y are the real and imaginary parts of ζ , respectively. These coordinates are given by the relations

$$x = 2a \cosh \psi \cos \theta$$
 (11)

$$y = 2a \sinh \psi \sin \theta$$
 (12)

The velocity distribution in terms of the airfoil parameters ψ and ϵ is given exactly for perfect fluid flow by the expression

$$\frac{\mathbf{v}}{\mathbf{V}} = \frac{\sin (\alpha_0 + \emptyset) + \sin(\alpha_0 + \epsilon_{\text{TE}})e^{\psi_0}}{\sqrt{\left(\sinh^2\psi + \sin^2\theta\right)\left[\left(1 - \frac{\mathrm{d}\epsilon}{\mathrm{d}\theta}\right)^2 + \left(\frac{\mathrm{d}\psi}{\mathrm{d}\theta}\right)^2\right]}}$$
(13)

where

v local velocity over surface of airfoil

V free-stream velocity

α_O section angle of attack

 ψ_0 average value of ψ , $\left(\frac{1}{2\pi}\int_0^{2\pi}\psi\,d\phi\right)$

€ TE value of € at trailing edge

The basic symmetrical shapes were derived by assuming suitable values of $d\varepsilon/d\phi$ as a function of ϕ . These values were chosen on the basis of previous experience and are subject to the conditions that

$$\int_0^\pi \frac{\mathrm{d}\epsilon}{\mathrm{d}\theta} = 0$$

and $d\varepsilon/d\emptyset$ at \emptyset is equal to $d\varepsilon/d\emptyset$ at $-\emptyset$. These conditions are necessary for obtaining closed symmetrical shapes. Values of $\varepsilon(\emptyset)$ were obtained simply by integrating $\frac{d\varepsilon}{d\emptyset} d\emptyset$. Values of $\psi(\emptyset)$ were found by obtaining the conjugate of the curve of $\varepsilon(\emptyset)$ and adding a value ψ_0 sufficient to make the value of ψ equal to zero at $\emptyset = \pi$. This condition assures a sharp trailing-edge shape.

Inasmuch as small changes in the velocity distribution at any point of the surface are approximately proportional to $1+\frac{d\varepsilon}{d\emptyset}$ (see reference 14), the initially assumed values of $d\varepsilon/d\emptyset$ were altered by a process of successive approximations until the desired type of velocity distribution was obtained. After the final values of ψ and ε were obtained, the ordinates of the basic thickness distribution were computed by equations (11) and (12).

When these computations were made, it appeared that there was an optimum value of the leading-edge radius dependent upon the airfoil thickness and the position of minimum pressure. If the leading-edge radius was too small, a premature peak in the pressure distribution occurred in the immediate vicinity of the leading edge as the angle of attack was increased. If the leading-edge radius was too large, a premature peak occurred a few percent of the chord behind the leading edge. With the correct leading-edge radius, the pressure distribution became nearly flat over the forward portion of the airfoil before the normal leading-edge peak formed at the higher lift coefficients. Curves of the parameters ψ , ε , $d\psi/d\phi$, $d\varepsilon/d\phi$ plotted against ϕ for the NACA 643-018 airfoil section are given in figure 4.

Experience has shown that, when the thickness ratio of an originally derived basic form was increased merely by multiplying all the ordinates by a constant factor, an unnecessarily large decrease in the critical speed of the resulting section occurred. Reducing the thickness ratio in a similar manner caused an unnecessarily large decrease in the low-drag range. For this reason, each of the earlier NACA 6-series sections was individually derived. It was later found that it was possible to derive basic airfoil parameters ψ and ε that could be multiplied by a constant factor to obtain airfoils of various thickness ratios, without having the aforementioned limitations in the resulting sections. Each of the more recent families of NACA 6-series airfoils, in which numerical subscripts are used in the designation. having minimum pressure at a given chordwise position was obtained by scaling up and down the basic values of the airfoil parameters \u00fc and ϵ .

Theoretical pressure distributions (indicated by $\left(\frac{v}{v}\right)^2$) for a family of NACA 65-series airfoils covering a range of thickness ratios are given in figure 5(a). This figure shows the typical increase in the magnitude of the favorable pressure gradient, increase in maximum velocity over the surface, and increase in the relative pressure recovery over the rear portion of the airfoil with increase in thickness ratio. Figure 5(b) shows the pressure distribution for a series of basic thickness forms having a thickness ratio of 0.15 and having minimum pressure at various chordwise positions. The value of the minimum pressure coefficient is seen to decrease and the magnitude of the pressure recovery over the rear portion of the airfoil to increase with rearward movement of the point of minimum pressure.

The pressure distribution for one of the basic symmetrical thickness distributions at various lift coefficients is shown in figure 6. At zero lift the pressure distributions over the upper and lower surfaces are the same. As the lift coefficient is increased, the slope of the pressure distribution over the forward portion of the upper surface decreases until it becomes flat at a lift coefficient of 0.22 (the end of the low-drag range). As the lift coefficient is increased beyond this value, the usual peak in the pressure distribution forms at the leading edge.

Rapid estimation of pressure distributions. In the discussion that follows, the term "pressure distribution" is used to signify the distribution of the static pressures on the upper and lower surfaces of the airfoil along the chord. The term "load distribution" is used to signify the distribution along the chord of the normal force resulting from the difference in pressure on the upper and lower surfaces.

The pressure distribution about any airfoil in potential flow may be calculated accurately by a generalization of the methods of the previous section. Although this method is not unduly laborious, the computations required are too long to permit quick and easy calculations for large numbers of airfoils. The need for a simple method of quickly obtaining pressure distributions with engineering accuracy has led to the development of a method (reference 15) combining features of thin- and thick-airfoil theory. This simple method makes use of previously calculated characteristics of a limited number of mean lines and thickness distributions that may be combined to form large numbers of airfoils.

Thin-airfoil theory (references 16 to 18) shows that the load distribution of a thin airfoil may be considered to consist of: (1) a basic distribution at the ideal angle of attack and (2) an additional distribution proportional to the angle of attack as measured from the ideal angle of attack.

The first load distribution is a function only of the shape of the thin airfoil, or (if the thin airfoil is considered to be a mean line) of the mean-line geometry. Integration of this load distribution along the chord results in a normal-force coefficient which, at small angles of attack, is substantially equal to a lift coefficient c_{li} , which is designated the ideal or design lift

coefficient. If, moreover, the camber of the mean line is changed by multiplying the mean-line ordinates by a constant factor, the resulting load distribution, the ideal or design angle of attack α_1 and the design lift coefficient c_{l_1} may be obtained simply by multiplying the original values by the same factor. The characteristics of a large number of mean lines are presented in both graphical and tabular form in the supplementary figures. The load-distribution data are presented both in the form of the resultant pressure coefficient P_R and in the form of the corresponding velocity-increment ratios $\Delta v/V$. For positive design lift coefficients, these velocity-increment ratios are positive on the upper surface and negative on the lower surface; the opposite is true for negative design lift coefficients.

The second load distribution, which results from changing the angle of attack, is designated herein the "additional load distribution" and the corresponding lift coefficient is designated the "additional lift coefficient." This additional load distribution contributes no moment about the quarter-chord point and, according to thin-airfoil theory, is independent of the airfoil geometry except for angle of attack. The additional load distribution obtained from thin-airfoil theory is of limited practical application, however, because this simple theory leads to infinite values of the velocity at the

NACA ACR No. 15005

leading edge. This difficulty is obviated by the exact thick-airfoil theory (reference 9) which also shows that the additional load distribution is neither completely independent of the airfoil shape nor exactly a linear function of the lift coefficient. For this reason, the additional load distribution has been calculated by the methods of reference 9 for each of the thickness distributions presented in the supplementary figures. These data are presented in the form of velocity-increment ratios $\Delta v_a/V$ corresponding to an additional lift coefficient of approximately unity. For positive additional lift coefficients, these velocity-increment ratios are positive on the upper surfaces and negative on the lower surfaces; the opposite is true for negative additional lift coefficients.

In addition to the pressure distributions associated with these two load distributions, another pressure distribution exists which is associated with the basic symmetrical thickness form or thickness distribution of the airfoil. This pressure distribution has been calculated by the methods described in the previous section for the condition of zero lift and is presented in the supplementary figures as $\left(\frac{v}{V}\right)^2$, which is equivalent at low Mach numbers to the pressure coefficient S, and as the local velocity ratio v/V. This local velocity ratio is always positive and is the same for corresponding points on the upper and lower surfaces of the thickness form.

The velocity distribution about the airfoil is thus considered to be composed of three separate and independent components as follows:

- (1) The distribution corresponding to the velocity distribution over the basic thickness form at zero angle of attack
- (2) The distribution corresponding to the design load distribution of the mean line
- (3) The distribution corresponding to the additional load distribution associated with angle of attack

The velocity-increment ratios $\Delta v/V$ and $\Delta v_a/V$ corresponding to components (2) and (3) are added to the velocity ratio corresponding to component (1) to obtain the total velocity at one point, from which the pressure coefficient S is obtained; thus,

$$S = \left(\frac{v}{V} \pm \frac{\Delta v}{V} \pm \frac{\Delta v_{B}}{V}\right)^{2} \tag{14}$$

NACA ACR No. 15005

When this formula is used, values of the ratios corresponding to one value of x are added together and the resulting value of the pressure coefficient S is assigned to the airfoil surface at the same value of x.

The values of v/V and of $\Delta v/V$ in equation (14) should, of course, correspond to the airfoil geometry. Methods of obtaining the proper values of these ratios from the values tabulated in the supplementary figures are presented in the previous section "Description of Airfoils."

When the ratio $\Delta v_a/V$ has the value of zero, the resulting distribution of the pressure coefficient S will correspond approximately to the pressure distribution of the airfoil section at the design lift coefficient c_{l_1} of the mean line, and the lift coefficient may be assigned this value as a first approximation. If the pressure-distribution diagram is integrated, however, the value of c_l will be found to be greater than c_l by an amount dependent on the thickness ratio of the basic thickness form.

The pressure distribution will usually be desired at some specified lift coefficient not corresponding to c_{l_1} . For this purpose the ratio $\Delta v_a/V$ must be assigned some value obtained by multiplying the tabulated value of this ratio by a factor $f(\alpha)$. For a first approximation this factor may be assigned the value

$$f(\alpha) = c_1 - c_{1_1} \tag{15}$$

where c_l is the lift coefficient for which the pressure distribution is desired. If greater accuracy is desired, the value of $f(\alpha)$ may be adjusted by trial and error to produce the actual desired lift coefficient as determined by integration of the pressure-distribution diagram.

Although this method of superposition of velocities has inadequate theoretical justification, experience has shown that the results obtained are adequate for engineering use. In fact, the results of even the first approximations agree well with experimental data and are adequate for at least preliminary consideration and selection of airfoils. A comparison of a first-approximation theoretical pressure distribution with an experimental distribution is shown in figure 7. Some discrepancy naturally occurs between the results of experiment and of any theoretical method based on potential flow because of the presence of the boundary layer. These effects are small, however, over the range of lift coefficients for which the boundary layer is thin and the drag coefficient is low.

Jelan milite ben

NACA ACR No. L5CO5

Numerical examples .- The following numberical examples are included to illustrate the method of obtaining the firstapproximation pressure distributions:

Example 1: Find the pressure coefficient S at the station x = 0.50 on the upper and lower surfaces of the NACA 653-418 airfoil at a lift coefficient of 0.2.

From the description of the NACA 6-series airfoils, it is determined that this airfoil is obtained by combining the NACA 652-018 basic thickness form with the a = 1.0 type mean line cambered to a design lift coefficient of 0.4. The following data are obtained from the supplementary figures for this thickness form and mean line at x = 0.50:

$$\frac{V}{V} = 1.235$$

$$\frac{\Delta V_{a}}{V} = 0.157$$

$$\frac{\Delta V}{V} = 0.250$$

The desired value of $\Delta v_a/V$ is computed as follows by use of equation (15):

$$\frac{\Delta v_{a}}{V} = (0.157)(0.2 - 0.4)$$
$$= -0.031$$

The desired value of $\Delta v/V$ is obtained by multiplying the tabulated value by the design lift coefficient as stated in the description of the NACA 6-series airfoils. Thus,

$$\frac{\Delta v}{v} = (0.250)(0.4)$$
= 0.100

Substituting these values in equation (14) gives the following values of S:

For the upper surface

$$S = (1.235 + 0.100 - 0.031)^{2}$$
$$= 1.700$$

For the lower surface

$$s = (1.235 - 0.100 + 0.031)^2$$
$$= 1.360$$

Example 2: Find the pressure coefficient S at the station x = 0.25 on the upper and lower surfaces of the NACA $65(215)^{-214}$, a = 0.5 airfoil at a lift coefficient of 0.6.

The airfoil designation shows that this airfoil was obtained by combining a thickness form obtained by multiplying the ordinates of the NACA 652-015 form by the factor 14/15 with the a=0.5 type mean line cambered to a design lift coefficient of 0.2.

The supplementary figures give a value of 1.182 for v/V at x = 0.25 for the NACA 652-015 basic thickness form. The desired value of v/V is obtained by applying formula (5) as follows:

$$\frac{v}{v} = (1.182 - 1)\frac{14}{15} + 1$$

$$= 1.170$$

From the supplementary figures the following values of $\Delta v_a/V$ are obtained at x=0.25 for the following basic thickness forms:

Thickness form	$\frac{\Delta v_a}{V} \text{ at}$ $x = 0.25$
NACA 652-015	0.290
NACA 651-012	.282

By interpolation the value of $\Delta v_a/V$ of 0.287 may be assigned to the 14-percent-thick form. The desired value of $\Delta v_a/V$ is then computed as follows by use of equation (15):

$$\frac{\Delta v_a}{V} = (0.287)(0.6 - 0.2)$$
$$= 0.115$$

Data presented in the supplementary figures for the a=0.5 type mean lines give the value of 0.333 for $\Delta v/V$ at x=0.25. As stated in the description of the NACA 6-series airfoils, the desired value of $\Delta v/V$ is obtained by multiplying the tabulated value by the design lift coefficient. Thus,

$$\frac{\Delta v}{v} = (0.333)(0.2)$$
= 0.067

Substituting the foregoing values in equation (14) gives the values of S as follows:

For the upper surface

$$S = (1.170 + 0.067 + 0.115)^2$$
$$= 1.828$$

For the lower surface

$$S = (1.170 - 0.067 - 0.115)^2$$
$$= 0.976$$

Example 3: Find the pressure coefficient S at the station x = 0.30 on the upper and lower surfaces of the NACA 2412 airfoil at a lift coefficient of 0.5.

The description of airfoils of the NACA four-digit series shows that the necessary data may be found from the NACA 0012 thickness form and 64 mean line in the supplementary figures. From these figures the following data are obtained:

At x = 0.30

$$\frac{v}{V} = 1.162$$

At x = 0.30

$$\frac{\Delta v_a}{V} = 0.239$$

For the NACA 64 mean line at x = 0.30

$$\frac{\Delta v}{V} = 0.260$$

For the NACA 64 mean line

$$c_{l_1} = 0.76$$

The values of $\Delta v/V$ and c_{l_i} corresponding to the airfoil geometry are obtained by multiplying the foregoing values by the factor 2/6 as explained in the description of these airfoils; thus,

$$\frac{\Delta v}{V} = (0.260)(\frac{2}{6})$$
$$= 0.087$$

$$c_{l_i} = (0.76)(\frac{2}{6})$$

$$= 0.253$$

The desired value of $\Delta v_a/V$ is obtained from equation (15) as follows:

$$\frac{\Delta v_a}{V} = (0.239)(0.5 - 0.253)$$
$$= 0.059$$

Substituting the proper values in equation (14) gives the values of S as follows:

For the upper surface

$$S = (1.162 + 0.087 + 0.059)^{2}$$
$$= 1.712$$

For the lower surface

$$S = (1.162 - 0.087 - 0.059)^2$$
$$= 1.032$$

Effect of camber on pressure distribution. At zero lift the pressure distributions over the upper and lower surfaces of a basic symmetrical thickness distribution are, of course, identical. The effect of camber on the pressure distribution at the design lift coefficient is to separate the pressures on the upper and lower surfaces by an amount corresponding approximately to the design load distribution of the mean line. When the local value of the design load distribution is positive, the pressure coefficient S on the upper surface is increased (decreased absolute pressure)

whereas that on the lower surface is decreased. This effect is shown in figure 8(a) for various amounts of camber.

The maximum value of the pressure coefficient on the upper surface at the design lift coefficient increases with the design lift coefficient and for a given design lift coefficient increases with decreasing values of a. The result is to cause the critical Mach number at the design lift coefficient to decrease with increasing camber or with the use of types of mean line concentrating the load near the leading edge. Figure 8(b) shows that the location of minimum pressure on both surfaces is not affected if a type of mean line is used having a value of a at least as large as the value of x/c at the position of minimum pressure on the basic thickness distribution. If a mean line with a smaller value of a is used, the possible extent of laminar flow along the upper surface will be reduced.

Critical Mach Number

The critical speed is defined as the free-stream speed at which the velocity at any point along the surface of the airfoil reaches the local velocity of sound. If the maximum value of the low-speed pressure coefficient S is known either experimentally or from theoretical methods, the critical Mach number may be predicted approximately by the von Kármán method (reference 19). A curve relating the critical Mach number and the low-speed pressure coefficient S has been calculated from the equations of reference 19 and included in the supplementary figures. These predicted critical Mach numbers are useful for preliminary considerations in the absence of test data and appear to correspond fairly well to the Mach numbers at which the local velocity of sound is reached in the high-criticalspeed range of lift coefficient. This criterion does not, however, appear to predict accurately the Mach numbers at which large changes in airfoil characteristics occur, especially when sharp pressure peaks exist at the leading edge. A discussion of the characteristics of airfoil sections at super-critical Mach numbers is beyond the scope of this report.

For convenience, curves of predicted critical Mach number plotted against the low-speed section lift coefficient have been included in the supplementary figures for a number of airfoils. These figures are somewhat similar to those of Heaslet (reference 20) but are plotted against the low-speed lift coefficient rather than against the high-speed lift coefficient, as in reference 20. High-speed lift coefficients corresponding to those of Heaslet may be obtained by multiplying the low-speed lift coefficient by the

factor $\frac{1}{\sqrt{1-M^2}}$. The critical Mach numbers have been predicted

from theoretical pressure distributions. For airfoils of the NACA four- and five-digit series and for the NACA 7-series airfoils, the theoretical pressure distributions were obtained by Theodorsen's method. For the other airfoils the theoretical pressure distributions were obtained by the approximate method described in the preceding section.

The data in the supplementary figures show that for any one type of airfoil, the maximum critical Mach number decreases rapidly as the thickness is increased. The effect of camber is to lower the maximum critical Mach number and to shift the range of high critical Mach numbers in the same manner as for the low drag range. For common types of camber the minimum reduction in critical speed for a given design lift coefficient is obtained with a uniform load type of mean line. A comparison of the data presented in the supplementary figures shows that NACA 6-series sections have considerably higher maximum critical Mach numbers than NACA 24-, 44-, and 230-series airfoils of corresponding thickness ratios.

Moment Coefficients

Methods of calculation. Theoretical moment coefficients may be approximated directly from the values presented in the supplementary figures for the various mean lines. These values were obtained from thin-airfoil theory and may be scaled up or down linearly with the design lift coefficient or with the mean-line ordinates. These theoretical values are sufficiently accurate for preliminary considerations, but experimental values should be used for stability and control calculations.

Numerical examples. - The following numerical examples illustrate the methods of calculating the moment coefficients:

Example 1: Find the theoretical moment coefficient about the quarter-chord point for the NACA 652-215, a = 0.5 airfoil.

The designation of the airfoil shows that the design lift coefficient of this airfoil is 0.2. From the data on the NACA a = 0.5 type mean line included in the supplementary figures, the value of $c_{\rm mc/4}$ is -0.139 for a design lift coefficient of 1.0. The desired value of the moment coefficient is accordingly

$$c_{m_C/4} = (-0.139)(0.2)$$

= -0.028

Example 2: Find the theoretical moment coefficient about the quarter-chord point for the NACA 4415 airfoil.

From the description of the NACA four-digit series airfoils, the required data is found to be presented for the NACA 64 mean line in the supplementary figures. The moment coefficient for this mean line is -0.157. The required value is then

$$c_{m_0/4} = (-0.157)^{\frac{14}{6}}$$

= -0.105

Angle of Zero Lift

Methods of calculation. Values of the ideal or design angle of attack α_i corresponding to the design lift coefficient c_{l_i} are included among the data for the various mean lines presented in the supplementary figures. The approximate values of the angle of zero lift may be obtained from the data by using the theoretical value of the lift-curve slope for thin airfoils, 2π per radian. The value of α_l in degrees is then

$$\alpha_{l_0} = \alpha_1 - \frac{57.3}{2\pi} c_{l_1}$$
 (16)

The tabulated values of α_i may be scaled linearly with the design lift coefficient or with the mean-line ordinates.

Although these theoretical angles of zero lift may be useful in preliminary design, they should not be used without experimental verification for such purposes as establishing the washout of a wing.

Numerical examples. The method of computing a is illustrated in the following examples:

Example 1: Find the theoretical angle of zero lift of the NACA 652-515, a = 0.5 airfoil.

This airfoil number indicates a design lift coefficient of 0.5. Data for the NACA a=0.5 mean line indicate that $\alpha_1=3.04^{\circ}$ when $c_{l_1}=1.0$. The desired value of α_1 is then

$$c_1 = (3.04)(0.5)$$

= 1.52°

Substituting in equation (16) gives

$$\alpha_{7_0} = 1.52 - \frac{(57.3)(0.5)}{2\pi}$$

$$= -3.0^{\circ}$$

Example 2: Find the theoretical angle of zero lift for the NACA 2415 airfoil.

The description of the NACA four-digit-series airfoils shows that the required values of α_i and c_{l_i} may be obtained by multiplying the corresponding values for the NACA 64 mean line (see supplementary figs.) by a factor 2/6; then

$$\alpha_{i} = (0.74)(\frac{2}{6})$$

$$= 0.25^{\circ}$$

$$c_{l_{i}} = (0.76)(\frac{2}{6})$$

$$= 0.253$$

and from equation (16)

$$\alpha_{7_0} = 0.25 - \frac{(57.3)(0.253)}{2\pi}$$

$$= -2.0^{\circ}$$

Description of Flow around Airfoils

Ferfect-fluid theory postulates that the flow follow the airfoil contour smoothly at all angles of attack with no loss of energy. Consequently, perfect-fluid theory itself gives no information concerning the profile drag or the maximum lift of airfoil sections. The explanation of these phenomena is found from a consideration of the effects of viscosity, which are of primary importance in a thin region near the surface of the airfoil called the boundary layer.

Boundary layers in general are of two types, namely, laminar and turbulent. The flow in the laminar layer is smooth and free from any eddying motion. The flow in the turbulent layer is characterized by the presence of a large number of relatively small eddies.

Because the eddies in the turbulent layer produce a transfer of momentum from the relatively fast-moving outer parts of the boundary layer to the portions closer to the surface, the distribution of average velocity is characterized by relatively higher velocities near the surface and a greater total boundary-layer thickness in a turbulent boundary layer than in a laminar boundary layer developed under otherwise identical conditions. Skin friction is therefore higher for turbulent boundary-layer flow than for laminar flow.

When the pressures along the airfoil surface are increasing in the direction of flow, a general deceleration takes place. At the outer limits of the boundary layer this deceleration takes place in accordance with Bernoulli's law. Closer to the surface, no such simple law can be given because of the action of the viscous forces within the boundary layer. In general, however, the relative loss of speed is somewhat greater for particles of fluid within the boundary layer than for those at the outer limits of the layer because the reduced kinetic energy of the boundary-layer air limits its ability to flow against the adverse pressure gradient. If the rise in pressure is sufficiently great, portions of the fluid within the boundary layer may actually have their direction of motion reversed and may start moving upstream. When this reverse occurs. the flow in the boundary layer is said to be "separated." Because of the increased interchange of momentum from different parts of the layer, turbulent boundary layers are much more resistant to separation than are laminar layers. Laminar boundary layers can only exist for a relatively short distance in a region in which the pressure increases in the direction of flow. Formulas for calculating many of the boundary-layer characteristics are given in references 21 to 23.

After laminar separation occurs, the flow may either leave the surface permanently or reattach itself in the form of a turbulent boundary layer. Not much is known concerning the factors controlling this phenomenon. Laminar separation on wings is usually not permanent at flight values of the Reynolds number except when it occurs near the leading edge under conditions corresponding to maximum lift. The size of the locally separated region that is formed when the laminar boundary layer separates and the flow returns to the surface decreases with increasing Reynolds number at a given angle of attack.

The flow over aerodynamically smooth airfoils at low and moderate lift coefficients is characterized by laminar boundary layers from the leading edge back to approximately the location of the first minimum-pressure point on both upper and lower surfaces. If the region of laminar flow is extensive, separation occurs

immediately downstream from the location of minimum pressure (reference 21) and the flow returns to the surface almost immediately at flight Reynolds numbers as a turbulent boundary layer. This turbulent boundary layer extends to the trailing edge. If the surfaces are not sufficiently smooth and fair, if the air stream is turbulent, or perhaps if the Reynolds number is sufficiently large, transition from laminar to turbulent flow may occur anywhere upstream of the calculated laminar separation point.

For low and moderate lift coefficients where inappreciable separation occurs, the airfoil profile drag is largely caused by skin friction and the value of the drag coefficient depends mainly on the relative amounts of laminar and turbulent flow. If the location of transition is known or assumed, the drag coefficient may be calculated with reasonable accuracy from boundary-layer theory by use of the methods of references 24 to 26.

As the lift coefficient of the airfoil is increased by changing the angle of attack, the resulting application of the additional type of lift distribution moves the minimum pressure point upstream on the upper surface, and the possible extent of laminar flow is thus reduced. The resulting greater proportion of turbulent flow, together with the larger average velocity of flow over the surfaces, causes the drag to increase with lift coefficient.

In the case of many of the older types of airfoils, this forward movement of transition is gradual and the resulting variation of drag with lift coefficient occurs smoothly. The pressure distributions for NACA 6-series airfoils are such as to cause transition to move forward suddenly at the end of the low-drag range of lift coefficients. A sharp increase in drag coefficient to the value corresponding to a forward location of transition on the upper surface results. Such sudden shifts in transition give the typical drag curve for these airfoils with a "sag" or "bucket" in the low-drag range. The same characteristic is shown to a smaller degree by some of the earlier airfoils such as the NACA 23015 when tested in a low-turbulence stream.

At high lift coefficients, a large part of the drag is contributed by pressure or form drag resulting from separation of the flow from the surface. The flow over the upper surface is characterized by a negative pressure peak near the leading edge, which causes laminar separation. The onset of turbulence causes the flow to return to the surface as a turbulent boundary layer. High Reynolds numbers are favorable to the development of turbulence and aid in this process. If the lift coefficient is sufficiently high or if the reestablishment of flow following laminar separation is undulydelayed by low Reynolds numbers, the turbulent layer will

separate from the surface near the trailing edge and will cause large drag increases. The eventual loss in lift with increasing angle of attack may result either from relatively sudden permanent separation of the laminar boundary layer near the leading edge or from progressive forward movement of turbulent separation. Under the latter condition, the flow over a relatively large portion of the surface may be separated prior to maximum lift. A more extended discussion of the flow conditions associated with maximum lift is given in reference 5.

EXPERIMENTAL CHARACTERISTICS

Sources of Data

The primary source of the wind-tunnel data presented is from tests in the Langley two-dimensional low-turbulence pressure tunnel (TDT). The methods used to obtain and correct the data are summarized in the appendix. Design data obtained from tests of 2-foot-chord models in this tunnel are presented in the supplementary figures.

Some wind-tunnel data presented were obtained in other NACA wind tunnels. In each case, the source of the data is indicated and the testing techniques and corrections used were conventional unless otherwise indicated.

Most of the flight data consist of drag measurements made by the wake-survey method on either the airplane wing or a "glove" fitted over the wing as the test specimen. Whenever the measurements were obtained for a glove, this fact is indicated in the presentation of the data. All data obtained at high speeds have been reduced to coefficient form by compressible-flow methods. In the case of all such NACA flight data, precautions have been taken to ensure that the results presented are not invalidated by cross flows of low-energy air into or out of the survey plane.

Drag Characteristics of Smooth Airfoils

Drag characteristics in low-drag range. The value of the drag coefficient in the low-drag range for smooth airfoils is mainly a function of the Reynolds number and the relative extent of the laminar layer and is moderately affected by the airfoil thickness ratio and camber. The effect on minimum drag of the position of minimum pressure which determines the possible extent of laminar flow is shown in figure 9 for some NACA 5-series airfoils. The data show a regular decrease in drag coefficient with rearward movement of minimum pressure.

The variation of minimum drag coefficient with Reynolds number for several airfoils is shown in figure 10. The drag coefficient generally decreases with increasing Reynolds number up to Reynolds numbers of the order of 20 x 100. Above this Reynolds number the drag coefficient of the NACA 65(421)-420 airfoil remained substantially constant up to a Reynolds number of nearly 40 x 106. The earlier increase in drag coefficient shown by the NACA 66(2x15)-116 airfoil may be caused by surface irregularities because the specimen tested was a practicalconstruction model. It may be noted that the drag coefficient for the NACA 653-418 airfoil at low Reynolds numbers is substantially higher than that of the NACA 0012, whereas at high Reynolds numbers the opposite is the case. The higher drag of the NACA 653-418 airfoil section at low Reynolds numbers is caused by a relatively extensive region of laminar separation downstream of the point of minimum pressure. This region decreases in size with increasing Reynolds number. These data illustrate the inadequacy of low Reynolds number test data either to estimate the full-scale characteristics or to determine the relative merits of airfoil sections at flight Reynolds numbers (references 27 and 28).

The variation of minimum drag coefficient with camber is shown in figure 11 for a number of smooth 18-percent-thick NACA 6-series airfoils. These data show very little change in minimum drag coefficient with increase in camber. A large amount of systematic data is included in figure 12 to show the variation of minimum drag coefficient with thickness ratio for a number of NACA airfoil sections ranging in thickness from 6 percent to 24 percent of the chord. The minimum drag coefficient is seen to increase with increase in thickness ratio for each airfoil series. This increase, however, is greater for the NACA four- and five-digit-series airfoils (fig. 12(a)) than for the NACA 6-series airfoils (figs. 12(b) to 12(e)).

The data presented in the supplementary figures for the NACA 6-series thickness forms show that the range of lift coefficients for low drag varies markedly with airfoil thickness. It has been possible to design airfoils of 12-percent thickness with a total theoretical low-drag range of lift coefficients of 0.2. This theoretical range increases by approximately 0.2 for each 3-percent increase of airfoil thickness. Figure 13 shows that the theoretical extent of the low-drag range is approximately realized at a Reynolds number of $9 \times 10^{\circ}$. Figure 13 also shows a characteristic tendency for the drag to increase to some extent toward the upper end of the low-drag range for moderately cambered airfoils, particularly for the thicker airfoils. All data for the NACA 6-series airfoils show a decrease in the extent of the low-drag

range with increasing Reynolds number. Extrapolation of the rate of decrease observed at Reynolds numbers below 9×10^6 would indicate a vanishingly small low-drag range at flight values of the Reynolds number. Tests of a carefully constructed model of the NACA $65_{(421)}$ -420 airfoil showed, however, that the rate of reduction of the low-drag range with increasing Reynolds number decreased markedly at Reynolds numbers above 9×10^6 (fig. 14). These data indicate that the extent of the low-drag range of this airfoil is reduced to about one-half the theoretical value at a Reynolds number of 35×10^6 .

The values of the lift coefficient for which low drag is obtained are determined largely by the amount of camber. The lift coefficient at the center of the low-drag range corresponds approximately to the design lift coefficient of the mean line. The effect on the drag characteristics of various amounts of camber is shown in figure 15. Section data indicate that the location of the low-drag range may be shifted by even such crude camber changes as those caused by small deflections of a plain flap. (See supplementary fig.)

The location of the low-drag range shows some variation from that predicted by simple thin-airfoil theory. This departure appears to be a function of the type of mean line used (reference 29) and the airfoil thickness. The effect of airfoil thickness is shown in figure 13, from which the center of the low-drag range is seen to shift to higher lift coefficients with increasing airfoil thickness. This shift is partly explained by the increase in lift coefficient above the design lift coefficient for the mean line obtained when the velocity increments caused by the mean line are combined with the velocity distribution for the basic thickness form according to the approximate methods previously described.

Drag characteristics outside low-drag range. At the end of the low-drag range the drag increases rapidly with increase in lift coefficient. For symmetrical and low-cambered airfoils, for which the lift coefficient at the upper end of the low-drag range is moderate, this high rate of increase does not continue. (See fig. 15.) For highly cambered sections, for which the lift at the upper end of the low-drag range is already high, the drag coefficient shows a continued rapid increase.

Comparison of data for airfoils cambered with a uniform-load mean line with data for airfoils cambered to carry the load farther forward shows that the uniform-load mean line is favorable for obtaining low drag coefficients at high lift coefficients (fig. 16 and reference 29).

Data for many of the airfoils given in the supplementary figures show large reductions in drag with increasing Reynolds number at high lift coefficients. This scale effect is too large to be accounted for by the normal variation in skin friction and appears to be associated with the effect of Reynolds number on the onset of turbulent flow following laminar separation near the leading edge (reference 30).

Effects of type of section on drag characteristics.- A comparison of the drag characteristics of the NACA 23012 and of three NACA 6-series airfoils is presented in figure 17. The drag for the NACA 6-series sections is substantially lower than for the NACA 23012 section in the range of lift coefficients corresponding to high-speed flight, and this margin may usually be maintained through the range of lift coefficients useful for cruising by suitable choice of camber. The NACA 6-series sections show the higher maximum values of the lift-drag ratio. At high values of the lift coefficient, however, the earlier NACA sections have generally lower drag coefficients than the NACA 6-series airfoils.

Effective aspect ratio. The combination of high drags at high lift coefficients, low drags at moderate lift coefficients, and the nonregular variation of drag with lift coefficient shown by the NACA 6-series airfoils may lead to paradoxical results when the span-efficiency concept (reference 31) is used for the calculation of airplane performance. In the usual application of this concept, the airplane drag characteristics are approximated by a curve of the type

$$C_{\rm D} = C_{\rm D_{\rm L}=0} + k C_{\rm L}^2$$
 (17)

This curve is usually matched to the actual drag characteristics at a rather low and at a moderately high value of the lift coefficient (reference 32).

The application of this concept to two hypothetical airplanes with NACA 230- and 65-series sections, respectively, is illustrated in figure 18(a). The wing drags of the airplanes have been calculated by adding the induced drags corresponding to an aspect ratio of 10 with elliptical loading to the profile-drag coefficients of the NACA 23018 and 653-418 airfoils. These sections are considered representative of average wing sections for a large airplane of this aspect ratio. Ordinate scales are given in figure 18(a) for the wing drag and for the total airplane drag coefficients obtained by adding a representative constant value of 0.0150 to the wing drag coefficients. The resulting drag coefficients

have been approximated by two curves corresponding to equation (17) and matched to the drag curves at lift coefficients of 0.2 and 1.0. These two curves correspond to effective aspect ratios of 9.29 for the airplane with NACA 23018 sections and of 8.30 for the airplane with NACA 653-418 sections and illustrate the typical large reduction in the effective aspect ratio obtained with such sections.

It should be noted, however, that although equation (17) provides a reasonably satisfactory approximation to the drag of the airplane with NACA 23018 sections, such is not the case for the airplane with the NACA 653-418 section. The most important reason for using high aspect ratios on large airplanes is to reduce the drag at cruising lift coefficients and to obtain high maximum values of the lift-drag ratio. For the two wings considered, the maximum value of this ratio is appreciably higher for the airplane with NACA 653-418 sections (19.8 as compared with 18.5) despite the fact that this airplane shows the lower effective aspect ratio. Figure 18(b) shows a similar comparison with similar results for two airplanes of aspect ratio 8 and NACA 2415 and 652-415 airfoils. It is accordingly concluded that the effective aspect ratio is not a satisfactory criterion for use in airfoil selection.

Effect of Surface Irregularities on Drag

Permissible roughness. Previous work has shown large drag increments resulting from surface roughness (reference 33). Although a large part of these drag increments was shown to result from forward movement of transition, substantial drag increments resulted from surface roughness in the region of turbulent flow. It is accordingly important to maintain smooth surfaces even when extensive laminar flow cannot be expected, but the gains that may be expected from maintaining smooth surfaces are greater for NACA 6- or 7-series airfoils when extensive laminar flows are possible.

No accurate method of specifying the surface condition necessary for extensive laminar flow at high Reynolds numbers has been developed, although some general conclusions have been reached. It may be presumed that for a given Reynolds number and chordwise position, the size of the permissible roughness will vary directly with the chord of the airfoil. It is known, at one extreme, that the surfaces do not have to be polished or optically smooth. Such polishing or waxing has shown no improvement in tests in the Langley two-dimensional low-turbulence tunnels when applied to satisfactorily sanded surfaces. Polishing or waxing a surface that is not aerodynamically smooth will, of course, result in improvement and such finishes may be of considerable practical value because

deterioration of the finish may be easily seen and possibly postpened. Large models having chord lengths of 5 to 8 feet tested in
the Langley two-dimensional low-turbulence tunnels are usually
finished by sanding in the chordwise direction with No. 320 carborundum
paper when an aerodynamically smooth surface is desired. Experience
has shown the resulting finish to be satisfactory at flight values
of the Reynolds number. Any rougher surface texture should be
considered as a possible source of transition, although slightly
rougher surfaces have appeared to produce satisfactory results in
some cases.

Wind tunnel experience in testing NACA 6-series sections and data of reference 34 show that small protuberances extending above the general surface level of an otherwise satisfactory surface are more likely to cause transition than small depressions. Dust particles, for example, are more effective than small scratches in producing transition if the material at the edges of the scratches is not forced above the general surface level. Dust particles adhering to the oil left on airfoil surfaces by fingerprints may be expected to cause transition at high Reynolds numbers.

Transition spreads from an individual disturbance with an included angle of about 15° (references 33 and 35). A few scattered specks, especially near the leading edge, will cause the flow to be largely turbulent. This fact makes necessary an extremely thorough inspection if low drags are to be realized. Specks sufficiently large to cause premature transition on full-size wings can be felt by hand. The inspection procedure used in the Langley two-dimensional low-turbulence tunnels is to feel the entire surface by hand after which the surface is thoroughly wiped with a dry cloth.

It has been noticed that transition resulting from individual small sharp protuberances, in contrast to waves, tends to occur at the protuberance. Transition caused by surface waviness appears to approach the wave gradually as the Reynolds number or wave size is increased. The height of a small cylindrical protuberance necessary to cause transition when located at 5 percent of the chord with its axis normal to the surface is shown in figure 19. These data were obtained at rather low values of the Reynolds number and show a large decrease in allowable height with increase in Reynolds number. This effect of Reynolds number on permissible surface roughness is also evident in figure 20, in which a sharp increase in drag at a Reynolds number of approximately 20 × 10° occurs for the model painted with camouflage lacquer.

The magnitude of the favorable gradient appears to have a small effect on the permissible surface roughness for laminar flow.

Figure 21 shows that the roughness becomes more important at the extremities of the low-drag range where the favorable pressure gradient is reduced on one surface. The effect of increasing the Reynolds number for a surface of marginal smoothness, which has an effect similar to increasing the surface roughness for a given Reynolds number, is to reduce rapidly the extent of the low-drag range and then to increase the minimum drag coefficient (fig. 21). The data of figure 21 were specially chosen to show this effect. In most cases, the effect of Reynolds number predominates over the effect of decreasing the magnitude of the favorable pressure gradient to such an extent that the only effect is the elimination of the low-drag range (reference 36).

Permissible waviness. - More difficulty is generally encountered in reducing the waviness to permissible values for the maintenance of laminar flow than in obtaining the required surface smoothness. In addition, the specification of the required freedom from surface waviness is more difficult than that of the required surface smoothness. The problem is not limited merely to finding the minimum wave size that will cause transition under given conditions because the number of waves and the shape of the waves require consideration.

If the wave is sufficiently large to affect the pressure distribution in such a manner that laminar separation is encountered, there is little doubt that such a wave will cause premature transition at all useful Reynolds numbers. A relation between the dimensions of a wave and the pressure distribution may be found by the methods of reference 37. The size of the wave required to reverse the favorable pressure gradient increases with the pressure gradient. Large negative pressure gradients would therefore appear to be favorable for wavy surfaces. Experimental results have shown this conclusion to be qualitatively correct.

Little information is available on waves too small to cause laminar separation or even reversal of the pressure gradient. Data for an airfoil section having a relatively long wave on the upper surface are given in figure 22. Marked increases in the drag corresponding to a rapid forward movement of the transition point were not noticeable below a Reynolds number of 44 × 100. On the other hand, transition has been caused at comparatively low Reynolds numbers by a series of small waves with a wave height of the order of a few ten-thousandths of an inch and a wave length of the order of 2 inches on the same 60-inch-chord model.

For the types of wave usually encountered on practicalconstruction wings, the test of rocking a straightedge over the surface in a chordwise direction is a fairly satisfactory criterion. The straightedge should rock smoothly without jarring or clicking. The straightedge test will not show the existence of waves that leave the surface convex, such as the wave of figure 22 and the series of small waves previously mentioned. Tests of a large number of practical-construction models, however, have shown that those models which passed the straightedge test were sufficiently free of small waves to permit low drags to be obtained at flight values of the Reynolds number.

It is not feasible to specify construction tolerances on airfoil ordinates with sufficient accuracy to ensure adequate freedom from waviness. If care is taken to obtain fair surfaces, normal tolerances may be used without causing serious alteration of the drag characteristics.

Drag with fixed transition.— If the airfoil surface is sufficiently rough to cause transition near the leading edge, large drag increases are to be expected. Figure 23 shows that, although the degree of roughness has some effect, the increment in minimum drag coefficient caused by the smallest roughness capable of producing transition is nearly as great as that caused by much larger grain roughness when the roughness is confined to the leading edge. The degree of roughness has a much larger effect on the drag at high lift coefficients. If the roughness is sufficiently large to cause transition at all Reynolds numbers considered, the drag of the airfoil with roughness only at the leading edge decreases with increasing Reynolds number (fig. 10 and reference 38).

The effect of fixing transition by means of a roughness strip of carborundum of 0.011-inch grain is shown in figure 24. The minimum drag increases progressively with forward movement of the roughness strip. The effect on the drag at high lift coefficients is not progressive; the drag increases rapidly when the roughness is at the leading edge. Figure 25 shows that the drag coefficients for the NACA 65(223)-422 and 63(420)-422 airfoils were nearly the same throughout most of the lift range when the extent of laminar flow was limited to 0.30c.

All recent airfoil data obtained in the Langley two-dimensional low-turbulence pressure tunnel include results with roughened leading edge, and these data are included in the supplementary figures. Tests with roughened leading edge were formerly made only for a limited number of airfoil sections, especially those having large thickness ratios (reference 39). The standard roughness selected for 24-inch-chord models consists of 0.011-inch carborundum grains applied to the airfoil surface at the leading edge over a surface length of 0.08c measured from the leading edge on both surfaces. The grains are thinly spread to cover 5 to 10 percent of this area.

This standard roughness is considerably more severe than that caused by the usual manufacturing irregularities or deterioration in service but is considerably less severe than that likely to be encountered in service as a result of accumulation of ice or mud or damage in military combet.

The variation of minimum drag coefficient with thickness ratio for a number of NACA airfoils with standard roughness is shown in figure 12. These data show that the magnitudes of the minimum drag coefficients for the NACA 6-series airfoils are less than the values for the NACA four- and five-digit-series airfoils. The rate of increase of drag with thickness is greater for the airfoils in the rough condition than in the smooth condition.

Drag with practical construction methods. The section drag coefficients of several airplane wings have been measured in flight by the wake-survey method (reference 40), and a number of practical-construction wing sections have been tested in the Langley two-dimensional low-turbulence pressure tunnel at flight values of the Reynolds number. Flight data obtained by the NACA (reference 40) are summarized in figure 26 and some data obtained by the Consolidated Vultee Aircraft Corporation are presented in figure 27. Data obtained in the Langley two-dimensional low-turbulence pressure tunnel for typical practical-construction sections are presented in figures 28 to 32. Figure 33 presents a comparison of the drag coefficients obtained in this wind tunnel for a model of the NACA 0012 section and in flight for the same model mounted on an airplane. For this case, the wind-tunnel and flight data agree to within the experimental error.

All wings for which flight data are presented in figure 26 were carefully finished to produce smooth surfaces. Great care was taken to reduce surface waviness to a minimum for all the sections except the NACA 2415.5, N-22, Republic S-3,13, and the NACA 27-212. Curvature-gage measurements of surface waviness for some of these airfoils are presented in reference 40. Surface conditions corresponding to the data of figure 27 are described in the figure. These data show that the sections permitting extensive laminar flow had substantially lower drag coefficients when smooth than the other sections.

The wind-tunnel tests of practical-construction wing sections as delivered by the manufacturer showed minimum drag coefficients of the order of 0.0070 to 0.0080 in nearly all cases regardless of the airfoil section used (figs. 28 to 32). Such values may be regarded as typical for good current construction practice. Finishing the sections to produce smooth surfaces always produced substantial drag reductions although considerable waviness usually

remained. None of the sections tested had fair surfaces at the front spar. Unless special care is taken to produce fair surfaces at the front spar, the resulting wave may be expected to cause transition either at the spar location or a short distance behind it. One practical-construction specimen tested with smooth surfaces maintained relatively low drags up to Reynolds numbers of approximately 30×10^6 (NACA 66(2x15)-ll6 airfoil of fig. 10). This specimen had no spar forward of about 35-percent chord from the leading edge and no sparwise stiffeners forward of the spars. This type of construction resulted in unusually fair surfaces and is being used on some modern high-performance airplanes.

A comparison of the effect of airfoil section on the minimum drag with practical-construction surfaces is very difficult because the quality of the surface has more effect on the drag than the type of section. Probably the best comparison can be obtained from pairs of models constructed at the same time by the same manufacturers. Data for such pairs of models are presented in figures 30 to 32. The results indicate that as long as current construction practices are used the type of section has relatively little effect at flight values of the Reynolds number for military airplanes.

Important savings in drag may be obtained at high Reynolds numbers by keeping the surfaces smooth even if extensive laminar flow is not realized. Drag increments resulting from surface roughness in turbulent flow have been shown to be important (reference 33). The effects of surface roughness on the variation of drag with Reynolds number are shown in figure 29, in which the favorable scale effect usually expected at high Reynolds numbers was not realized. This type of scale effect may be compared with that shown for the NACA 63(420)-422 airfoil with rough leading edge but otherwise smooth surfaces (fig. 10). Drag increments obtained in flight resulting from roughness in the turbulent boundary layer with fixed transition are presented in reference 41.

The effect of the application of de-icers to the leading edge of two smooth airfoils is shown in figure 34. The de-icer "boots" were installed in both cases by the manufacturer to represent good typical installations. The minimum drag coefficients for both sections with de-icers installed were of the order of 0.0070 at high Reynolds numbers.

Effects of propeller slipstream and airplane vibration. Very few data are available on the effect of propeller slipstream on transition or airfoil drag; the data that are available do not show consistent results. This inconsistency may result from variations in lift coefficient, surface condition, air-stream turbulence,

propeller advance-diameter ratio, and number of blades. Tests in the Langley 8-foot high-speed tunnel indicated transition occurring from 5 to 10 percent of the chord from the leading edge (reference 42). Drag measurements made in the Langley 19-foot pressure tunnel (fig. 35) indicated only moderate drag increments resulting from a windmilling propeller. Although the data of figure 35 may not be very accurate because of the difficulty of making wake surveys in the slipstream, these data seem to preclude very large drag increments such as would result from movement of the transition to a position close to the leading edge. These data also seem to be confirmed by recent NACA flight data (fig. 36), which show transition as far back as 20 percent of the chord in the slipstream. Other unpublished NACA flight data on transition on an S-3,14.6 airfoil in the slipstream indicated that laminar flow occurred as far back as 0.2c.

Even less data are available on the effects of vibration on transition. Tests in the Langley 8-foot high-speed tunnel (reference 42) showed negligible effects but the range of frequencies tested may not have been sufficiently wide. Some unpublished flight data showed small but consistent rearward movements of transition outside the slipstream when the propellers were feathered. This effect was noticed even when the propeller on the opposite side of the airplane from the survey plane was feathered and was accordingly attributed to vibration. Recent tests in the Ames full-scale tunnel showed premature adverse scale effect on drag coefficients measured by the wake-survey method when a model-support strut vibrated.

Lift Characteristics of Smooth Airfoils

Two-dimensional data .- As explained in the section "Angle of Zero Lift," the angle of zero lift of an airfoil is largely determined by the camber. Thin-airfoil theory provides a means for computing the angle of zero lift from the mean-line data presented in the supplementary figures. The agreement between the calculated and the experimental angle of zero lift depends on the type of mean line used. Comparison of the experimental values of the angle of zero lift obtained from the supplementary figures and the theoretical values taken from the mean-line data shows that the agreement is good except for the uniform-load type (a = 1.0) mean line. The angles of zero lift for this type mean line generally have values more positive than those predicted. The experimental values of the angles of zero lift for a number of NACA fourand five-digit and NACA 6-series airfoils are presented in figure 37. The airfoil thickness appears to have little effect on the value of the angle of zero lift regardless of the airfoil series. For the

NACA four-digit-series airfoils, the angles of zero lift are approximately 0.93 of the value given by thin-airfoil theory; for the NACA 230-series airfoils, this factor is approximately 1.08; and for the NACA 6-series airfoils with uniform-load type mean line, this factor is approximately 0.74.

The lift-curve slopes (fig. 38) for airfoils tested in the Langley two-dimensional low-turbulence pressure tunnel are higher than those previously obtained in the tests reported in reference 8. It is not clear whether this difference in slope is caused by the difference in air-stream turbulence or by the differences in test methods, since the section data of reference 8 were inferred from tests of models of aspect ratio 6. The present values of the liftcurve slope were measured for a Reynolds number of 9 x 100 and at values of the lift coefficient approximately equal to the design lift coefficient of the airfoil section. For the NACA 6-series airfoils this lift coefficient is approximately in the center of the low-drag range. For airfoils having thicknesses in the range from 6 to 10 percent the NACA four- and five-digit series and the NACA 64-series airfoil sections have values of lift-curve slope very close to the value for thin airfoils (2π per radian or 0.110 per degree). Variation in Reynolds number between 3 x 106 and 9 x 106 and variations in airfoil camber up to 4 percent chord appear to have no systematic effect on values of lift-curve slope. The airfoil thickness and the type of thickness distribution appear to be the primary variables. For the NACA four- and five-digit-series airfoil sections, the lift-curve slope decreases with increase in airfoil thickness. For the NACA 6-series airfoil sections, however, the lift-curve slope increases with increase in thickness and forward movement of the position of minimum pressure of the basic thickness form at zero lift.

Some NACA 6-series airfoils show jogs in the lift curve at the end of the low-drag range, especially at low Reynolds numbers. This jog becomes more pronounced with increase of camber or thickness and with rearward movement of the position of minimum pressure on the basic thickness form. This jog decreases rapidly in severity with increasing Reynolds number, becomes merely a change in lift-curve slope, and is practically nonexistent at a Reynolds number of 9×10^6 for most airfoils that would be considered for practical application. This jog may be a consideration in the selection of airfoils for small low-speed airplanes. An analysis of the flow conditions leading to this jog is presented in reference 30.

The variation of maximum lift coefficient with airfoil thickness ratio at a Roynolds number of 6×10^6 is shown in figure 39 for a number of NACA airfoil sections. The airfoils for which data are presented in this figure have a range of thickness ratio

from 6 to 24 percent and cembers up to 4-percent chord. From the data for the NACA four- and five-digit-series airfoil sections (fig. 39(a)), the maximum lift coefficients for the plain airfoils appear to be the greatest for a thickness of 12 percent. In general, the rate of change of maximum lift coefficient with thickness ratio appears to be greatest for airfoils having a thickness less than 12 percent. The data for the NACA 6-series airfoils (figs. 39(b) to (e)) also show a rapid increase in maximum lift coefficient with increasing thickness ratio for thickness ratios of less than 12 percent. For NACA 6-series airfoil sections cambered to give a design lift coefficient of not more than 0.2, the optimum thickness ratio for maximum lift coefficient appears to be between 12 and 15 percent, except for the airfoils having the position of minimum pressure at 60 percent chord. The optimum thickness ratio for the NACA 66-series sections cambered for a design lift coefficient of not more than 0.2 appears to be 15 percent or greater. The available data indicate that a thickness ratio of 12 percent or less is optimum for airfoils having a design lift coefficient of 0.4.

The maximum lift coefficient is least sensitive to variations in position of minimum pressure on the basic thickness form for airfoils having thickness ratios of 6, 18, or 21 percent. The maximum lift coefficients corresponding to intermediate thickness ratios increase with forward movement of the position of minimum pressure, particularly for those airfoils having design lift coefficients of 0.2 or less.

The maximum lift coefficients of moderately cambered NACA 6-series sections increase with increasing camber (fig. 39(b) to 39(e)). The addition of camber to the symmetrical airfoils causes the greatest increments of maximum lift coefficient for airfoil thickness ratios varying from 6 to 12 percent. The effectiveness of camber as a means of increasing the maximum lift coefficient generally decreases as the airfoil thickness increases beyond 12 or 15 percent. The available data indicate that the combination of a 12-percent-thick section and a mean line cambered for a design lift coefficient of 0.4 yields the highest maximum lift coefficient.

The variation of maximum lift with type of mean line is shown in figure 40 for one 6-series thickness distribution. No systematic data are available for mean lines with values of a less than 0.5. It should be noted, however, that airfoils such as the NACA 230-series sections with the maximum camber far forward show large values of maximum lift. Airfoil sections with maximum camber far forward and with thickness ratios of 6 to 12 percent usually stall from the leading edge with large sudden losses in lift. A more desirable gradual stall is obtained when the location of maximum camber is farther back, as for the NACA 24-, 44-, and 6-series sections with normal types of camber.

A comparison of the maximum lift coefficients of NACA 64-series airfoil sections cambered for a design lift coefficient of 0.4 with those of the NACA 44- and 230-series sections (fig. 39) shows that the maximum lift coefficients of the NACA 64-series airfoils are as high or higher than those of the NACA 44-series sections in all cases. The NACA 230-series airfoil sections have maximum lift coefficients somewhat higher than those of the NACA 64-series sections.

The scale effect on the maximum lift coefficient of a large number of NACA airfoil sections for Reynolds numbers from 3×10^6 to 9×10^6 is shown in figure 41. The scale effect for the NACA 24-, 44-, and 230-series airfoils (figs. 41(a) and (b)) having thickness ratios from 12 to 24 percent is favorable and nearly independent of the airfoil thickness. Increasing the Reynolds number from 3×10^6 to 9×10^6 results in an increase in the maximum lift coefficient of approximately 0.15 to 0.20. The scale effect on the NACA 00-and 14-series airfoils having thickness ratios less than 0.12c is very small.

The scale-effect data for the NACA 6-series airfoils (figs. 41(c) to (f)) do not show an entirely systematic variation. In general, the scale effect is favorable for these airfoil sections. For the NACA 63- and 64-series airfoils with small camber, the increase in maximum lift coefficient with increase in Reynolds number is generally small for thickness ratios of less than 12 percent but is somewhat larger for the thicker sections. The character of the scale effect for the NACA 65- and 66-series airfoil sections is similar to that for the NACA 63- and 64-series airfoils but the trends are not so well defined. In most cases the scale effect for NACA 6-series airfoil sections cambered for a design lift coefficient or 0.4 or 0.6 does not vary much with airfoil thickness ratio. The data of figure 42 show that the maximum lift coefficient for the NACA 63(420)-422 airfoil continues to increase with Reynolds number, at least up to a Reynolds number of 26 × 10.5.

The values of the maximum lift coefficient presented were obtained for steady conditions. The maximum lift coefficient may be higher when the angle of attack is increasing. Such a condition might occur during gusts and landing maneuvers. (See reference 43.)

The systematic investigation of NACA 6-series airfoils included tests of the airfoils with a simulated split flap deflected 60°. It was believed that these tests would serve as an indication of the effectiveness of more powerful types of trailing-edge high-lift devices although sufficient data to verify this assumption have not been obtained. The maximum lift coefficients for a large number of NACA airfoil sections obtained from tests with the simulated split flap are presented in figure 39.

The data for the NACA 00- and 14-series airfoils equipped with split flap for thickness ratios from 6 to 12 percent show a considerable increase in maximum lift coefficient with increase in thickness ratio. Corresponding data for the NACA 44-series airfoils with thickness ratios from 12 to 24 percent show very little variation in maximum lift coefficient with thickness. For NACA 6-series airfoils equipped with split flaps the maximum lift coefficients increase rapidly with increasing thickness over a range of thickness ratio, the range beginning at thickness ratios between 6 and 9 percent, depending upon the camber. The upper limit of this range for the symmetrical NACA 64- and 65-series airfoils appears to be greater than 21 percent and for the NACA 63- and 66-series airfoils approximately 18 percent. Between thickness ratios of 6 and 9 percent the values of maximum lift coefficient for the symmetrical NACA 6-series airfoils are essentially the same regardless of thickness ratio and position of minimum pressure on the basic thickness form. The maximum lift coefficient decreases with rearward movement of minimum pressure for the airfoils having thickness ratios between 9 and 18 percent.

Substantial increments in maximum lift coefficient with increase in camber are shown for the NACA 6-series airfoils of moderate thickness ratios (10 to 15 percent chord) with split flaps. For the airfoils having thickness ratios of 6 percent and for the airfoils having thickness ratios of 18 or 21 percent, the maximum lift coefficient is affected very little by a change in camber. For thickness ratios greater than 15 percent, the maximum lift coefficients of the NACA 63- and 64-series airfoils cambered for a design lift coefficient of 0.4 equipped with split flaps are greater than the corresponding maximum lift coefficients of the NACA 44-series airfoils.

Three-dimensional data. No recent systematic three-dimensional wing data obtained at high Reynolds numbers are available, so that it is difficult to make any comparison with the section data. When the maximum-lift data for three-dimensional wings are compared with section data, account should be taken of the span load distribution over the wing. The predicted maximum lift coefficient for the wing will be somewhat lower than the maximum lift coefficients of the sections used because of the nonuniformity of the spanwise distribution of lift coefficient. The difference amounts to about 4 to 7 percent for a rectangular wing with an aspect ratio of 6.

Maximum-lift data obtained from tests of a number of wings and airplane models in the Langley 19-foot pressure tunnel are presented in table II. Although section data at the Reynolds numbers necessary to permit a detailed comparison are not available, the maximum lift coefficient for plain wings given in table II appears

to be in general agreement with values expected from section data. The data for the airplane models are presented to indicate the maximum lift coefficients obtained with various airfoils and configurations.

Lift Characteristics of Rough Airfoils

Two-dimensional data. - Most recent airfoil tests, especially of airfoils with the thicker sections, have included tests with roughened leading edge (reference 39), and the available data are included in the supplementary figures.

The effect on maximum lift coefficient of various degrees of roughness applied to the leading edge of the NACA 63(420)-422 airfoil is shown in figure 23. The maximum lift coefficient decreases progressively with increasing roughness (reference 38). For a given surface condition at the leading edge, the maximum lift coefficient increases slowly with increasing Reynolds number (fig. 43). Figure 24 shows that roughness strips located more than 0.20c from the leading edge have little effect on the maximum lift coefficient or lift-curve slope. The results presented in figure 38 show that the effect of standard leading edge roughness is to decrease the lift-curve slope, particularly for the thicker airfoils having the position of minimum pressure far back. These data are for a Reynolds number of 6 x 100. Maximum-lift-coefficient data at a Reynolds number of 6×10^6 for a large number of NACA airfoil sections with standard roughness are presented in figures 39 and 41. The variation of maximum lift coefficient with thickness for the NACA four- and five-digit-series airfoil sections with standard roughness shows the same trends as those for the smooth airfoils except that the values are considerably reduced for all of these airfoils other than the NACA 00-series airfoils of 6 percent thickness. For a given thickness ratio greater than 15 percent, the values of maximum lift coefficient for the four- and five-digit series airfoils are substantially the same.

Much less variation in maximum lift coefficient with thickness ratio is shown by the NACA 6-series airfoil sections in the rough condition than with smooth leading edge. The maximum lift coefficients of the 6-percent-thick airfoils are essentially the same for both smooth and rough conditions. The variation of maximum lift coefficient with camber, however, is about the same for the airfoils with standard roughness as for the smooth sections. The maximum lift coefficient of airfoils with standard roughness generally decreases somewhat with rearward movement of the position of minimum pressure except for airfoils having thickness ratios greater than 18 percent, in which case some slight gain in maximum lift coefficient results from a rearward movement of the position of minimum pressure.

Except for the NACA 44-series airfoils of 12 to 15 percent thickness, the present data indicate that the rough NACA 64-series airfoil sections cambered for a design lift coefficient of 0.4 have maximum lift coefficients consistently higher than the rough airfoils of the NACA 24-, 44-, and 230-series airfoils of comparable thickness. Standard roughness causes decrements in maximum lift coefficient of the airfoils with split flaps that are substantially the same as those observed for the plain airfoils.

The maximum lift coefficient may be lowered by failure to maintain the true airfoil contour near the leading edge, but no systematic data on this effect have been obtained. Examples of this effect that were accidentally encountered are presented in figure 44, in which lift characteristics are given for accurate and slightly inaccurate models. The model inaccuracies were so small that they were not found previous to the tests.

Three-dimensional data. Tests of several airplanes in the Langley full-scale tunnel (reference 44) show that many factors besides the airfoil sections affect the maximum lift coefficient of airplanes. Such factors as roughness, leakage, leading-edge air intakes, armament installations, nacelles, and fuselages make it difficult to correlate the airplane maximum lift with the airfoils used, even when the flaps are retracted. The various flap configurations used make such a correlation even more difficult when the flaps are deflected. When the flaps were retracted, both the highest and the lowest maximum lift coefficients obtained in recent tests of airplanes and complete mock-ups of conventional configurations in the Langley full-scale tunnel were those obtained with NACA 6-series airfoils.

Results obtained from tests of a model of an airplane in the Langley 19-foot pressure tunnel and of the airplane in the Langley full-scale tunnel are presented in figure 45. Both tests were made at approximately the same Reynolds number. The results show that the airplane in the service condition had a maximum lift coefficient more than 0.2 lower than that of the model, as well as a lower lift-curve slope. Some improvement in the airplane lift characteristics was obtained by sealing leaks. These results show that airplane lift characteristics are strongly affected by details not reproduced on large-scale smooth models.

Lift characteristics obtained in the Langley 19-foot pressure tunnel for two airplane models in the smooth condition and with transition fixed at the front spar are presented in figures 46 and 47. In both cases, the lift-curve slope was decreased throughout most of the lift range with fixed transition. The maximum lift coefficient was decreased in one case but was increased in the other case.

Unconservative Airfoils

The attempt to obtain low drags, especially for long-range airplanes, leads to high wing loadings together with relatively low span loadings. This tendency results in wings of high aspect ratio that require large spar depths for structural efficiency. The large spar depths require the use of thick root sections.

This trend to thick root sections has been encouraged by the relatively small increase in drag coefficient with thickness ratio of smooth airfoils (fig. 12). Unfortunately, airplane wings are not usually constructed with smooth surfaces and, in any case, the surfaces cannot be relied upon to stay smooth under all service conditions. The effect of roughening the leading edges of thick airfoils is to cause large increases in the drag coefficient at high lift coefficients. The resulting drag coefficients may be excessive at cruising lift coefficients for heavily loaded, high-altitude airplanes. Airfoil sections that have suitable characteristics when smooth but have excessive drag coefficients when rough at lift coefficients corresponding to cruising or climbing conditions are classified as unconservative.

The decision as to whether a given airfoil section is conservative will depend upon the power and the wing loading of the airplane. The decision may be affected by expected service and operating conditions. For example, the ability of a multiengine airplane to fly with one or more engines inoperative in icing conditions or after suffering damage in combat may be a consideration.

As an aid in judging whether the sections are conservative, the lift coefficient corresponding to a drag coefficient of 0.02 was determined from the supplementary figures for a large number of NACA airfoil sections with roughened leading edges. The variation of this critical lift coefficient with airfoil thickness ratio and camber is shown in figure 48. These data show that, in general, the lift coefficient at which the drag coefficient is 0.02 decreases with rearward movement of position of minimum pressure. The thickness ratio for which this lift coefficient is a maximum usually lies between 12 and 15 percent; variations in thickness ratio from this optimum range generally cause rather sharp decreases in the critical lift coefficient. The addition of camber to the symmetrical airfoils usually causes an increase in the critical lift coefficient except for the very thick sections, in which case increasing the camber becomes relatively ineffectual and may be actually harmful. All the data of figure 49 correspond to a Reynolds number of 6×10^6 .

As shown in figure 49, the drag coefficient at flight values of the Reynolds number may be considerably lower than the drag coefficient at a Reynolds number of 6×10^{6} if the roughness is confined to the leading edge.

Pitching Moment

The variation of the quarter-chord pitching-moment coefficient at zero angle of attack with airfoil thickness ratio and camber is presented in figure 50 for several NACA airfoil sections. The quarter-chord pitching-moment coefficients of the NACA four- and five-digit-series airfoils become less negative with increasing airfoil thickness. Almost no variation in quarter-chord pitching-moment coefficient with airfoil thickness ratio or position of minimum pressure is shown by the NACA 6-series airfoil sections. As might be expected, increasing the amount of camber causes an almost uniform negative increase in the pitching-moment coefficient.

As discussed previously, the pitching moment of an airfoil section is primarily a function of its camber, and thin-airfoil theory provides a means for estimating the pitching moment from the mean-line data presented in the supplementary figures. A comparison of the experimental moment coefficient and theoretical values for the mean lines is presented in figure 51. The experimental values of the moment coefficients for NACA 6-series airfoils cambered with the uniform-load type mean line are usually about three-quarters of the theoretical values (figs. 50 and 51). Airfoils employing mean lines with values of a less than unity, however, have moment coefficients somewhat more negative than those indicated by theory. The use of a mean line having a value of a less than unity, therefore, brings about only a slight reduction in pitching-moment coefficient for a given design lift coefficient when compared with the value obtained with a uniform-load type mean line. The experimental moment coefficients for the NACA 24-, 44-, and 230-series airfoils are also less negative than those indicated by theory but the agreement is closer than for airfoils having the uniform-load type mean line.

The pitching-moment data for the airfoils equipped with simulated split flaps deflected 60° (fig. 50) indicate that the value of the quarter-chord pitching-moment coefficient becomes more negative with increasing thickness for all the airfoils tested. For the thicker NACA 6-series sections the magnitude of the moment coefficient increases with rearward movement of the position of minimum pressure.

Position of Aerodynamic Center

The variation of chordwise position of the aerodynamic center corresponding to a Reynolds number of 6×10^6 for a large number of NACA airfoils is presented in figure 52. From the data given in the supplementary figures there appears to be no systematic variation of chordwise position of aerodynamic center with Reynolds number. The data for the NACA 00- and 14-series airfoils, presented for thickness ratios less than 12 percent, show that the chordwise position of the aerodynamic center is at the quarter-chord point and does not vary with airfoil thickness. For the NACA 24-, 144-, and 230-series airfoils with thickness ratios ranging from 12 to 24 percent, the chordwise position of the aerodynamic center is ahead of the quarter-chord point and moves forward with increase in thickness ratio.

The chordwise position of the aerodynamic center is behind the quarter-chord point for the NACA 6-series airfoils and moves rearward with increase in airfoil thickness, which is in accordance with the trends indicated by perfect-fluid theory. There appears to be no systematic variation of chordwise position of the aerodynamic center with camber or position of minimum pressure on the basic thickness form for these airfoils.

The data of reference 45 show important forward movements of the aerodynamic center with increasing trailing-edge angle for a given airfoil thickness. For the NACA 24-, 44-, and 230-series airfoils (fig. 52) the effect of increasing trailing-edge angle is apparently greater than the effect of increasing thickness. For the NACA 6-series airfoils, the opposite appears to be the case.

High-Lift Devices

Lift characteristics for two NACA 6-series airfoils equipped with plain flaps are presented in figure 53. These dat 2 show that the maximum lift coefficient increases less rapidly with flap deflection for the more highly cambered section. Lift characteristics of three NACA 6-series airfoils with split flaps are presented in reference 46 and figure 54. The maximum-lift increments for the 12-percent-thick sections were only about three-fourths of that for the 16-percent-thick section. The maximum lift coefficient for the thicker section with flap deflected is about the same as that obtained for the NACA 23012 airfoil in the now obsolete Langley variable-density tunnel (reference 47) and in the Langley 7- by 10-foot tunnel (reference 48).

Tests of a number of slotted flaps on NACA 6-series airfoils (supplementary figures and reference 49) indicate that the design parameters necessary to obtain high maximum lifts are essentially similar to those for the NACA 230-series sections (references 50 and 51). Lift data obtained for typical hinged single-slotted 0.25c flaps (fig. 55(a)) on the NACA 63,4-420 airfoil are presented in figure 55(b). A maximum lift coefficient of approximately 2.95 was obtained for one of the flaps. Lift characteristics for the NACA 653-118 airfoil fitted with a double-slotted flap (reference 49 and fig. 56(a)) are presented in figure 56(b). A maximum lift coefficient of 3.28 was obtained. It may be concluded that no special difficulties exist in obtaining high maximum lift coefficients with slotted flaps on moderately thick NACA 6-series sections.

Tests of airplanes in the Langley full-scale tunnel (reference 44) have shown that expected increments of maximum lift coefficient are obtained for split flaps (fig. 57) but not for slotted flaps (fig. 58). This failure to obtain the expected maximum-lift increments with slotted flaps may be attributed to inaccuracies of flap contour and location, roughness near the flap leading edge, leakage, interference from flap supports, and deflection of flap and lip under load.

Lateral-Control Devices

An adequate discussion of lateral-control devices is outside the scope of this report. The following brief discussion is therefore limited to considerations of effects of airfoil shape on aileron characteristics.

The effect of airful shape on alleron effectiveness may be inferred from the data of figure 59 and reference 52. The section flap-effectiveness parameter $\Delta\alpha_{\rm p}/\Delta\delta$ is plotted against the aileron-chord ratio ca/c for a number of airfoils of different type in figure 59. Table III, which presents supplementary information regarding the data, is placed opposite figure 59 to facilitate its use. Also shown in this figure are the theoretical values of the parameter for thin airfoils. The data show no large consistent trends of aileron-effectiveness variation with airfoil section for a wide range of thickness distributions and thickness ratios. In order to evaluate aileron characteristics from section data, a method of analysis is necessary that will lead to results comparable to the usual curves of stick force against helix angle pb/2V for three-dimensional data. The analysis that follows is considered suitable for comparing the relative merits of ailerons from two-dimensional data.

Two-dimensional data are presented in the form of the equivalent change in section angle of attack Δαο required to maintain a constant section lift coefficient for various deflections of the aileron from neutral. This equivalent change in angle of attack is plotted against the hinge-moment parameter Acus, which is the product of the alleron deflection from neutral and the resulting increment of hinge-moment coefficient based on the wing chord. This method of analysis takes into account the aileron effectiveness, the hinge moments, and the possible mechanical advantage between the controls and the ailerons. The larger the value of $\Delta \alpha_0$ for a given value of the hinge-moment parameter, the more advantageous the combination should be for providing a large value of pb/2V for a given control force. The assumption that the aileron operates at a constant lift coefficient as the airplane rolls is not entirely correct, however, and involves an over estimation of the effect of changing angle of attack on the hingemoment coefficient. In addition, the span of the ailerons and other possible three-dimensional effects are not considered. In spite of these inaccuracies, the method provides a useful means of comparing the two-dimensional characteristics of different ailerons.

For the purpose of evaluating the effect of airfoil shape on the aileron characteristics, it is desirable to make the comparison with unbalanced ailerons to avoid confusion. Plots of the parameters for plain unbalanced flaps of true airfoil contour on three airfoil sections are shown in figure 60. The characteristics of the NACA 66(215)-216, a = 0.6 section are essentially the same as those for the NACA 0009 airfoil within the range of deflection for which data are available. The NACA 64,2-(1.4)(13.5) airfoil shows appreciably smaller values of $\Delta c_{\rm H}\delta$ for a given value of $\Delta c_{\rm O}$ than the other sections presented. No explanation for this difference can be offered, although some of the difference may result from the slightly smaller chord of the flap for this combination.

The effects of using straight-sided ailerons instead of ailerons of true airfoil contour are shown in figure 61 for two NACA 6-series airfoils. One of the two combinations for which data are available was provided with an internal balance whereas the other combination was without balance. This difference prevents any comparison between the two combinations but does not affect comparison of the two contours for each case. For the NACA 66(215)-216, a = 0.6 airfoil, the straight-sided aileron has more desirable characteristics for the range of deflections for which data are available. It appears, however, that the straight-sided aileron would be less advantageous than the aileron of true contour for positive deflections greater than 12°. In the case of the NACA 63,4-4(17.8) airfoil, the straight-sided aileron appears

NACA ACR No. 15005

to have no advantage over the aileron of true airfoil contour. The advantage of using straight-sided ailerons appears to depend markedly on the airfoil used but sufficient data are not available to determine the significant airfoil parameters. Figure 62 shows that in one case the effect of leading-edge roughness on the aileron characteristics is unfavorable.

Leading-Edge Air Intakes

The problem of designing satisfactory leading-edge air intakes is to maintain the lift, drag, and critical-speed characteristics of the sections while providing low intake losses over a wide range of lift coefficients and intake velocity ratios. The data of reference 67 show that desirable intake and drag characteristics can easily be maintained over a rather small range of lift coefficients for NACA 6-series airfoils. The data of reference 67 show that the intake losses increase rapidly at moderately high lift coefficients for the shapes tested. Unpublished data taken at the Langley Laboratory indicate that shapes such as those of reference 67 have low maximum-lift coefficients. Recent data show that air-intake shapes can be provided for such airfoil sections with desirable air-intake characteristics and without loss in maximum lift coefficient (fig. 63). Some pressure-distribution data for the air intakes shown in figure 63 indicate that the critical speed of the section has been lowered only slightly and that falling pressures in the direction of flow were maintained for some distance from the leading edge on both surfaces at lift coefficients near the design lift coefficient for the section. Sufficient information is not available to permit such desirable configurations to be designed without experimental development.

Interference

The main problem of interference at low Mach numbers is considered to be that of avoiding boundary-layer separation resulting from rapid flow expansions caused by the addition of induced velocities about bodies and the boundary-layer accumulations near intersections. No recent systematic investigations of interference such as the investigation of reference 68 have been made.

Some tests have been made of airfoil sections with intersecting flat plates (reference 69). These configurations may be considered to represent approximately the condition of a wing intersection with a large flat-sided fuselage. In this case, the interference may be considered to result from the effect on the wing of the fully developed turbulent boundary layer on the fuselage or flat plate and

the accumulation of boundary layer in the intersection. These tests showed little interference except in cases for which the boundary layer on the airfoil alone was approaching conditions of separation such as were noted with the less conservative airfoils at moderately high lift coefficients.

Some scattered data on the characteristics of nacelles mounted on airfoils permitting extensive laminar flow are presented in references 70 to 72. The data appear to indicate that the interference problems for conservative NACA 6-series sections are similar to those encountered with other types of airfoil. The detail shapes for optimum interfering bodies and fillets may, however, be different for various sections if local excessive expansions in the flow are to be avoided.

Some lift and drag data for an airfoil with pusher-propeller-shaft housings are presented in reference 73. These results indicate that protuberances near the trailing edge of wings should be carefully designed to avoid unnecessary drag increments.

Another type of interference of particular importance for high-speed airplanes results in the reduction of the critical Mach number of the combination because of the addition of the induced velocities associated with each body (reference 74). This effect may be kept to a minimum by the use of bodies with low induced velocities, by separation of interfering bodies to the greatest possible extent, and by such selection and arrangement of combinations that the points of maximum induced velocity for each body do not coincide.

APPLICATION TO WING DESIGN

Detail consideration of the various factors affecting wing design lies outside the scope of this report. The following discussion is therefore limited to some important aerodynamic features that must be considered in the application of the data presented.

Application of Section Data

Wing characteristics are usually predicted from airfoilsection data by use of methods based on simple lifting-line theory (references 75 to 78). Application of such methods to wings of conventional plan form without spanwise discontinuities yields results of reasonable engineering accuracy (reference 79),

especially with regard to such important characteristics as the angle of zero lift, the lift-curve slope, the pitching moment, and the drag. Basically similar methods not requiring the assumption of linear section lift characteristics (references 80 and 81) appear capable of yielding results of greater accuracy, especially at high lift coefficients. Further refinement may be made by consideration of the chordwise distribution of lift (reference 82). Wings with large amounts of sweep require special consideration (reference 83).

The usual wing theory assumes that the resultant air force and moment on any wing section are functions of only the section lift coefficient (or angle of attack) and the section shape. According to this assumption, the air forces and moments on any section are not affected by adjacent sections or other features of the wing except as such sections or features affect the lift distribution and thus the local lift of the section under consideration. These assumptions obviously are not valid near wing tips, near discontinuities in deflected flaps or ailerons, near disturbing bodies, or for wings with pronounced sweep or sudden changes in plan form, section, or twist. Under such circumstances, cross flows result in a breakdown of the concept of two-dimensional flow over the airfoil sections. In addition to these cross flows. induced effects exist that are equivalent to a change in camber. Such effects are particularly marked near the wing tips for wings of normal plan form and for wings of low aspect ratio or unusual plan form. Lifting-surface theory (see, for example, reference 83) provides a means for calculating wing characteristics more accurately than the simple lifting-line theory.

Although span load distributions calculated for wings with discontinuities such as are found with partial-span flaps (references 84 and 85) may be sufficiently accurate for structural design, such distributions are not suitable for predicting maximumlift and stalling characteristics. Until sufficient data are obtained to permit the prediction of the maximum-lift and stalling characteristics of wings with discontinuities, these characteristics may best be estimated from previous results with similar wings or, in the case of unusual configurations, should be obtained by test.

The characteristics of intermediate wing sections must be known for the application of wing theory, but data for such sections are seldom available. Tests of a number of such intermediate sections obtained by several manufacturers for wings formed by straight-line fairing have indicated that the characteristics of such sections may be obtained with reasonable accuracy by interpolation of the root and tip characteristics according to the thickness variation.

Selection of Root Section

The characteristics of a wing are affected to a large extent by the root section. In the case of tapered wings formed by straight-line fairing, the resulting nonlinear variation of section along the span causes the shapes of the sections to be predominantly affected by the root section over a large part of the wing area. The desirability of having a thick wing that provides space for housing fuel and equipment and reduces structural weight or permits large spans usually leads to the selection of the thickest root section that is aerodynamically feasible. The comparatively small variation of minimum drag coefficient with thickness ratio for smooth airfoils in the normal range of thickness ratios and the maintenance of high lift coefficient for thick sections with flaps deflected usually result in limitation of thickness ratio by characteristics other than maximum lift and minimum drag.

The critical Mach number of the section is the most serious limitation of thickness ratio for high-speed airplanes. It is desirable to select a root section with a critical Mach number sufficiently high to avoid serious drag increases resulting from compressibility effects at the highest level-flight speed of the airplane, allowance being made for the increased velocity of flow over the wing resulting from interference of bodies and slipstream. Available data indicate that a small margin exists between the critical Mach number and the Mach number at which the drag increases sharply. As airplane speeds increase, it becomes increasingly difficult and finally impossible to avoid the drag increases resulting from compressibility effects by reduction of the airfoil thickness ratio.

In the cases of airplanes of such low speeds that compressibility considerations do not limit the thickness ratio to values less than about 0.20, the maximum thickness ratio is limited by excessive drag coefficients at moderate and high lift coefficients with the surfaces rough. In these cases, the actual surface conditions expected for the airplane should be considered in selecting the section. Consideration should also be given to unusual conditions such as ice, mud, and damage caused in military combat, especially in the case of multiengine airplanes for which . ability to fly under such conditions is desired with one or more engines inoperative. In cases for which root sections having large thickness ratios are under consideration to permit the use of high aspect ratios, a realistic appraisal of the drag coefficients of such sections with the expected surface conditions at moderately high lift coefficients will indicate an optimum aspect ratio beyond which corresponding increases in aspect ratio and root thickness ratio will result in reduced performance.

Inboard sections of wings on conventional airplanes are subject to interference effects and may be in the propeller slipstream. The wing surfaces are likely to be roughened by access doors, landing-gear retraction wells, and armament installations. Attainment of extensive laminar flows is, therefore, less likely on the inboard wing panels than on the outboard panels. Unless such effects are minimized, little drag reduction is to be expected from the use of sections permitting extensive laminar flow. Under these conditions, the use of sections such as the NACA 63-series will provide advantages if the sections are thick, because such sections are more conservative than those permitting more extensive laminar flow.

Selection of Tip Section

In order to promote desirable stalling characteristics, the tip section should have a high maximum lift coefficient and a large range of angle of attack between zero and maximum lift as compared with the root section. It is also desirable that the tip section stall without a large sudden loss in lift. The attainment of a high maximum lift coefficient is often more difficult at the tip section than at the root section for tapered wings because of the lower Reynolds number of the tip section. For wings with small camber, the most effective way of increasing the section maximum lift coefficient is to increase the camber. The amount of camber used will be limited in most cases by either the critical-speed requirements or by the requirement that the section have low drag at the high-speed lift coefficient.

The selection of the optimum type of camber for the tip section presents problems for which no catergorical answers can be given on the basis of existing data. The use of a type of camber that imposes heavy leads on the ailerons complicates the design of the lateral-control system and increases its weight. The use of a type of camber that carries the lift farther forward on the section and thus relieves the ailerons will, however, have little effect on the maximum lift coefficient of the section unless the maximum-camber position is well forward, as for the NACA 230-series sections. In this case a sudden loss of lift at the stall may be expected. The effects on the camber of modifications to the airfoil contour near the trailing edge, which may be made in designing the ailerons, should not be overlooked in estimating the characteristics of the wing.

If the root sections are at least moderately thick, it is usually desirable to select a tip section with a somewhat reduced thickness ratio. This reduction in thickness ratio, together with

the absence of induced velocities from interfering bodies, gives a margin in critical speed that permits the camber of the tip section to be increased. This reduction in thickness ratio will probably be limited by the loss in maximum lift coefficient resulting from too thin a section.

A small amount of aerodynamic washout may also be useful as an aid in the avoidance of tip stalling. The permissible amount of washout may not be limited by the increase in induced drag, which is small for 1° or 2° of washout (reference 75). The limiting washout may be that which causes the tip section to operate outside the low-drag range at the high-speed lift coefficient. This limitation may be so severe as to require some adjustment of the camber to permit the use of any washout.

A change in airfoil section between the root and tip may be desirable to obtain favorable stalling characteristics or to take advantage of the greater extent of laminar flow that may be possible on the outboard sections. Thus, such combinations as an NACA 230-series root section with an NACA 44-series tip section or an NACA 63-series root section with an NACA 65-series tip section may be desirable.

It should be noted that the tip sections may easily be so heavily loaded by the use of an unfavorable plan form as to cause tip stalling with any reasonable choice of section and washout. Both high taper ratios and large amounts of sweepback are unfavorable in this respect and are particularly bad when used together, because the resulting tip stall promotes longitudinal instability at the stall in addition to the usual lateral instability.

CONCLUSIONS

The following conclusions may be drawn from the data presented. Most of the data, particularly for the lift, drag, and pitching-moment characteristics, were obtained at Reynolds numbers from 3 to 9×10^{6} .

- 1. Airfoil sections permitting extensive laminar flow, such as the NACA 6- and 7-series sections, result in substantial reductions in drag at high-speed and cruising lift coefficients as compared with other sections if, and only if, the wing surfaces are fair and smooth.
- 2. Experience with full-size wings has shown that extensive laminar flows are obtainable if the surface finish is as smooth as

that provided by sanding in the chordwise direction with No. 320 carborundum paper and if the surface is free from small scattered defects and specks. Satisfactory results are usually obtained if the surface is sufficiently fair to permit a straightedge to be rocked smoothly in the chordwise direction without jarring or clicking.

- 3. For wings of moderate thickness ratios with surface conditions corresponding to those obtained with current construction methods, minimum drag coefficients of the order of 0.0080 may be expected. The values of the minimum drag coefficient for such wings depend primarily on the surface condition rather than on the airfoil section.
- 4. Substantial reductions in drag coefficient at high Reynolds numbers may be obtained by smoothing the wing surfaces, even if extensive laminar flow is not obtained.
- 5. The maximum lift coefficients for moderately cambered smooth NACA 6-series airfoils with the uniform-load type of mean line are as high as those for NACA 24- and 44-series airfoils. The NACA 230-series airfoils have somewhat higher maximum lift coefficients for thickness ratios less than 0.20.
- 6. The maximum lift coefficients of airfeils with flaps are about the same for moderately thick NACA 6-series sections as for the NACA 23012 section but appear to be considerably lower for thinner NACA 6-series sections.
- 7. The lift-curve slopes for smooth NACA 6-series airfoils are slightly higher than for NACA 24-, 44-, and 230 series airfoils and usually exceed the theoretical value for thin airfoils.
- 8. Leading-edge roughness causes large reductions in maximum lift coefficient for both plain airfoils and airfoils equipped with split flaps deflected 60°. The decrement in maximum lift coefficient resulting from standard roughness is essentially the same for the plain airfoils as for the airfoils equipped with the 60° split flaps.
- 9. The effect of leading-edge roughness is to decrease the lift-curve slope, particularly for the thicker sections having the position of minimum pressure far back.
- 10. Characteristics of airfoil sections with the expected surface conditions must be known or estimated to provide a satisfactory basis for the prediction of the characteristics of practical-construction wings and the selection of airfoils for such wings.

- 11. The NACA 6-series airfoils provide higher critical Mach numbers for high-speed and cruising lift coefficients than earlier types of sections and have a reasonable range of lift coefficients within which high critical Mach numbers may be obtained.
- 12. The NACA 6-series sections provide lower predicted critical Mach numbers at moderately high lift coefficients than the earlier types of sections. The limited data available suggest, however, that the NACA 6-series sections retain satisfactory lift characteristics up to higher Mach numbers than the earlier sections.
- 13. The NACA 6-series airfoils do not appear to present unusual problems with regard to the application of ailerons.
- 14. Problems associated with the avoidance of boundary-layer separation caused by interference are expected to be similar for conservative NACA 6-series sections and other good airfoils. Detail shapes for optimum interfering bodies and fillets may be different for various sections if local excessive expansions in the flow are to be avoided.
- 15. Satisfactory leading-edge air intakes may be provided for NACA 6-series sections, but insufficient information exists to allow such intakes to be designed without experimental development.

Langley Memorial Aeronautical Laboratory
National Advisory Committee for Aeronautics
Langley Field, Va.

APPENDIX

METHODS OF OBTAINING DATA IN THE LANGLEY

TWO-DIMENSIONAL LOW-TURBULENCE TUNNELS

By Milton M. Klein

Description of Tunnels

The Langley two-dimensional low-turbulence tunnels are closed-throat wind tunnels having rectangular test sections 3 feet wide and $7\frac{1}{2}$ feet high and are designed to test models completely spanning the width of the tunnel in two-dimensional flow. The low-turbulence level of these tunnels, amounting to only a few hundredths of 1 percent, is achieved by the large contraction ratio in the entrance cone (approx. 20:1) and by the introduction of a number of fine-wire small-mesh turbulence-reducing screens in the widest part of the entrance cone. The chord of models tested in these tunnels is usually about 2 feet, although the characteristics at low lift coefficients of models having chords as large as 8 feet may be determined.

The Langley two-dimensional low-turbulence tunnel operates at atmospheric pressure and has a maximum speed of approximately 155 miles per hour. The Langley two-dimensional low-turbulence pressure tunnel operates at pressures up to 10 atmospheres absolute and has a maximum speed of approximately 300 miles per hour at atmospheric pressure. Standard airfoil tests in this tunnel are made of 2-foot-chord wooden models up to Reynolds numbers of approximately 9 × 106 at a pressure of 4 atmospheres absolute.

The lift and drag characteristics of airfoils tested in these tunnels are usually measured by methods other than the use of balances. The lift is evaluated from measurements of the pressure reactions on the floor and ceiling of the tunnel. The drag is obtained from measurements of static and total pressures in the wake. Moments are usually measured by a balance.

Symbols

A₁, A₂,... A_n coefficients of potential function for a symmetrical body

fraction of chord from leading edge over which design load is uniform

В	dimensionless constant determining width of wake
С	chord
cd	drag coefficient corrected for tunnel-wall effects
cd'	drag coefficient uncorrected for tunnel-wall effects
cqL	drag coefficient measured in tunnel
cl	section lift coefficient corrected for tunnel-wall effects
c _l '	section lift coefficient uncorrected for tunnel-wall effects
cli	design lift coefficient
cll	lift coefficient measured in tunnel
c _{mc/4}	moment coefficient about quarter-chord point corrected for tunnel-wall effects
c _{mc/4}	moment coefficient about quarter-chord point measured in tunnel
F	average of velocity readings of orifices on floor and ceiling used to measure blocking at high lifts
F F _O	average of velocity readings of orifices on floor and ceiling used to measure blocking at high lifts average value of F in low-lift range
	ceiling used to measure blocking at high lifts
Fo	ceiling used to measure blocking at high lifts average value of F in low-lift range
F _O	ceiling used to measure blocking at high lifts average value of F in low-lift range potential function used to obtain n-factor
F _o f H _o	ceiling used to measure blocking at high lifts average value of F in low-lift range potential function used to obtain n-factor total pressure in front of airfoil total pressure in wake of airfoil coefficient of loss of total pressure in the
Fo f Ho	ceiling used to measure blocking at high lifts average value of F in low-lift range potential function used to obtain n-factor total pressure in front of airfoil total pressure in wake of airfoil
Fo f Ho	ceiling used to measure blocking at high lifts average value of F in low-lift range potential function used to obtain n-factor total pressure in front of airfoil total pressure in wake of airfoil coefficient of loss of total pressure in the
Fo f Ho Hl Hc	ceiling used to measure blocking at high lifts average value of F in low-lift range potential function used to obtain η -factor total pressure in front of airfoil total pressure in wake of airfoil coefficient of loss of total pressure in the wake $\left(\frac{H_0-H_1}{q_0}\right)$

L	true lift resulting from a point vortex
L ^t	lift associated with a point vortex as measured by integrating manometers
m	upstream limit of integration of floor and ceiling pressures
n	downstream limit of integration of floor and ceiling pressures
P_{R}	resultant pressure coefficient; difference between local upper- and lower-surface pressure coefficients
P ₁	static pressure in the wake
q _o	free-stream dynamic pressure
S	static-pressure coefficient $\left(\frac{H_0-p}{q_0}\right)$ static-pressure coefficient in the wake $\left(\frac{H_0-p_1}{q_0}\right)$
Sl	static-pressure coefficient in the wake $\left(\frac{H_0 - p_1}{q_0}\right)$
S	distance along airfoil surface
u	velocity, due to row of vortices, at any point along tunnel walls
V	free-stream velocity
Δ	increment in free-stream velocity due to blocking
A.	corrected indicated tunnel velocity
Λ ₁₁	tunnel velocity measured by static-pressure orifices
V	local velocity at any point on airfoil surface
W	potential function for flow past a symmetrical body
х	distance along chord or center line of tunnel
Y	variable of integration $\left(\frac{By}{c}\right)$
У	distance perpendicular to stream direction

Уt	ordinate of symmetrical thickness distribution
y_w	distance perpendicular to stream direction from position of H _{cmax}
dyt dx	slope of surface of symmetrical thickness distribution
Z	complex variable (x + iy)
ar _o	angle of zero lift
ao	section angle of attack corrected for tunnel-wall effects
ao t	section angle of attack measured in tunnel
Γ	strength of a single vortex
η	ratio of measured lift to actual lift for any type of lift distribution
ηα	η-factor for additional-type loading
ηЪ	η-factor for basic mean-line loading
$\eta_{\mathbf{x}}$	η-factor applying to a point vortex
Λ	component of blocking factor dependent on shape of body
Š	quantity used for correcting effect of body upon velocity measured by static-pressure orifices
σ	component of blocking factor dependent on size of body
Ø	potential function
Ψ	stream function

Measurement of Lift

The lift carried by the airfoil induces an equal and opposite reaction upon the floor and ceiling of the tunnel. The lift may therefore be obtained by integrating the pressure distribution along the floor and ceiling of the tunnel, the integration being accomplished with an integrating manometer. Because the pressure field theoretically extends to infinity in both the upstream and the

downstream directions, not all the lift is included in the length over which the integration is performed. It is therefore necessary to apply a correction factor η that gives the ratio of the measured lift to the actual lift for any lift distribution. The calculation was performed by first finding the correction factor $\eta_{\mathbf{x}}$ applying to a point vortex and then determining the weighted average of this factor over the chord of the model.

The factor $\eta_{\mathbf{x}}$ was obtained as follows: The image system which gives only a tangential component of velocity along the tunnel walls is made up of an infinite vertical row of vortices of alternating sign as shown in figure 64. If the sign of the vortex at the origin is assumed to be positive, the complex potential function f for this image system is

$$f = \frac{i\Gamma}{2\pi} \log \sinh \frac{\pi z}{2h_T} - \frac{i\Gamma}{2\pi} \log \sinh \pi \left(\frac{z - ih_T}{2h_T}\right)$$
 (18)

where

r strength of a single vortex

z complex variable (x +iy)

hm tunnel height

The velocity u, due to the row of vortices, at any point along the tunnel walls where

$$y = \frac{hT}{2}$$

is then obtained as

$$u = \frac{\Gamma}{2h_T} \operatorname{sech} \frac{\pi x}{h_T} \tag{19}$$

where x is the horizontal distance from the point on the wall to the origin. The resultant pressure coefficient PR is then given by

$$P_{R} = \frac{4u}{V}$$

$$= \frac{2\Gamma}{h_{\rm T}V} \operatorname{sech} \frac{\pi x}{h_{\rm T}} \tag{20}$$

where V is the free-stream velocity.

The lift manometers integrate the pressure distribution along the floor and ceiling from the downstream position n to the upstream position m (fig. 64). For a point vortex located a distance x from the origin along the center line of the tunnel, the limits of integration become n - x and m - x. The lift L' associated with a point vortex, as measured by the integrating manometers, is given by

$$L' = \int_{m-x}^{n-x} q_0 P_R dx \qquad (21)$$

where qo is the free-stream dynamic pressure.

The true lift L resulting from the point vortex is given by

 $L = \frac{2q_0 \Gamma}{V}$

The correction factor η_{X} is then

$$u^{\mathbf{X}} = \frac{\Gamma}{\Gamma_i}$$

$$= \frac{1}{h_T} \int_{m-x}^{n-x} \operatorname{sech} \frac{\pi x}{h_T} dx$$

which yields

$$\eta_{x} = \frac{2}{\pi} \tan^{-1} \left[\frac{e^{-\pi x/h_{T}} \left(e^{\pi n/h_{T}} - e^{\pi m/h_{T}} \right)}{1 + e^{-2\pi x/h_{T}} e^{\pi (m + n)/h_{T}}} \right]$$
(22)

In the Langley two-dimensional low-turbulence tunnels, the orifices in the floor and ceiling of the tunnel used to measure the lift extend over a length of approximately 13 feet. A plot of $\eta_{\mathbf{X}}$ against x for the Langley two-dimensional low-turbulence pressure tunnel is shown in figure 65. The η -factor for a given lift distribution is obtained from the expression

$$\eta = \frac{\int_{\text{chord}} P_{R} \eta_{x} d\left(\frac{x}{c}\right)}{\int_{\text{chord}} P_{R} d\left(\frac{x}{c}\right)}$$
(23)

The values of η_b and η_a for the Langley two-dimensional low-turbulence pressure tunnel are given in the following table for a model having a chord length of 2 feet, where η_b is the η -factor corresponding to the basic mean-line loading (indicated by the value of a) and η_a is the η -factor for the additional type of loading as given by thin-airfoil theory:

a	ηρ
1.0 .8 .6 .4 .2	0.9347 .9342 .9336 .9330 .9325 .9322

 $\eta_a = 0.9296$

In order to check the variation of η_a with variations in the additional type of lift distribution, the value of η_a was recalculated for the class C additional lift distribution given in figure 6 of reference 76. The value of η_a for this case was 0.9304, as compared with 0.9296 for a thin airfoil. Because of the small variation of η_a with the type of additional lift, the value for thin-airfoil additional lift was used for all calculations. The lift coefficient of the model in the tunnel uncorrected for blocking c_1 ' is given in terms of the lift coefficient measured in the tunnel c_{l_T} and the design lift coefficient of the airfoil c_l , by the following expression:

$$c_{l}' = \frac{c_{l_{T}}}{\eta_{a}} - \left(\frac{\eta_{b}}{\eta_{a}} - 1\right) c_{l_{1}}$$
 (24)

Because η_b does not differ much from η_a , it is not necessary that the basic loading or the design lift coefficient be known with great accuracy.

Because of tunnel-wall and other effects, the lift distribution over the airfoil in the tunnel does not agree exactly with the assumed lift distribution. Because of the small variations of η with lift distribution, errors caused by this effect are considered negligible. It can also be shown that errors caused by neglecting the effect of airfoil thickness on the distribution of the lift reaction along the tunnel walls are small.

NACA ACR No. 15005

Measurement of Drag

The drag of an airfoil may be obtained from observations of the pressures in the wake (reference 86). An approximation to the drag is given by the loss in total pressure of the air in the wake of the airfoil. The loss of total pressure is measured by a rake of total-pressure tubes in the wake. When the total pressures in front of the airfoil and in the wake are represented by Ho and Hi, respectively, the drag coefficient obtained from loss of total pressure cdm is

$$c_{d_{T}} = \int_{\text{wake}}^{\gamma} \frac{dy_{w}}{c}$$
 (25)

where

 H_c coefficient of loss of total pressure in the wake $\left(\frac{H_o - H_1}{q_o}\right)$

distance perpendicular to stream direction from position yw of H_{cmax}

If the static pressure in the wake is represented by p1, the true drag coefficient uncorrected for blocking cd' may be shown to be (reference 86)

$$c_{d}' = \int_{\text{wake}} 2\sqrt{s_1 - H_c} \left(1 - \sqrt{1 - H_c}\right) \frac{dy_w}{c}$$
 (26)

where S₁ is the static-pressure coefficient in the wake H₀ - P₁.

The assumption is made that the variation of total pressure across the wake can be represented by a normal probability curve. The drag coefficient cd' is then easily obtainable from measurements of cdr by means of a factor K, the ratio of cd to cdr,

which depends only on S_1 and the maximum value of H_c . If the maximum value of H_c is represented by $H_{c_{\max}}$, the equation of the normal probability curve is

$$H_{c} = H_{c_{max}} e^{-\left(\frac{By_{w}}{c}\right)^{2}}$$

where B is a dimensionless constant that determines the width of the wake. If a convenient variable of integration $Y = \frac{By_w}{c}$ is used, the ratio K is

$$K = \frac{c_{d}!}{c_{dT}}$$

$$= \frac{2}{\sqrt{\pi}} \frac{1}{H_{c_{max}}} \int_{-\infty}^{\infty} \sqrt{S_1 - H_c} (1 - \sqrt{1 - H_c}) dY \qquad (27)$$

and is independent of the width of the wake. The quantity K has been evaluated for various values of $H_{C_{\max}}$ and S_1 by assuming S_1 to be constant across the wake. The drag coefficient c_d may thus be obtained from tunnel measurements of c_{d_T} , $H_{C_{\max}}$, and S_1 . A plot of K as a function of $H_{C_{\max}}$ with S_1 as parameter is given in figure 66. A parallel treatment of this problem is given in reference 87.

Tunnel-Wall Corrections

In two-dimensional flow, the tunnel walls may be conveniently considered as having two distinct effects upon the flow over a model in a tunnel: (1) an increase in the free-stream velocity in the neighborhood of the model because of a constriction of the flow and (2) a distortion of the lift distribution from the induced curvature of the flow.

The increase in free-stream velocity caused by the tunnel walls (blocking effect) is obtained from consideration of an infinite vertical row of images of a symmetrical body as given in reference 88; the images represent the effect of the tunnel walls.

The potential function w for a symmetrical body is given by

$$W = Vz + \frac{A_1}{z} + \frac{A_2}{z^2} + \cdots + \frac{A_n}{z^n}$$
 (28)

where V is the free-stream velocity and the coefficients A₁, A₂, ... are complex. If the tunnel height is large compared

to the size of the body, powers of 1/z greater than 1 may be neglected and

$$W = Vz + \frac{A_1}{z} \tag{29}$$

This operation is equivalent to replacing the body by a circle of which the doublet strength is $2\pi A_1$; the term A_1/z represents the disturbance to the free-stream flow. The total induce velocity at the center of the body due to all the images is expressed in reference 88 as

$$\Delta V = \frac{A_1}{h_m^2} \frac{\pi^2}{3} \tag{30}$$

where the term A_1 is the same as the term $\frac{1}{4}\lambda t^2 V$ of reference 88 .

For convenience in tunnel calculations, the expression of ΔV may be written

$$\frac{\Delta V}{V} = \Lambda \sigma \tag{31}$$

where

$$\sigma = \frac{\pi^2}{48} \left(\frac{c}{h_T} \right)^2 \tag{32}$$

$$\Lambda = \frac{16A_1}{c^2V} \tag{33}$$

The factor σ depends only on the size of the body and is easily calculated. The factor Λ depends on the shape of the body and is more difficult to calculate. For bodies such as Rankine ovals and ellipses, simple formulas may be obtained for calculating Λ . In the general case, the value of Λ may be obtained from the velocity distribution over the body by the expression

$$\Lambda = \frac{16}{\pi} \int_0^1 \frac{y}{c} \frac{v}{v} \sqrt{1 + \left(\frac{dy_t}{dx}\right)^2} d\left(\frac{x}{c}\right)$$
(34)

where v is the velocity at any point on the airfoil surface and dy_t/dx is the slope of the airfoil surface at any point of which the ordinate is y_t .

In order to obtain this expression, consider the flow past a symmetrical body as shown in figure 67. The potential function for this flow is given by equation (28). Differentiating and multiplying equation (28) by z gives

$$z \frac{dw}{dz} = Vz - \frac{A_1}{z} - \frac{2A_2}{z^2} - \frac{-nA_n}{z^n}$$

The line integral about a closed curve $\int_C z \, \frac{dw}{dz} \, dz$ will depend only on the term $-A_1/z$ and, from the theory of residues, is given by

$$\int_{C} z \frac{dw}{dz} dz = -2\pi i A_{1}$$

but

$$z \frac{dw}{dz} dz = z dw$$

$$= (x + iy)(d\emptyset + i d\psi)$$

where \emptyset is the potential function and ψ is the stream function. On the surface of the body $d\psi=0$, so that

$$\int_{C} z \frac{dw}{dz} dz = \int_{C} x d\phi + i \int_{C} y d\phi$$
 (35)

Since the body is symmetrical, the term $x d\emptyset$ will have equal numerical values but opposite signs at corresponding points of the upper and lower surfaces, and $\int_C x d\emptyset$ will vanish. The term $y d\emptyset$ will have equal values at corresponding points of the upper and lower surfaces, and $\int_C y d\emptyset$ may be replaced by an integration over the upper surface; therefore,

$$\int_{C}^{z} \frac{dw}{dz} dz = 2i \int y d\phi \text{ (counterclockwise direction)}$$

or

$$A_1 = -\frac{1}{\pi} \int y \, d\phi$$

Reversing the path of integration, replacing dØ by v ds, replacing ds by $\sqrt{1+\frac{dy_t}{dx}}\frac{2}{dx}$, and solving for $\Lambda=\frac{16A_1}{c^2V}$ gives

$$\Lambda = \frac{1.6}{\pi} \int_{0}^{1} \frac{y}{c} \frac{v}{v} \sqrt{1 + \left(\frac{dy_{t}}{dx}\right)^{2}} d\left(\frac{x}{c}\right)$$

where the integration is taken from the leading edge to the trailing edge over the upper surface.

In addition to the error caused by blocking, an error exists in the measured tunnel velocity because of the interference effects of the model upon the velocity indicated by the static-pressure orifices located a few feet upstream of the model and halfway between floor and ceiling. In order to correct for this error an analysis was made of the velocity distribution along the streamline halfway between the upper and the lower tunnel walls for Rankine ovals of various sizes and thickness ratios. The analysis showed that the correction could be expressed, within the range of conventional-airfoil thickness ratios, as a product of a thickness factor given by the blocking factor Λ and a factor ξ which depended upon the size of the model and the distance from the static-pressure orifices to the midchord point of the model. The corrected indicated tunnel velocity V^{\bullet} could then be written

$$V^{\bullet} = V^{\bullet \bullet} (1 + \Lambda^{e}) \tag{36}$$

where V" is the velocity measured by the static-pressure orifices. In the Langley-two dimensional low-turbulence tunnels, the distance from the static-pressure orifices to the midchord point of the model is approximately 5.5 feet; the corresponding value of \(\xi \) for a 2-foot-chord model is approximately 0.002.

In order to calculate the effect of the tunnel walls upon the lift distribution, a comparison is made of the lift distribution of a given airfoil in a tunnel and in free air on the basis of

NACA ACR No. 15005

thin-airfoil theory. It is assumed that the flow conditions in the tunnel correspond most closely to those in free air when the additional lift in the tunnel and in free air are the same (reference 89). On this basis the following corrections are derived (reference 89), in which the primed quantities refer to the coefficients measured in the tunnel:

$$c_{\chi} = \left[1 - 2\Lambda(\sigma + \xi) - \sigma\right]c_{\chi}^{-1} \tag{37}$$

$$\alpha_{0} = (1 + \sigma)\alpha_{0}^{\dagger} + \frac{4\sigma c_{m_{0}}/4^{\dagger}}{dc_{1}^{\dagger}/d\alpha_{0}^{\dagger}} - \sigma\alpha_{0}$$
 (38)

$$c_{m_{c}/4} = \left[1 - 2\Lambda(\sigma + \tilde{s})\right] c_{m_{c}/4} + \sigma \frac{c_{l}}{4}$$
 (39)

In the foregoing equations, the terms $\frac{4\sigma c_{m_c/l_1}!}{dc_l!/dc_o!}$, c_l , and $\sigma c_l!/4$

are usually negligible for 2-foot-chord models in the Langley two-dimensional low-turbulence tunnels.

When the effect of the tunnel walls on the pressure distribution over the model is small, the wall effect on the drag is merely that corresponding to an increase in the tunnel speed. The correction to the drag coefficient is therefore given by the following relation:

$$c_{d} = \left[1 - 2\Lambda(\sigma + g)\right]c_{d}$$
 (40)

Similar considerations have been applied to the development of corrections for the pressure distribution in reference 89.

Equation (40) neglects the blocking due to the wake, such blocking being small at low to moderate drags. The effect of a pressure gradient in the tunnel upon loss of total pressure in the wake is not easily analyzed but is estimated to be small. The effect of the pressure gradient upon the drag has therefore been disregarded. When the drag is measured by a balance, the effect of the pressure gradient upon the drag is directly additive and a correction should be applied. For large models, especially at high lift coefficients, the effect of the tunnel walls is to distort the pressure distribution appreciably. Such distortions of the pressure distribution may cause large changes in the boundary flow and no adequate corrections to any of the coefficients, particularly the drag, can be found.

Correction for Blocking at High Lifts

So long as the flow follows the airfoil surface, the foregoing relations account for the effects of the tunnel walls with sufficient accuracy. When the flow leaves the surface, the blocking increases because of the predominant effect of the wake upon the free-stream velocity. Since the wake effect shows up primarily in the drag, the increase in blocking would logically be expressed in terms of the drag. The accurate measurement of drag under these conditions by means of a rake is impractical because of spanwise movements of lowenergy air. A method of correcting for increased blocking at high angles of attack without drag measurements has therefore been devised for use in the Langley two-dimensional low-turbulence tunnels.

Readings of the floor and ceiling velocities are taken a few inches ahead of the quarter-chord point and averaged to remove the effect of lift. This average F, which is a measure of the effective tunnel velocity, is essentially constant in the low-lift range. The quantity F/F_0 , where F_0 is the average value of F in the low-lift range, however, shows a variation from unity in the high-lift range for any airfoil tested in the tunnel; this variation indicates a change in blocking at high lifts. A plot of F/F_0 against angle of attack α_0 for a 2-foot-chord model of the NACA 643-418 airfoil is given in figure 68. The quantity F/F_0 is nearly constant for values of α_0 up to 12°; but for values of α_0 greater than 12°, F/F_0 increases and the increase is particularly noticeable at and over the stall.

A theoretical comparison was made of the blocking factor Λ σ , and the velocity measured by the floor and ceiling crifices for a series of Rankine ovals of various sizes and thickness ratios. The quarter-chord point of each oval was located at the pivot point, the usual position of an airfoil in the tunnel. The analysis showed the relation between the blocking factor $\Lambda\sigma$ and the change in F to be unique for chord lengths up to 50 inches in that different bodies having the same blocking factor $\Lambda\sigma$ gave approximately the same value of F. For chords up to 50 inches, the relationship is

$$\frac{\Delta V}{V} = 0.45 \left(\frac{F}{F_0} - 1 \right). \tag{41}$$

where $\Delta V/V$ is the true increment in tunnel velocity due to blocking. The foregoing relation was adopted to obtain the correction to the blocking in the range of lifts where $\frac{F}{F_O}>1$.

Considerable uncertainly exists regarding the correct numerical value of the coefficient occurring in equation (41). If a row of

NACA ACR No. 15005

sources, rahter than the Rankine ovals used in the present analysis, is considered to represent the effect of the wake, the value of the coefficient in equation (41) would be approximately twice the value used. Fortunately, the correction amounts to only about 2 percent at maximum lift for an extreme condition with a 2-foot-chord model. Further refinement of this correction has therefore not been attempted.

Comparison with Experiment

A check of the validity of the tunnel-wall corrections has been made in reference 89, which gives lift and moment curves for models having various ratios of chord to tunnel height, uncorrected and corrected for tunnel-wall effects. The general agreement of the corrected curves shows that the method of correcting the lifts and moments is valid.

A comparison is made in reference 89 between the theoretical correction factor (equation (40)) and the experimentally derived corrections of reference 90. The theoretical correction factors were found to be in good agreement with those obtained experimentally.

In order to check the validity of the η -factor, a comparison has been made of lift values obtained from pressure distributions with those obtained from the integration of the floor and ceiling pressures in the tunnel. A comparison for two airfoils given in figure 69 shows that the two methods of measuring lift give results that are in good agreement. The η -factor has also been checked by comparison of the lift obtained from balance measurements with the integrating-manometer values in figure 70.

Finally, a check has been made of the method of correcting pressure distributions (reference &9) for NACA 6-series airfoils of two chord lengths at zero angle of attack in figure 71, in which the pressure coefficients are plotted against chordwise position x/c. The agreement between the corrected pressure distributions for both models verifies the method of making the tunnel-wall corrections.

REFERENCES

- 1. Jacobs, Eastman N., Ward, Kenneth E., and Finkerton, Robert M.:
 The Characteristics of 78 Related Airfoil Sections from Tests
 in the Variable-Density Wind Tunnel. NACA Rep. No. 460, 1933.
- 2. Jacobs, Eastman N., and Pinkerton, Robert M.: Tests in the Variable-Dencity Wind Tunnel of Related Airfoils Having the Maximum Camber Unusually Far Forward. NACA Rep. No. 537, 1935.
- 3. Jacobs, Eastman N., Pinkerton, Robert M., and Greenberg, Harry:
 Tests of Related Forward-Camber Airfoils in the VariableDensity Wind Tunnel. NACA Rep. No. 610, 1937.
- 4. Stack, John, and von Doenhoff, Albert E.: Tests of 16 Related Airfoils at High Speeds. NACA Rep. No. 492, 1934.
- 5. Jacobs, Eastman N., and Sherman, Albert: Airfoil Section Characteristics as Affected by Variations of the Reynolds number. NACA Rep. No. 586, 1937.
- 6. Pinkerton, Robert M., and Greenberg, Harry: Aerodynamic Characteristics of a Large Number of Airfoils Tested in the Variable-Density Wind Tunnel. NACA Rep. No. 628, 1938.
- 7. Jones, B. Melvill: Flight Experiments on the Boundary Layer. Jour. Aero. Sci., vol. 5, no. 3, Jan. 1938, pp. 81-94.
- 8. Jacobs, Eastman N., and Abbott, Ira H.: Airfoil Section Data Obtained in the N.A.C.A. Variable-Density Tunnel as Affected by Support Interference and Other Corrections. NACA Rep. No. 669, 1939.
- 9. Theodorsen, Theodore: Theory of Wing Sections of Arbitrary Shape. NACA Rep. No. 411, 1931.
- 10. Stack, John: Tests of Airfoils Designed to Delay the Compressibility Burble. NACA TN No. 976, Dec. 1944. (Reprint of NACA ACR, June 1939.)
- 11. Jacobs, Eastman N.: Preliminary Report on Laminar-Flow Airfoils and New Methods Adopted for Airfoil and Boundary-Layer Investigations. NACA ACR, June 1939.

- 12. von Doenhoff, Albert E., and Stivers, Louis S., Jr.: Aerodynamic Characteristics of the NACA 747A315 and 747A415 Airfoils from Tests in the NACA Two-Dimensional Low-Turbulence Pressure Tunnel. NACA CB No. L4I25, 1944.
- 13. Naiman, Irven: Numerical Evaluation by Harmonic Analysis of the &-Function of the Theodorsen Arbitrary-Airfoil Potential Theory. NACA ARR No. L5H18, 1945.
- 14. Theodorsen, Theodore: Airfoil-Contour Modification Based on E-Curve Method of Calculating Pressure Distribution NACA ARR No. 14605, 1944.
- 15. Allen, H. Julian: A Simplified Method for the Calculation of Airfoil Pressure Distribution. NACA TN No. 708, 1939.
- 16. Munk, Max M.: Elements of the Wing Section Theory and the Wing Theory. NACA Rep. No. 191, 1924.
- 17. Glauert, H.: The Elements of Aerofoil and Airscrew Theory. Cambridge Univ. Press, 1926, pp. 87-93.
- 18. Theodorsen, Theodore: On the Theory of Wing Sections with Particular Reference to the Lift Distribution. NACA Rep. No. 383, 1931.
- 19. von Kármán, Th.: Compressibility Effects in Aerodynamics. Jour. Aero. Sci., vol. 8, no. 9, July 1941, pp. 337-356.
- 20. Heaslet, Max. A.: Critical Mach Numbers of Various Airfoil Sections. NACA ACR No. 4G18, 1944.
- 21. von Doenhoff, Albert E.: A Method of Rapidly Estimating the Position of the Laminar Separation Point. NACA TN No. 671, 1938.
- 22. Jacobs, E. N., and von Doenhoff, A. E.: Formulas for Use in Boundary-Layer Calculations on Low-Drag Wings. NACA ACR, Aug. 1941.
- 23. von Doenhoff, Albert E., and Tetervin, Neal: Determination of General Relations for the Behavior of Turbulent Boundary Layers. NACA ACR No. 3Gl3, 1943.
- 24. Squire, H. B., and Young, A. D.: The Calculation of the Profile Drag of Aerofoils. R. & M. No. 1838, British A.R.C., 1938.

- 25. Nitzberg, Gerald E.: A Concise Theoretical Method for Profile-Drag Calculation. NACA ACR No. 4B05, 1944.
- 26. Tetervin, Neal: A Method for the Rapid Estimation of Turbulent Boundary-Layer Thicknesses for Calculating Profile Drag.
 NACA ACR No. L4G14, 1944.
- 27. Quinn, John H., Jr., and Tucker, Warren A.: Scale and Turbulence Effects on the Lift and Drag Characteristics of the NACA 653-418, a = 1.0 Airfoil Section. NACA ACR No. L4Hll, 1944.
- 28. Tucker, Warren A., and Wallace, Arthur R.: Scale-Effect Tests in a Turbulent Tunnel of the NACA 65,-418, a = 1.0 Airfoil Section with 0.20-Airfoil-Chord Split Flap. NACA ACR No. 14122, 1944.
- 29. Davidson, Milton, and Turner, Harold R., Jr.: Effects of Mean-Line Loading on the Aerodynamic Characteristics of Some Low-Drag Airfoils. NACA ACR No. 3127, 1943.
- 30. von Doenhoff, Albert E., and Tetervin, Neal: Investigation of the Variation of Lift Coefficient with Reynolds Number at a Moderate Angle of Attack on a Low-Drag Airfoil.

 NACA CB, Nov. 1942.
- 31. Oswald, W. Bailey: General Formulas and Charts for the Calculation of Airplane Performance. NACA Rep. No. 408, 1932.
- 32. Millikan, Clark B.: Aerodynamics of the Airplane. John Wiley & Sons, 1941, pp. 108-109.
- 33. Hood, Manley J.: The Effects of Some Common Surface Irregularities on Wing Drag. NACA TN No. 695, 1939.
- 34. Loftin, Laurence K., Jr.: Effects of Specific Types of Surface Roughness on Boundary-Layer Transition. NACA ACR No. L5J29a, 1946.
- 35. Charters, Alex C.: Transition between Laminar and Turbulent Flow by Transverse Contamination. NACA TN No. 891, 1943.
- 36. Braslow, Albert L.: Investigation of Effects of Various Camouflage Paints and Painting Procedures on the Drag Characteristics of an NACA 65(421)-420, a = 1.0 Airfoil Section. NACA CB No. L4G17, 1944.

- 37. Allen, H. Julian: Notes on the Effect of Surface Distortions on the Drag and Critical Mach Number of Airfoils.
 NACA ACR No. 3129, 1943.
- 38. Abbott, Frank T., Jr., and Turner, Harold R., Jr.: The Effects of Roughness at High Reynolds Numbers on the Lift and Drag Characteristics of Three Thick Airfoils. NACA ACR No. L4H21, 1944.
- 39. Jacobs, Eastman N., Abbott, Ira H., and Davidson, Milton:
 Investigation of Extreme Leading-Edge Roughness on Thick
 Low-Drag Airfoils to Indicate Those Critical to Separation.
 NACA CB. June 1942.
- 40. Zalovcik, John A.: Profile-Drag Coefficients of Conventional and Low-Drag Airfoils as Obtained in Flight. NACA ACR No. L4E31, 1944.
- 41. Zalovcik, John A., and Wood, Clotaire: A Flight Investigation of the Effect of Surface Roughness on Wing Profile Drag with Transition Fixed. NACA ARR No. L4125, 1944.
- 42. Hood, Manley J., and Geydos, M. Edward: Effects of Propellers and of Vibration on the Extent of Laminar Flow in the N.A.C.A. 27-212 Airfoil. NACA ACR, Oct. 1939.
- 43. Silverstein, Abe, Katsoff, S., and Hootman, James A.: Comparative Flight and Full-Scale Wind-Tunnel Measurements of the Maximum Lift of an Airplane. NACA Rep. No. 618, 1938.
- 44. Sweberg, Harold, H., and Dingeldein, Richard C.: Summary of Measurements in the Langley-Full-Scale Tunnel of Maximum Lift Coefficients and Stalling Characteristics of Airplanes. NACA ACR L5C24, 1945.
- 45. Purser, Paul E., and Johnson, Harold S.: Effects of Trailing-Edge Modifications on Pitching-Moment Characteristics of Airfoils. NACA CB No. L4I30, 1944.
- 46. Fullmer, Felicien F., Jr.: Wind-Tunnel Investigation of NACA 66(215)-216, 66,1-212, and 65,-212 Airfoils with 0.20-Airfoil-Chord Split Flaps. NACA CB No. L4G10, 1944.
- 47. Abbott, Ira H., and Greenberg, Harry: Tests in the Variable-Density Wind Tunnel of the N.A.C.A. 23012 Airfoil with Plain and Split Flaps. NACA Rep. No. 661, 1939.

- 48. Wenzinger, Carl J., and Harris, Thomas A.: Wind-Tunnel Investigation of NACA 23012, 23021, and 23030 Airfoils with Various Sizes of Split Flap. NACA Rep. No. 668, 1939.
- 49. Bogdonoff, Seymour M.: Wind-Tunnel Investigation of a Low-Drag Airfoil Section with a Double Slotted Flap. NACA ACR No. 3I20, 1943.
- 50. Wenzinger, Carl J., and Harris, Thomas A.: Wind-Tunnel Investigation of an N.A.C.A. 23012 Airfoil with Various Arrangements of Slotted Flaps. NACA Rep. No. 664, 1939.
- 51. Wenzinger, Carl J., and Harris, Thomas A.: Wind-Tunnel Investigation of an N.A.C.A. 23021 Airfoil with Various Arrangements of Slotted Flaps. NACA Rep. No. 677, 1939.
- 52. Swanson, Robert S., and Crandall, Stewart M.: Analysis of Available Data on the Effectiveness of Ailerons without Exposed Overhang Balance. NACA ACR No. 14E01, 1944.
- 53. Street, William B., and Ames, Milton B., Jr.: Pressure-Distribution Investigation of an N.A.C.A. 0009 Airfoil with a 50-percent-Chord Plain Flap and Three Tabs. NACA TN No. 734, 1939.
- 54. Ames, Milton B., Jr., and Sears, Richard I.: Pressure-Distribution Investigation of an NACA 0009 Airfoil with an 80-Percent-Chord Plain Flap and Three Tabs. NACA TN No. 761, 1940.
- 55. Ames, Milton B., Jr., and Sears, Richard I.: Pressure-Distribution Investigation of an NACA 0009 Airfoil with a 30-Fercent-Chord Plain Flap and Three T.bs. NACA TN No. 759, 1940.
- 56. Sears, Richard I.: Wind-Tunnel Investigation of Control-Surface Characteristics. I Effect of Gap on the Aerodynamic Characteristics of an NACA 000 9 Airfoil with a 30-Percent-Chord Plain Flap. NACA ARR, June 1941.
- 57. Jones, Robert T., and Ames, Milton B., Jr.: Wind-Tunnel Investigation of Control-Surface Characteristics. V The Use of a Beveled Trailing Edge to Reduce the Hinge Moment of a Control Surface. NACA ARR, March 1942.
- 58. Sears, Richard I., and Liddell, Robert B.: Wind-Tunnel Investigation of Control-Surface Characteristics. VI A 30-Percent-Chord Plain Flap on the NACA 0015 Airfoil. NACA ARR, June 1942.

- 59. Wenzinger, Carl J., and Delano, James B.: Pressure Distribution over an N.A.C.A. 23012 Airfoil with a Slotted and a Plain Flap. NACA Rep. No. 633, 1938.
- 60. Gillis, Clarence L., and Lockwood, Vernard E.: Wind-Tunnel Investigation of Control-Surface Characteristics.

 XIII Various Flap Overhangs Used with a 30-Percent-Chord Flap on an NACA 66-009 Airfoil. NACA ACR No. 3G20, 1943.
- 61. Rogallo, F.M.: Collection of Balanced-Aileron Test Data.
 NACA ACR No. 4All, 1944.
- 62. Denaci, H.G., and Bird, J.D.: Wind-Tunnel Tests of Ailerons at Various Speeds. II Ailerons of 0.20 Airfoil Chord and True Contour with 0.60 Aileron-Chord Sealed Internal Balance on the NACA 66,2-216 Airfoil. NACA ACR No. 3F18, 1943.
- 63. Purser, Paul E., and Riebe, John M.: Wind-Tunnel Investigation of Control-Surface Characteristics. XV Various Contour Modifications of a 0.30-Airfoil-Chord Plain Flap on an NACA 66(215)-014 Airfoil. NACA CR No. 3L20, 1943.
- 64. Braslow, Albert L.: Wind-Tunnel Investigation of Aileron Effectiveness of 0.20-Airfoil-Chord Plain Ailerons of True Airfoil Contour on NACA 652-415, 653-418, and 654-421 Airfoil Sections. NACA CB No. 14H12, 1944.
- 65. Sears, Richard I., and Purser, Paul E.: Wind-Tunnel Investigation of Control-Surface Characteristics. XIV NACA 0009 Airfoil with a 20-Percent-Chord Double Plain Flap. NACA ARR No. 3F29, 1943.
- 66. Crane, Robert M., and Holtzclaw, Ralph W.: Wind-Tunnel Investigation of Ailerons on a Low-Drag Airfoil. I The Effect of Aileron Profile. NACA ACR No. 4A14, 1944.
- 67. von Doenhoff, Albert E., and Horton, Elmer A.: Preliminary
 Investigation in the NACA Low-Turbulence Tunnel of Low-DragAirfoil Sections Suitable for Admitting Air at the Leading
 Edge. NACA ACR, July 1942.
- 68. Jacobs, Eastman N., and Ward, Kenneth E.: Interference of Wing and Fuselage from Tests of 209 Combinations in the N.A.C.A. Variable-Density Tunnel. NACA Rep. No. 540, 1935.
- 69. Abbott, Ira H.: Interference Effects of Longitudinal Flat Plates on Low-Drag Airfoils. NACA CB, Nov. 1942.

- 70. Ellis, Macon C., Jr.: Some Lift and Drag Measurements of a Representative Bomber Nacelle on a Low-Drag Wing II.

 NACA CB, Sept. 1942.
- 71. Ellis, Macon C., Jr.: Effects of a Typical Nacelle on the Characteristics of a Thick Low-Drag Airfoil Critically Affected by Leading-Edge Roughness. NACA CB No. 3D27, 1943.
- 72. Allen, H. Julian, and Frick, Charles W., Jr.: Experimental Investigation of a New Type of Low-Drag Wing-Nacelle Combination. NACA ACR, July 1942.
- 73. Abbott, Frank T., Jr.: Lift and Drag Data for 30 Pusher-Propeller Shaft Housings on an NACA 65,3-018 Airfoil Section. NACA ACR No. 3Kl3, 1943.
- 74. Robinson, Russell G., and Wright, Ray H.: Estimation of Critical Speeds of Airfoils and Streamline Bodies. NACA ACR, March 1940.
- 75. Anderson, Raymond F.: Determination of the Characteristics of Tapered Wings. NACA Rep. No. 572, 1936.
- 76. Jacobs, Eastman N., and Rhode, R. V.: Airfoil Section Characteristics as Applied to the Prediction of Air Forces and Their Distribution on Wings. NACA Rep. No. 631, 1938.
- 77. Soule, H. A., and Anderson, R. F.: Design Charts Relating to the Stalling of Tapered Wings. NACA Rep. No. 703, 1940.
- 78. Harmon, Sidney M.: Additional Design Charts Relating to the Stalling of Tapered Wings. NACA ARR, Jan. 1943.
- 79. Anderson, Raymond F.: The Experimental and Calculated Characteristics of 22 Tapered Wings. NACA Rep. No. 627, 1938.
- 80. Tani, Itiro: A Simple Method of Calculating the Induced Velocity of a Monoplane Wing. Rep. No. 111 (Vol. IX,3), Aero. Res. Inst., Tokyo Imperial Univ., Aug. 1934.
- 81. Sherman, Albert: A Simple Method of Obtaining Span Load Distributions. NACA TN No. 732, 1939.
- 82. Jones, Robert T.: Correction of the Lifting-Line Theory for the Effect of the Chord. NACA TN No. 817, 1941.
- 83. Cohen, Doris: Theoretical Distribution of Load over a Swept-Back Wing. NACA ARR, Oct. 1942.

- 84. Pearson, H. A.: Span Load Distribution for Tapered Wings with Partial-Span Flaps. NACA Rep. No. 585, 1937.
- 85. Pearson, Henry A., and Anderson, Raymond F.: Calculation of the Aerodynamic Characteristics of Tapered Wings with Partial-Span Flaps. NACA Rep. No. 665, 1939.
- 86. The Cambridge University Aeronautics Laboratory: The Measurement of Profile Drag by the Pitot-Traverse Method. R. & M. No. 1688, British A.R.C., 1936.
- 87. Silverstein, A., and Katzoff, S.: A Simplified Method for Determining Wing Frofile Drag in Flight. Jour. Aero. Sci., vol. 7, no. 7, May 1940, pp. 295-301.
- 88. Glauert, H.: Wind Tunnel Interference on Wings, Bodies and Airscrews. R. & M. No. 1566, British A.R.C., 1933.
- 89. Allen, H. Julian, and Vincenti, Walter G.: Wall Interference in a Two-Dimensional-Flow Wind Tunnel with Consideration of the Effect of Compressibility. NACA ARR No. 4K03, 1944.
- 90. Fage, A.: On the Two-Dimensional Flow past a Body of Symmetrical Cross-Section Mounted in a Channel of Finite Breadth. R. & M. No. 1223, British A.R.C., 1929.

TABLE I
ANALYSIS OF AIRFOIL DERIVATION

Airfoil designation	Basic		Mean-line combination1													
designation	thickness form	a = 0	a = 0.1	a = 0.2	a = 0.3	a = 0.4	a = 0.5	a = 0.6	a = 0.7	a = 0.8	a = 0.9	a = 1.0				
747A315	747A015					0.763			-0.463							
747A415	747A015					0.763			-0.463			0.100				
						-										
						1.						-				
											v					

The numbers in the various columns headed "Mean-line combination" indicate the magnitude of the design lift coefficient used.

NATIONAL ADVISORY COMMITTEE FOR AERONAUTICS

TABLE II

MAXIMUM LIFT AND STALLING CHARACTERISTICS OF MODELS TESTED IN THE NACA 19-FOOT PRESSURE TUNNEL

Model	Configur	ation	Geometric	Fl	ap	Fla ang (de	le	(per	ap ord cent			R	CLmax	Stalling characteristics
MOGGI	Plan view	Front view	characteristics	Inboard	Outboard	501	δfo	cfi	cfo	bfi	bfo		max	
•				None	None			None	None	None	None	2.6 × 10 ⁶ 3.6 4.6	1.26 1.36 1.41	
				Split		6.		10		53		2.6 3.6 4.6	1.72 1.78 1.84	
			Sections: Root: NACA 66(215)-216					20				2.6 3.6 4.6	1.94 1.98 2.07	Abrupt stall progresses from root toward tip for flaps
, I			Tip: NACA 66(215)-216 A = 7.00 \(\) = 1.00 Geometric washout, 0.00		+		+	30	†		1	2.6 3.6 4.6	1.97 2.03 2.06	neutral and partial-span flaps deflected; no data for full- span flaps
			Geometric washout, 0.0		Split		60	10	10		37	2.6 3.6 4.6	2.04 2.11 2.15	
						20	20			2.6 3.6 4.6	2.40 2.50 2.51			
		1	+	1	+	30	30	1	'	2.6 3.6 4.6	2.43 2.49 2.52			
				Fowler	Fowler	0	0	30	30	53	37	2.1 × 10 ⁶ 2.8 3.3	1.15 1.29 1.27	
II			Sections: Root: NACA 66(215)-116 Tip: NACA 66(215)-216 A = 7.0 \(\lambda = 0.5\)			30						2.1 2.9 3.4	2.29	With flaps neutral, satisfactory; with flaps deflected, extremely abrupt stall envelopes entire
			λ = 0.5 Geometric washout, 1.5°			35	+					2.1 2.9 3.4	2.36 2.49 2.54	wing
		*		1	+	30	30	1	+	1	•	2.1 2.9 3.4	3.13 3.31 3.29	
III			Sections: Root: NACA 65(318)-019 Tip: NACA 65(318)-015 A = 7.36 \(\lambda = 0.25\) Geometric washout, 3.60	MOIN	None							3.0 × 10 ⁶ 5.1 7.4	1.18 1.37 1.43	Abrupt stall with satisfactory progression toward tips
Iv			Sections: Root: NACA 65(318)-015 T1p: NACA 65(318)-015 A = 7.36 A = 0.25 Geometric washout, 4.06 Sweepback of 0.25 chord line, 21.930	None	None							3.3 × 10 ⁶ 5.6 7.2	1.17 1.31 1.34	Unsatisfactory stall; a strong outflow resulted in severe tip stall

NATIONAL ADVISORY
COMMITTEE FOR AERONAUTICS

TABLE II - Continued

MAXIMUM LIFT AND STALLING CHARACTERISTICS OF MODELS - Continued

Model	Configu	ration	Geometric	Fl	ap	81	lap ngle deg)	c]	lap hord rcent c)	3)	lap pan rcent b)			
	Plan view	Front view	characteristics	Inboard	Outboard	δfi	δfi δfo c				-	R	CLmax	Stalling characteristics
v			Sections: Root: NACA 66(215)-(1.8)(15.5), a = 0.6 Tip: NACA 66(215)-(1.8)12. a = 0.6 A = 5.82 $\lambda = 0.46$ Geometric washout, 2.5°	Plain	None	0		25		60		3.2 × 10 ⁶ 7.8 3.3 5.8 7.0	1.40 1.52 1.55 2.10 2.19 2.21 2.23	Abrupt stall with satis- factory progression toward tips
VI		-0	Sections: Root: NACA 66(215)-(1.8)(15.5), a = 0.6 Tip: NACA 66(215)-(1.8)12, a = 0.6 A = 5.82 \(\lambda = 0.46 \) Geometric washout, 2.5°	Plain	None	50		25		60		3.3 × 10 ⁶ 5.3 6.0 3.3 5.1 5.8	1.34 1.39 1.39 1.87 1.91	Abrupt stall with satis- factory progression toward tips
VII			Sections: Root: Mod. NACA 65,3-318,	Double slotted	Double slotted	0 55	0 30	25	25	50	48	5.1 × 10 ⁶	1.33	Satisfactory
AIII			Sections: Root: NACA 67(115)-116 Tip: NACA 67,1-115 A = 6.7 \(\) = 0.\(\) Geometric washout, 2.0°	Zap J Split	Zap 	0 48 60 †	48	35	35 20 	60	38 1 38	2.4 × 10 ⁶ 2.4 2.5 2.5	1.32 2.25 2.77 1.91 2.22	No data

NACA

ACR

No.

L5C05

TABLE II - Continued

MAXIMUM LIFT AND STALLING CHARACTERISTICS OF MCDELS - Continued

Model	Configu	ration	Geometric characteristics	Flag	,	Flap angle (deg)		Flap chord (percent c)		ent (per		R	CLmax	Stalling characteristics	
	Plan view	Front view	Characteristics	Inboard	Outboard	δfi	δfo	c _f i	c _{fo}	bfi	bfo		-max		
IX			Root: NACA 64(215)-418 Tip: NACA 66,2x-415 A = 8.92 \$\text{\$\text{\$\delta}\$} = 0.33\$ Geometric washout, 1.00	None Split	None	 55		20		60		3.5 × 10 ⁶ 3.6	1.38	Satisfactory	
x		-000	Sections: Root: NACA 64(215)-418 Tip: NACA 66,2x-415 A = 8.92 \(\) = 0.33 Geometric washout, 1.00	None Split	None Split	55	55	20	20	60	30	3.5 × 10 ⁶ 3.6 3.5	1.42 1.87 2.11	Satisfactory	
XI		•0•	Sections: Root: NACA 64(215)-418 Tip: NACA 66,2x-415 A = 8.92 \(= 0.33 \) Geometric washout, 1.00	None Split	None	55		20		60	1112 2123 3133 3133 3133 3133 3133 3133	4.0 × 10 ⁶	1.47	Satisfactory	
	٨		Sections: Root: NACA 63(420)-418,	Extensible slotted	None	0		25		70		3.1 × 10 ⁶ 4.1 4.8	1.37 1.42 1.45		
XII		HOM	a = 1.0 Tip: NACA 652-415, a = 1.0	-		35						3.1 4.9	a2.19 a2.20 a2.21	Satisfactory	
	V		$\lambda = 0.50$ Geometrie washout, 2.8°	Split	+	60		+		+		3.1 4.1 4.8	2.00 2.06 2.06		
			/	None	None							2.h × 10 ⁶ 5.3	1.21 1.37 1.45		
				Split		60		20		65		2.4	1.76 1.89 1.96		
XIII		-0	Sections: Root: NACA 66(215)-016 Tip: NACA 66(215)-016 A = 5.34	Extensible trailing edge	,	45	+					2.5 3.7 5.2	1.72 1.86 1.98	Satisfactory	
	V		$\lambda = 0.68$ Geometric washout, 0.0°	+	Split	4	60		20		30	2.4	1.99 2.03 2.13		
				Split	+	60	*	+	+	+	+	2.4	2.01 2.15 2.21		

apropellers windmilling.

NATIONAL ADVISORY COMMITTEE FOR AERONAUTICS.

TABLE II - Continued

MAXIMUM LIFT AND STALLING CHARACTERISTICS OF MODELS - Continued

							-							
Model	Configur	ration	Geometric	Flag)	a	lap ngle neg)	(per	lap nord cent	(perc	ap ent	R	C	
	Plan view	Front view	characteristics	Inboard	Outboard	δfi	500			bfi		A	CLmax	Stalling characteristics
				Extensible slotted	None	0		20		60		3.6 × 10 ⁶ 5.1 6.1	1.32 1.42 1.46	>
XIV		0	Sections: Root: NACA 65(318)-1(18.5) Tip: NACA 66(215)-216 A = 5.52	+		35						3.6 5.2 6.3	2.27 2.34 2.37	Abmit at 22 at the at 10
	V		A = 5.52 $A = 0.48$ Geometric washout, 3.0°	Slotted		50						3.5 4.9 5.9	2.04 2.13 2.16	Abrupt stall with satisfactory pro- gression toward tips
				Split	+	50		+		+		3.5 4.8 5.9	2.02 2.12 2.17	
xv		0	Sections: Root: NACA 23015.6 Tip: NACA 23009	Slotted	None	0		20		60		3.4 × 10 ⁶ 4.8 5.6	1.55 1.58 1.60	Wery abrupt stall, left wing stalling
			A = 5.5 $A = 0.52$ Geometric washout, 0.0°	'	+	50		+		+		3.4 4.8 5.6	2.46 2.50 2.52	very rapidly, for all conditions
	A		Sections: Root: NACA 66,2-118	Extensible	None	0		24		50		3.0 × 10 ⁶ 4.1 5.0	1.34	Extremely abrupt stall, left wing
XVI		0	Tip: NACA $66(2x15)-116$ A = 6.9 Geometric washout, 2.0°	\$ Split		38						2.9	2.01 2.15 2.21 52.29 51.98	stalls first for the extensible slotted flap, satisfactory for split flap
XVII		0	Sections: Root: NACA 65(216)-215, a = 0.8 Tip: NACA 65(216)-215, a = 0.5 A = 9.08 \$\lambda = 0.45\$ Geometric washout, 1.00 0.2 ohord line straight	Double slotted	Double slotted	0 55	0 1	25	25	65	31	3.6 × 10 ⁶ 3.1 2.8	1.38 2.45 2.69	Satisfactory
XVIII		-0	Sections: Root: NAGA 65(216)-215, a = 0.8 Tip: NAGA 65(216)-215, A = 9.08 A = 0.15 Geometrio washout, 1.0° -0.10 ohord line straight	Double slotted	Double slotted	0 55	0 1	25	25	65	31	3.6 × 10 ⁶ 3.1 2.8	1.37 2.44 2.76	Satisfactory
XIX		0	Sections: Root: NACA 65(216)-215, a = 0.8 Tip: NACA 65(216)-215, a = 0.5 \[\lambda = 0.5 \] \[\lambda = 0.45 \]	Double slotted	Double	0 55	0 1	25	25	65	31	3.6 × 106 3.1 2.8	1.45 2.57 2.86	Unsatisfactory, severe tip stall for all conditions except full- span flap

b Pillets removed.

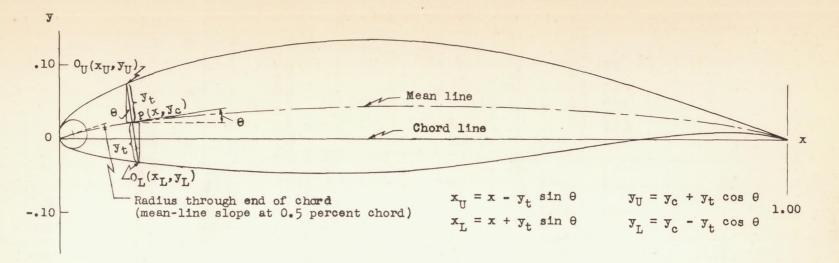
NATIONAL ADVISORY COMMITTEE FOR AERONAUTICS.

TABLE II - Concluded

MAXIMUM LIFT AND STALLING CHARACTERISTICS OF MODELS - Concluded

				- 4				FI	ap	Fl	ap			
Model	Configu	ration	Geometric characteristics	F	lap	an	ap igle leg)	ch	cent	(per	cent	R	CImax	Stalling characteristics
MOGGE	Plan view	Front view	characteristics	Inboard	Outboard	5fi	δfo	cf1	°f _o	bfi	bfo			
xx	-AAA	000	Sections: Root: NACA 65(216)-215,	Double slotted	Double slotted	0 55	o ↓	25	25	65	31	5.5 × 10 ⁶ 5.5 5.5	1.45 2.37 2.65	Satisfactory
XXI			Root: MACA 66,2-118 T1p: NACA 66(2x15)-116 A = 6.25 A = 0.35 Geometrie washout, 2.50 0.375 ohord line straight	None	None	45		20		50		2.9 × 10 ⁶ 4.0 4.9 3.0 4.0 4.9	1.23 1.43 1.51 1.80 1.85 1.96	Satisfactory
	V		o.yij shord The stranger		Split	60	60		20	-	40	3.0 4.3 5.1 5.2	1.90 2.01 2.04 2.43	
XXII		-	Sections: Root: NACA 66,2-118 Tip: NACA 66(2x15)-116 A = 6.25 \(\lambda = 0.35\) Geometric washout, 2.5° 0.375 chord line straight	None Split	None	45		20		50		4.1 × 10 ⁶ 4.9	1.50 1.60 2.02	Satisfactory
xxIII			Sections: Root: NACA 66,2-118 Tip: NACA 66(2x15)-116 A = 6.25 A = 0.35 Geometrie washout, 2.50 0.375 chord line swept forward 3.50	None Split	None	45		20		50		2.9 × 10 ⁶ 4.1 4.9 2.9 4.1 5.0	1.38 1.57 1.61 1.83 1.99 2.02	Satisfactory
XXIV			Sections: Root: NAOA 66,2-118 Tip: NAOA 66(2x15)-116 A = 6.1 A = 0.17 Geometric washout, 2.5° 0.375 chord line straight	None	Hone	45		20		50		2.9 × 10 ⁶ 4.2 5.0 3.0 4.2 5.1	1.34 1.56 1.63 1.85 1.92 2.01	Satisfactory
xxv		b & d o	Sections: Root: NACA 65(223)-221, a = 1.0 Tip: MACA 66(215)-316, a = 0.6 A = 12.8 \[\lambda = 0.33 \] Geometric washout, 0.0°	Fowler	None	40		18		53		1.5 × 10 ⁶ 2.2 2.8 1.4 1.9 2.7	1.17 1.27 1.37 2.21 2.23 2.30	Poor, initial stall occurs at tips

NATIONAL ADVISORY COMMITTEE FOR AERONAUTICS.



			SAMI			FOR DER	IVATION (a = 1.0)	OF THE			
x	y _t (a)	у _с (b)	tanθ	sin0	cosθ	y _t sin0	ytcosθ	x _U	yU	xL	y_L
0 .005 .05 .25 .50 .75	0 .0132l ₄ .03831 .08093 .08593 .04456	0 .00200 .01264 .03580 .04412 .03580	.18744	0.31932 .18422 .06979 0	.98288 .99756	.00565	0 .01255 .03765 .08073 .08593 .04445	0 .00077 .04294 .24435 .50000 .75311 1.00000	0 .01455 .05029 .11653 .13005 .08025	.25565	0 01055 02501 04493 04181 00865

^aThickness distribution obtained from ordinates of the NACA 65,3-018 airfoil. b Ordinates of the mean line, 0.8 of the ordinate for $c_{l_1} = 1.0$.

cSlope of radius through end of chord.

NATIONAL ADVISORY
COMMITTEE FOR AERONAUTICS

Figure 1.- Method of combining mean lines and basic thickness forms.

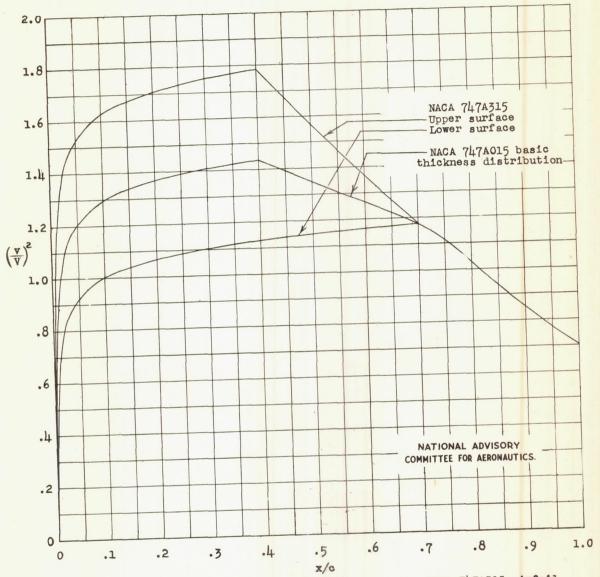


Figure 2.- Theoretical pressure distribution for the NACA 747A315 airfoil section at the design lift coefficient and the NACA 747A015 basic thickness distribution.

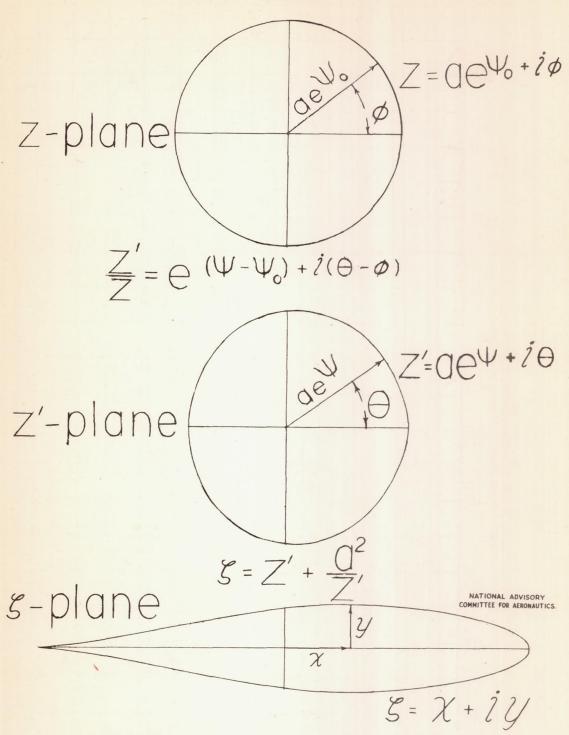


Figure 3.-Illustration of transformations used to derive airfoils and calculate pressure distributions.

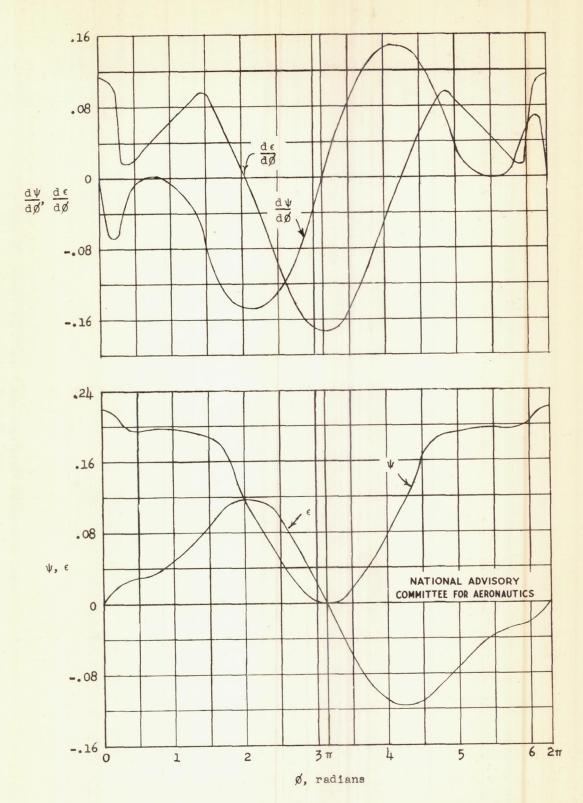
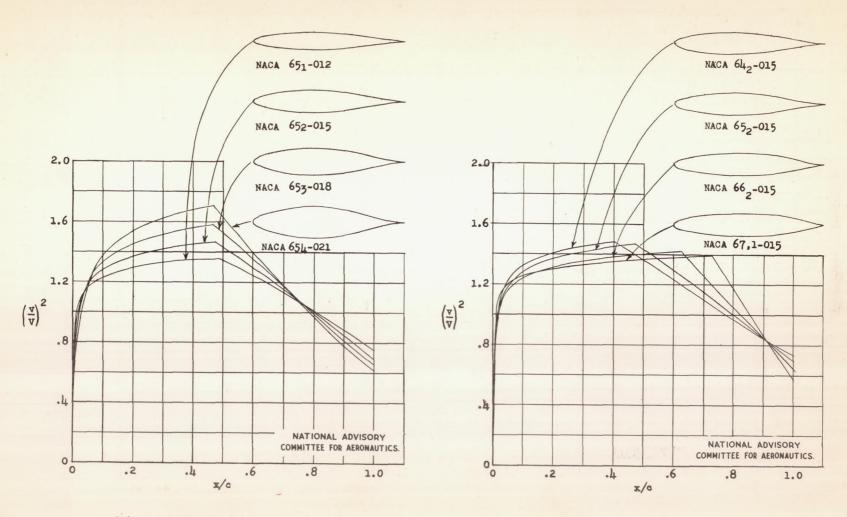


Figure 4.- Variation of airfoil parameters ψ , ϵ , $\frac{\mathrm{d}\psi}{\mathrm{d}\theta}$, $\frac{\mathrm{d}\epsilon}{\mathrm{d}\theta}$ with θ for the NACA 643-018 airfoil-section basic thickness form.



(a) Variation with thickness.

(b) Variation with position of minimum pressure.

Figure 5.- Theoretical pressure distributions for some basic symmetrical NACA 6-series airfoils at zero lift.

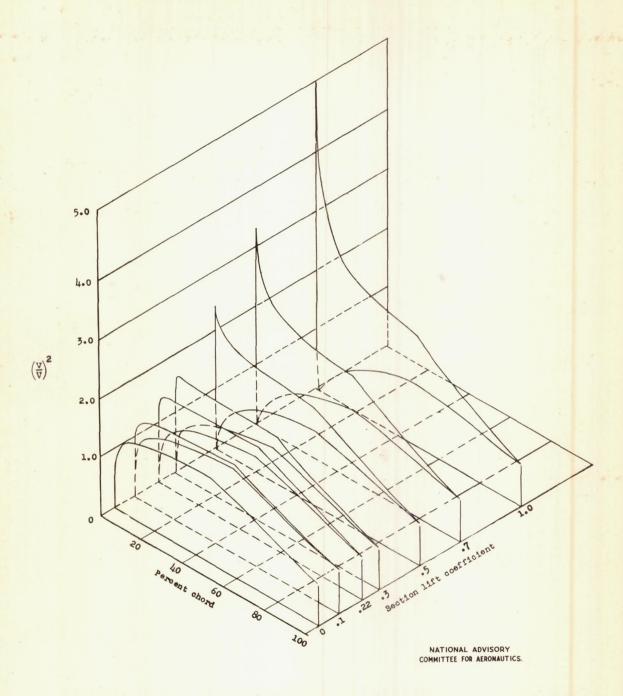


Figure 6.- Theoretical pressure distributions for the NACA 652-015 airfoil at several lift coefficients.

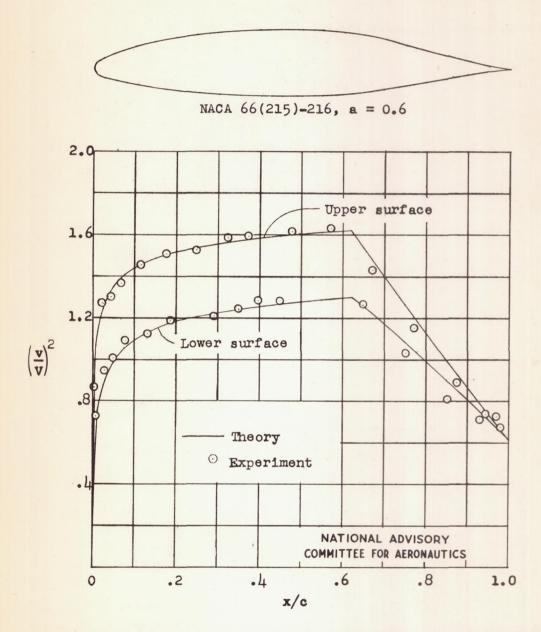
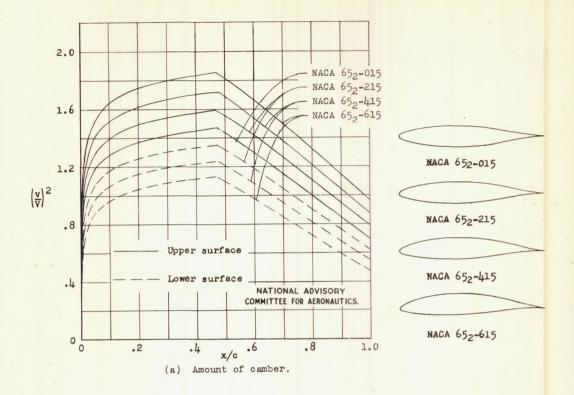


Figure 7.- Comparison of theoretical and experimental pressure distributions for the NACA 66(215)-216, a = 0.6 airfoil; c₁ = 0.23.



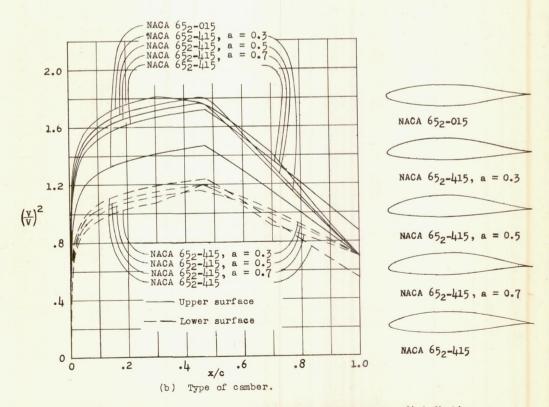


Figure 8.- Effect of amount and type of camber on pressure distribution at design lift.

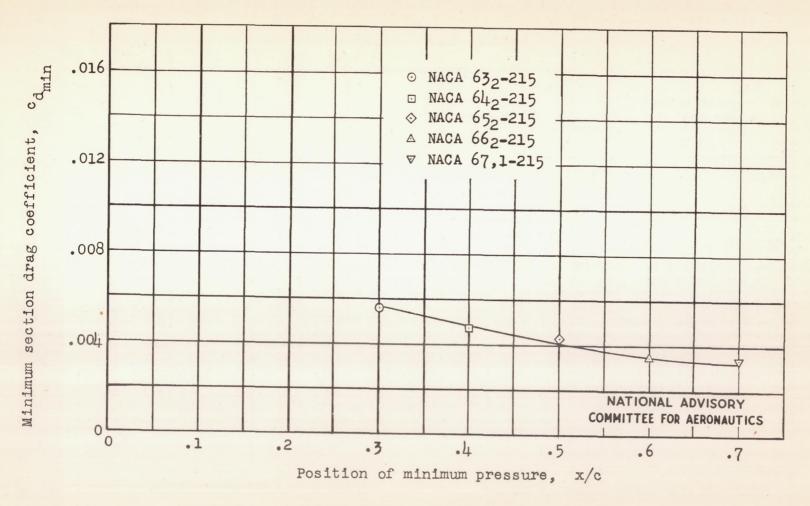


Figure 9.- Variation of minimum drag coefficient with position of minimum pressure for some NACA 6-series airfoils of the same camber and thickness. R, 6×10^6 .

9

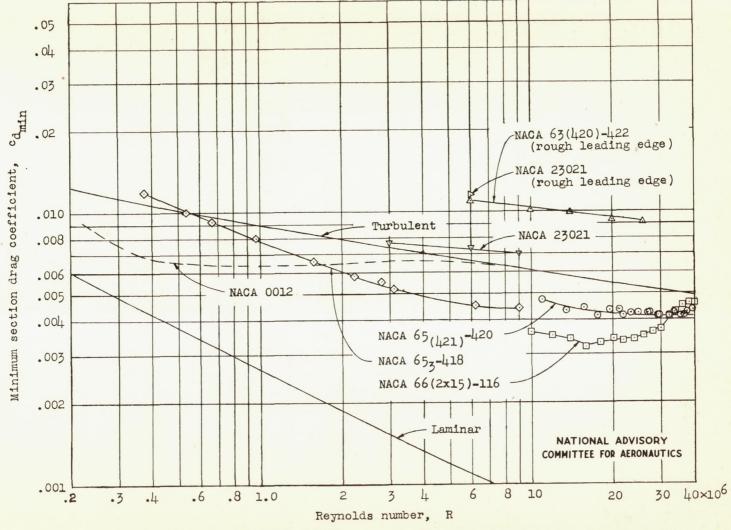


Figure 10.- Variation of minimum drag coefficient with Reynolds number for several airfoils, together with laminar and turbulent skin-friction coefficients for a flat plate.

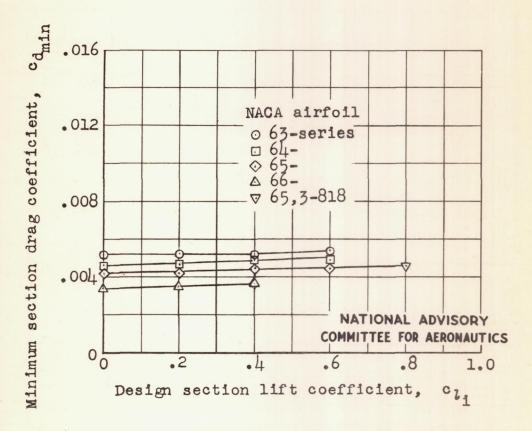
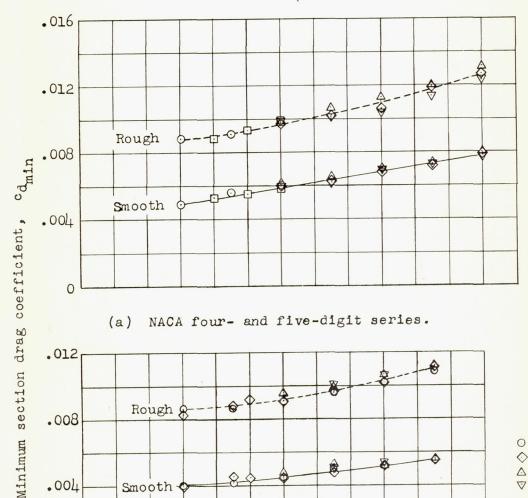
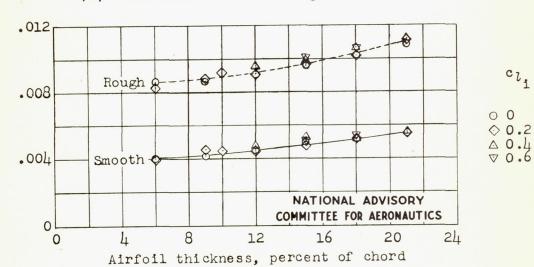


Figure 11.- Variation of section minimum drag coefficient with camber for several NACA 6-series airfoil sections of 18-percent thickness ratio. R, 6 × 106.

Series

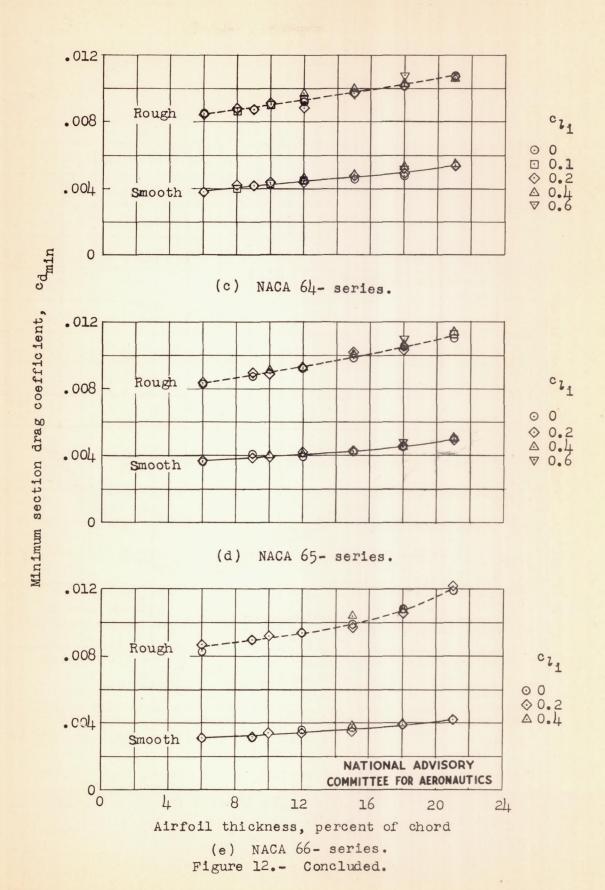


(a) NACA four- and five-digit series.



(b) NACA 63- series.

Figure 12.- Variation of section minimum drag coefficient with airfoil thickness ratio for several NACA airfoil sections of different cambers in both smooth and rough conditions. R, 6×10^6 .



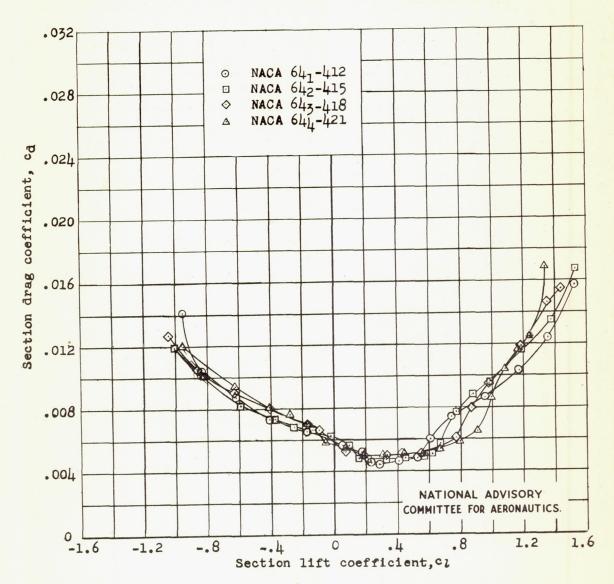
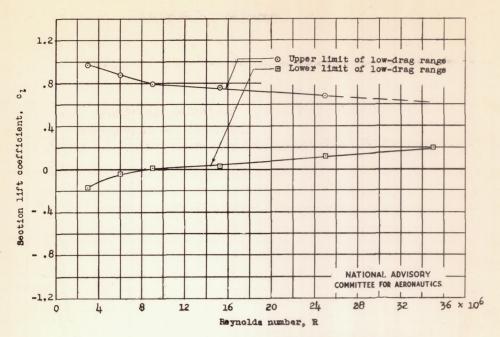
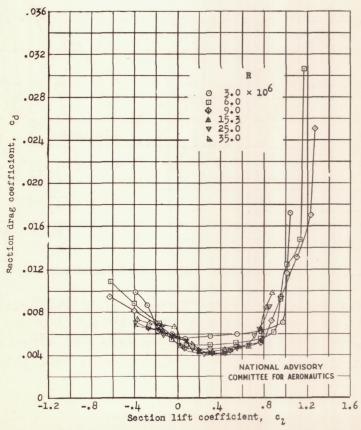


Figure 13.- Drag characteristics of some NACA 64-series airfoil sections of various thicknesses, cambered to a design lift coefficient of 0.4; R, 9 × 10⁶, TDT tests 682, 733, 735, and 691.



(a) Variation of upper and lower limits of low-drag range with Reynolds number.



(b) Section drag characteristics at various Reynolds numbers.

Figure 14.- Variation of low-drag range with Reynolds number for the NACA 65(421)-420 airfoil; TDT tests 300, 312, and 328.

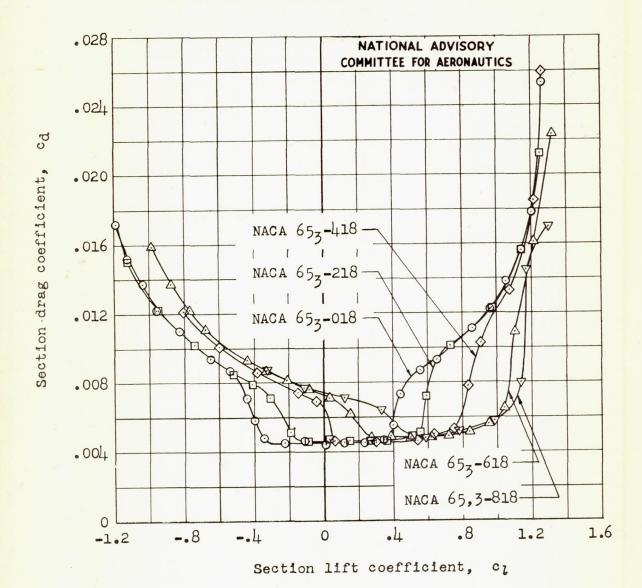


Figure 15.- Drag characteristics of some NACA 65-series airfoil sections of 18 percent thickness with various amounts of camber. R, 6×10^6 ; TDT tests 163, 314, 802, 813, and 830.

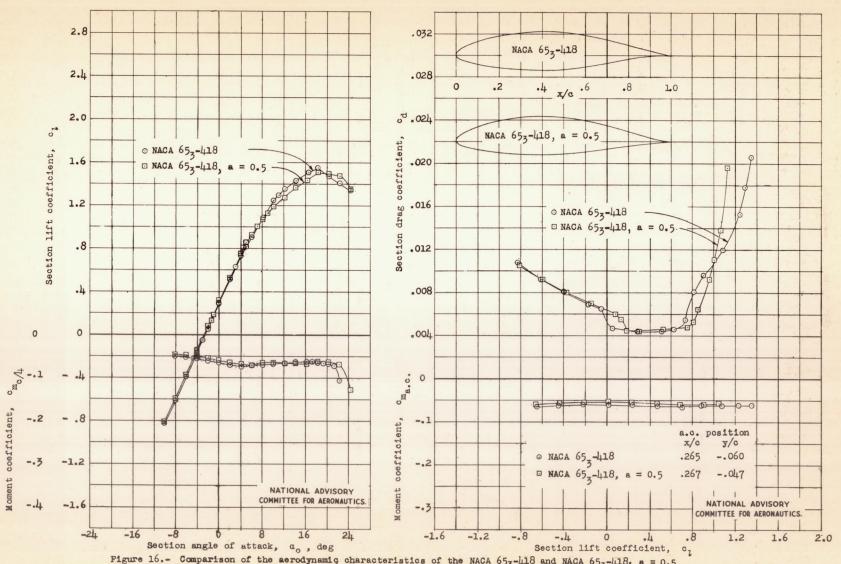


Figure 16.- Comparison of the aerodynamic characteristics of the NACA 65_3 -418 and NACA 65_3 -418, a = 0.5 airfoils at a Reynolds number of 9×10^6 ; TDT tests 314, 320, 406, and 411.

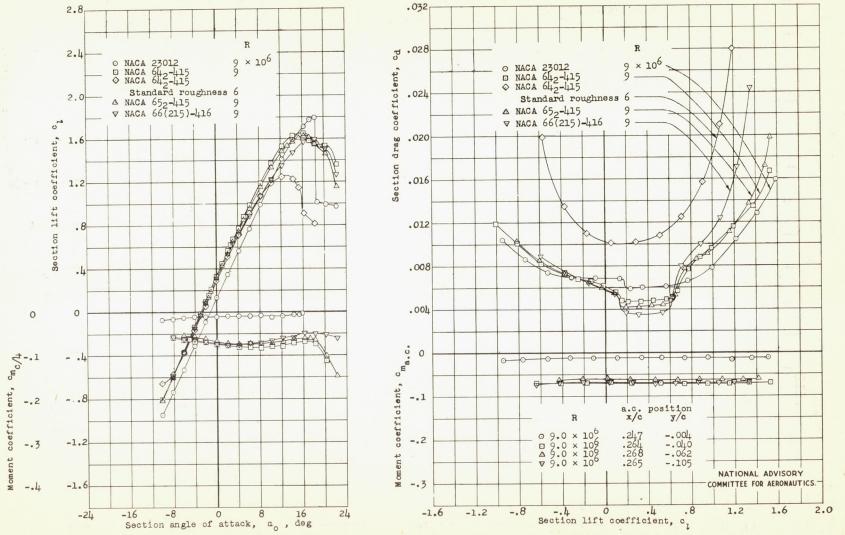


Figure 17.- Comparison of the aerodynamic characteristics of some NACA airfoils from tests in the Langley two-dimensional low-turbulence pressure tunnel.

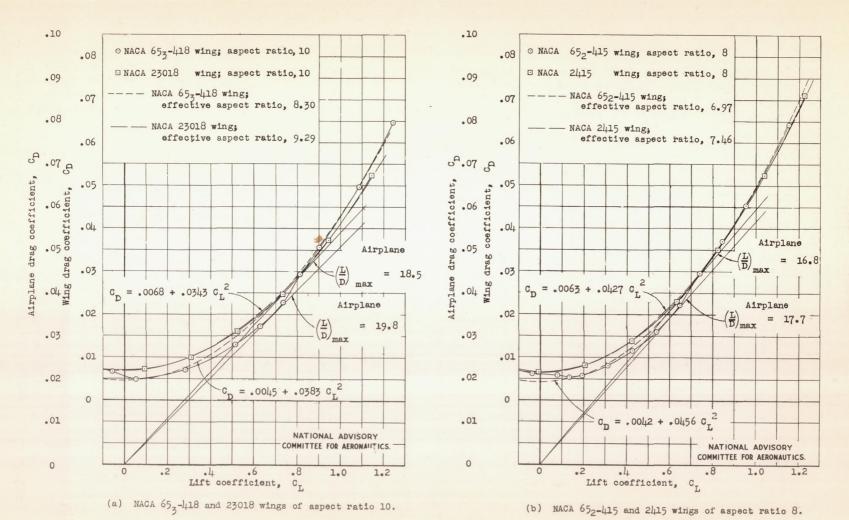


Figure 18.- Comparison of finite aspect-ratio drag characteristics for two types of airfoils obtained by adding the induced drag corresponding to an elliptical span loading to the section drag coefficients.

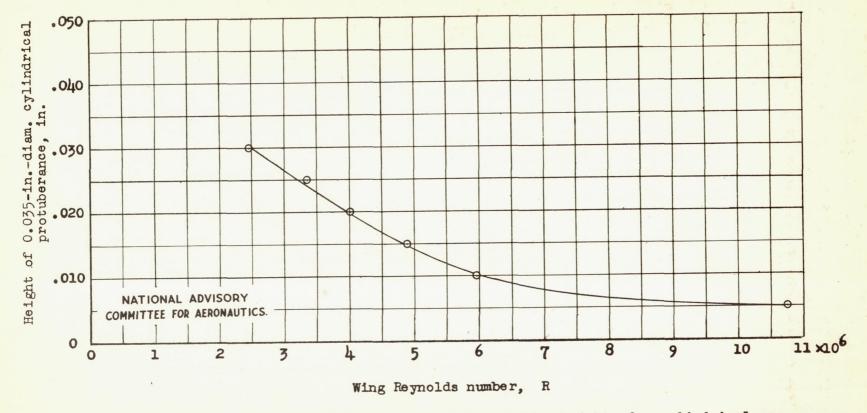
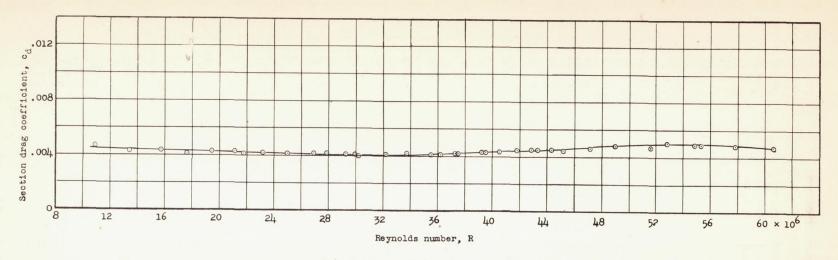
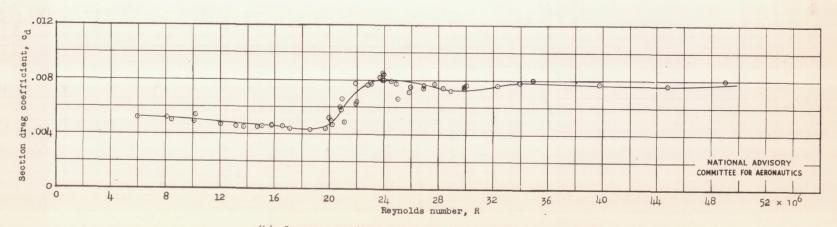


Figure 19.- Variation with wing Reynolds number of the minimum height of a cylindrical protuberance necessary to cause premature transition. Protuberance has 0.035-inch diameter with axis normal to wing surface and is located at 5-percent-chord of a 90-inch-chord symmetrical 6-series airfoil section of 15-percent thickness and with minimum pressure at 70-percent chord.



(a) Smooth condition; TDT test 328.



(b) Lacquer camouflage unimproved after painting; TDT test h61.

Figure 20.- Variation of drag coefficient with Reynolds number for a 60-inch-chord model of the NACA 65 (421) 420 airfoil for two surface conditions.

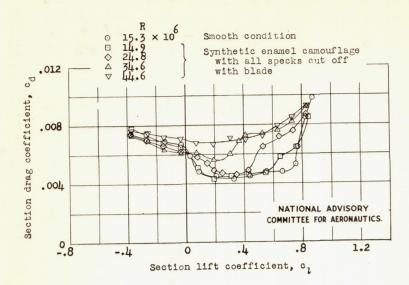


Figure 21.- Drag characteristics of NACA 65 (421)-420 airfoil for two surface conditions; TDT tests 300 and 486.

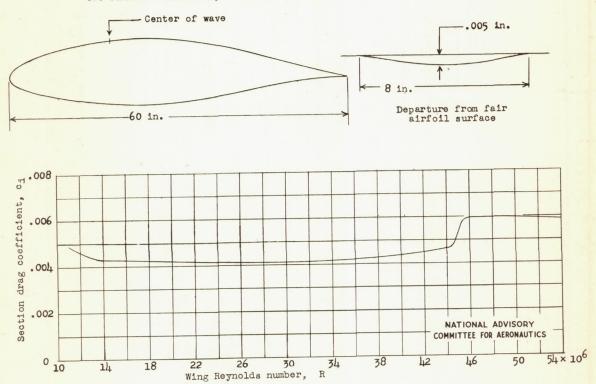


Figure 22.- Experimental curve showing variation of drag coefficient with Reynolds number for the NACA $65(421)^{-420}$ airfoil section with a small amount of surface waviness.

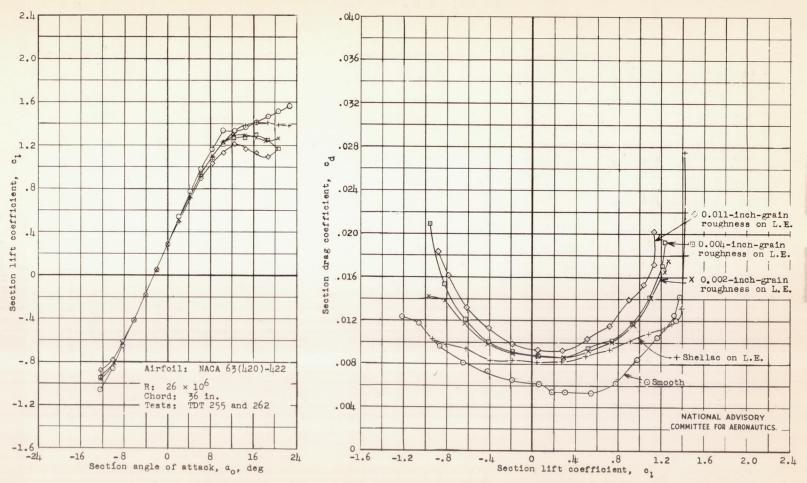


Figure 23.- Lift and drag characteristics of an NACA 63(420)-422 airfoil with various degrees of roughness at the leading edge.

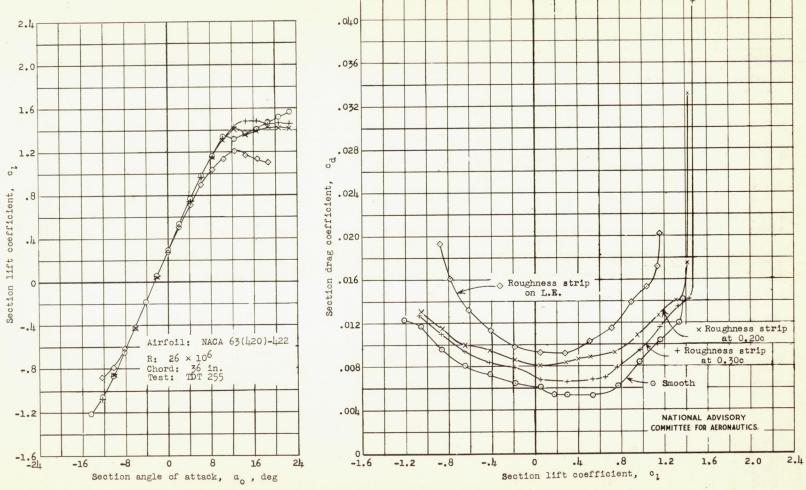


Figure 24.- Lift and drag characteristics of an NACA 63(420)-422 airfoil with 0.011-inch-grain roughness at various chordwise locations.

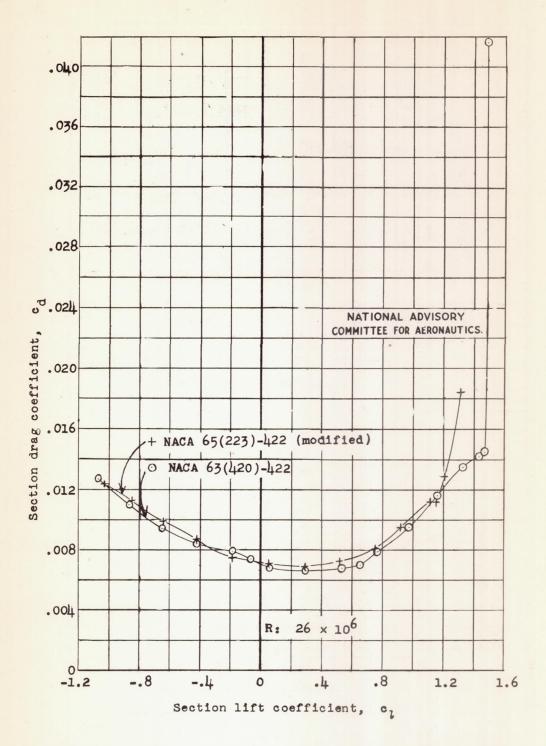
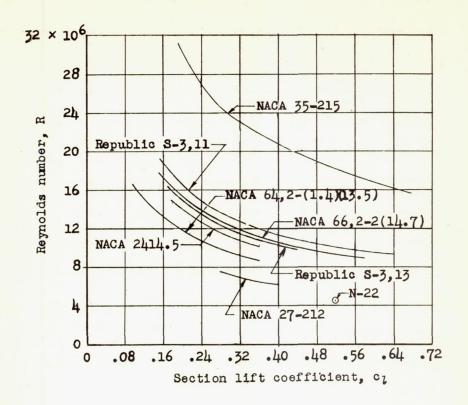


Figure 25.- Drag characteristics of two NACA 6-series airfoils with 0.011-inch-grain roughness at 0.30c.



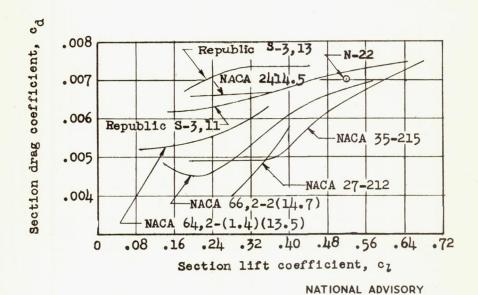


Figure 26.- Comparison of section drag coefficients obtained in flight on various airfoils. Tests of NACA 27-212 and 35-215 sections made on gloves.

COMMITTEE FOR AERONAUTICS

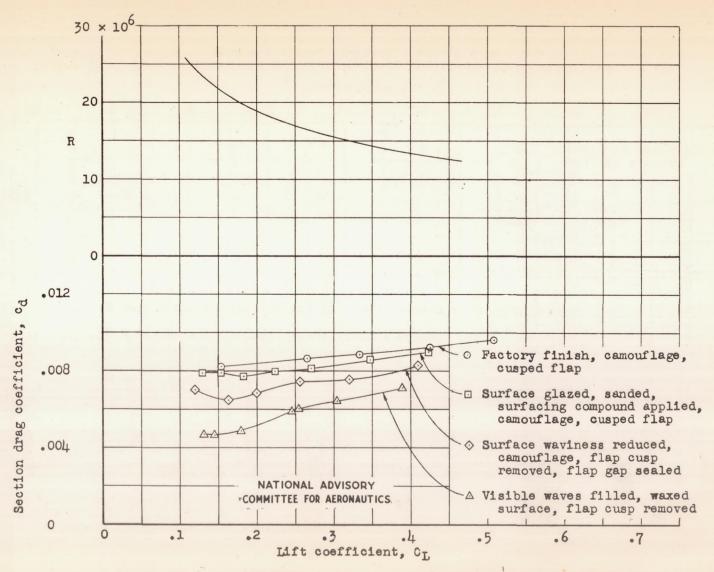
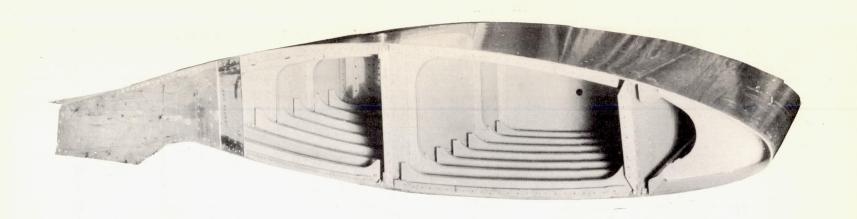


Figure 27.- Consolidated-Vultee flight measurements of the effect of wing surface condition on drag of an NACA 66(215)-1(14.5) wing section.



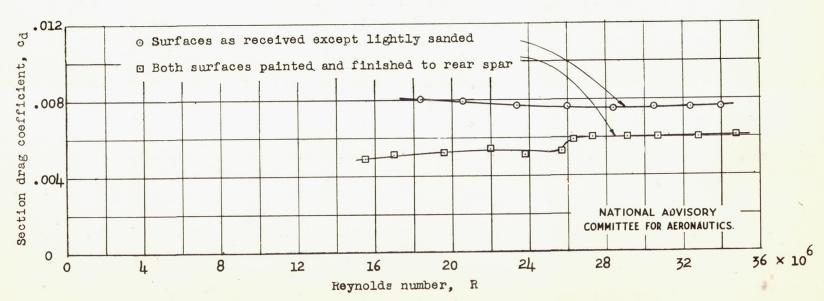


Figure 28.- Drag scale effect on 100-inch-chord practical-construction model of the NACA 65(216)-3(16.5) (approx.) airfoil section. $c_1 = 0.2$ (approx.).

Laminar

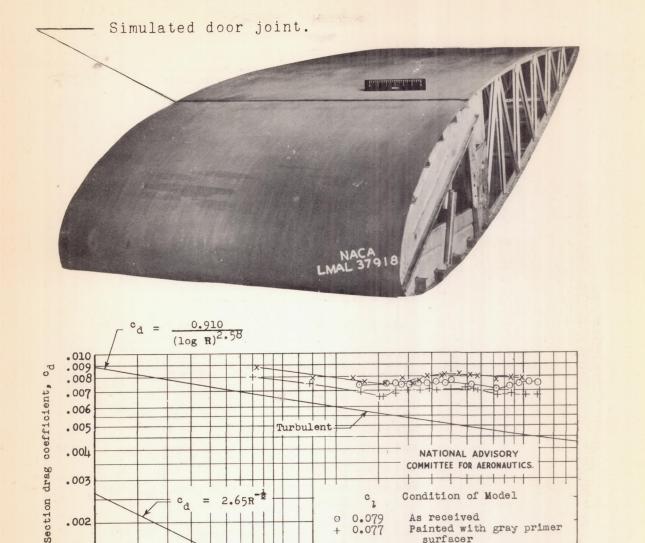
2

3

4 5 6

.001

1



Reynolds number, R

10

0.077

0.074

surfacer

Camouflage painted with simulated door joints

50 60

30 40

100×106

Figure 29.- Variation of the drag coefficient with Reynolds number for the NACA 23016 airfoil section together with laminar and turbulent skin-friction coefficients for a flat plate.

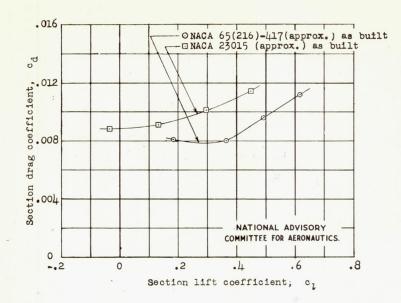


Figure 30.- Drag characteristics of the NACA 65,2-417 (approx.) and NACA 23015 (approx.) airfoil sections built by practical-construction methods by the same manufacturer. R = 10.23 × 10.

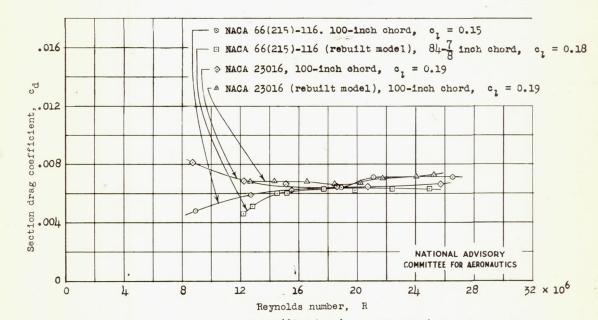


Figure 31.- Scale effect on drag of the NACA 66(215)-116 and NACA 23016 airfoil sections built by practical-construction methods by the same manufacturer and tested as received.

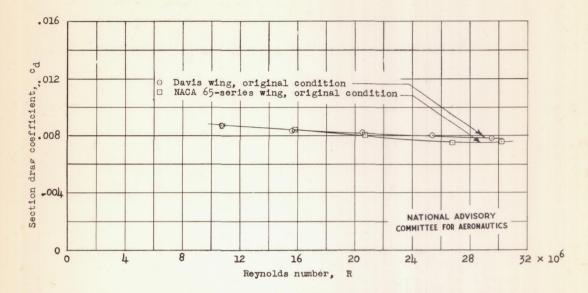


Figure 32.- Drag scale effect for a model of the NACA 65-series airfoil section 18.27 percent thick and the Davis airfoil section 18.27 percent thick, built by practical-construction methods by the same manufacturer. c₁ = 0.46 (approx.).

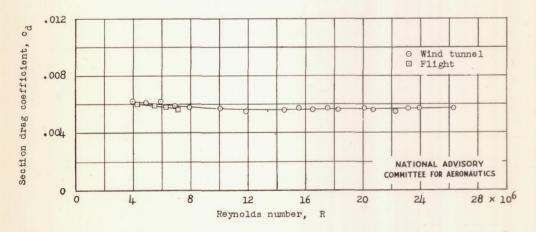


Figure 33.- Comparison of drag coefficients measured in flight and wind tunnel for the NACA 0012 airfoil section at zero lift.

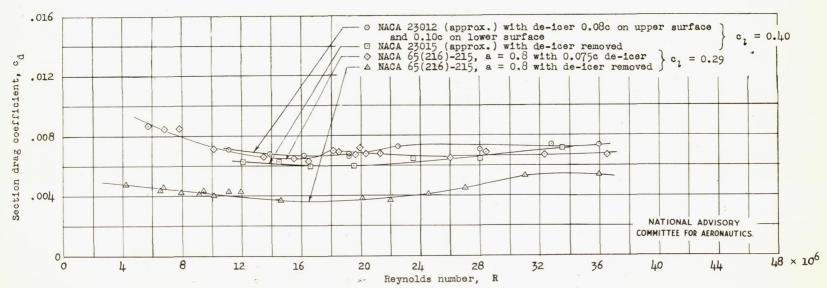


Figure 34.- Effect of de-icers on the drag of two practical-construction airfoil sections with relatively smooth surfaces.

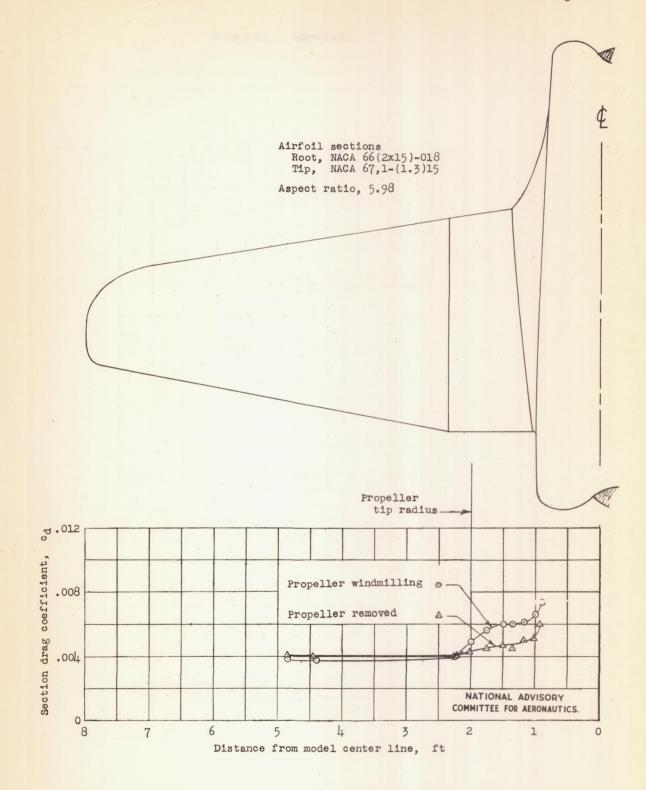


Figure 35.- The effect of propeller operation on section drag coefficient of a fighter-type airplane, from tests of a model in the Langley 19-foot pressure tunnel; C_L = 0.10; R, 3.7 × 10⁶.

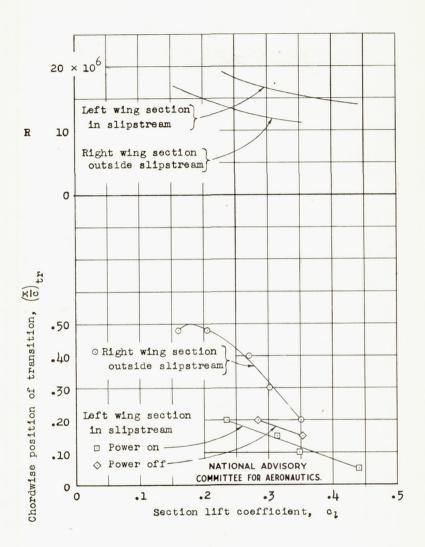


Figure 36.- Flight measurements of transition on an NACA 66-series wing within and outside the slipstream.

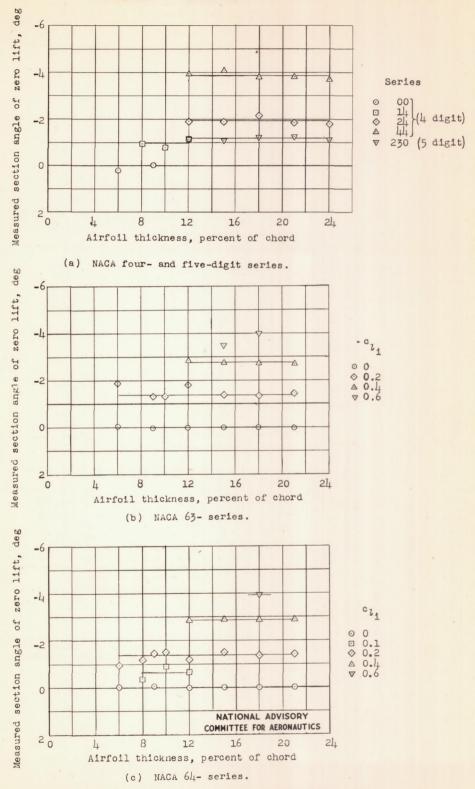
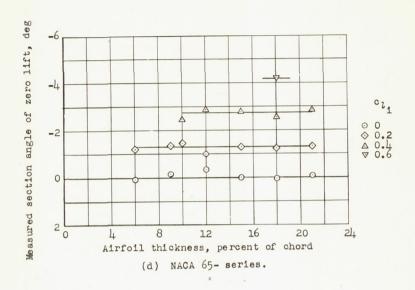


Figure 37.- Measured section angles of zero lift for a number of NACA airfoil sections of various thicknesses and camber. R, 6×10^6 .



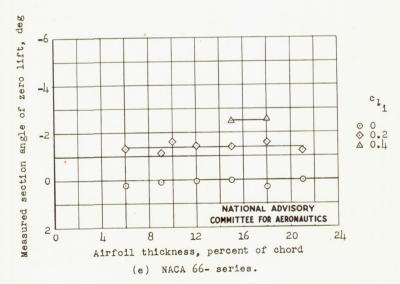
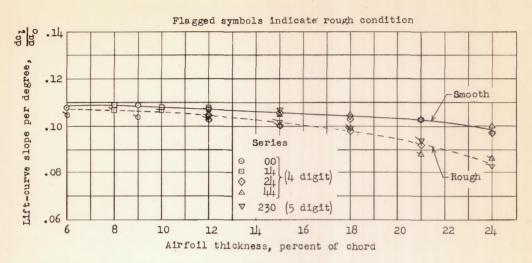
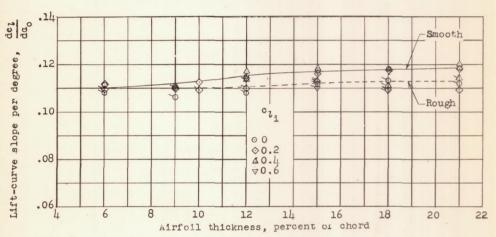


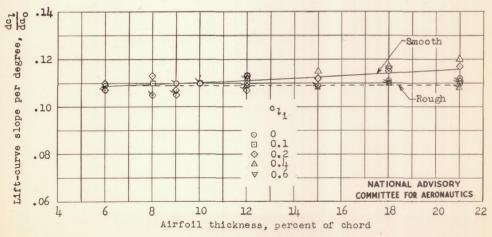
Figure 37 .- Concluded.



'(a) NACA four- and five-digit series.

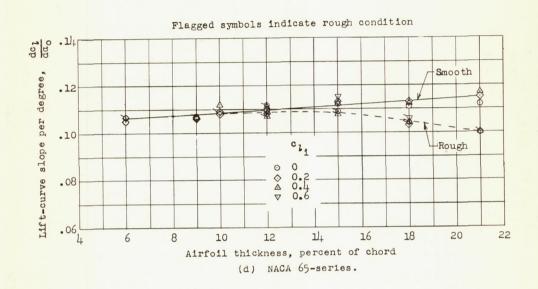


(b) NACA 63- series.



(c) NACA 64- series.

Figure 38.- Variation of lift-curve slope with airfoil thickness ratio and camber for a number of NACA airfoil sections in both the smooth and rough conditions. R, 6×10^6 .



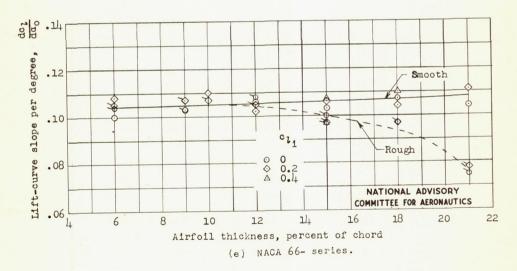


Figure 38.- Concluded.

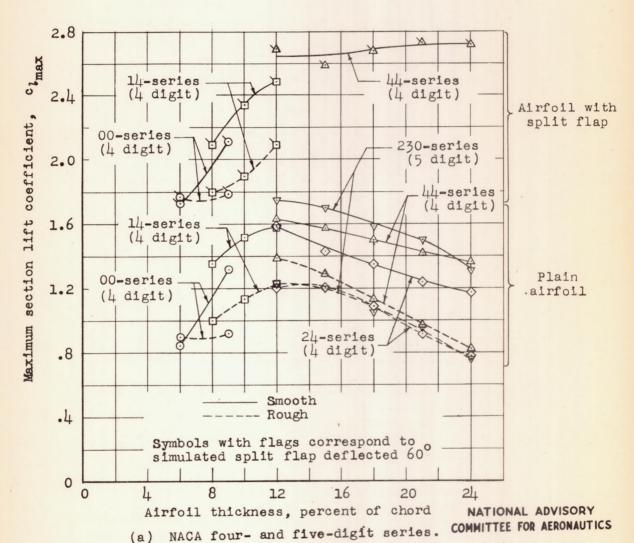


Figure 39.- Variation of maximum section lift coefficient with airfoil thickness ratio and camber for several NACA airfoil sections with and without simulated split flaps and standard roughness. R, 6 x 106.

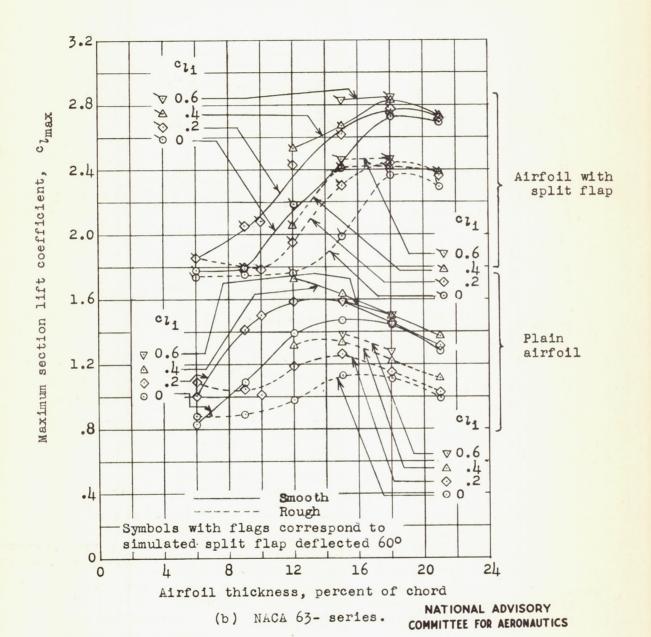


Figure 39.- Continued.

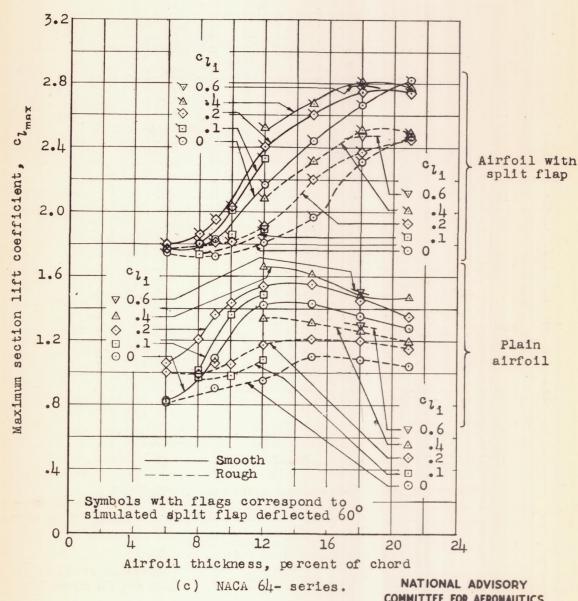


Figure 39 .- Continued.

COMMITTEE FOR AERONAUTICS

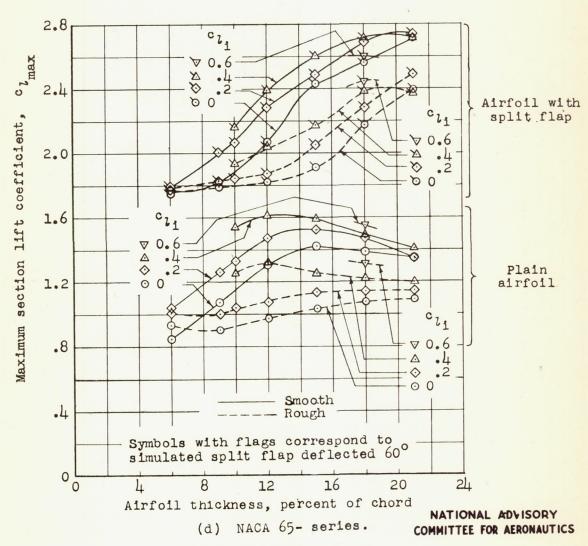


Figure 39.- Continued.

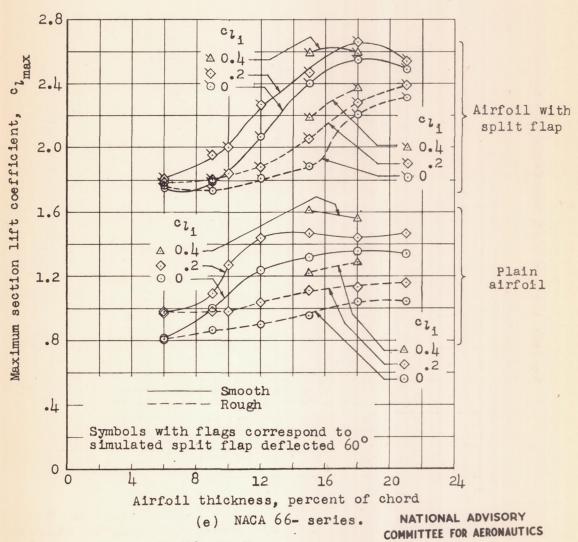


Figure 39.- Concluded.

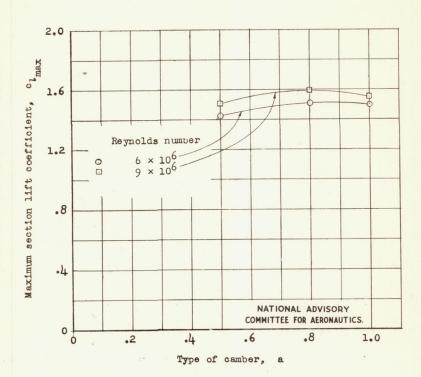


Figure 40.- Variation of maximum lift coefficient with type of camber for some NACA 653-418 airfoil sections from tests in the Langley two-dimensional low-turbulence pressure tunnel.

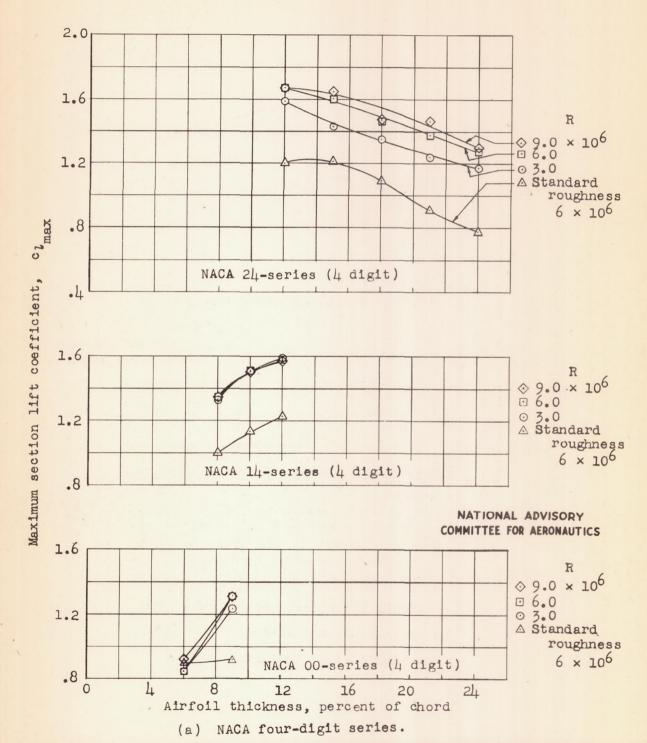
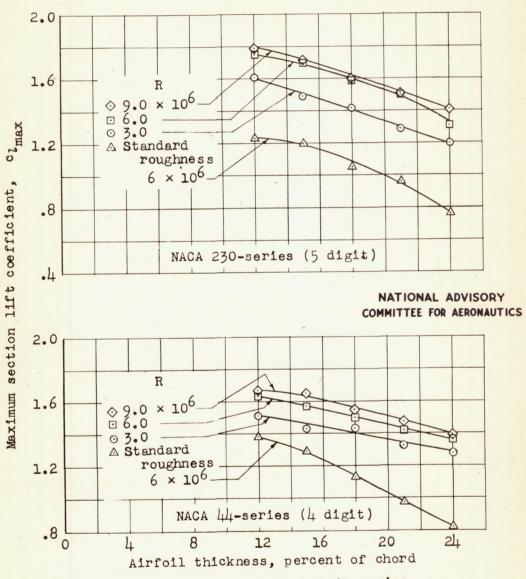


Figure 41.- Variation of maximum section lift coefficient with airfoil thickness ratio at several Reynolds numbers for a number of NACA airfoil sections of different cambers.



(b) NACA four- and five-digit series.
Figure 41.- Continued.

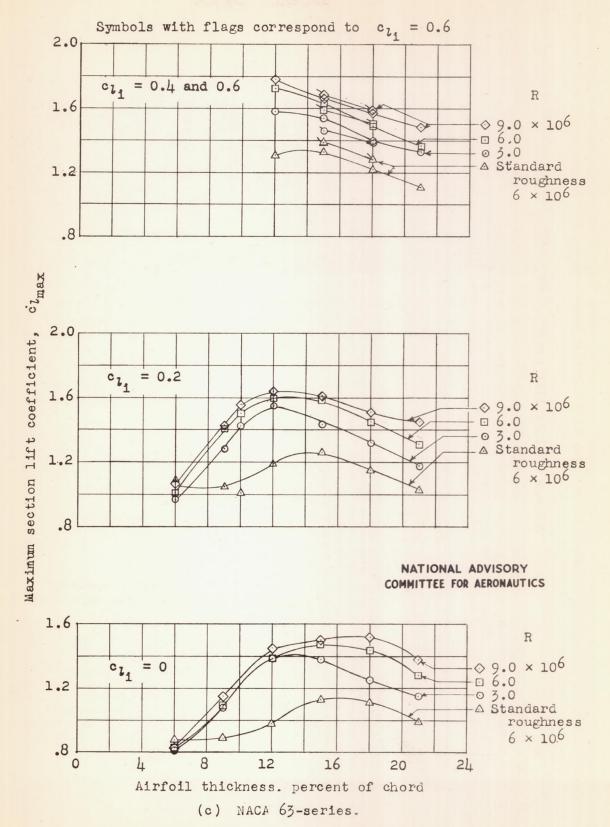


Figure 41 .- Continued.

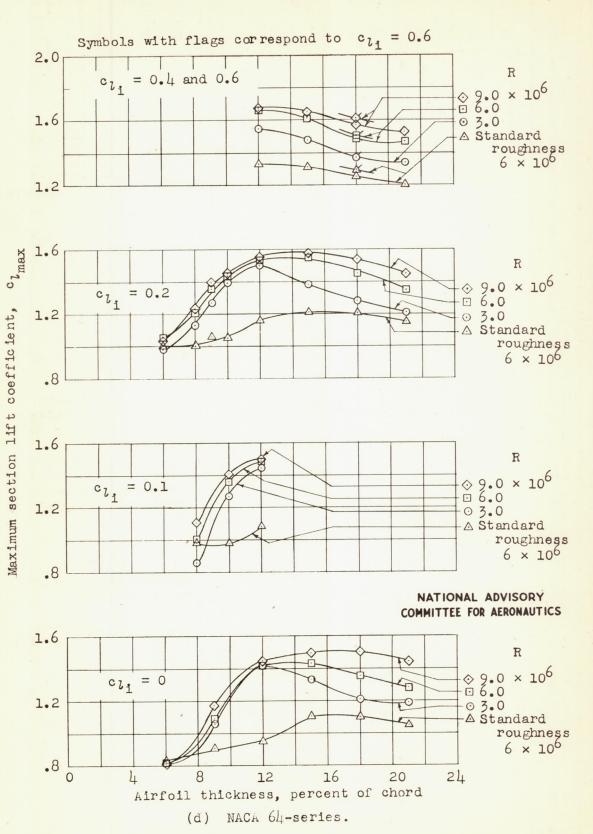
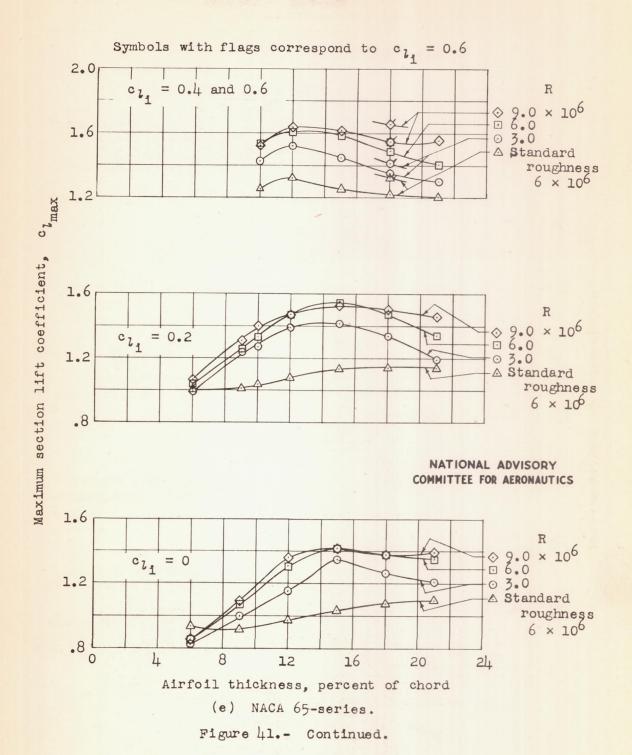


Figure 41. - Continued.



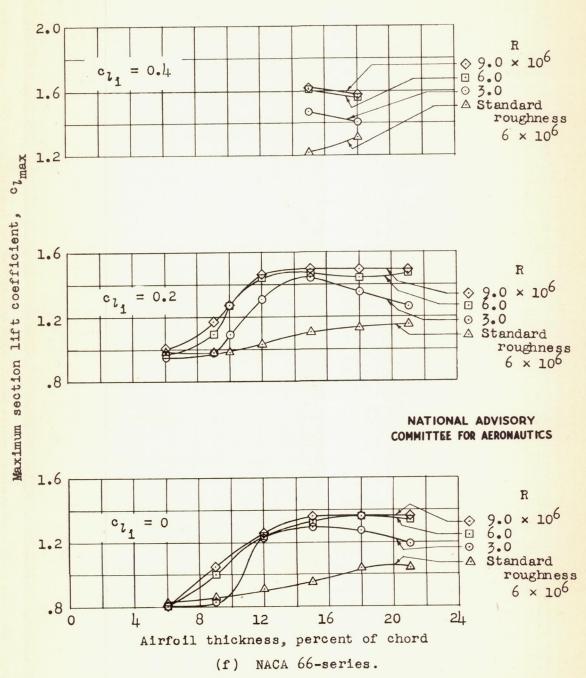


Figure 41.- Concluded.

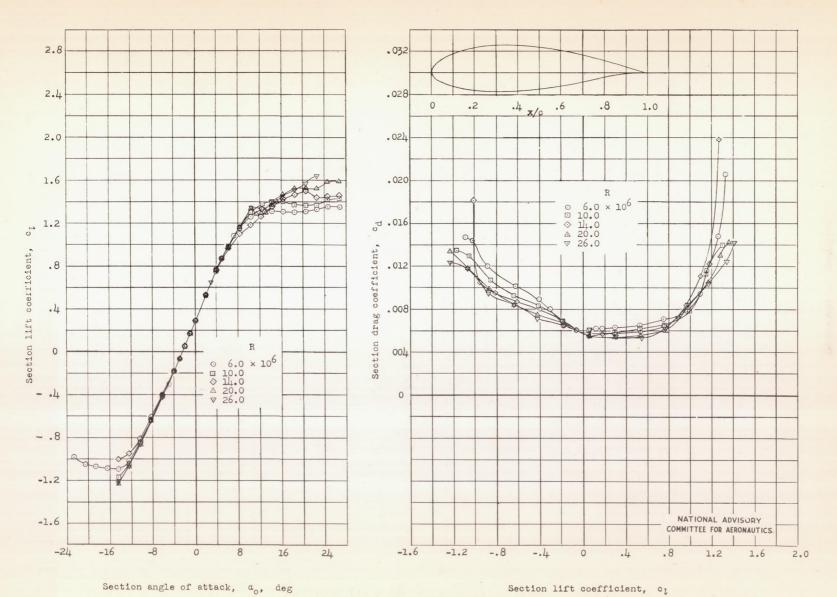


Figure 42.- Lift and drag characteristics of the NACA 63(420)-422 airfoil at high Reynolds number; TDT tests 228 and 255.

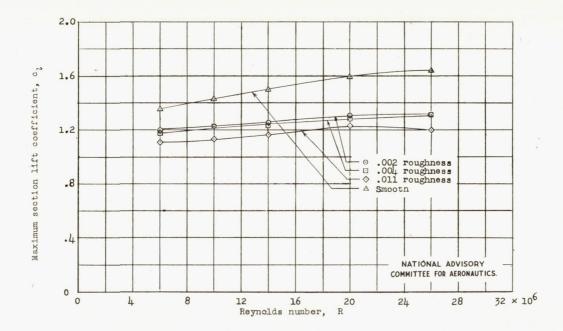


Figure 43.- Effects of Reynolds number on maximum section lift coefficient c_1 of the NACA 63(420)-422 airfoil with roughened and smooth leading edge.

Figure 44.- Lift characteristics of the NACA 23012, 2412, and 2415 airfoil sections as affected by normal model inaccuracies; R, 9×10^6 (approx.).

2.0

log-

□ As delivered by shop,

TDT test 468

○ Final condition,

TDT test 520

16

8

Section angle of attack, a, deg NACA 2412

0

b

24

o 1.6

1.2

.8

.4

0

Section lift coefficient,

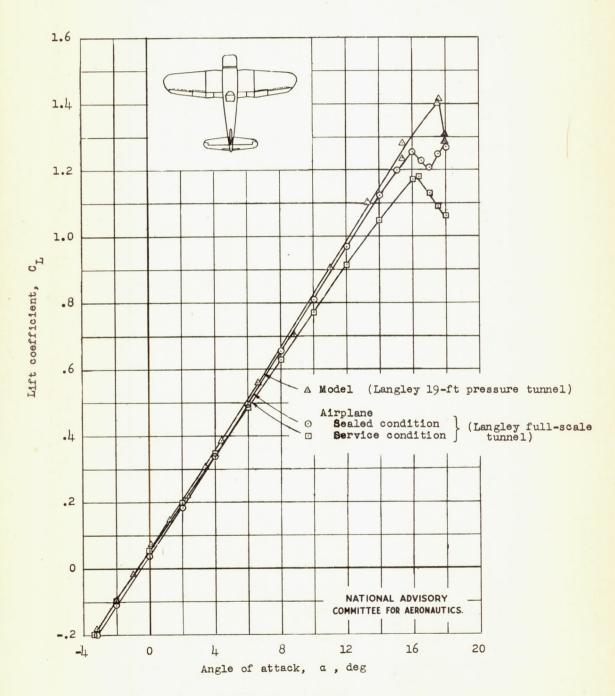


Figure 45.- The effects of surface conditions on the lift characteristics of a fighter-type airplane; R, 2.8 \times 106.

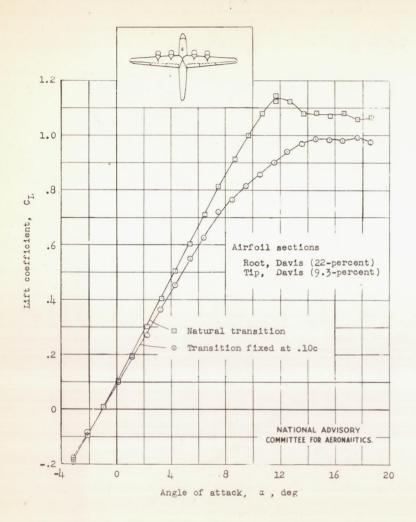


Figure 46.- The effect on the lift characteristics of fixing the transition on a model in the Langley 19-foot pressure tunnel; R, 2.7×10^6 . (model with Davis airfoil sections.)

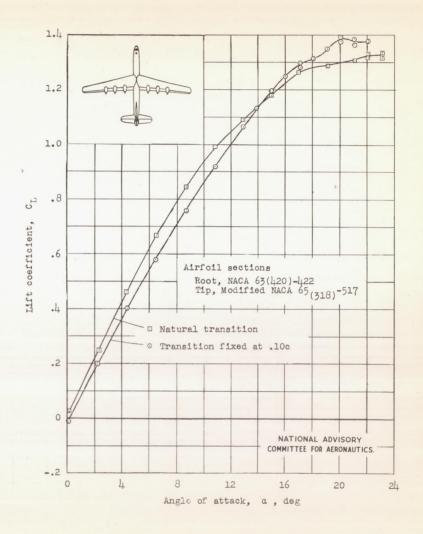


Figure 47.- The effect on the lift characteristics of fixing the transition on a model in the Langley 19-foot pressure tunnel; R, 2.7×10^6 . (Model with NACA airfoil sections.)

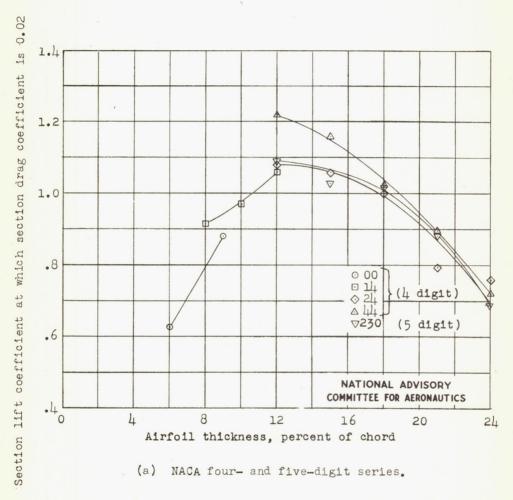


Figure 48.- Variation of the lift coefficient corresponding to a drag coefficient of 0.02 with thickness and camber for a number of NACA airfoil sections with roughened leading edges. R, 6 × 106.

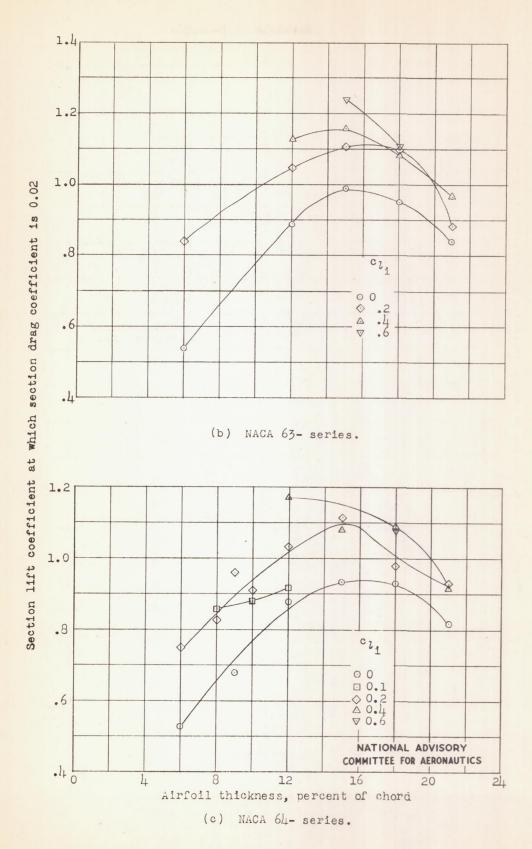


Figure 48.- Continued.

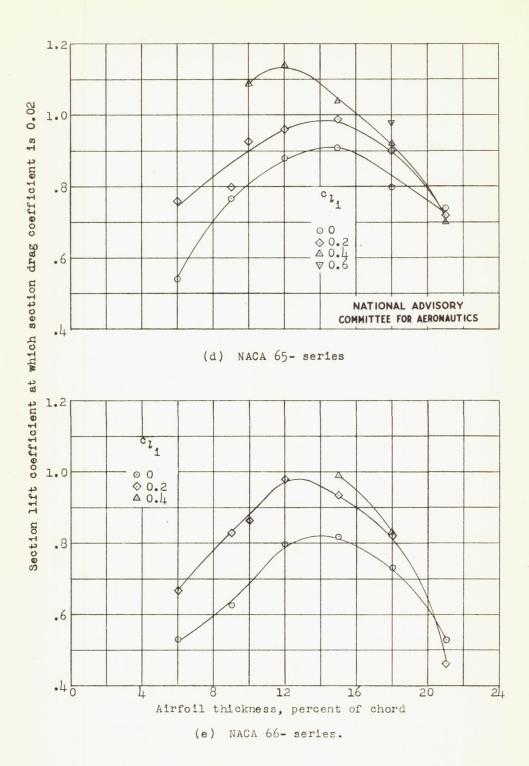


Figure 48.- Concluded.

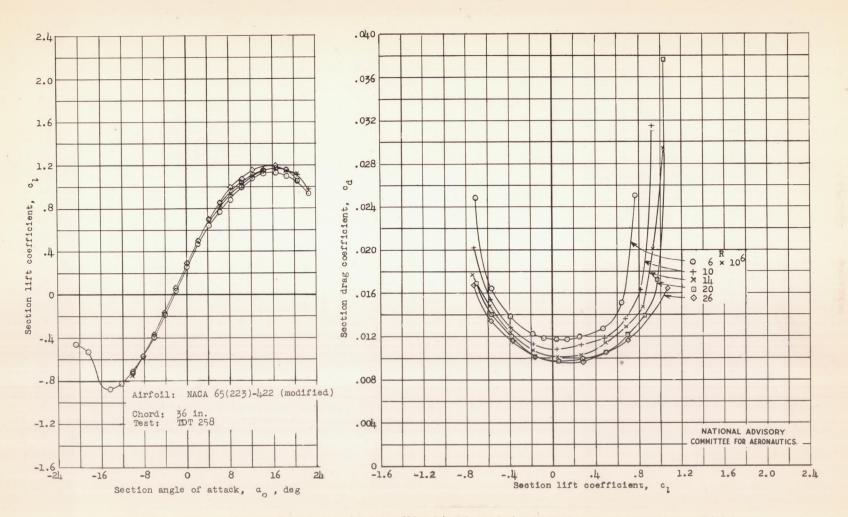


Figure 49.- Lift and drag characteristics of an NACA 65(223)-422 (modified) airfoil with standard roughness applied to the leading edge.

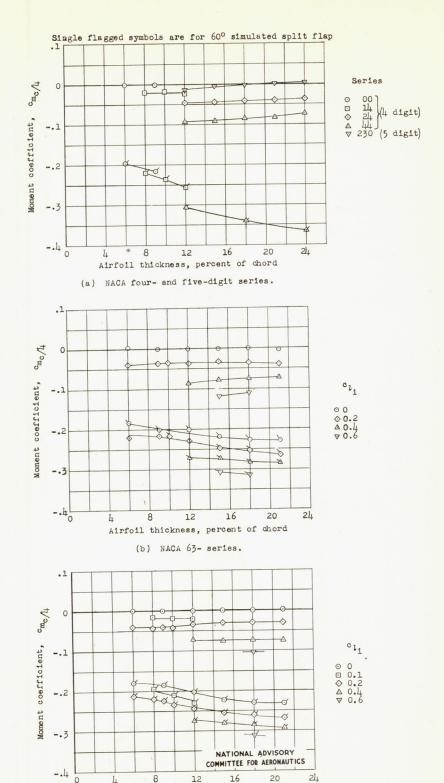
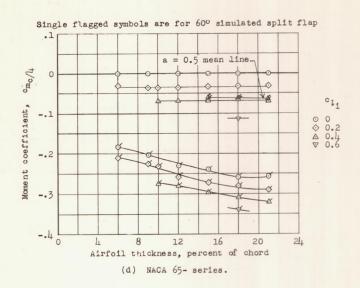


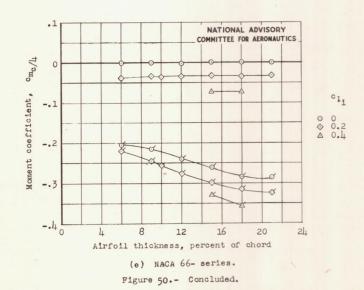
Figure 50.- Variation of section quarter-chord pitching-moment coefficient (measured at an angle of attack of zero degrees) with airfoil thickness ratio for several NACA airfoil sections of different camber. R, 6×10^6 .

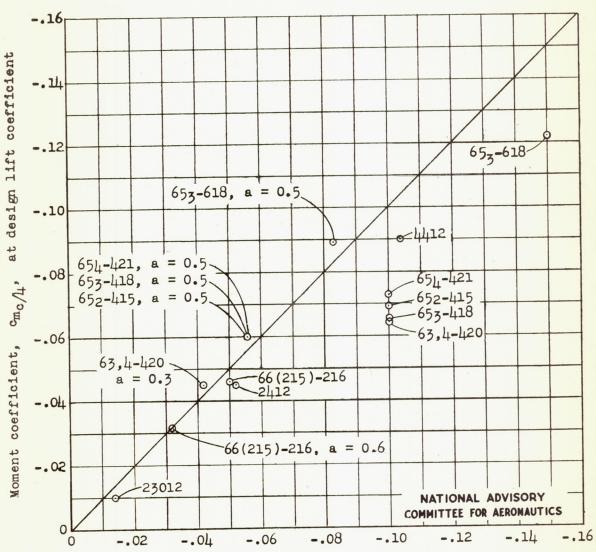
Airfoil thickness, percent of chord (c) NACA 64- series.

4

8

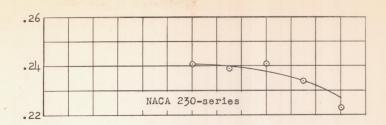






Theoretical moment coefficient for the airfoil mean line about quarter-chord point

Figure 51.- Comparison of theoretical and measured pitching-moment coefficients for some NACA airfoils; R, 6×10^6 .



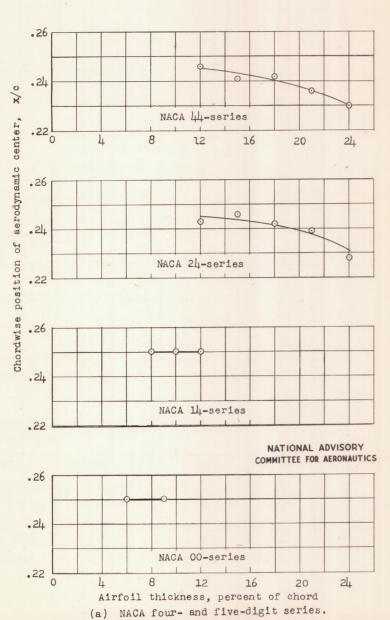


Figure 52. - Variation of section chordwise position of the aerodynamic center with airfoil thickness ratio for several NACA airfoil sections of different cambers. R, 6 × 100.

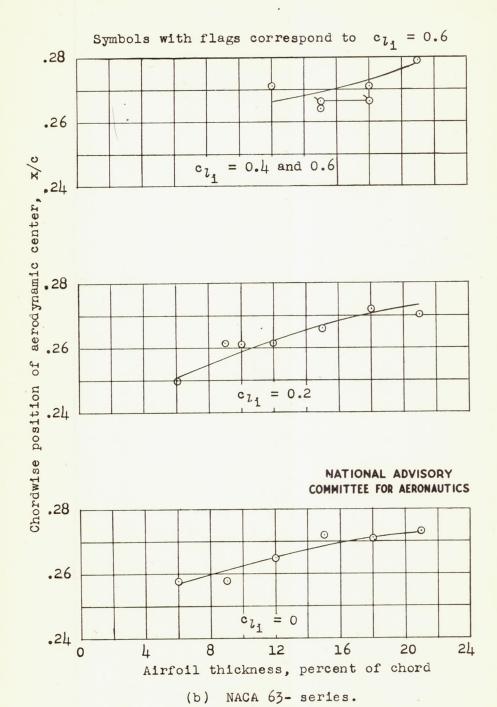


Figure 52.- Continued.

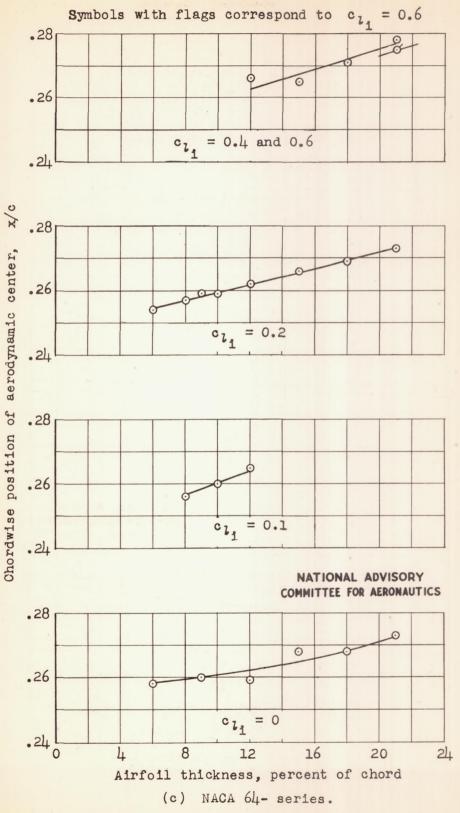
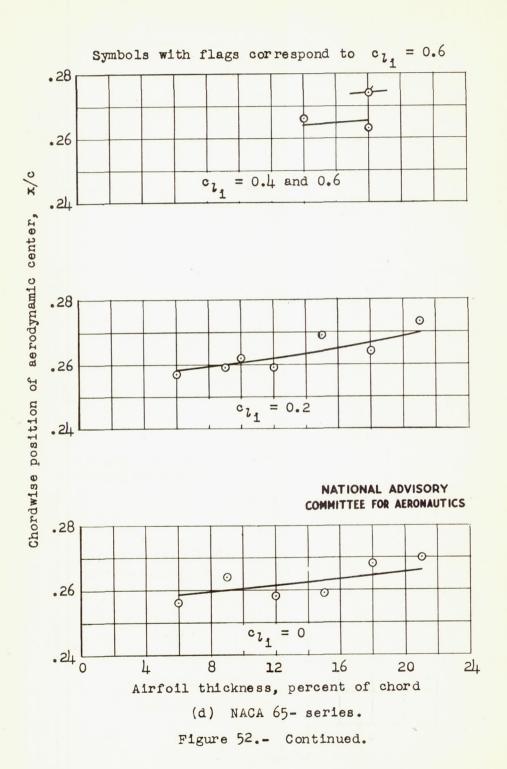
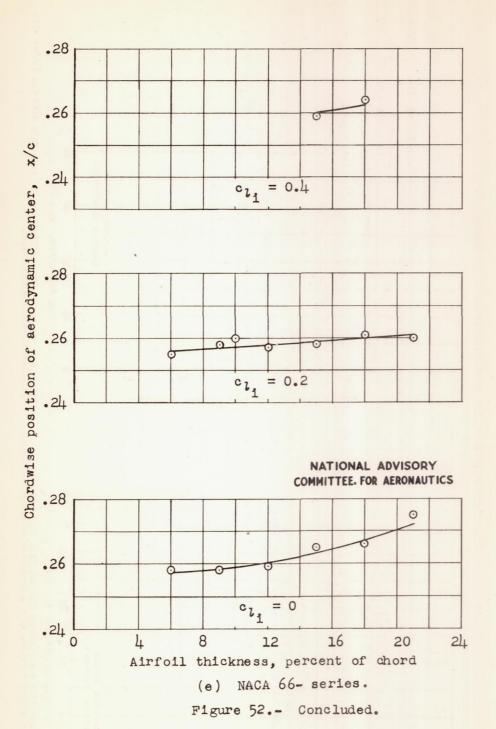


Figure 52 .- Continued.





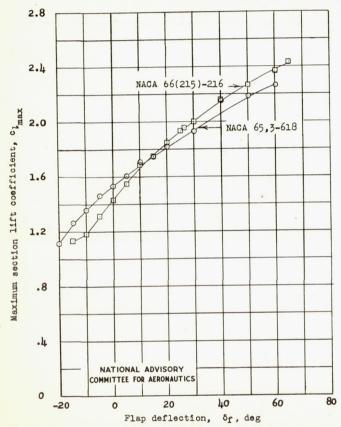


Figure 53.- Maximum lift coefficients for the NACA 65,3-618 and NACA 66(215)-216 airfoils fitted with 0.20-airfoil-chord plain flaps; R, 6×10^6 .

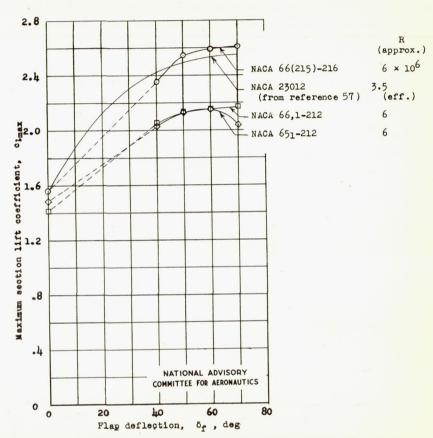
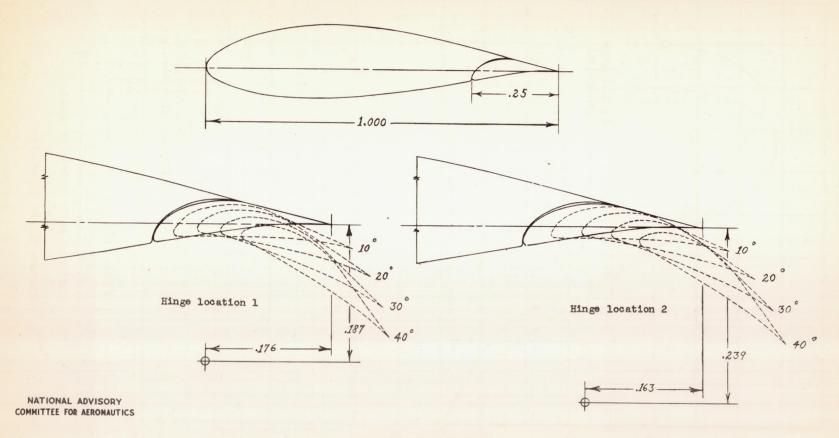
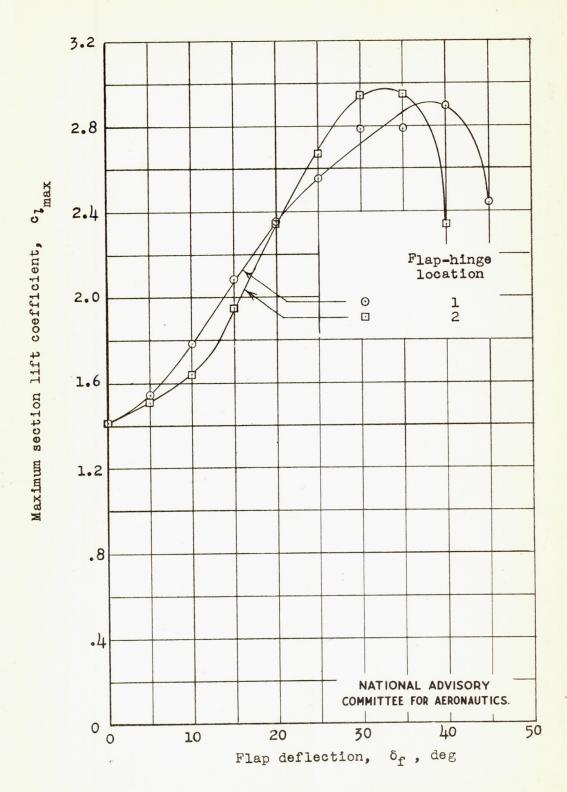


Figure 54.- Maximum lift coefficients for some NACA airfoils fitted with 0.20-airfoil-chord split flaps.



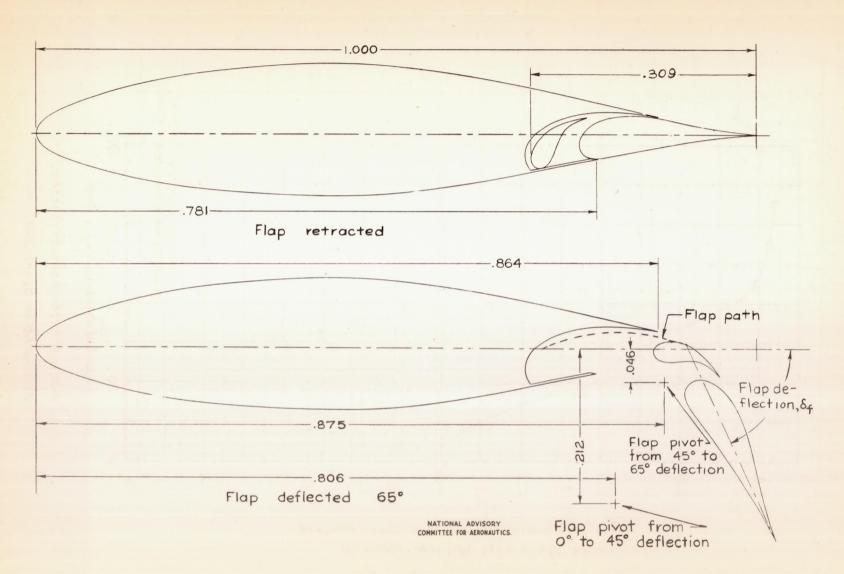
(a) Flap configuration.

Figure 55.- Flap configuration and maximum lift coefficients for the NACA 63,4-420 airfoil with a 0.25-airfoil-chord hinged slotted flap; R, 6×10^6 .



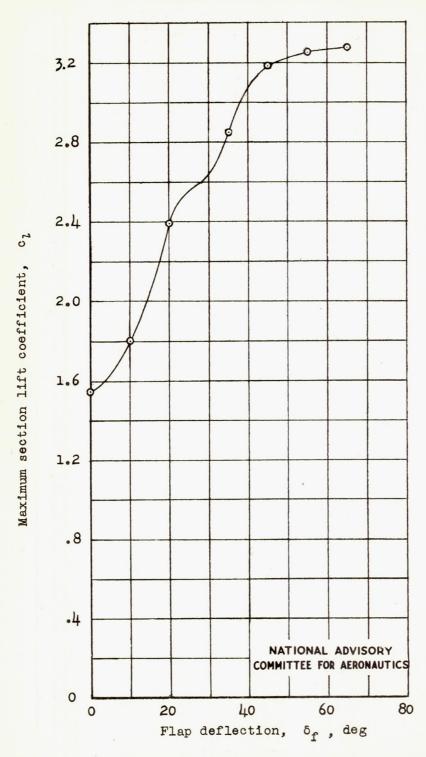
(b) Maximum lift characteristics.

Figure 55.- Concluded.



(a) Flap configuration.

Figure 56.- Flap configuration and maximum lift coefficients for the NACA 653-118 airfoil with a double slotted flap; R, 6×10^6 .



(b) Maximum lift characteristics.

Figure 56.- Concluded.

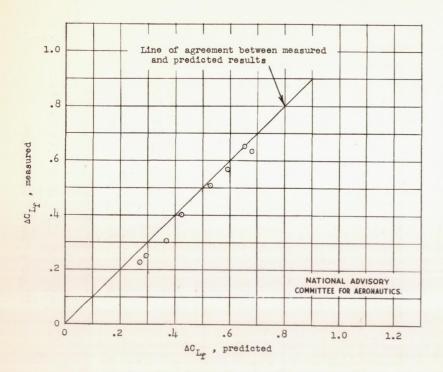


Figure 57.- Comparison between measured values of the increments in lift coefficients due to flap deflection and values predicted from two-dimensional data. Split flap.

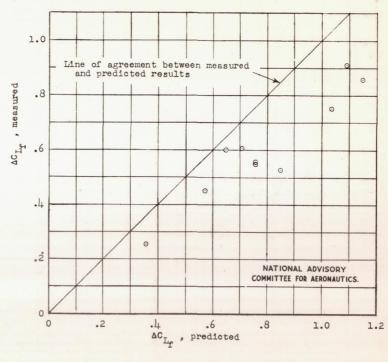


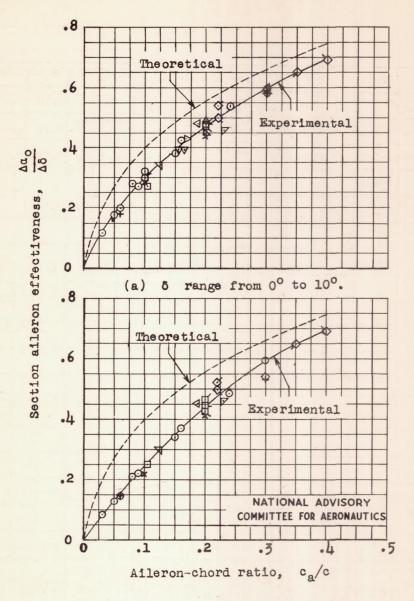
Figure 58.- Comparison between measured values of the increments in lift coefficients due to flap deflection and values predicted from two-dimensional data. Slotted flap.

TABLE III. SUPPLEMENTARY INFORMATION REGARDING TESTS

OF TWO-DIMENSIONAL MODELS

Model				Air-flow characteristics			
Desig- nation	Sym- bol	Basic airfoil	Type of flap	τ	М	R	Refer-
		NACA 0009	Plain	1.93	0.08		53 to 57
1	+				0.10	1.4 × 10 ⁶	58
2	-	NACA 0015	Plain	1.60		2.2 × 10 ⁶	59, 50
3	×	NACA 23012	Plain	1.50	0.11		39, 30
4		NACA 66(2 x 15)=009	Plain, straight contour	1.93	0.10	1.4 × 10 ⁶	
5	\Diamond	NACA 66-009	Plain	1.93	0.11	1.4 × 10 ⁶	60
6	Δ	NACA 63,4-417.8) approx.	Internally balanced	Approach- ing 1.00	0.17	2.5 × 10 ⁶	61
7	∇	NACA 66(2x15)-216, a = 0.6	Internally balanced	Approach- ing 1.00	0.18	5.3 × 10 ⁶	61
8	D	NACA 66(2x15)-116, a = 0.6	Internally balanced	Approach- ing 1.00	0.14	6.0 × 10	61
9	٥	NACA 64,2-(1.4 X13.5)	Plain	Approach- ing 1.00		13.0 × 10 ⁶	
10	7	NACA 65,2-318 approx.	Internally balanced	Approach- ing 1.00	0.14	6.0 × 10 ⁶	61
11	4	NACA 63(420)-521 approx.	Internally balanced	Approach- ing 1.00		8.0 × 10 ⁶	
12	<u>\</u>	NACA 66(215)-216 a = 0.6	Internally balanced	Approach- ing 1.00	0.20 to 0.48	2.8 × 10 ⁶ 6.8 × 10 ⁶	62
13	Δ	NACA 66(215)-014	Plain	1.93	0.09	1.2 × 10 ⁶	63
1/4	Q	NACA 66(215)-216 a = 0.6	Plain	Approach- ing 1.00		6.0 × 10 ⁶	
15	۵	NACA 652-415	Plain	Approach- ing 1.00	0.13	6.0 × 10 ⁶	64
16	<u> </u>	NACA 65 ₃ -418	Plain	Approach- ing 1.00	0.13	6.0 × 10 ⁶	64
17	TQ	NACA 65 ₁ -421	Plain	Approach- ing 1.00	0.13	6.0 × 10 ⁶	64
18	\$	NACA 65(112)-213	Internally balanced	Approach- ing 1.00	0.14	8.0 × 10 ⁶	
19	\\ \alpha	NACA 745A317 approx.	Internally balanced	Approach- ing 1.00	0.13	6.0 × 10 ⁶	
20	\$	NACA 64,3-013 approx.	Internally balanced	Approach- ing 1.00	0.13	6.0 × 10 ⁶	
21	♦	NACA 64,3-1(15.5) approx.	Internally balanced	Approach- ing 1.00	0.13	6.0 × 10 ⁶	

NATIONAL ADVISORY COMMITTEE FOR AERONAUTICS



(b) δ range from 0° to 20° .

Figure 59.- Variation of section aileron effectiveness with aileron chord ratio for true-airfoil-contour ailerons without exposed overhang balance on a number of airfoil sections; gaps sealed; $c_1 = 0$.

(Symbols designating different airfoil sections are identified in table III.)

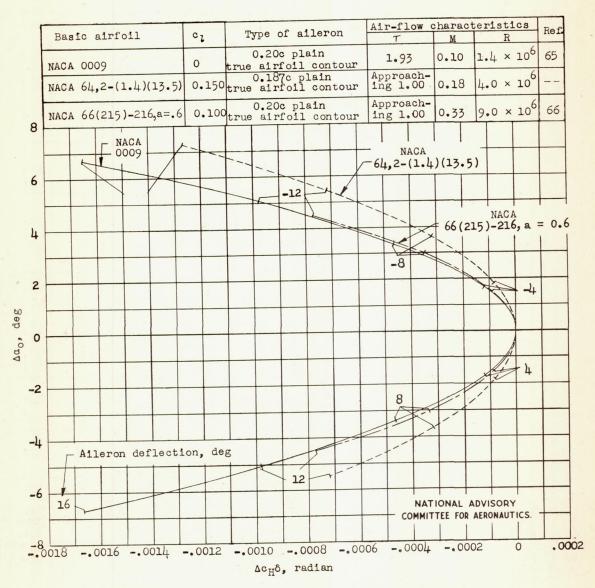


Figure 60.- Variation of the hinge-moment parameter $\Delta c_H \delta$ with the equivalent change in section angle of attack required to maintain a constant section lift coefficient for deflection of the aileron on the NACA 0009, NACA 64,2-(1.4)(13.5), and NACA 66(215)-216, a = 0.6 airfoil sections; gaps sealed.

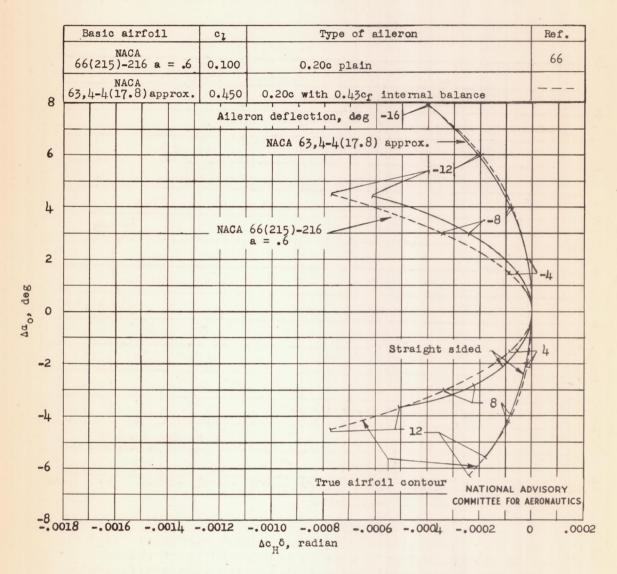


Figure 61.- Variation of the hinge-moment parameter $\Delta c_{\rm H} \delta$ with the equivalent change in section angle of attack required to maintain a constant section lift coefficient for deflection of true-airfoil-contour and straight-sided ailerons on the NACA 66(215)-216, a = 0.6, and the NACA 63,4-4(17.8) (approx.) airfoil sections; gaps sealed.

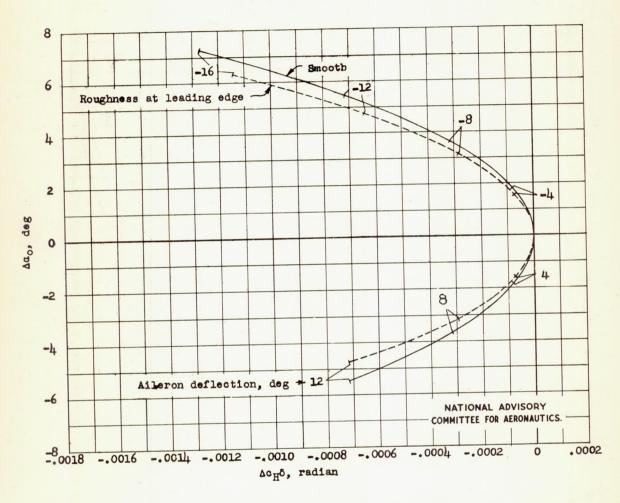


Figure 62.- Variation of the hinge-moment parameter ΔcHδ with the equivalent change in section angle of attack required to maintain a constant section lift coefficient for deflection of the aileron on the NACA 64,2-(1.4)(13.5) airfoil section smooth and with roughness at the leading edge of the airfoil. (For description of aileron, see fig. 60.)

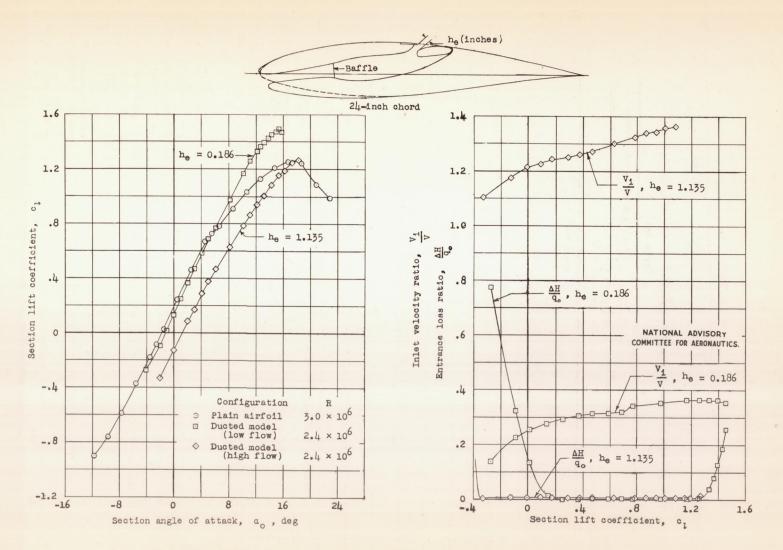


Figure 63.- Lift and flow characteristics of an NACA 7-series type airfoil section with leading-edge air intake.

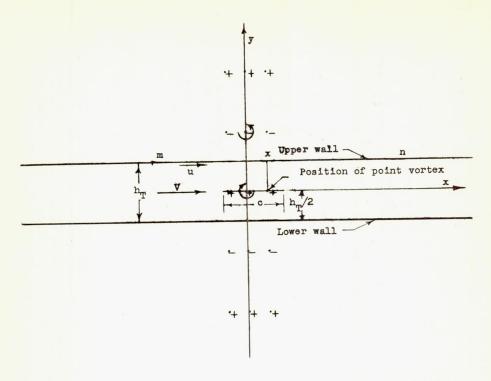


Figure 64.- Image system for calculation of $\,\eta\text{-factor}$ in the Langley two-dimensional low-turbulence tunnels.

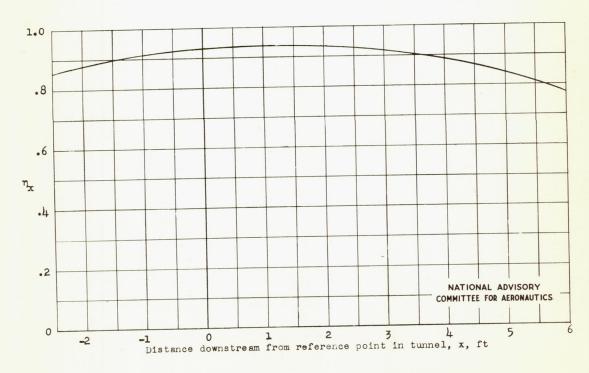


Figure 65.- Lift efficiency factor $\eta_{\mathbf{X}}$ for a point vortex situated at various positions along the center line of the tunnel.

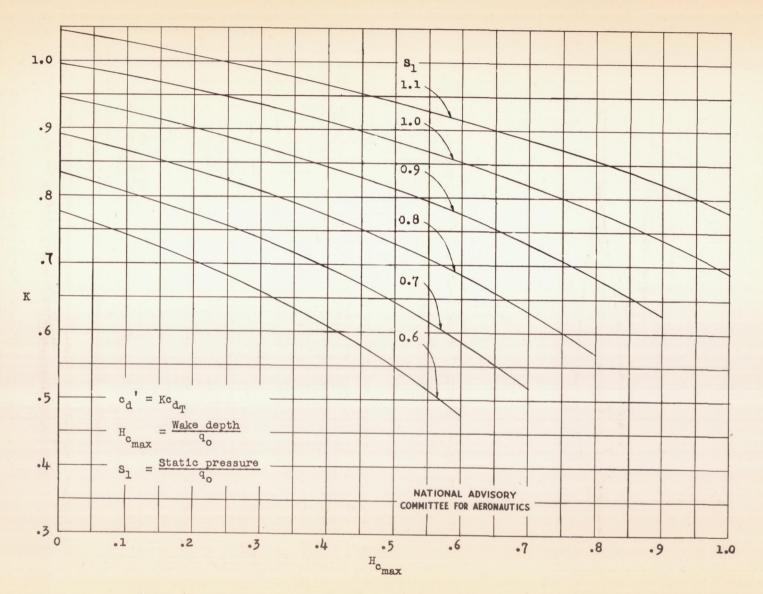


Figure 66.- Plot of K as a function of $\mathrm{H}_{\mathbf{C}_{\text{max}}}$ with S_1 as a parameter.

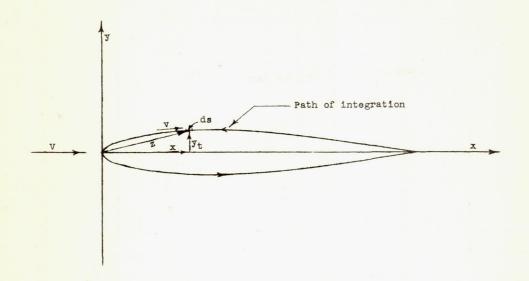


Figure 67.- Sketch for derivation of A-factor.

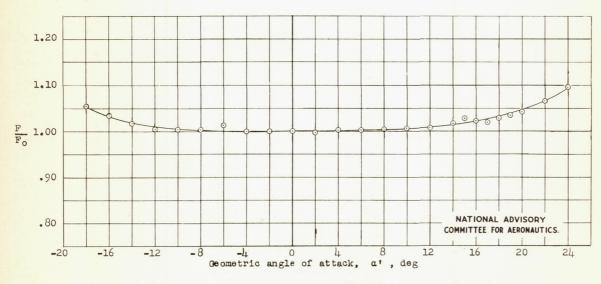


Figure 68.- Additional blocking factor at the tunnel walls plotted against angle of attack for the NACA 643-418 airfoil.

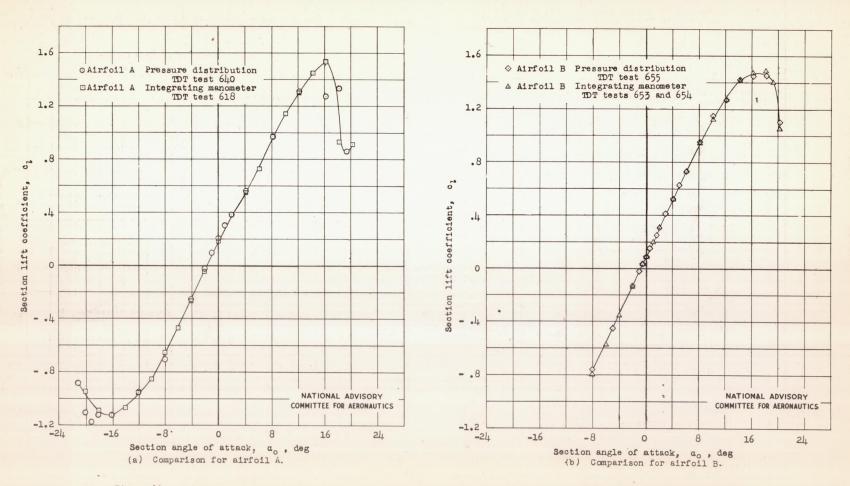


Figure 69.- Comparison between lifts obtained from pressure-distribution measurements and lifts obtained from reactions on the floor and ceiling of the tunnel.

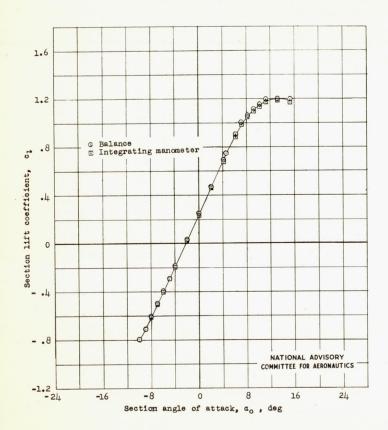


Figure 70.- Comparison between balance measurements and lifts obtained from reactions on the floor and ceiling of the tunnel.

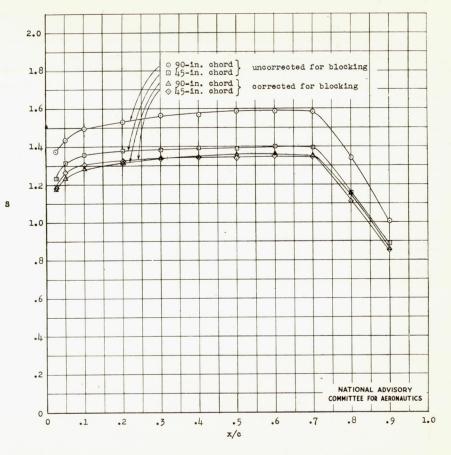


Figure 71.- Comparison between corrected and uncorrected pressure distributions for two chord sizes of a symmetrical NACA 6-series airfoil of 15-percent thickness. $\alpha_{\rm O}=0^{\circ}.$

SUPPLEMENTARY DATA

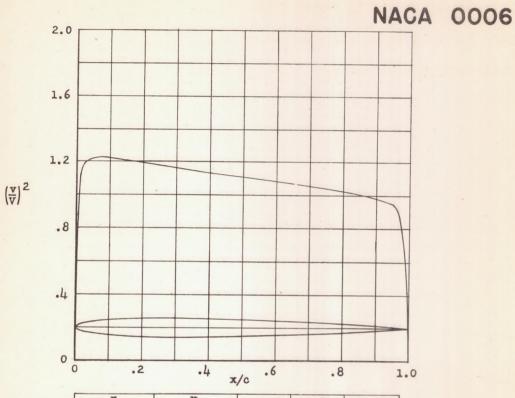
I - BASIC THICKNESS FORMS

NACA ACR No. L5CO5

		I - BASIC	;	TI	HIC	KN	E	SS	FC	RI	1S				S2
	NACA	0006 basic thickness form	n									,			S4
	NACA	0008 basic thickness form	n												S4a
	NACA	0009 basic thickness form	a												S5
	NACA	0010 basic thickness form	n												S5a
	NACA	0012 basic thickness form	1												s6
	NACA	0015 basic thickness form	1												S7
	NACA	0018 basic thickness form	1										. •		s8
	NACA	0021 basic thickness form	1												\$9
	NACA	0024 basic thickness form	1												S10
	NACA	16-006 basic thickness fo	r	m											Sll
	NACA	16-009 basic thickness fo	r	m											S12
	NACA	16-012 basic thickness fo	r	m											S13
	NACA	16-015 basic thickness fo)I"	m											S14
	NACA	16-018 basic thickness fo	r	m											S15
	NACA	16-021 basic thickness fo	r	m											S16
	NACA	63,4-020 basic thickness	f	or	m										S17
	NACA	63-006 basic thickness fo	r	m											Sl7a
	NACA	63-009 basic thickness fo	r	m											S17b
	NACA	63-010 basic thickness fo	M	m											Sl7c
		631-012 basic thickness f													
		632-015 basic thickness f													
		633-018 basic thickness f													
]	NACA	63h-021 basic thickness for	01	rm											Sl7g

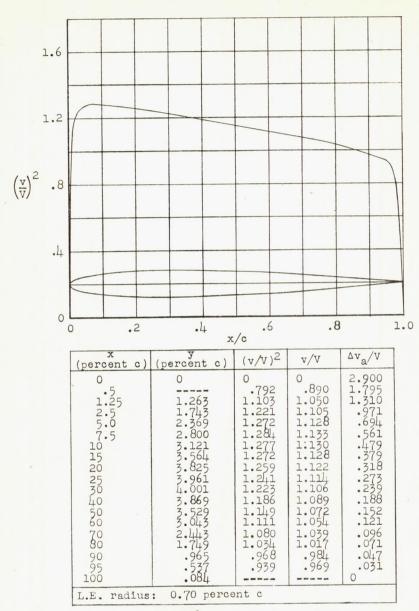
NACA	642-015 basic thickness form .									S20
NACA	643-018 basic thickness form .									S21
NACA	644-021 basic thickness form .									522
NACA	65,2-016 basic thickness form									S23
NACA	65,2-023 basic thickness form									S24
NACA	65,3-018 basic thickness form									S25
NACA	65-006 basic thickness form .									S25a
	65-008 basic thickness form .									
NACA	65-009 basic thickness form .							٠		S25c
	65-010 basic thickness form .									
NACA	651-012 basic thickness form .									S27
	652-015 basic thickness form .									
	653-018 basic thickness form .									
NACA	654-021 basic thickness form .									S30
	66,1-012 basic thickness form									
NACA	66,2-015 basic thickness form									S32
NACA	66,2-018 basic thickness form									S33
NACA	66-006 basic thickness form .									S33a
NACA	66-008 basic thickness form .									S33b
NACA	66-009 basic thickness form .		•						•	S33c
NACA	66-010 basic thickness form .			,						S33d
NACA	661-012 basic thickness form .									S34
NACA	662-015 basic thickness form .									S35
NACA	663-018 basic thickness form .									s36

NACA ACR No. L5C05	S3a
NACA 664-021 basic thickness form	S37
NACA 67,1-015 basic thickness form	s38
NACA 747A015 basic thickness form	S39

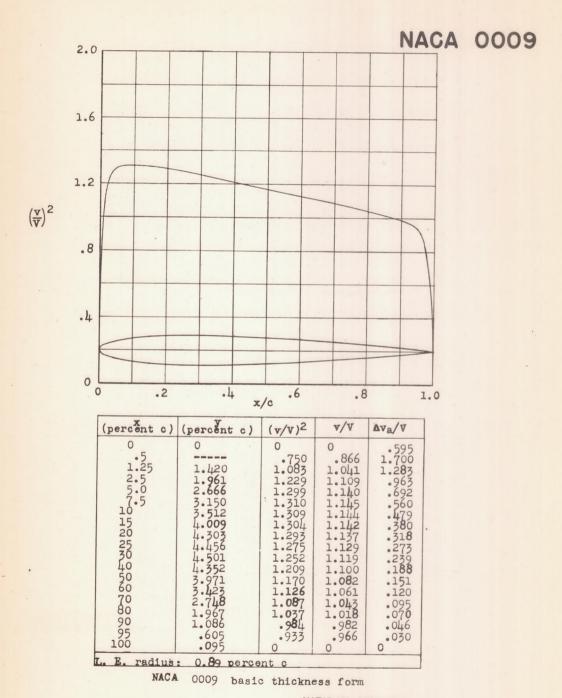


NACA 0006 basic thickness form

NACA 0008

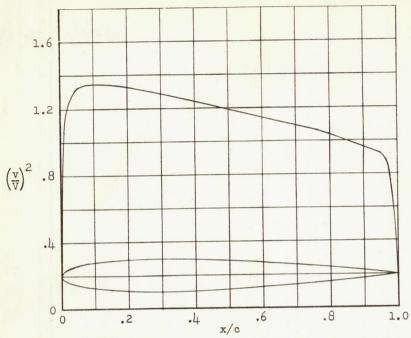


NACA 0008 basic thickness form



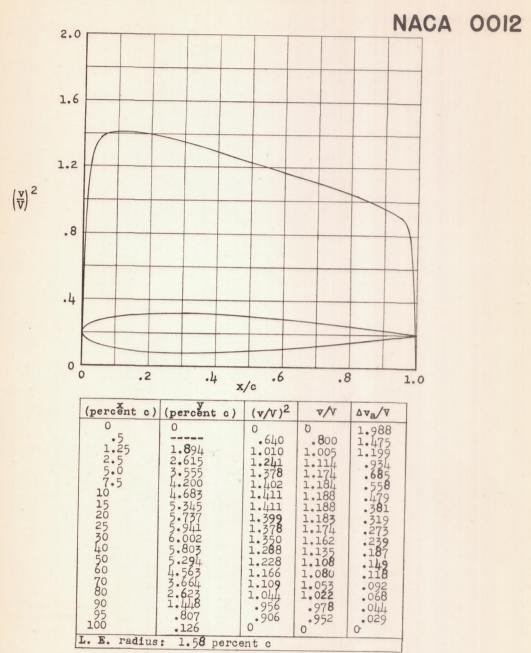
NATIONAL ADVISORY COMMITTEE FOR AERONAUTICS.

NACA OOIO

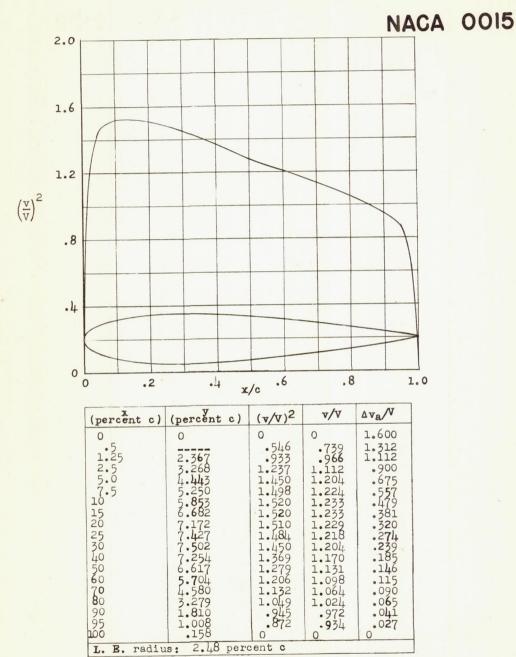


(percent c)	(percent c)	$(v/V)^2$	v/v	Δv _a /V
0 1.25 2.5 5.0 7.5 10 15 20 25 30 40 50 70 80 90 90 90 100	0 1.578 2.178 2.178 2.960 3.960 3.9455 4.782 4.950 4.803 3.2.803 3.2.803 3.2.803 3.2.803 3.2.803	0 .712 1.061 1.237 1.325 1.341 1.341 1.329 1.309 1.237 1.190 1.138 1.094 1.040 .925	0 .844 1.030 1.112 1.151 1.158 1.158 1.153 1.144 1.133 1.112 1.046 1.046 1.046 1.020	2.72 1.6155 .6959 .438 .225 .438 .2238 .150 .0045 .0045 .0045 .0045 .0045

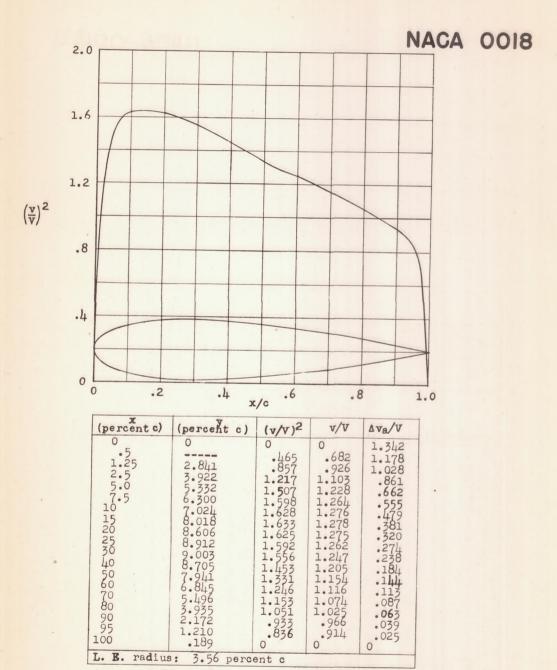
NACA 0010 basic thickness form



NACA 0012 basic thickness form

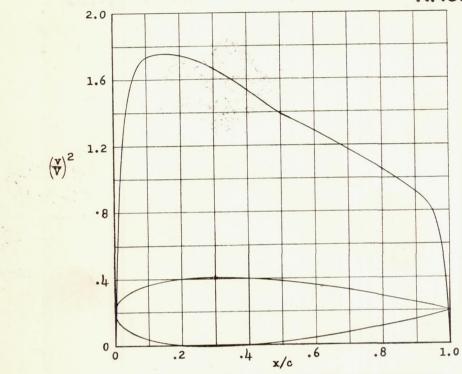


NACA 0015 basic thickness form



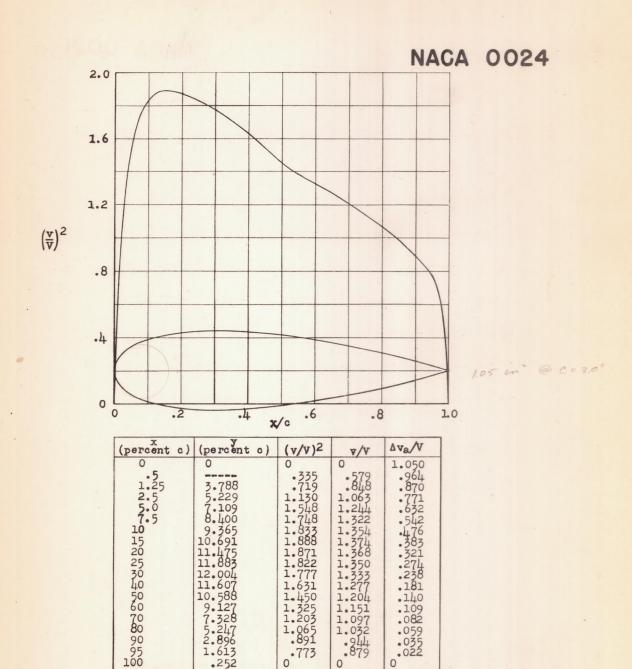
NACA 0018 basic thickness form





(percent c)	(percent c)	$(v/v)^2$	v/v	Δv _a /v
0 •555 2•5 5 •5 •5 •5 •6 •6 •6 •6 •6 •6 •6 •6 •6 •6	3.315 4.576 6.221 7.350 8.195 9.354 10.040 10.504 10.504 10.504 10.5504 10.556 9.265 7.986 6.412 4.591 2.534 1.412	0 37723324626488847756 11.56835406488847756 11.7638847756 11.7638847756 11.763884 11.0980 10.0	0 .630 .887 1.242 1.247 1.317 1.325 1.320 1.3290 1.178 1.178 1.087 .957 .895	1.167 1.0656 .948 .648 .5478 .320 .2738 .142 .081 .081 .0923
L. E. radius	s: 4.85 perc	ent c		

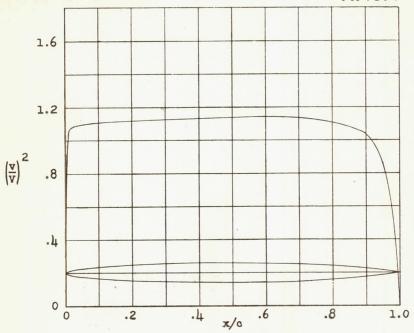
NACA 0021 basic thickness form



NACA 0024 basic thickness form

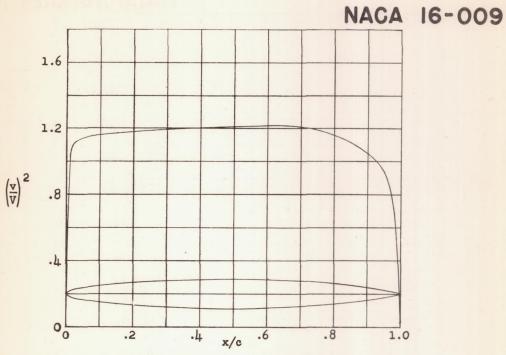
1.613 .252 L. E. radius: 6.33 percent c





(percent c)	(percent c)	(v/V) ²	v/v	Δv _a /V	
01.25 25.05 25.05 105 200 300 450 600 780 9950	0 .903 1.255 1.516 1.729 2.067 2.332 2.709 2.927 3.000 2.917 2.6399 1.259 .707	0 1.059 1.085 1.097 1.105 1.112 1.116 1.123 1.132 1.132 1.131 1.132 1.141 1.132 1.104	0 1.029 1.042 1.047 1.051 1.055 1.057 1.060 1.064 1.068 1.064 1.051 1.017	5.471 1.376 .980 .689 .557 .476 .379 .244 .196 .160 .130 .104 .077 .049 .032	
L. E. radius: 0.176 percent c					

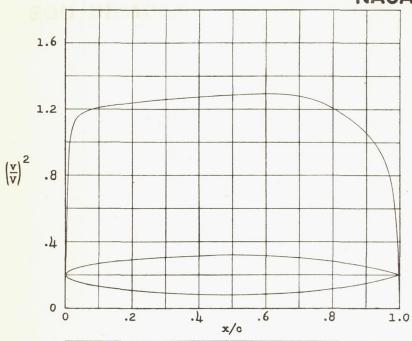
NACA 16-006 basic thickness form



1.25	(percent c)	(percent c)	$(v/v)^2$	v/v	Δva/V
90 1.888 1.043 1.022 .01	2.5 7.0 10 150 20 40 50 780 995	1.354 1.824 1.822 2.5901 2.5901 3.40691 4.5762 3.9948 4.5762 3.1881	1.109 1.139 1.152 1.158 1.168 1.177 1.190 1.202 1.211 1.214 1.206 1.156 1.043	1.021 1.053 1.067 1.073 1.076 1.081 1.085 1.091 1.096 1.100 1.106 1.099 1.075	3.644 1.334 6.655 1.477 3.768 1.477 1.657 1.760

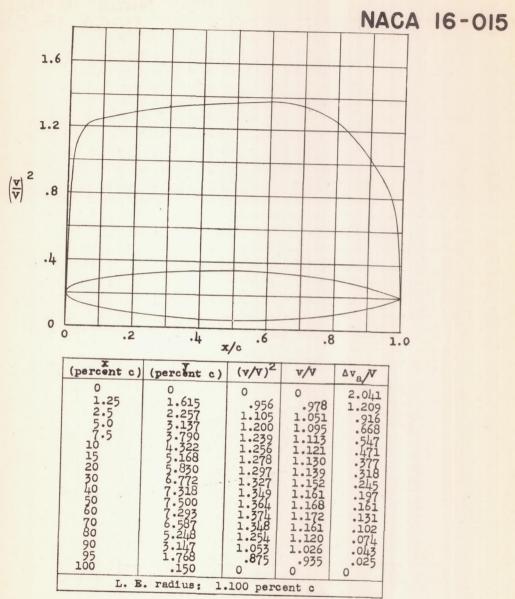
NACA 16-009 basic thickness form





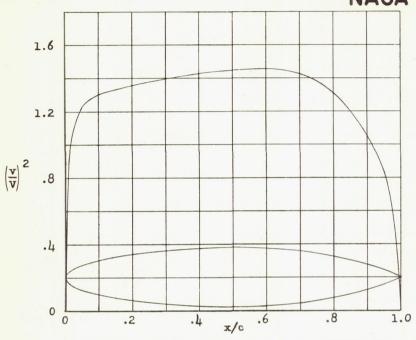
(percent c)	(percent c)	(v/V) ²	v/V	Δv _{a/} V
0 1.25	0 11.85035754750 280035754750 11.85033699756 11.85033699750 11.85033699750 11.85033699750 11.85033699750	0 1.002 1.109 1.173 1.208 1.2237 1.237 1.276 1.276 1.275 1.275 1.275 1.203	0 1.001 1.053 1.093 1.099 1.106 1.112 1.121 1.128 1.137 1.129 1.025 .953	2.624 1.268 .942 .677 .551 .473 .378 .319 .245 .197 .161 .102 .075 .045
L. I	3. radius: 0	.703 per	cent c	

NACA 16-012 basic thickness form



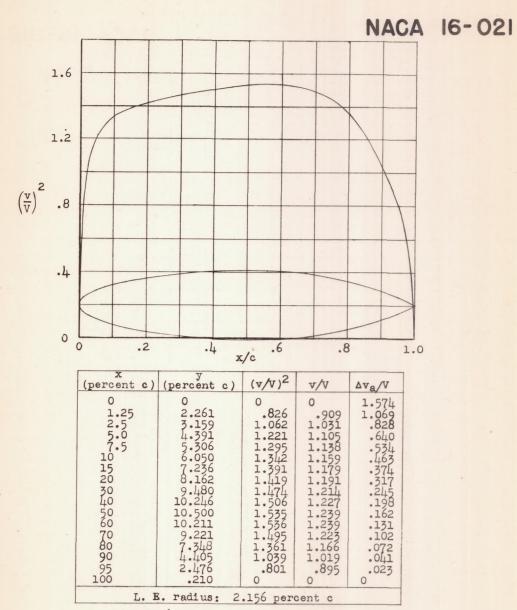
NACA 16-015 basic thickness form

NACA 16-018

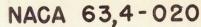


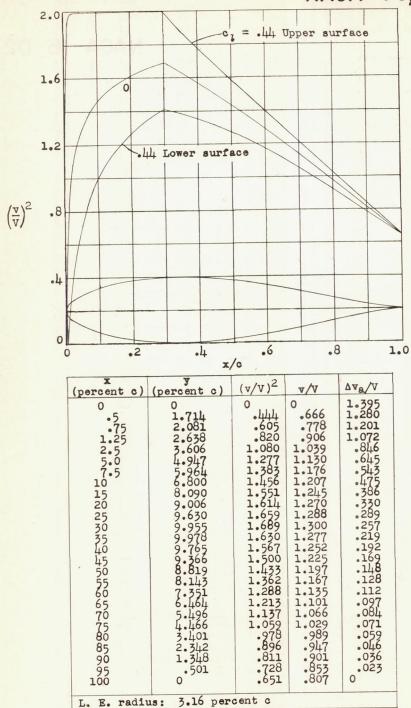
(percent c)	(percent c)	(v/v) ²	v/V	Δva/V
01.55 25 7.50 105 150 150 150 150 150 150 150 150 1	0 1.388	0 .903 1.092 1.217 1.271 1.332 1.3357 1.447 1.452 1.452 1.306 1.051	0 .950 1.045 1.103 1.141 1.154 1.183 1.203 1.203 1.205 1.194 1.025	1.744 1.140 .883 .6571 .4686 .3718 .1982 .1312 .0024 0
L. 1	s. radius: 1	.584 per	cent c	

NACA 16-018 basic thickness form



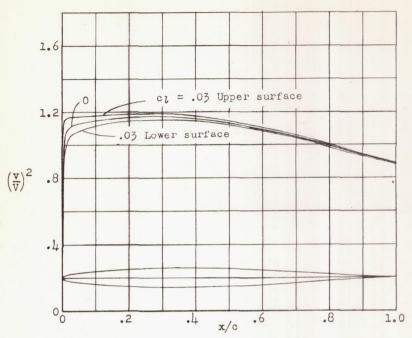
NACA 16-021 basic thickness form





NACA 63,4-020 basic thickness form

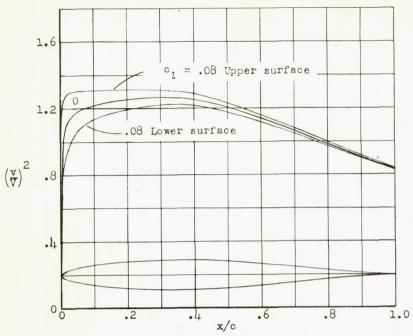
NACA 63-006



percent c)	(percent c)	$(v/v)^2$	V/V	ΔVa/V
0 12570 5725 5 12570 12050 10050 100	0 5099 77572 11,7666 12,0866 12,0866 12,0866 12,0866 12,0866 12,0866 12,0866 12,0866 13,0866 14,7610 14,7610 14,7610 14,7610 16,0866 16,08	0 .973 1.050 1.080 1.110 1.149 1.159 1.165 1.170 1.170 1.161 1.170 1.151 1.177 1.196 1.094 1.094 1.094 1.094 1.094 1.094 1.088	0 986 1.025 1.039 1.069 1.077 1.079 1.082 1.079 1.084 1.075 1.047 1.047 1.023 1.010 1.098 1.099	1.399 .981 .692 .562 .484 .384 .321

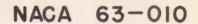
NACA 63 -006 basic thickness form
NATIONAL ADVISORY
COMMITTEE FOR AERONAUTICS

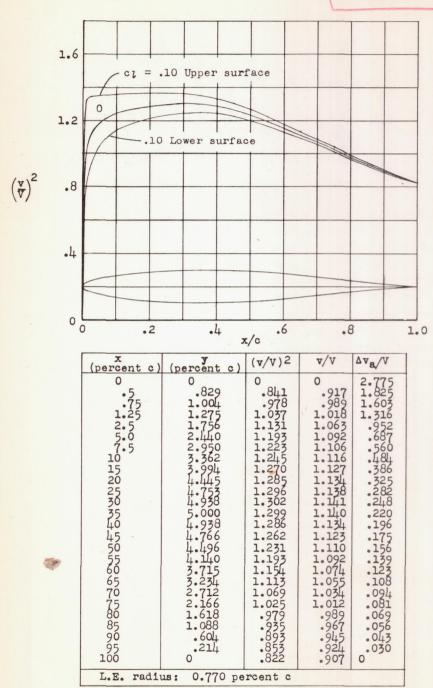
NACA 63-009



percent c) (po 0 .75 1.25 2.5 7.5 10 15 20 25 30	0 •749 •906	.885	0 .941	3.058 1.889
250 50 50 50 50 50 50 50 50 50 50 50 50 5	1122333344444443332211	1.002 1.051 1.180 1.202 1.245 1.2266	1.001 1.025 1.063 1.086 1.098 1.105 1.114 1.120 1.125 1.120 1.111 1.099 1.084 1.051 1.032 1.012 992 971 950 950 950 950	1

NACA 63-009 basic thickness form



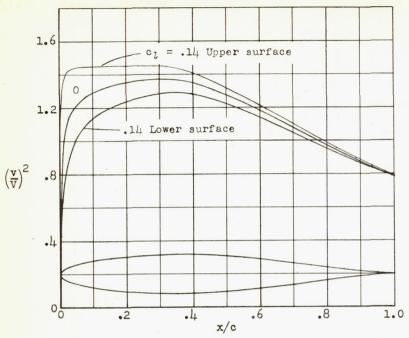


NACA 63 -010 basic thickness form

NATIONAL ADVISORY

COMMITTEE FOR AERONAUTICS

NACA 631-012



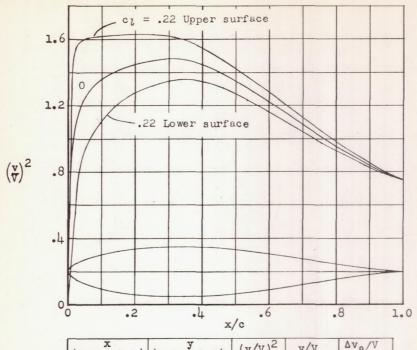
(percent c)	(percent c)	(v/v) ²	v/V	Δva/V
0 •••• 5725 5725 5 1225 70 150 50 50 50 50 50 50 50 50 50 50 50 50 5	0 11510252 989492 98949 989492 98949 989492 98949	0 7525 1.0059 1.22614 1.2294 1.3367 1.337668 1.337668 1.337669 1.33679 1.3679 1.3679 1.3679 1.3679 1.3679 1.3679 1.3699 1.3699 1.3699	0 .866 .9033 1.0633 1.1238 1.1531 1.167 1.169 1.1648 1.1399 1.0873 1.0873 1.0899 1.9899 99399	2.336 1.695 1.5136 .685 1.263 .682 .559 .484 .3876 .283 .221 .1961 .1757 .121 .1061 .0797 .0429 0
L.E. radius: 1.087 percent c				

NACA 631-012 basic thickness form

NATIONAL ADVISORY

COMMITTEE FOR AERONAUTICS

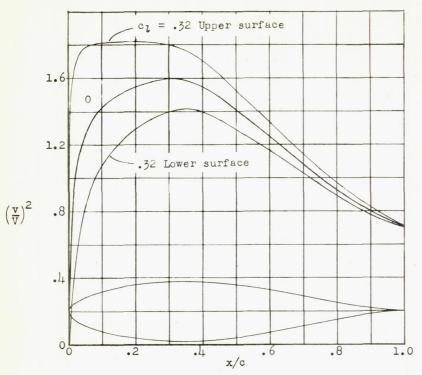
NACA 632-015



v/v v/v

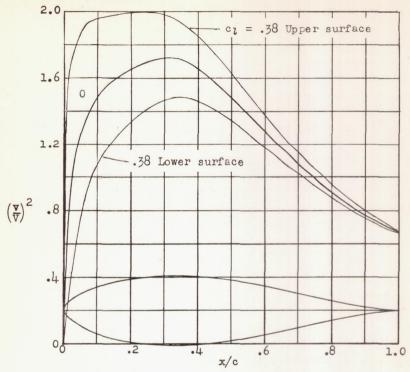
NACA 632-015 basic thickness form
NATIONAL ADVISORY
COMMITTEE FOR AERONAUTICS

NACA 633-018



NACA 633-018 basic thickness form
NATIONAL ADVISORY
COMMITTEE FOR AERONAUTICS

NACA 634-021



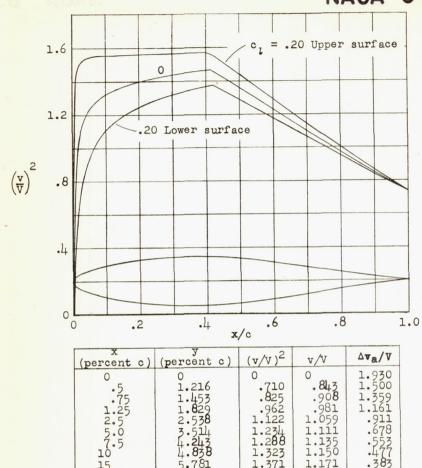
(percent c)	(percent c)	(v/v) ²	v/V	ΔVa/V
0 125 70505050505050505050505050505050505050	0 1.952 7.506.20 1.05.25 1.	0 275 564 1010 1.260 1.394 1.487 1.555 1.658 1.721 1.709 1.578 1.779 1.480 1.280 1.280 1.280 1.280 1.280 1.280 1.280 1.280 1.280 1.280 1.280 1.280 1.280 1.280 1.676	0 .524 .751 1.005 1.122 1.181 1.219 1.262 1.303 1.312 1.307 1.286 1.256 1.216 1.175 1.132 1.086 1.091 .916 .880 .8149 .822	1.439 1.236 1.156 1.034 8.42 6.530 4.484 3.392 2.555 1.98 1.730 1.130 1.12 0.96 0.81 0.068 0.057 0.023 0
L.E. radius: 2.650 percent c				

NACA 634-021 basic thickness form

NATIONAL ADVISORY

COMMITTEE FOR AERONAUTICS

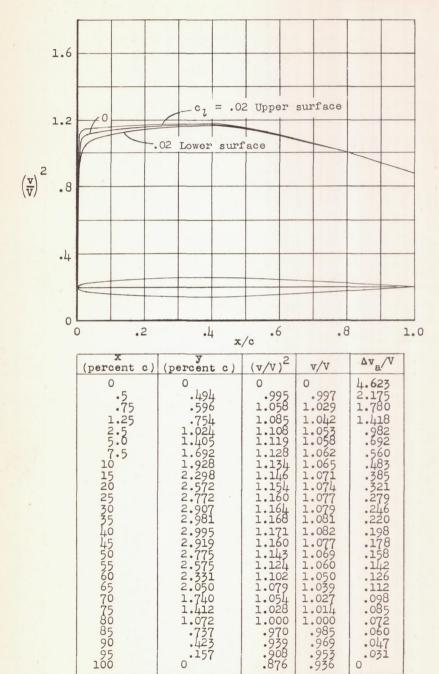
NACA 64,2-015



(percent c)	(percent c)	(v/V) ²	v/V	∆va/V
0 125705 572505 12570505050505050505050	0111234456677777666544886811 215231458147776665174488669153099655	0 710 .8252 1.2288 1.3288 1.3421 1.4459 1.4459 1.4566 1.2266 1.1039 9710 9710 9710 9710 9710 9710 9710 971	0 843 981 1.959 1.111 1.155 1.171 1.184 1.200 1.207 1.192 1.207 1.199 1.111 1.005 1.019 9.01 9.01 9.01 9.01 9.01 9.01 9.0	1.930 1.500 1.359 1.161 .911 .678 .553 .477 .383 .225 .253 .227 .175 .137 .102 .086 .080 .071 .039 .027
L. E. radius: 1.65 percent c				

NACA 64,2-015 basic thickness form

NACA 64 - 006

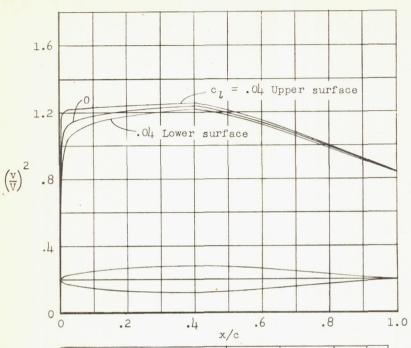


NACA 64 - 006 basic thickness form

L.E. radius: 0.256 percent c

.031

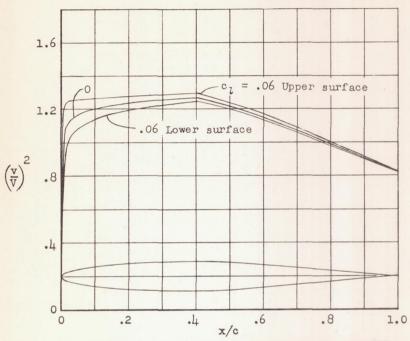
NACA 64-008



(percent c)	(percent c)	(v/v) ²	v/v	Δv _a /V
0 •7725 •725 •50 •5725 •65 •65 •65 •65 •65 •65 •65 •65 •65 •6	0 .658 .794 1.005 1.365 1.875 2.259 2.574 3.069 3.437 3.704 3.979 3.988 3.411 3.081 2.704 2.291 1.404 .550 .206	0 .912 1.016 1.084 1.127 1.152 1.167 1.179 1.225 1.230 1.225 1.230 1.163 1.133 1.102 1.063	0 955 1.008 1.041 1.062 1.080 1.086 1.099 1.107 1.109 1.111 1.105 1.078 1.064 1.050 1.034 1.050 1.034 1.050 1.034 1.050 1.034 1.050 1.034 1.050 1.034 1.050 1.034 1.050 1	3.544 1.994 1.686 1.6867 9.688 5.560 1.480 1.768 1.125 1.100 1.096 1.098 1.096
L.E. radius	: 0.455 per	cent c		

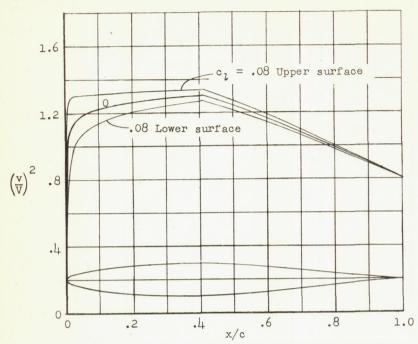
NACA 64-008 basic thickness form

NACA 64-009



NACA 64 - 009 basic thickness form

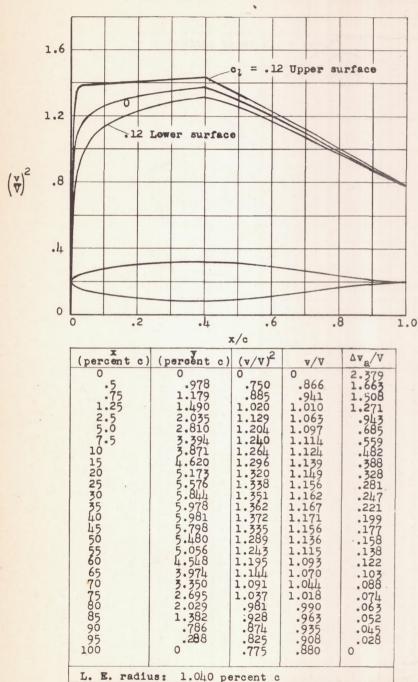
NACA 64 - 010



(percent c)	(percent c)	$(v/V)^2$	v/V	Δva/V
0 • 5 5 5 5 5 5 5 5 5 5 5 5 5 6 5 6 5 6 5	0 .9890 .9890 1.7346 2.822 3.8224 4.8622 2.83534 4.980 8.3638 4.980 8.3638 4.980 8.3638 4.980 8.3638 9.203 2.6338 4.980 8.3638 2.7276 1.6718 0	0 834 962 1.061 1.130 1.181 1.206 1.245 1.262 1.275 1.286 1.279 1.241 1.161 1.1080 1.086 990 850 855	0 .913 .981 1.030 1.087 1.098 1.105 1.123 1.129 1.134 1.131 1.131 1.096 1.077 1.058 1.058 1.972 .949 .922 .897	2.815 1.817 1.5813 1.517 1.5580 1.3157 1.5580 1.328 1.21420 1.158 1.139 1.1095 1.069 1.069 1.030
L.E. radius: 0.720 percent c				

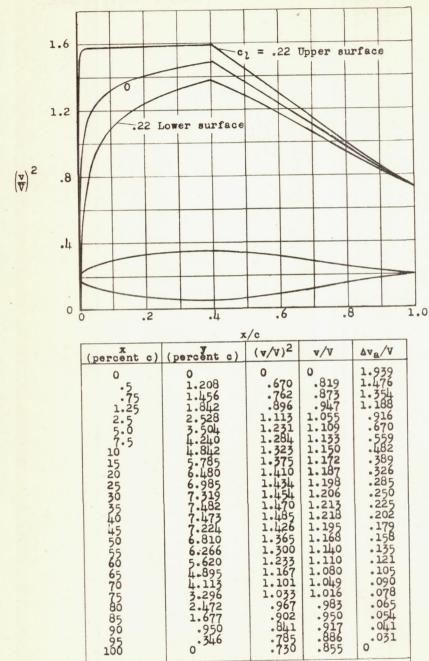
NACA 64 - 010 basic thickness form

NACA 64,-012



NACA 64, -012 basic thickness form

NACA 642-015



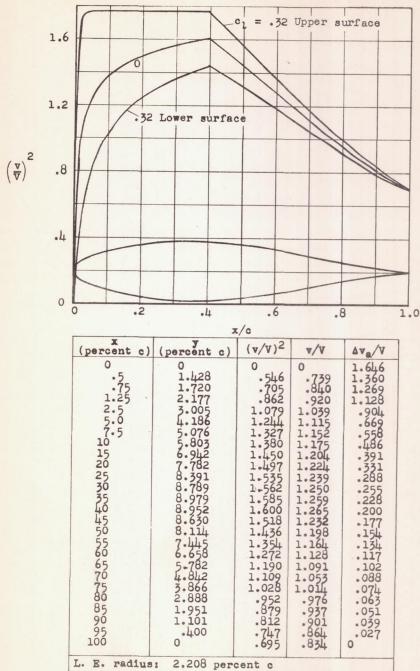
NACA 642-015 basic thickness form

L. E. radius: 1.590 percent c

NATIONAL ADVISORY COMMITTEE FOR AERONAUTICS.

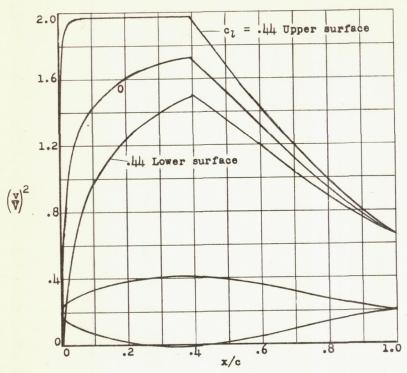
0.031

NACA 643-018



NACA 643-018 basic thickness form

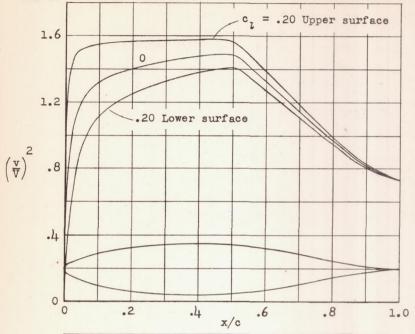
NACA 64-021



0
0.01

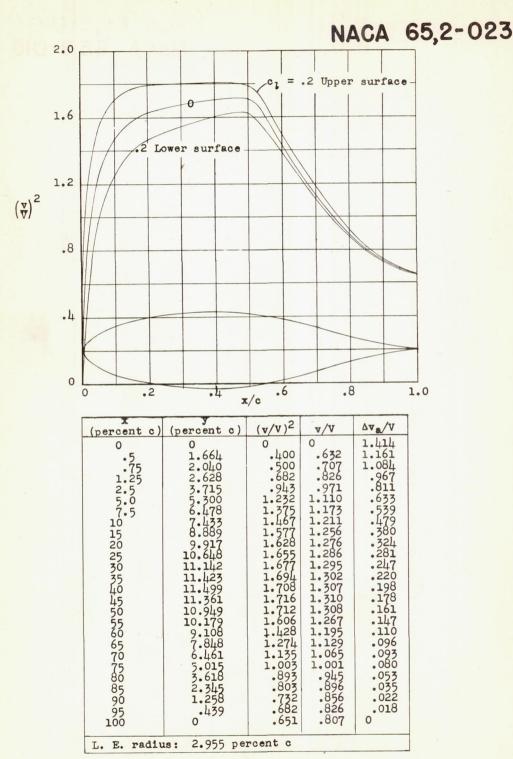
NACA 644-021 basic thickness form

NACA 65,2-016



21/0					
(percent c)	(percent c)	$(v/v)^2$	v/V	Δva/V	
0 .5555 7.255 1.2550 5 1.50 5 1.50 250 5 1.50 5 1.5	011123445677777777654321 011123445677777777654321 0	0 5690 60928	0 748 8318 1 033 1 134 1 152 1 174 1 187 1 205 1 218 1 221 1 192 1 152 1 111 1 028 985 944 3 856	1.950 1.650 1.500 1.275 .920 .545 .480 .5255 .225 .225 .200 .180 .140 .125 .066 .050 .045	
L. E. radius: 1.704 percent c					

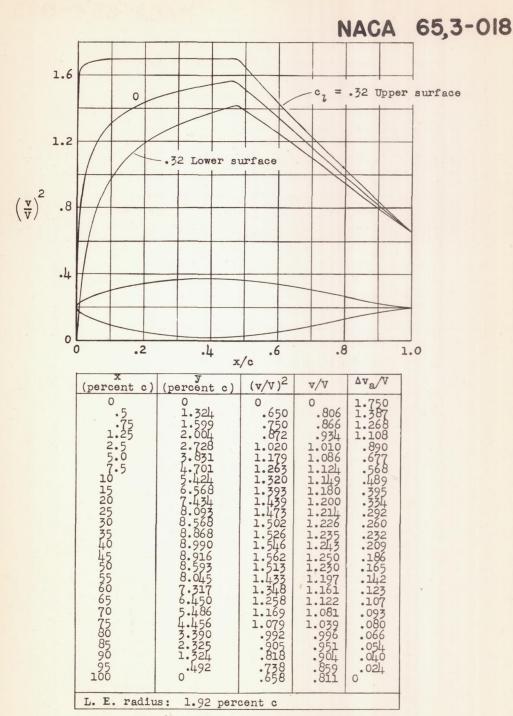
NACA 65,2-016 basic thickness form



NACA 65,2-023 basic thickness form

NATIONAL ADVISORY

COMMITTEE FOR AERONAUTICS.

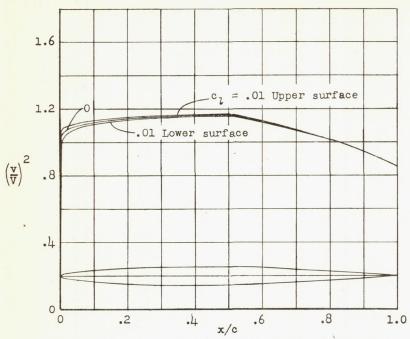


NACA 65,3-018 basic thickness form

NATIONAL ADVISORY

COMMITTEE FOR AERONAUTICS.

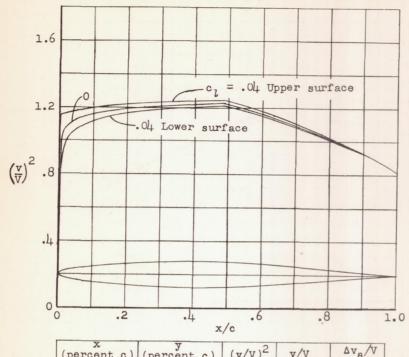
NACA 65-006



(percent c)	(percent c)	(√∆) 3	v/V	$\Delta v_a/V$
0	0 .474 .77510 .5717510 .5717510 .57189447 .57189447 .57189447 .57189447 .57189 .5718	0 1.044 1.055 1.063 1.100 1.112 1.120 1.149 1.159 1.165 1.166 1.165 1.165 1.165 1.164 1.100 1.07 1.044 1.003 1.043 1.043 1.043 1.043 1.043 1.043 1.044 1.043 1.044 1.043 1.044	0 1.022 1.027 1.031 1.049 1.058 1.065 1.075 1.077 1.078 1.079 1.079 1.036 1.049 1.036 1.049 1.036 1.049 1.036 1.049	4.815 2.110 1.780
L.E. radiu	s: 0.240 per	cent c		

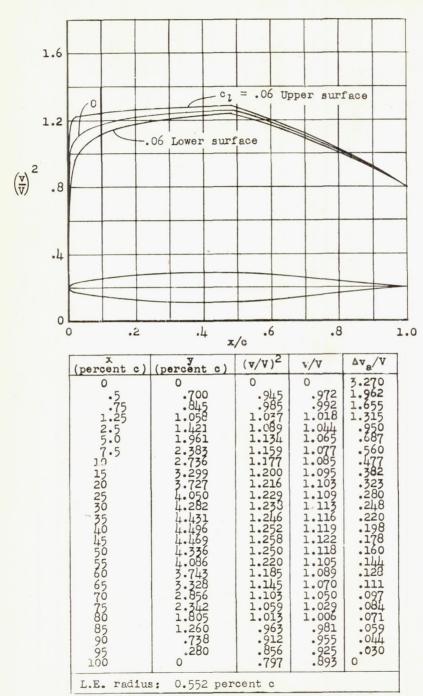
NACA 65 - 006 basic thickness form

NACA 65-008



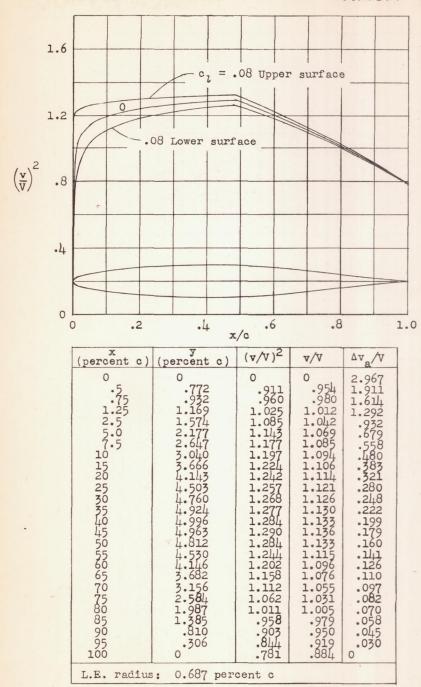
NACA 65 - 008 basic thickness form

NACA 65-009



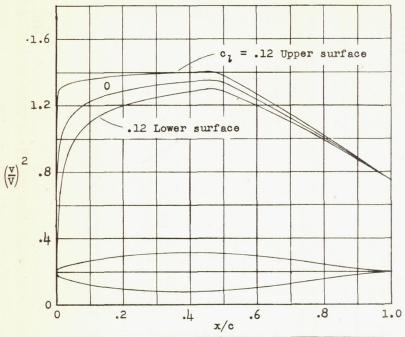
NACA 65 - 009 basic thickness form

NACA 65 - 010



NACA 65 - 010 basic thickness form

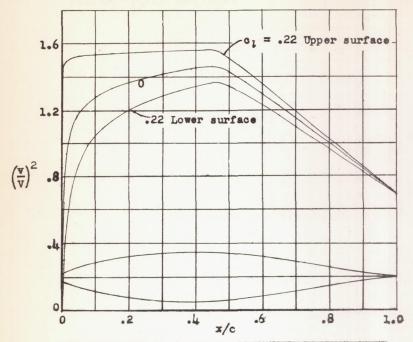
NACA 65,-012



(percent c)	(percent c)	(v/v) ²	v/v	Δv _a /V	
0	397562725662797231395076 913861649747997231395076 91112334455555554433321 0	0	0 99004786006887449925985056554055 110067655 1111111111111111111111111111111111	2.444 1.776 1.465 1.465 1.7668 97068 4889 3285 22088 1.4271 1.971 1.0076 1.004	
L. E. radius: 1.000 percent c					

NACA 651-012 basic thickness form

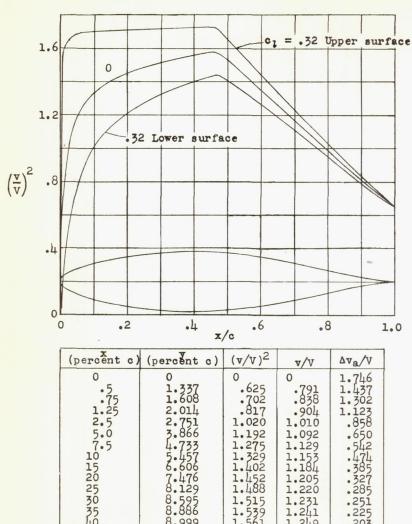
NACA 652-015



	(percent c)	(percent c)	(▼ / ▼) ²	v/V	ΔVa/V
	0 ••••• 572505 12257050505050505050505050505050505050505	0 11.3562 12562 12562 15562 15562 15562 15562 15562 15562 15562 15662 1677 1677 1677 1677 1677 1677 1677 1	0 6544 93634 1.1841 1.281 1.3777 1.4438 1.4564 1.3697 1.2251 1.0024 6846 7697	0 .809 .904 .9631 1.088 1.112 1.156 21.191 1.199 1.2010 1.197 1.103 1.00	2.0799602377340577340 1.3799668877340577340 1.1199688286 1.11997688286 0.05326
L	L. E. rac	lius: 1.505	percent	С	

NACA 652-015 basic thickness form

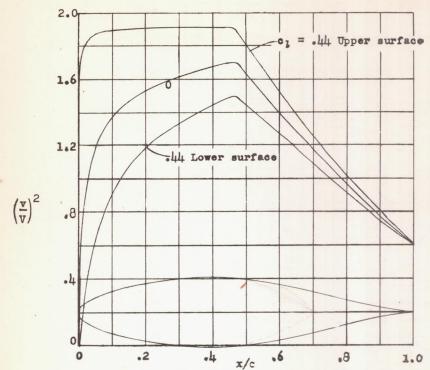
NACA 653-018



75

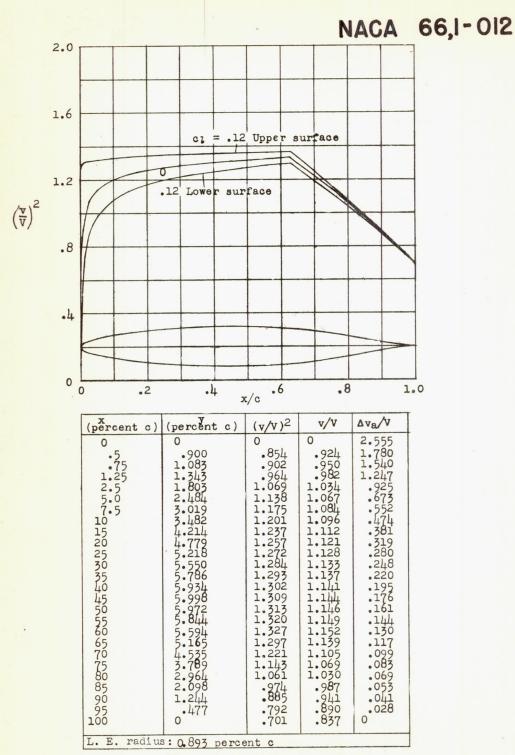
NACA 653-018 basic thickness form

NACA 654-021



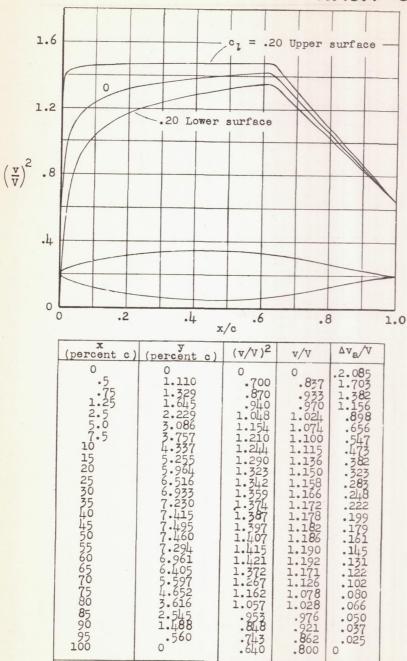
(percent c)	(percent c)	(V/V)2	v/V	Ava/V
0 1257050 572505 12570505050505050505050	22814282 238014282 52830147982 52830147982 52830147982 52830147982 529000749662 529008443 529008443 529087653 52100 529087653 52100 529087653 52100 52008 52	0 5107400 5	0 .717 .7769 .860 .989 1.171 1.2257 1.2257 1.228 1.2296 1.307 1.228 1.2288 1.2288 1.2288 1.2288 1.288	1.531 1.2063 8.649 1.2063 8.65478 8.5289 1.201 1

NACA 654-021 basic thickness form



NACA 66,1-012 basic thickness form

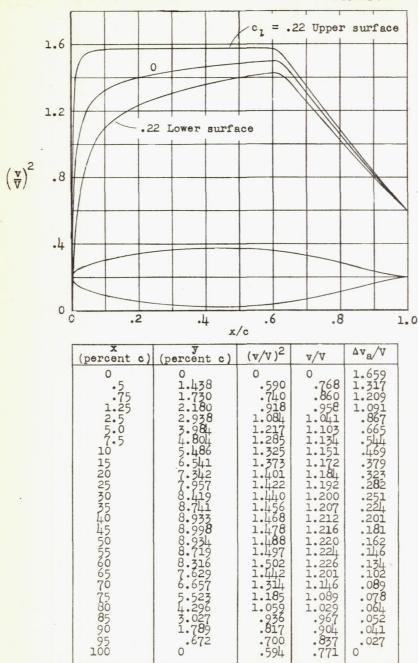
NACA 66,2-015



NACA 66,2-015 basic thickness form

L. E. radius: 1.384 percent c

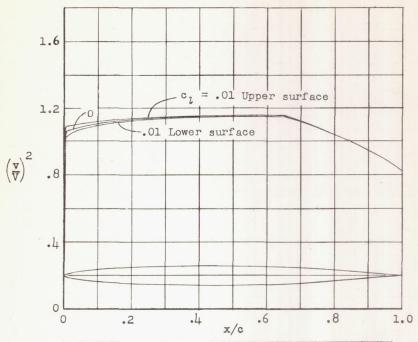
NACA 66,2-018



NACA 66,2-018 basic thickness form

L. E. radius: 2.30 percent c

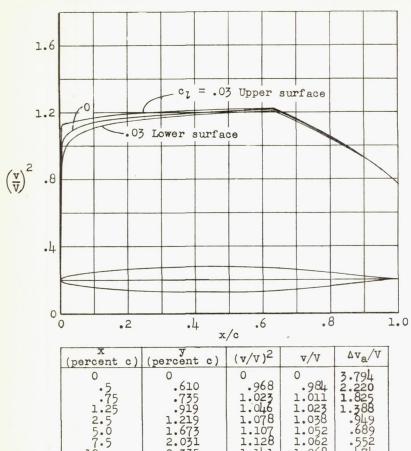
NACA 66 - 006



v
.5

NACA 66 - 006 basic thickness form

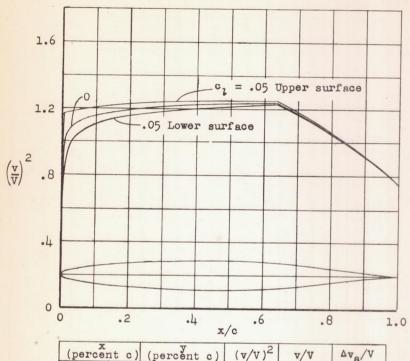
NACA 66-008



(percent c)	(percent c)	(v/v) ²	v/v	Δv _a /V
0 125705 572505 12570505050505050505050	0 .610 .7359 .92173 .22735 .238201 .22.38201 .22.38201 .22.38201 .24.78620 .24.78620 .24.7745624 .25.24667 .26.2467 .26.24	0 968 1.048 1.076 1.128 1.178 1.178 1.178 1.196 1.205	0 984 1.0113 1.023 1.0352 1.0688 1.0762 1.0885 1.0998 1.0998 1.0996 1.0965 1.09	794 220 1 8258 9 6852 1 779 1 8779 1 8779 1 8779 1 8779 1 8779 1 1988 1 1087
L.E. radius	0.411			

NACA 66 - 008 basic thickness form

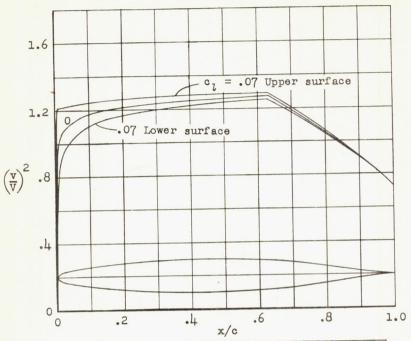
NACA 66-009



(percent c)	(percent c)	(v/v) ²	v/v	Δv _a /V
0 125.50 125.70 125	0 -874 -8230 -88230 -888 -888 -888 -888 -888 -888 -888 -8	0 .930 .999 1.036 1.079 1.119 1.178 1.190 1.210 1.221 1.222 1.237 1.240 1.237 1.172 1.172 1.172 1.173 1.050 .985 .915 .839 .747	0 .964 .9999 1.018 1.039 1.069 1.077 1.085 1.091 1.091 1.105 1.105 1.108 1.114 1.109 1.083 1.055	3.352 2.100 1.750 1.340 .946 .5473 .323 .2846 .2220 .197 .178 .161 .145 .130 .146 .100 .085 .077 .048
L.E. radius	: 0.530 per	cent c		

NACA 66 - 009 basic thickness form

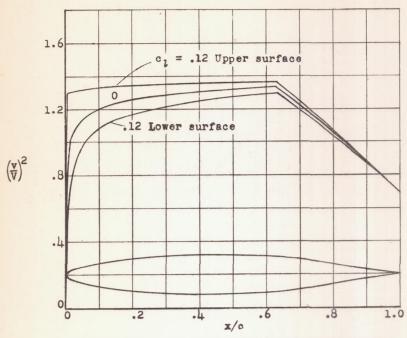
NACA 66-010



x (percent c)	(percent c)	$(v/v)^2$	v/v	Δv _a /V
5.725 5.725 10.505 10.5	0	0	0 .947 .986 1.011 1.038 1.061 1.074 1.095 1.107 1.115 1.118 1.095 1.127 1.118 1.0959 1.026 .989 .9514	3.002 2.012 1.686 1.296 .931 .473 .3722 .2146 .229 .198 .161 .146 .130 .114 .085 .070 .027
L.E. radiu	s: 0.662			

NACA 66 - 010 basic thickness form

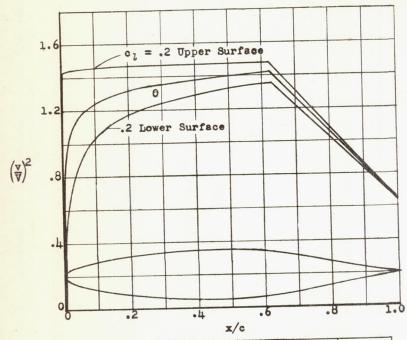
NACA 661-012



(percent c)	(percent c)	(v/v) ²	v/V	Ava/V							
0 • 12 5 7 5 5 5 12 5 7 6 5 0 5 0 5 0 5 0 5 0 5 0 5 0 5 0 5 0 5	6788676418837056895174344 90850939303604063831648377 908509393930360406383115790024	0 .800 .980378 .980378 1.1704 1.225797 1.22293318 1.330221 1.3530221 1.0968 .8788 .887	0 .894 .957 .936 1.067 1.122 1.129 1.134 1.145 1.145 1.150 1.154 1.141 1.067 1.026 .938 .829	2.569 1.847 1.5757 1.52513 2.475 2.3883 2.246 2.221 2.176 2.1152 2.1158 2.0849 2.053							
L. E. radius: 0.952 percent c											

NACA 661-012 basic thickness form

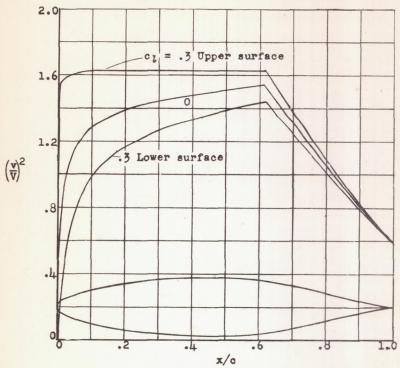
NACA 662-015



(percent c)	(percent c)	$(v/v)^2$	V/V	Ava/V
0 5755 12.5 5725 10 50 50 50 50 50 50 50 50 50 50 50 50 50	01112334556677777766554321 01112334556677777766554321 01112334556677777766654321	0 .760 .840 .929 1.168 1.2048 1.3456 1.3570 1.3570 1.3570 1.420 1.	0 .872 .916 .961 .1027 1.078 1.099 1.114 1.158 1.164 1.179 1.184 1.192 1.169 1.122 1.075 1.026 .9740 .929 .799	2.139 1.652 1.431 1.895 .6637 .5473 .3822 .280 .2482 .200 .1636 .1313 .096 .085 .025 0
L. E. radius	s: 1.435 pe	rcent c		

NACA 662-015 basic thickness form

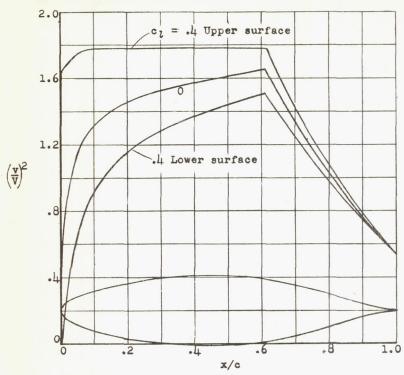
NACA 663-018



(percent c)	(percent c)	(v/v) ²	v/v	ΔVa/V
0 • 7755 • 1.2 5 • 10 50 50 50 50 50 50 50 50 50 50 50 50 50	011123456777888888888765421 01112345677888888888766446	0	0 .806 .857 .897 1.002 1.111 1.134 1.162 1.180 1.202 1.210 1.223 1.238 1.238 1.199 1.083 1	1.773 1.456 1.312 1.121 .858 .649 .545 .282 .250 .223 .201 .181 .163 .147 .131 .114 .095 .061 .048 .037 .022
L. E. radius	: 1.955 per	cent c		

NACA 663-018 basic thickness form

NACA 664-021

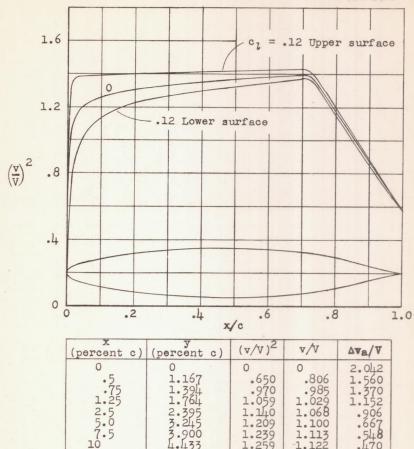


NACA 664-021 basic thickness form

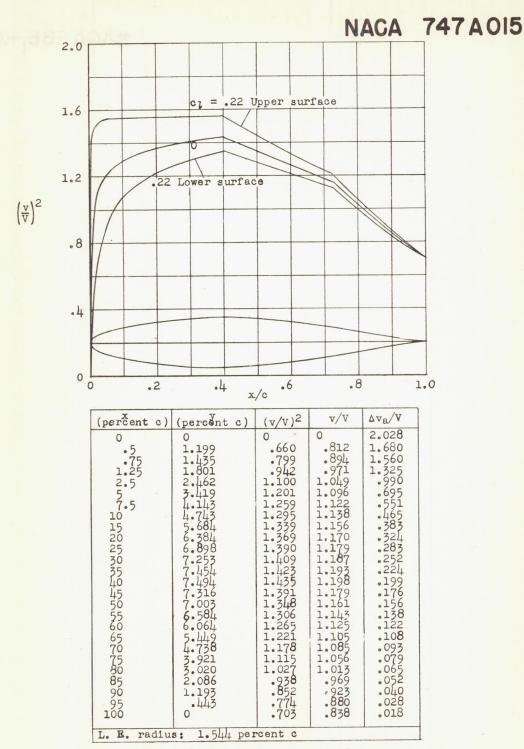
NATIONAL ADVISORY

COMMITTEE FOR AERONAUTICS

NACA 67,1-015



NACA 67,1-015 basic thickness form

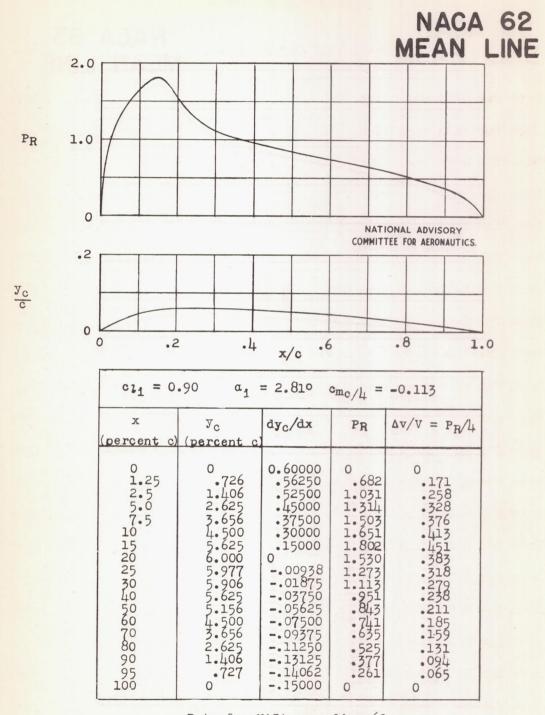


NACA 747A015 basic thickness form

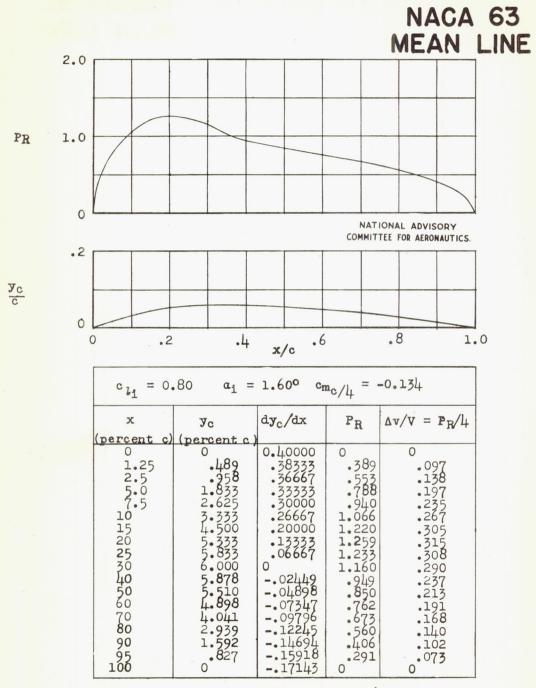
II - MEAN LINES

NACA ACR No. L5CO5

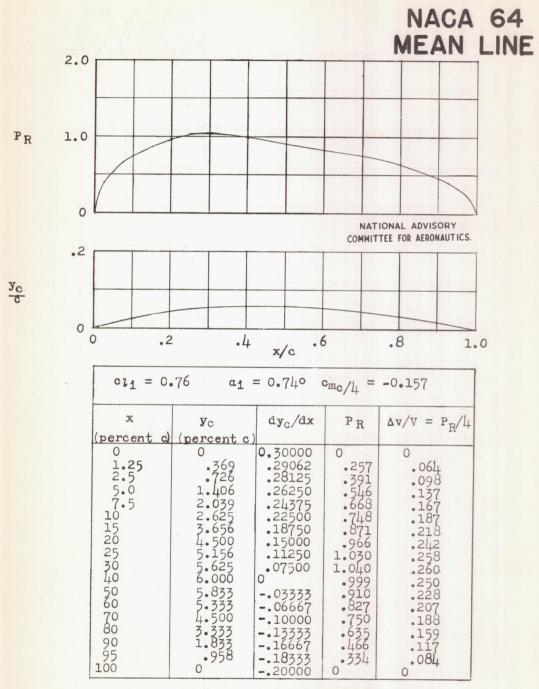
					I	I	-	M	CAI	I	II	VES	5						S41
Data	for	NACA	mean	line	62														S42
Data	for	NACA	mean	line	63														S43
Data	for	NACA	mean	line	64														S44
Data	for	NACA	mean	line	65														S45
Data	for	NACA	mean	line	66														S46
Data	for	NACA	mean	line	67														S47
Data	for	NACA	mean	line	210														548
Data	for	NACA	mean	line	220		,												S49
Data	for	NACA	mean	line	230														S50
Data	for	NACA	mean	line	240														S51
Data	for	NACA	mean	line	250														S52
Data	for	NACA	mean	line	а	=	0												S53
Data	for	NACA	mean	line	a	=	0.	1											S54
Data	for	NACA	mean	line	а	=	0.	2											S55
Data	for	NACA	mean	line	a	=	0.	3											S56
Data	for	NACA	mean	line	a	=	0.	4	٠										S57
Data	for	NACA	mean	line	а	=	0.	5											S58
Data	for	NACA	mean	line	а	=	0.	6											S59
Data	for	NACA	mean	line	a	=	0.	7											s60
Data	for	NACA	mean	line	a	=	0.	8											s61
Data	for	NACA	mean	line	8.	=	0.	9											s62
Data	for	NACA	mean	line	a	=	1.	0											s63



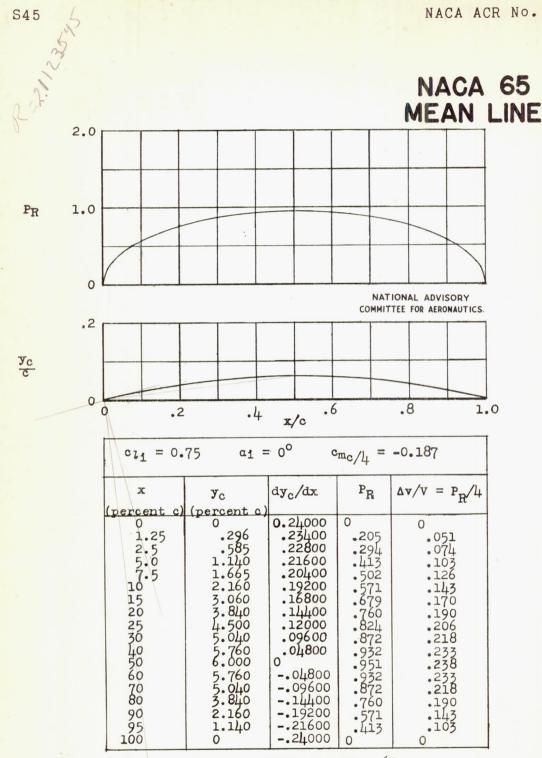
Data for NACA mean line 62



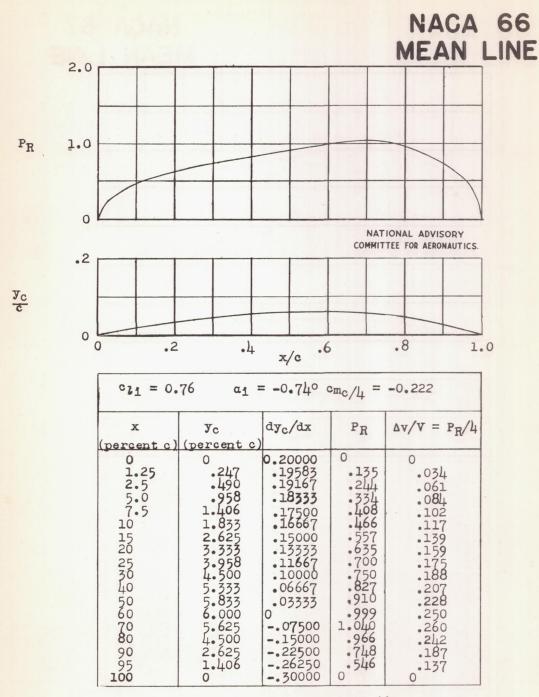
Data for NACA mean line 63



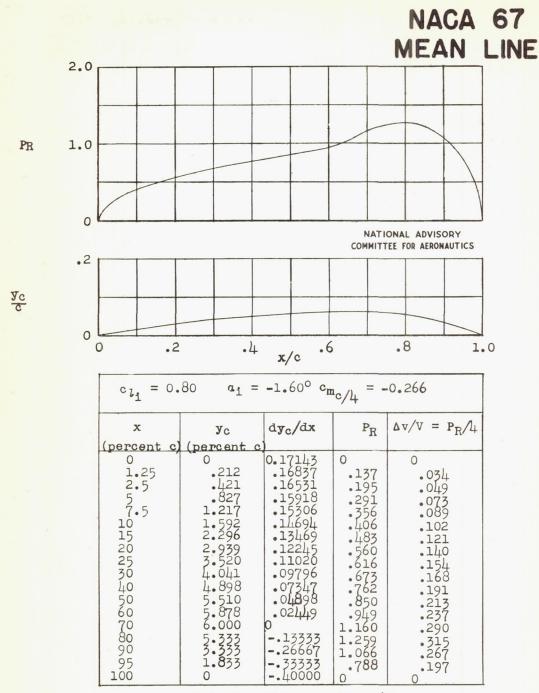
Data for NACA mean line 64



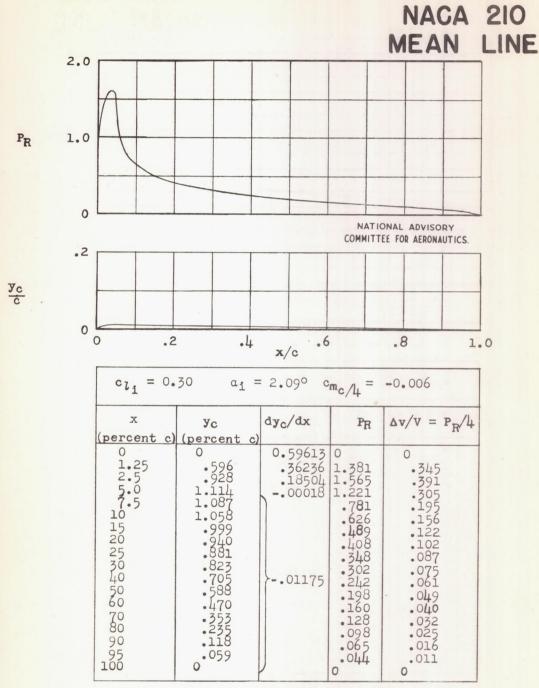
Data for NACA mean line 65



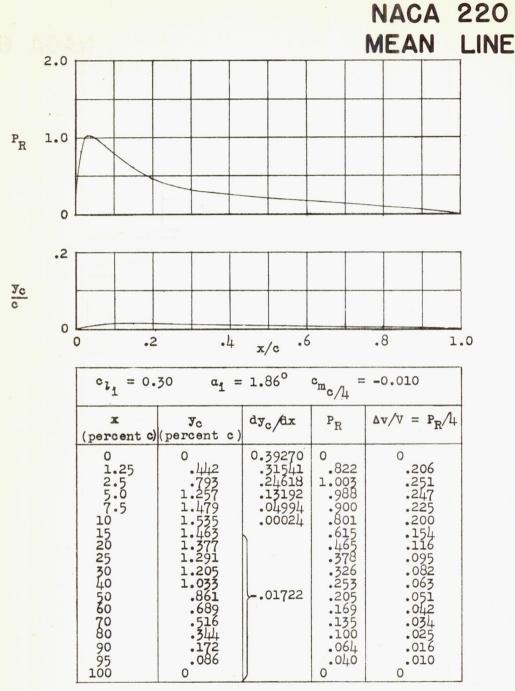
Data for NACA mean line 66



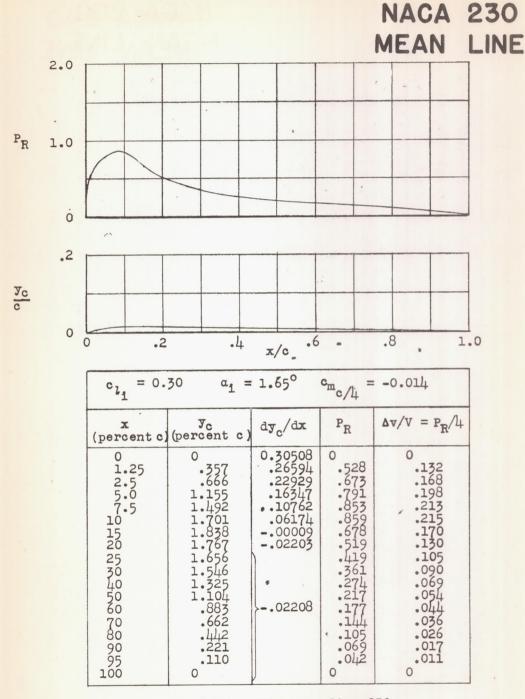
Data for NACA mean line 67



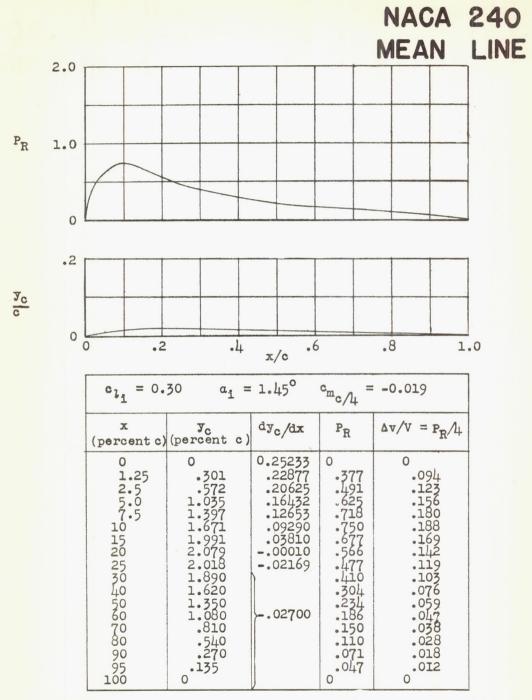
Data for NACA mean line 210



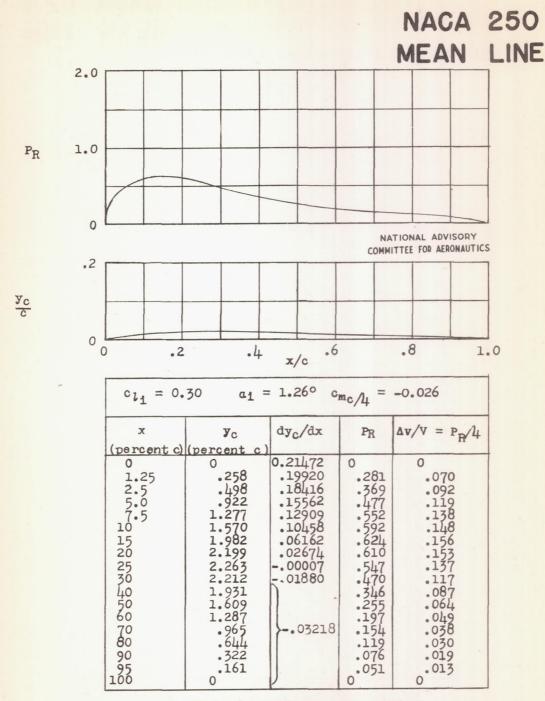
Data for NACA mean line 220



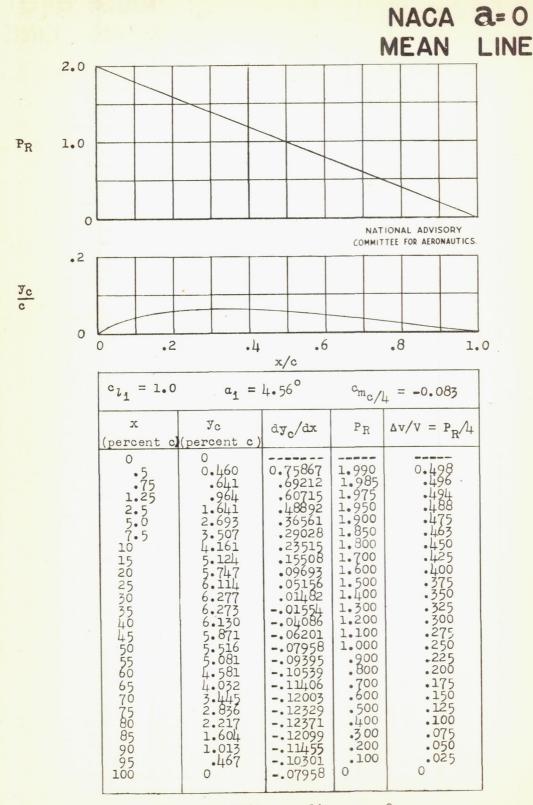
Data for NACA mean line 230



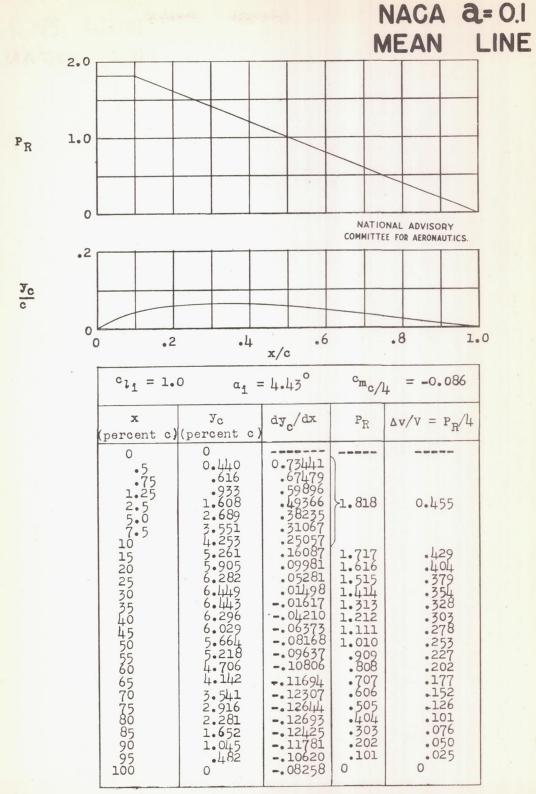
Data for NACA mean line 240



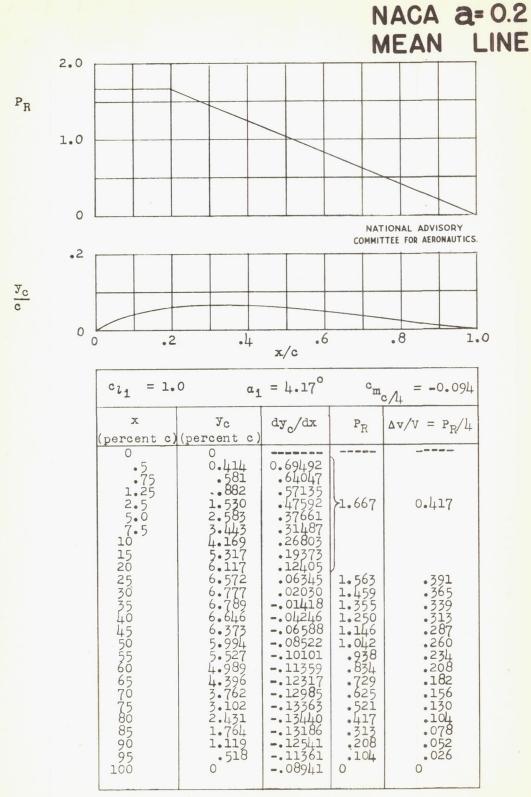
Data for NACA mean line 250



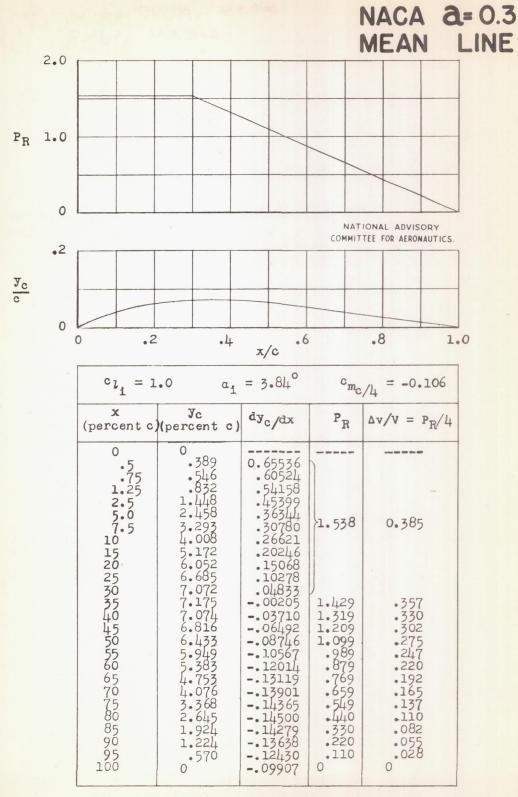
Data for NACA mean line a = 0



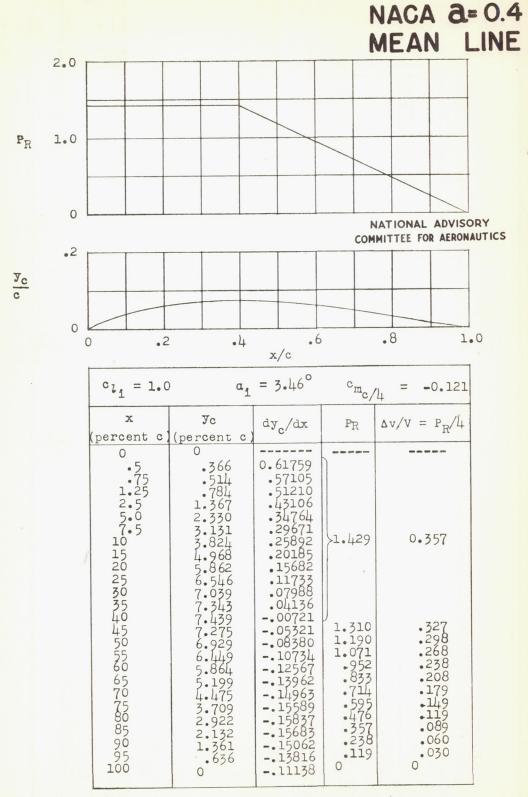
Data for NACA mean line a = 0.1



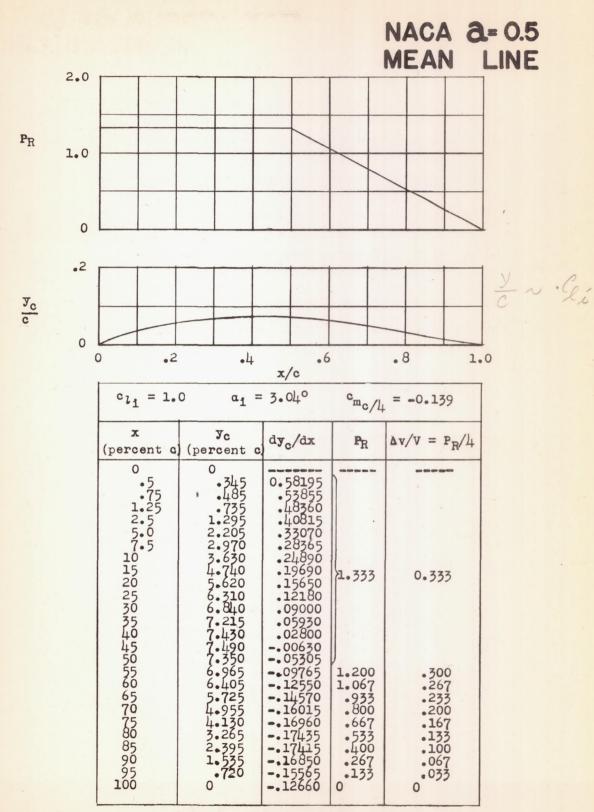
Data for NACA mean line a = 0.2



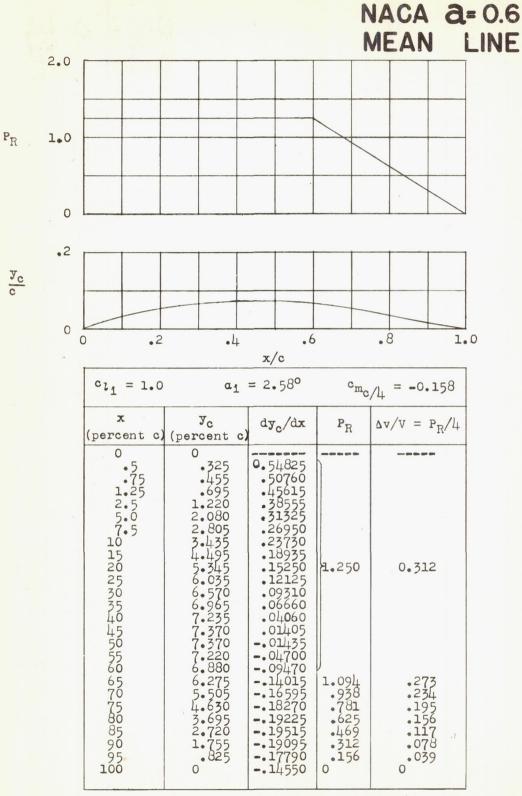
Data for NACA mean line a = 0.3



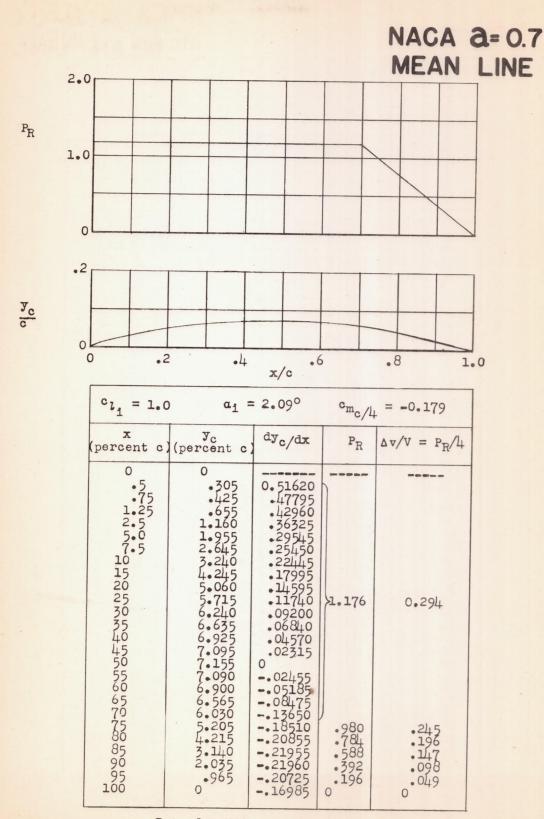
Data for NACA mean line a = 0.4



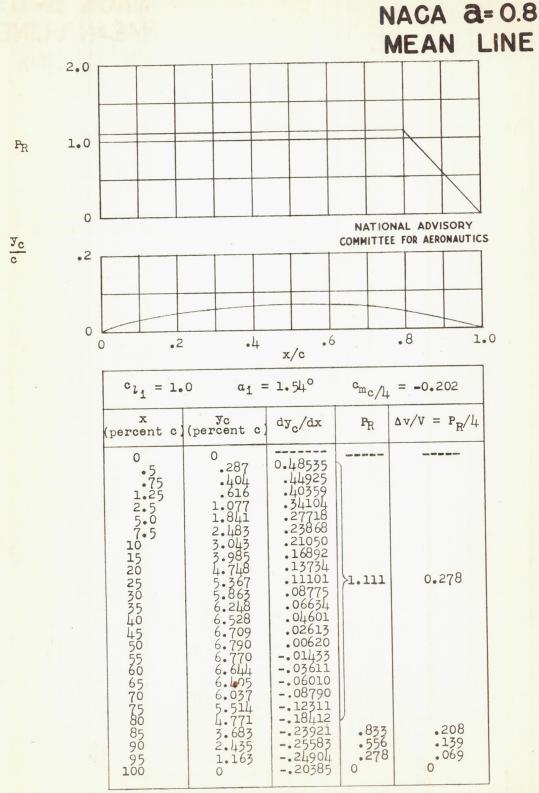
Data for NACA mean line a = 0.5



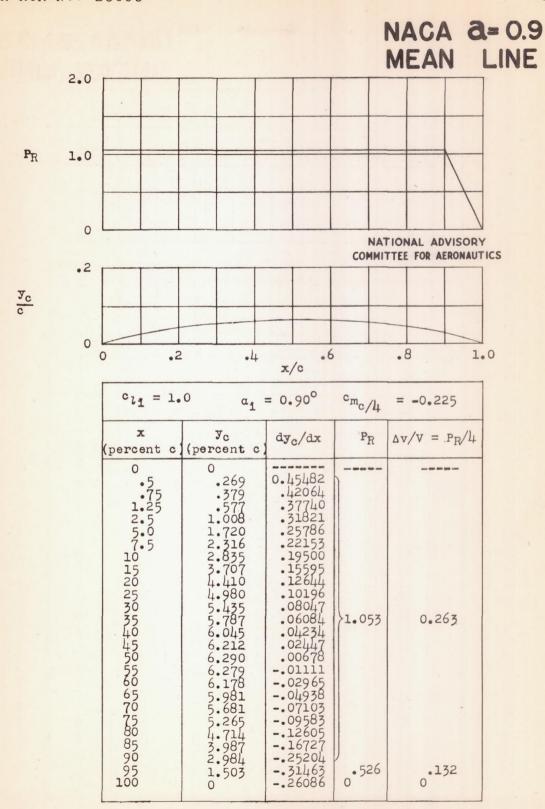
Data for NACA mean line a = 0.6



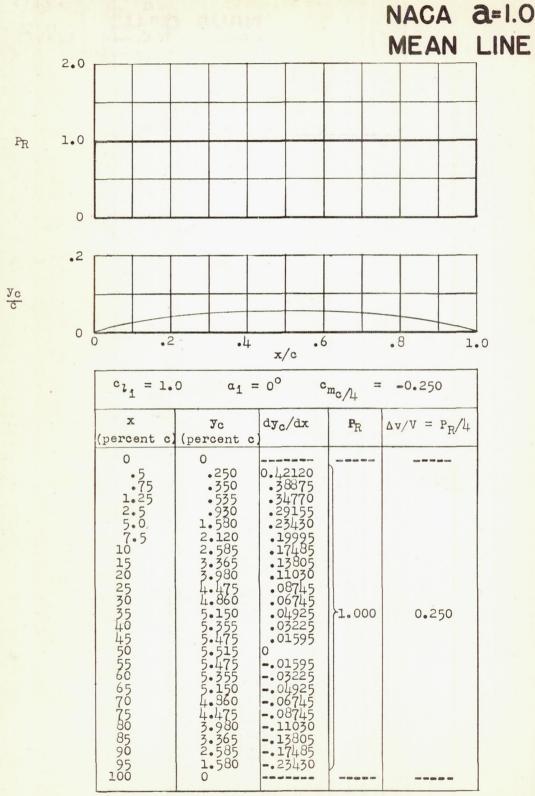
Data for NACA mean line a = 0.7



Data for NACA mean line a = 0.8



Data for NACA mean line a = 0.9



Data for NACA mean line a = 1.0

III - AIRFOIL ORDINATES

III - AIRFOIL ORDINATES

NACA	0006													•							S66a
NACA	0009													•							S66a
NACA	1408												٠,								S66b
NACA	1410																				s66b
NACA	1412																				s66b
NACA	2412																				s67
NACA	2415							,													s67
NACA	2418								•					•							s67
NACA	2421																٠			•	s67
NACA	2424			• .																	s68
NACA	4412										ě										s68
NACA	4415																			,	s68
NACA	4418						•														s68
NACA	4421														٠						s69
NACA	4424																				s69
NACA	23012	2			•																s69
NACA	23015	5																			s69
NACA	23018	3											•								S70
NACA	23021	L	•			٠.							•								570
NACA	23021	+						•													570
NACA	63,4-	-42	20												•						S70
	63,4-																	· in			
	63(42																				

NACA ACR No. L5C05

NACA	63 (420)	-51	7																. S71
NACA	63-006									•									.S7la
NACA	63-009																		.S7la
NACA	63-206																		.S7la
NACA	63-209																٠		.S7la
NACA	63-210													,					.S71b
NACA	631-012																		.S71b
NACA	631-212								•										.S71b
NACA	631-412				•			,											.S71b
NACA	632-015																		.S71c
NACA	632-215																		.S7lc
NACA	632-415															٠.			.S71.c
NACA	632-615																		.S71c
NACA	633-018																		.S71d
NACA	633-218									 ••						•			.S7ld
NACA	633-418					•							•						.S71d
NACA	633-618																		.S71d
NACA	634-021																		.S7le
NACA	634-221																		.S7le
NACA	634-421						, .												.S7le
NACA	64-006																		.S7lf
NACA	64-009.																		.S71f
NACA	64-108																	77.	.S71f
NACA	64-110																		.S71f

							I.	IAC	A	AC	R	No		L5	CO	5							S65c
NACA	65-206 .	,																					S73a
NACA	65-209 .										. ,												S73a
NACA	65-210 .																						S73b
NACA	65-410 .						3																S73b
NACA	651-012																						S73b
NACA	651-212																						S73b
NACA	651-212,	а	=	0	.6																		S74
NACA	651-412						,																S74
NACA	652-015							٠									•						S74
NACA	652-215																						S74
NACA	652-415												•										S74a
NACA	652-415,	a	=	0	.5										•							*	S74a
NACA	653-018	•				e																	S74a
NACA	653-218																						S74a
NACA	653-418								٠										٠.				S75
NACA	653-418,	a	=	0	.5											•			•				. S75
NACA	653-618										.0												S75
NACA	653-618,	a	=	0	.5																		S75
NACA	654-021													٠.									S75a
NACA	654-221															•		٠	٠.				S75a
NACA	654-421																						S75a
NACA	654-421,	a	=	0	.5																		S75a
NACA	65(215)-1	14	+		•																		S75b
NACA	65(421)-1	120)			7																	S75b

NACA ACR No. L5CO5

I	NACA	66,1-212											1.		•			S75b
I	NACA	66(215)-01	16							•								S76
]	NACA	66(215)-23	16															s76
		66 (215) - 21																S76
	NACA	66(215)-43	16						٠,									S76
	NACA	66-006 .				-				,								S77
	NACA	66-009 .		 						•								S77
		66-206 .																S77
	NACA	66-209 .																S77
																		S77a
		661-012																S77a
		661-212						*										S77a
		662-015																S77a
		662-215														1		S77b
		662-415																S77b
		663-018						•					٠					S77b
		663-218																S77b
		663-418																S77c
		66,-021															•	S77c
		664-551																~
		67,1-215																
		747A315																
		747A415																
	412707	- /	-	-	-													

[Stations and ordinates given in percent of airfoil chord]

Upper	Surface	Lower	Surface
Station	Ordinate	Station	Ordinate
0 1.5 25 2.5 5.5 10 15 25 25 25 25 20 45 20 60 90 90 90 90 90 90 90 90 90 90 90 90 90	0 1138 9518 9518 968 970 968 970 968 970 968 971 971 971 971 971 971 971 971 971 971	0 1.25 2.5 7.5 10 15 20 25 40 40 40 90 90 90 100 100	0 -1378 -11368970 -22837-22837-22837-2406)
L.E. radi	us: 0.40		

NACA 0009

[Stations and ordinates given in percent of airfoil chord]

Upper	Surface	Lower	Surface
Station	Ordinate	Station	Ordinate
0.25 2.55 7.10 120 120 120 120 120 120 120 120 120 1	01125511060572579061 01125544444559479061	0 1.25 2.5 5.0 7.5 10 15 20 25 30 40 50 60 70 80 90 90 100 100	0 12 -1.96 -2.67 -2.67 -3.51 -4.30 -4.55 -3.97 -2.97 -2.97 -1.960 (-0)

[Stations and ordinates given in percent of airfoil chord]

Station	Ordinate		1
	Or or Third or	Station	Ordinate
0 1.1898 24.8966 7.8887 14.8964 29.9260 29.9250 40.000 50.001 80.0024 90.0016 100.000	0 1.3242 2.422 2.6602 3.1357 1.557 1.4.5819 9.9862 1.5939 1.5939 1.5939 1.6984 1.6984	0 1.311 2.582 5.104 7.614 10.117 15.111 20.096 25.074 30.050 49.980 59.966 69.959 79.961 89.973 94.984 100.000	0 -1.200 -1.620 -2.134 -2.458 -2.682 -2.953 -3.074 -3.101 -3.669 -2.556 -2.153 -1.193 -1.193 -378 -378

NACA 1410

[Stations and ordinates given in percent of airfoil chord]

Upper	Surface	Lower	Surface
Station	Ordinate	Station	Ordinate
0 1.74 2.3970 7.358 9.8561 119.880 24.907 240.0025 29.937 240.0025 60.0451 90.021 100.000	0 1.29 63974782 2.193382 3.558845 5.5889468 7.5888 1.5838	0 1.326 2.602 5.130 7.142 10.146 15.139 20.120 25.993 70.000 49.9758 69.949 79.951 89.979 100.000	0 -1.515 -2.055 -2.726 -3.157 -3.162 -4.031 -4.031 -4.061 -3.459 -2.930 -1.629 -512 -1.105

NACA 1412

[Stations and ordinates given in percent of airfoil chord]

Upper S	Burface	Lower	Surface
Station	Ordinate	Station	Ordinate
0 1.158 2.378 4.845 7.330 9.824 119.857 24.889 29.925 40.000 50.029 70.061 80.058 90.040 95.025 100.000	0 1.95436 2.77836 7.7536 1.151 5.486 6.903 6.903 6.903 1.7936 1.7936 1.916	0 1.342 2.652 7.670 10.176 15.167 20.143 25.111 40.000 49.971 59.939 79.949 89.960 94.975 100.000	0

Stations and ordinates given in percent of airfoil chord

Station	Ordinate	Station	Ordinate
0 12.50 25.05 25.05 12.50 15.05 15.0	2.159934-9934-9934-9934-9934-9934-9934-9934	0 1.55 25 25.05 10.50 10	0 -1.65 -2.271 -3.046 -3.750 -3.750 -4.133 -4.133 -4.150 -2.150 -

NACA 2415

Stations and ordinates given in percent of airfoil chord

	The same of the sa	Table Const.	
Station	Ordinate	Station	Ordinate
0 1.25 2.50 7.5 10 15 20 25 30 40 50 70 80 90 90 100	71176637707857001154667899707857001154667899987644114346	0 1 2 5 5 0 5 1 0 5 0 0 5 0 0 0 0 0 0 0 0 0 0	0223344594602579055788

NATIONAL ADVISORY
COMMITTEE FOR AERONAUTICS.

NACA 2418

Stations and ordinates given in percent of airfoil chord

Upper	urface	Lower	Surface
Station	Ordinate	Station	Ordinate
0 1.25 2.50 7.5 10 15 20 25 30 40 50 60 70 80 90 90 100	3.28 4.45 6.03 7.17 8.35 10.15 10.65 10.71 9.88 10.71 9.89 5.08 1.55 1.55 1.55 1.55 1.55 1.55 1.55 1.5	0 125 25 25 5 50 25 10 120 25 30 25 30 25 40 50 90 90 90 100	0 45 -2.45 -3.445 -4.488 -5.48 -6.74 -7.71 -7.71 -5.99 -2.80 -2.80 -1.587 -1.99

L. E. radius: 3.56 Slope of radius through L. E.: 0.10

NACA 2421

Stations and ordinates given in percent of airfoil chord

Upper Surface		Lower	Surface
Station	Ordinate	Station	Ordinate
0.25 .25 .50 .7.5 .15 .20 .25 .20 .25 .20 .25 .20 .25 .20 .25 .20 .25 .20 .25 .20 .25 .20 .25 .20 .25 .20 .25 .20 .25 .20 .20 .20 .20 .20 .20 .20 .20 .20 .20	7.871 7.200 8.299 9.289 10.70 11.559 12.158 12.16 11.22 9.794 5.718 1.76 (.22)	0 1.25 2.50 7.5 10 120 230 250 700 890 9950 1000	0 -2.82 -4.02 -5.51 -6.48 -7.18 -7.18 -8.52 -8.62 -8.16 -7.17 -4.87 -4.87 -5.148 -1.06 (-22)

L. E. radius: 4.85 Slope of radius through L. E.: 0.10

[Stations and ordinates given in percent of airfoil chord]

Ordinate	Station	0-11
	Doggion	Ordinate
0 3.892 5.449 7.552 9.052 10.215 11.888 12.959 13.593 13.606 12.532 10.903 8.824 6.352 1.930	0 1.615 9880 10.627 25.620 10.667 20.54400 49.669 7756 79.8900 10.669 10	03-4-6-69-69-69-69-69-69-69-69-69-69-69-69-6
	5.449 7.552 9.052 10.215 11.888 12.959 13.593 13.874 13.606 12.532 10.903 8.824 6.352	3.892 1.615 5.449 2.988 7.552 5.620 9.052 8.180 10.215 10.700 11.888 15.667 12.959 20.573 13.593 25.445 13.606 40.000 13.606 40.000 12.532 49.882 10.903 59.756 8.824 69.756 6.352 79.767 3.502 89.892 1.930 94.902

NACA 4412

Stations and ordinates given in percent of airfoil chord

Upper S	Surface	Lower	Surface
Station	Ordinate	Station	Ordinate
0 1.25 25 25 70 5 10 150 25 10 150 25 10 150 25 10 10 10 10 10 10 10 10 10 10 10 10 10 1	0 2.44 3776 759 90 116 99 116 1178 1178 1178 1178 1178 1178 1178	0 1.25 2.55 5.0 7.5 10 150 25 30 40 50 60 70 80 90 100	0 -1.43 -1.95 -2.49 -2.74 -2.88 -2.74 -2.26 -1.80 -1.40 -1.00 -2.39 -2.22 -1.30 (-13)

NATIONAL ADVISORY COMMITTEE FOR AERONAUTICS.

NACA 4415

Stations and ordinates given in percent of airfoil chord

Upper Surface		Lower	Surface
Station	Ordinate	Station	Ordinate
0 1.25 2.5 5.0 7.5 10 15 20 25 40 50 60 70 80 90 90 100	3.07 4.17 5.71 5.71 6.21 7.25 10.25 11.25 10.25 11.25 10.36 1.66 1.67 1.66 1.67	0 125 255 7 105 105 105 100 100 100	0 -1.79 -2.27 -3.27 -3.718 -4.158 -4.158 -3.77 -3.77 -3.77 -3.77 -3.77 -3.60 -1.553 -1.553 -1.553 -1.553 -1.553 -1.553

L. E. radius: 2.48 Slope of radius through L. E.: 0.20

NACA 4418

Stations and ordinates given in percent of sirfoil chord

Upper &	Burface	Lower	Surface
Station	Ordinate	Station	Ordinate
0 1.25 25 25 10 5 5 10 5 6 7 0 0 9 9 5 0 10 0 0 0 9 9 5 0 10 0 0 0 0 0 0 0 0 0 0 0 0 0 0 0 0	3.76 5.00 6.75 8.06 9.11 10.66 11.72 12.40 12.76 12.70 11.85 10.144 8.55 6.22 3.46 1.89	0 1.25 2.50 7.5 10 120 250 250 40 500 700 900 900 900 1000	0 2.11 1996 1996 1996 1996 1996 1996 1996 1

L. E. radius: 3.56 Slope of radius through L. E.: 0.20

Stations and ordinates given in percent of airfoil chord

Upper Surface		Lower S	Surface
Station	Ordinate	Station	Ordinate
0 25 25 25 50 5 10 15 25 25 26 60 70 80 995 100 100	4-1-5 5-84 7-82 9-24 10-35 12-17 13-88 14-16 13-18 11-60 9-50 6-91 3-85 14-16 13-81	0 1.5 25 25 5.5 10 150 25 25 25 25 25 25 25 25 25 25 25 25 25	0 428 428 47.62 -5.155 -6.976 -6.34 -5.34 -7.22 -1.72 -1.72 -1.72 -1.72 -1.72

L. E. radius: 4.85

Slope of radius through L. E.: 0.20

NACA 4424

Stations and ordinates given in percent of airfoil chord

Upper Surface		Lower S	Burface
Station	Ordinate	Station	Ordinate
0 1,536 3,775 6,753 8,611 13,674 18,858 24,111 19,400 50,235 60,405 70,487 80,454 90,320 95,196 100,000	0 3.964 5.624 7.651 11.015 14.416 15.287 15.738 14.474 12.674 12.674 12.674 12.674	0 1.970 3.464 6.225 8.847 11.389 16.326 21.142 25.889 30.599 40.000 49.765 59.513 79.536 89.6804 100.000	0 -3-472 -4-656 -6-931 -7-512 -8-416 -8-413 -7-606 -5-5698 -5-562 -1-555 -1-6555 -0

L. E. radius: 6.33

Slope of radius through L. E.: 0.20

NATIONAL ADVISORY
COMMITTEE FOR AERONAUTICS.

NACA 23012

Stations and ordinates given in percent of airfoil chord

Upper	Surface	Lowe	r Surface
Station	Ordinate	Station	Ordinate
0 1.25 2.5 7.5 10 20 20 20 20 40 50 60 70 90 90 90 90 100	2.67 3.91 5.89 5.43 7.50 7.50 7.55 1.47 4.368 1.68 9.33	0 25 25 2 50 7 5 105 205 200 205 200 200 200 200 200 200 2	0 -1.23 -1.26 -2.61 -2.92 -3.50 -3.97 -4.48 -4.417 -3.67 -3.06 -1.23 -70 (-13)

L. E. radius: 1.58

Slope of radius through L. E.: 0.305

NACA 23015

Stations and ordinates given in percent of airfoil chord

Upper	Upper Surface		Surface
Station	Ordinate	Station	Ordinate
0 1.25 2.55 2.50 2.55 10 20 20 20 20 20 20 20 20 20 20 20 20 20	3-14 15-890 7-6552 8-005 9-005 9-005 7-68 9-005 7-68 9-005 9	0 1.25 2.5 2.5 10 1.5 20 25 30 40 50 60 70 80 90 95 100	-1.54 -2.25 -3.661 -5.17.96 -5.17.96 -5.17.96 -5.17.99 -1.59.91 -1

L. B. radius: 2.48

Slope of radius through L.B.: 0.305

Stations and ordinates given in percent of airfoil chord

Upper S	Upper Surface		Surface
Station	Ordinate	Station	Ordinate
0 1.5 2.5 2.5 2.5 10 15 120 25 25 20 25 20 25 20 25 20 25 20 20 25 20 25	09922 09922 099088 09008 00000 00000 00000 00000 00000 00000 0000	0 125 255 255 205 205 200 200 200 200 200 2	0 851 -2.780 -5.660 -5.186 -7.77 -7.457 -6.80 -7.457 -6.80 -7.457 -6.982 -5.982 -5.982 -7.199

L. R. radius: 3.56

Slope of radius through L. E.: 0.305

NACA 23021

Stations and ordinates given in persent of airfoil shord

Upper Surface		Lower	Surface
Station	Ordinate	Station	Ordinate
0 125 255 10 255 10 255 10 250 10 250	1.87 6.14 7.93 9.13 10.03 11.80 12.06 11.49 10.49 7.09 5.76 1.53 1.53	0 1.25 2.50 7.55 10 10 20 25 30 45 60 70 80 90 90 90 100 100	0 0 0 0 0 0 0 0 0 0 0 0 0 0 0 0 0 0 0

L. B. radius: 4.85

Slope of redime through I. E.: 0.305

NATIONAL ADVISORY COMMITTEE FOR AERONAUTICS.

NACA 23024

Stations and ordinates given in percent of airfoil shord

Upper Surface		Lower S	Surface
Station	Ordinate	Station	urdinate
0 .277 1.331 3.853 6.601 9.123 15.001 20.253 25.262 10.256 50.235 60.202 70.162 80.116 90.064 95.036	0 4.017 5.764 9.844 11.528 12.527 13.534 11.690 10.008 7.687 5.115	0.2.23 3.6647 2.23 3.6647 2.35 2.35 2.37 2.37 2.37 2.37 2.37 2.37 2.37 2.37	0 -3.303 -4.432 -5.862 -6.860 -7.647 -9.703 -10.427 -10.427 -9.482 -9.482 -9.482 -6.664 -6.663 -2.673 -1.504

L. E. radius: 6.33

Slope of radius through L.E.:0.305

NACA 63,4-420

Stations and ordinates given in percent of airfeil shord

Upper Surface		Lower S	urface
Station	Ordinate	Station	Ordinate
0 2150 8822 4705284406 1906663323 1906663323 1906663 1	0 1.796 2.196 2.196 2.827 3.95573 7.81249 11.8036 11.5523 11.95655 11.5523 2.425984 2.6473 10.445984 11.5673 1	0 .785 1.070 1.613 2.918 5.462 7.976 10.474 15.446 20.337 30.268 35.126 45.060 50.000 54.948 59.948 59.948 69.852 74.871 89.995 100	0 -1.590 -1.916 -2.399 -3.210 -4.2937 -5.7492 -7.405 -7.40

L. E. radius: 3.16

Slope of radius through L. E.:0.168

NACA 63,4-420

a = 0.3
[Stations and ordinates given in percent of airfoil chord]

Upper	Surface	Lower	Surface
Station	Ordinate	Station	Ordinate
0 .0661 .69568 .69568 .69568 .728478 .40728458 .4088	0 1.814 2.24128 4.128 5.2366 10.1320 11.296 10.1320 11.296 12.7818 12.089 11.3516 9.497 7.589 7.589	0 1.809 3.71220 1.809 3.71220 1.5.5496 10.75531992 230.349.557266615 7.798862 230.349.556667 1.5.66615 7.798862 230.349.9700 230.349.9700	0 -1.82198 -2.296110186 -2.296119708 -3.6199708 -5.6199708 -7.7185561 -7.718566 -7.7185651 -3.5666 -7.581356562

NACA 63(420)-517

Stations and ordinates given in percent of airfoil chord

			_
Upper	Surface	Lower	Surface
Station	Ordinate	Station	Ordinate
0 .200 .866 2.058 4.511 6.996 9.497 19.578 24.642 29.715 39.866 44.936 50.000 55.075 70.157 70.157 70.157 70.157 90.100	0 11-512 5127896440 5-14-9864-0-502 6-15-0-502 6-16-0-502 6-16-0-502 10-0-5	0 100000000000000000000000000000000000	01.12.186 3.59.1686 3.59.1686 3.59.1686 3.59.1686 3.59.1686 3.09.208 3.59.1686 3.09.208 3.09.

Slope of radius through L.E.: 0.211

NACA 63(420)-422 [Stations and ordinates given in percent of airfoil chord]

Station Ordinate Station Ordinate 0 0 0 0 1.87 1.959 .813 -1.759 .398 2.402 1.102 -2.122 .850 3.088 1.650 -2.660 2.041 4.312 2.959 -3.568 4.492 6.050 5.508 -4.786 6.977 7.387 8.023 -5.691 9.478 8.496 10.522 -6.428 14.509 10.231 15.491 -7.539 19.563 11.489 20.437 -8.797 29.705 12.893 30.295 -9.002 34.784 13.034 35.216 -8.914 39.861 12.883 40.139 -8.599 14.934 12.493 45.066 -8.113 50.000 11.907 50.000 -7.495 55.057 11.147 54.949 -5.949 -5.943 -6.767 -6.767 60.104
187 1.959 813 -1.759 .398 2.402 1.102 -2.122 .850 3.088 1.650 -2.660 2.041 4.312 2.959 -3.568 4.492 6.050 5.508 -4.786 6.977 7.387 8.023 -5.991 9.478 8.496 10.522 -6.428 14.509 10.231 15.491 -7.539 19.563 11.489 20.437 8.305 24.630 12.377 25.370 -8.797 29.705 12.890 30.295 -9.002 34.784 13.034 35.216 8.914 39.861 12.883 40.139 -8.599 14.934 12.493 45.066 -8.113 50.000 11.907 50.000 -8.797 55.057 11.147 54.943 -6.767
60.10µ 10.227 59.896 -5.9µ3 65.1µ0 9.169 64.860 -5.0µ9 70.163 7.988 69.837 -4.100 75.172 6.700 74.828 -5.120 80.165 5.329 79.835 -2.1µ5 85.1µ2 3.918 84.858 90.103 2.513 89.897 95.051 1.181 9µ.9µ9 100.000 0 100.000 0

NACA 63-006

Stations and ordinates given in percent of airfoil chord

Upper S	Surface	Lower S	Surface
Station	Ordinate	Station	Ordinate
0 .458 .7037 .1932 .1932 .1932 .1932 .1932 .1939 .1934 .19,950 .29,960 .34,971 .50,000 .55,008 .65,002 .85,019 .95,006 .100,000	0 .5517 .8776 1.2776 2.1526 2.5058 3.5058 1.9726 2.5058 3.9726 2.5058 3.9726 2.5058 3.9726 2.5058 3.5058 3.5058 2.2180 2.2180 3.2280 3.450 4.506	0 5,42 7,797 1 . 3,62 2 . 5,62 2 . 5,671 10 . 0,70 15 . 0,66 20 . 0,50 25 . 0,50 25 . 0,50 45 . 0,09 45 . 0,09 54 . 9,98 64 . 9,92 54 . 9,98 64 . 9,97 77 9,97 79 . 9,78 84 . 9,94 100 . 0,00	0451537662869 -1.144 -1.341 -1.492 -1.712 -1.982 -1.970 -1.982 -1.620 -1.422 -1.196 -952 -698 -447212 -010 .178 0

NACA 63-206

Stations and ordinates given in percent of airfoil chord

Upper	Surface	Lower Surface	
Station	Ordinate	Station	Ordinate
0 .12.5.0.5 5.725.0.5 1.2.5.7.0 1.2.5.7.0 1.2.5.7.0 1.2.5.7.0 1.2.5.0.5 1.2.	0 .503 .609 .771 .1057 .1.462 .2.386 .2.6541 .2.954 .3.907 .2.8777 .2.7217 .2.7217 .2.7217 .348 .683 .683 .138 .0	0 .5755 12.50 .5 .150 .5 .5 .5 .5 .5 .5 .5 .5 .5 .5 .5 .5 .5	0503609771 -1.057 -1.462 -1.766 -2.841 -2.954 -3.000 -2.971 -2.877 -2.723 -2.517 -2.267 -1.982 -1.670 -1.342 -1.008683138 0

NACA 63-009

[Stations and ordinates given in percent of airfoil chord]

Upper	Surface	Lower Surface	
Station	Ordinate	Station	Ordinate
0 5725 725 0 5 12 5 0 5 10 15 20 5 20 5 0 5 10 25 0 5 10 0 5	0	0 5755 5725 12 570 5 150 50 50 50 50 50 50 50 50 50 50 50 50 5	0 - 7496 -1.1582 -2.1965 -2.6024 -3.5991 -3.5991 -4.42966 -4.77528 -4.42966 -1.471 -1.5996 -1.471 -1.5996

NACA 63-209

Stations and ordinates given in percent of airfoil chord

Upper S	Surface	Lower S	urface
Station	Ordinate	Station	Ordinate
0	0 .97555 9.27555 11.751077932 9.25555 9.252679694 9.2526667 9.252667 9.252667 9.252667 9.252667 9.252667 9.252667 9.252667 9.252667 9.252667 9.252667 9.252667 9.252667 9.252667 9.252	0 .563 .820 1.592 5.1036 10.106 15.098 25.008 25.0060 35.004 45.014 50.000 54.973 64.971 64.971 64.971 64.971 64.971 64.971 64.973 94.991	0696 833 -1.041 -1.393 -1.878 -2.229 -2.505 -2.917 -3.200 -3.470 -3.476 -3.201 -2.954 -2.287 -1.898 -1.486 -1.071 675 3120 0

L.E. radius: 0.631 Slope of radius through L.E.: 0.0842

NACA 63-210

Stations and ordinates given in percent of airfoil chord

Upper S	Surface	Lower Surface	
Station	Ordinate	Station	Ordinate
0 .430 .669 .162 .2398 .4382 .4382 .14.890 .19.902 .24.917 .29.933 .34.951 .39.968 .44.985 .50.000 .55.013 .65.032 .70.036 .75.038 .80.036 .85.030 .95.010 .000	0 .876 1.107 1.379 1.379 2.7572 2.7573 2.666 5.910 6.861 5.930 5.2786 4.268 4.268 4.268 4.268 4.268 4.268 4.330 6.061 1.762 1.762 0	0 .570 .8338 2.602 5.114 70.118 15.110 20.098 30.067 35.0049 45.015 50.000 54.987 59.976 64.964 77.9664 84.977 94.990 100.000	0 .776 -967 -1965 -1567 -2.5843 -3.6857 -3.8566 -3.966 -3.9867 -3.3945 -2.2044 -1.740 -1.822 -415 -087
L.E. radius		ough L.E.:	0.0842

NACA 631 -212 Stations and ordinates given in percent of airfoil chord

Upper	Surface	Lower	Surface
Station	Ordinate	Station	Ordinate
0 .4177 1.1488 4.38638 4.38638 19.8868 19.9201 24.9900 24.99201 34.9862 50.0016 65.0029 65.0049 65.0042 85.035 90.000	0 1.032 1.260 1.622 2.238 3.4554 45.4770 66.901 7.993 66.4730	0 .583 .843 1.3552 5.1372 10.141 15.132 20.118 25.100 35.0538 45.018 50.0538 45.018 50.0538 45.018 50.0538 45.0538 50.9575 74.9575 74.9575 74.962 69.9575 74.962 69.9575 74.962 69.9575 74.962 69.9575 74.962 69.9575 94.968	0 - 932 -1.120 -1.408 -1.912 -2.606 -5.115 -1.545 -1.545 -1.545 -1.609 -1.4.809 -1.609 -2.238 -1.661 -1.106 -1.900 0

Slope of radius through L.E.: 0.0842

NACA 631-012

Stations and ordinates given in percent of airfoil chord

Upper	Surface	Lower	Surface
Station	Ordinate	Station	Ordinate
0 125705 125705 125705050505050505050505050	0 .985 1949 1.102 2.505 3719 2.255 3719 2.255 3719 2.255 3719 3727 3725 3725 3725 3725 3725 3725 3725	0	0 985 -1.1949 -2.1022 -2.5129 -4.5039 -4.5722 -5.7930 -5.97342 -5.9735 -4.420 -3.240 -3.240 -3.256 -1.9074 -1.707 -2.50 0
L.E. radiu	1.087		

NACA 63 -412

[Stations and ordinates given in percent of airfoil chord]

Unner	Surface	Lower	Sunface
opper	Juriace	Dower .	Juriace
Station	Ordinate	Station	Ordinate
0 .336 .5041 2.2577 7.218 9.718 14.7355 24.8882 29.8882 29.8882 39.924 55.031 60.057 670.089 80.089 80.089 90.049 90.049	0 1.071 1.3710 1.3710 1.371460 1.371460 1.371460 1.371460 1.371460 1.37160 1.3	0 .664 .933 1.459 2.743 5.273 10.285 20.235 20.235 20.235 20.235 20.160 35.118 40.0736 50.000 554.969 54.911 79.913 64.911 79.913 89.951 94.977 100.000	0 - 871 -1 040 -1 291 -1 716 -2 280 -2 995 -3 745 -3 919 -3 919 -3 978 -3 978 -
L.E. radiu		ough L.E.:	0.1685

NACA 632-015

Stations and ordinates given in percent of airfoil chord

NACA 632 -415

Stations and ordinates given in percent of airfoil chord

Upper	Surface	Lower	Surface
Station	Ordinate	Station	Ordinate
0 .5291 2.198 4.660 7.647 14.669 19.7050 29.800 34.802 39.9055 50.0039 60.0039 60.0039 70.1009 80.020 890.020	0 1.587 1.587 1.587 1.444 1.587 1.489 1.20 1.45 1.67 1.21 1.489 1.52 1.49 1.52 1.49 1.53 1.53 1.53 1.53 1.53 1.53 1.53 1.53	0 .70709 1.58040 35331 2.5.35351 15.33532,2500 8 15.320,200 8 15.320,2	0 -1.306 -1.306 -2.306 -3.6420 -3.5006 -5.006 -5.006 -5.442 -5.3442 -5.3443 -2.906 -1.33 -1.33 -1.33 -1.33 -1.33 -1.33

Slope of radius through L.E.: 0.1685

NACA 632-215

Stations and ordinates given in percent of airfoil chord

2			-	
Upper S	Surface	Lower	Surface	
Station	Ordinate	Station	Ordinate	
0 .3997 1.1248 4.3233 14.8323 14.8355 9.8323 14.8355 9.87900 9.9000 9.9000 9.0000 9.0000 9.0000 9.0000 9.0000 9.00	0 1.59820 1.59820 2.528020 1.598264792279657856889920749202749837492027492047920479204792047920479204792	0 .601 .863 1.380 2.652 5.171 7.677 15.168 25.125 30.100 35.0023 50.000 35.0000 54.965 64.9947 74.945 79.986 100.000	0 -1.150 -1.388 -1.7420 -3.3289 -1.53365 -5.8259 -6.44705 -6.50132 -5.0382 -2.25157 -8.3366 -2.25157 -3.3644 -	
T F redi	I F reding: 1 50/			

L.E. radius: 1.594
Slope of radius through L.E.: 0.0842

NACA 632-615

Stations and ordinates given in percent of airfoil chord]

Upper	Surface	Lower	Surface
Station	Ordinate	Station	Ordinate
0 205 4166 2.050 4.4973 14.5525 9.455525 29.7708 34.7978 35.005 560.1055 65.1139 775.163 80.1129 95.042 100.000	0 1.317 1.1549 2.1299 1.56678 8.01066 9.83317 10.5984 10.5984 10.5984 10.5984 10.5984 10.5985 7.88097 6.88097 6.5598 10.5598 10.5598	0 7952 1.06350 5.5527 10.57502 10.57502 10.574942 25.332223 40.0002 25.33223 45.0002 45.0002 54.8347 79.8347 79.8347 84.950 94.958 100.000	0 -1.017 -1.214 -1.517 -2.0154 -3.125 -3.476 -3.972 -4.460 -4.499 -4.499 -4.472 -3.354 -2.8239 -1.629 -1.015 -3.476 -3.972 -4.372 -2.8239 -1.629 -1.430 -3.476 -3.476 -3.476 -3.476 -3.476 -3.476 -3.476 -3.476 -3.476 -3.476 -3.476 -3.476 -3.476 -4.499 -4.4

L.E. radius: 1.594 Slope of radius through L.E.: 0.2527

NACA 633-018

Stations and ordinates given in percent of airfoil chord

Upper S	Surface	Lower S	Surface
Station	Ordinate	Station	Ordinate
0 125705	0 1.404 1.713 2.1068 2.1088 2.	0 .1.2.5.0.5 5.7.2.5.0.5 1.2.5.7.0.50 1.2.5.	0 -1 -404 -1 -1717 -2 -104 -2 -136288 -7 -15628 -7 -15628 -7 -15628 -7 -15629 -7 -15629 -1 -1562
L.E. radius: 2.120			

NACA 633 -418

Stations and ordinates given in percent of airfoil chord

Upper Surface		Lower S	Surface
Station	Ordinate	Station	Ordinate
0 .267 .487 .945 .2.140 .4.593 .7.077 .9.577 .14.602 .19.645 .24.699 .29.760 .31.826 .31.946 .55.046 .55.046 .60.083 .65.110 .70.125 .75.128 .60.1125 .75.069 .95.032 .100.000	0 1.484 1.833 2.4150 2.4150 7.587 8.560 2.585 10.956 10.95728 10.95728 10.95728 10.95728 10.1446 10.14466 7.55264 10.1530 2.1530 2.1530 978	0 733 1.0550 5.40733 1.5550 5.427 10.3398 20.3301 15.3398 20.3301 20.3301 1714 45.0095 4.917 69.8891 84.931 94.968 100.000	0 -1 .284 -1 .553 -1 .982 -2 .711 -3 .413 -5 .868 -6 .846 -6 .966 -6 .930 -6 .9702 -5 .766 -6 .7302 -5 .766 -6 .7302 -5 .766 -1 .878 -1 .988 -1 .988 -1 .988 -1 .988
L.E. radius: 2.120 Slope of radius through L.E.: 0.1685			

NACA 633-218

Stations and ordinates given in percent of airfoil chord

Upper Surface		Lower	Surface
Station	Ordinate	Station	Ordinate
0 .382 .617 1.096 2.319 4.798 7.788 14.880 29.880 34.911 39.943 55.023 65.055 70.002 65.062 75.064 80.059 85.019 90.030 100.000	0 1 4789 44789 5328738 477328738 477328738 457678 488 4970 4576 4576 4576 4576 4576 4576 4576 4576	0 .618 .883 .1.404 .2.681 .7.712 .10.212 .15.199 .20.1750 .30.120 .35.089 .745.027 .50.007 .54.958 .64.938 .64.938 .9566 .9941 .84.9566 .94.984 .100.000	0 -1 - 3438
L.E. radius: 2.120 Slope of radius through L.E.: 0.0842			

NACA 633 -618

Stations and ordinates given in percent of airfoil chord

Upper Surface		Lower S	Surface
Station	Ordinate	Station	Ordinate
0 .156 .361 .797 1.965 .4.393 6 .868 9.367 14.469 .24.549 .29.560 .34.734 .919 .500 .500 .601 .601 .601 .601 .601 .601 .601 .6	0 1.511 1.878 2.491 5.268 6.5,42 7.586 9.219 10.18 11.273 11.822 12.086 11.767 11.251 10.566 11.767 11.251 10.5667 7.5330 5.073 3.531 1.293	0 844 1.793 1.7935 5.6072 10.6373 15.5931 15.5936 120.5451 20.5451 20.031 50.031 50.031 50.4883 4.8825 4.8825 779.8825 89.992 94.900	0 -1.211 -1.4549 -2.5000 -3.3798 -4.484 -5.603 -5.9990 -5.603 -5.9990 -5.637 -3.241 -2.4752 -1.9607 -2.238 -2.4752 -1.9607 -2.238 -2.603 -2.60
L.E. radius: 2.120 Slope of radius through L.E.: 0.2527			

NACA 634-021

Stations and ordinates given in percent of airfoil chord

upper 3	Surface	Lower	Surface
Station	Ordinate	Station	Ordinate
0	0 1.583 1.937 2.527 3.577 3.577 3.577 3.5727 3.5727 3.652 10.410 10.453 10.410 10.453 10.452 10.5098 9.2090 10.253 8.443960 4.1692 10.132 0	0 5755 12.50 5 10 70 5 150 250 50 50 50 50 50 50 50 50 50 50 50 50 5	0 -1.583 -1.95277 -2.5777 -5.0652 -7.080 -8.441 -9.410 -10.503 -10.412 -10.5098 -9.8206 -8.390 -7.441 -6.3290 -3.054 -2.021 -1.113 -3.392 0

NACA 634 -421

Stations and ordinates given in percent of airfoil chord

Upper S	urface	Lower S	Surface
Station	Ordinate	Station	Ordinate
0 .237 .452 .902 .902 .906 .4.527 .506 .14.535 .24.649 .29.719 .34.783 .29.719 .34.937 .50.004 .65.126 .75.145 .80.135 .85.111 .90.078 .937 .00.000	0 1.661 2.7717 3.925 5.675 7.010 8.097 9.7714 10.9377 12.352 12.5539 12.441 11.412 10.582 8.4552 8.4552 7.947 3.3644 1.022	0	0 -1.461 -1.7749 -3.181 -4.411 -5.314 -6.029 -7.082 -7.809 -8.464 -8.455 -7.6664 -7.020 -5.298 -4.335 -4.335 -3.347 -1.4592 -2.242 0
L.E. radius: 2.650 Slope of radius through L.E.: 0.1685			

NACA 634-221

Stations and ordinates given in percent of airfoil chord

Upper S	Surface	Lower	Surface
Station	Ordinate	Station	Ordinate
0 .607 .607 .2763 .7777 .7779 .19.889 .19.889 .900 .007 .007 .29.49 .889 .900 .007 .007 .007 .007 .007 .007 .00	0 1.627 2.0628 3.757 5.375 6.607 9.111 10.204 11.383 11.529 11.369 10.309 9.485 7.1262 5.054 5.054 7.08	0 . 630	0 -1.527 -1.861 -2.4345 -4.75562 -7.75562 -7.756162 -9.1459 -9.2756 -9.1459 -9.27566 -9.27566 -9.27566 -9.27566 -9.27566 -1.3366 -1.3566 -1.36

L.E. radius: 2.650 Slope of radius through L.E.: 0.0842

NACA 64-006

[Stations and ordinates given in percent of airfoil chord]

Upper Surface		Lower	Surface
Station	Ordinate	Station	Ordinate
0 .725 505 12.50	0 .494 .596 .754 1.024 1.4692 1.928 2.298 2.2772 2.987 2.772 2.981 2.995 2.775 2.375	0 125,05 125	0

NACA 64-009

Stations and ordinates given in percent of airfoil chord

	Surface	Donoz	Surface
Station	Ordinate	Station	Ordinate
0 57250 57250 12557 10 1257 1250 12	0 73928 115339 115339 112222358 12349 123498	0 -12.50 -57.25 -57.05 -12.57 -15.05 -12.57 -15.05	0 -739 -892 -1.128 -1.533 -2.1543 -2.898 -3.4558 -4.1703 -4.479 -4.3136 -2.561 -2.0694 -1.069

NACA 64-108

[Stations and ordinates given in percent of airfoil chord]

Stations and ordinates given in percent of airfoil chord

Upper S	Surface	Lower S	Surface
Station	Ordinate	Station	Ordinate
0 .465 .712 1.207 2.450 4.945 7.444 1.953 2.4.959 2.9.967 3.4.975 3.9.994 2.50.000 55.000 65.016 70.019 85.016 90.012 690.012	0 .044 1.023 1.793 2.037 2.037 4.790 2.037 4.798 4.798 4.798 4.798 4.798 4.798 4.798 4.798 4.798 4.798 4.798 4.798 4.798 4.798 4.798 6.798	0 5358 72930 525576 12.5556 15.05577 10.05577 10.05577 10.0556 15.0000 15.0000 15.0000 15.0000 15.0000 15.0000 15.0000 15.00000	01.60 d2.20 -

NACA 64-IIO

L.E. radius: 0.720 Slope of radius through L.E.: 0.042

NACA 64-206

[Stations and ordinates given in percent of airfoil chord]

Station	Ordinate	Station	Ordinate
0 1-194 1-194 1-194 1-193	0 .6649 .208 .208 .1.195 .2.197077 .6679 .2.208 .1.195 .6707	0 5496 1.356668 1.356668 7.506688 7.506688 7.506688 7.50668 7.50668 7.50668 7.50668 7.50668 7.50668 7.50668 7.50668 7.5068 7.9985 7.9985 7.9985 7.9985 7.9985 7.9985 7.9985 7.9985 7.9985 7.90	0 - 142 - 524 - 645 - 836 - 1.087 - 1.267 - 1.410 - 1.621 - 1.951 - 1.951 - 1.961 - 1.672 - 1.480 - 1.260 - 1.020 - 768 - 517 - 276 - 064 - 159

L.E. radius: 0.256 Slope of radius through L.E.: 0.084

NACA 64-209

[Stations and ordinates given in percent of airfoil chord]

Upper	Surface	Lower	Surface
Station	Ordinate	Station	Ordinate
0 1,38 .680 1.172 2.411 4.901 7.398 9.899 14.986 34.956 34.956 55.012 65.030 70.035 75.035 85.030 90.021 100.000	0 .9274 785926 795926 795926 792714 792714 792714 792714 792714 792711 792711 792711 79271	0 562 8328 9328 1.5899 10.101 15.0075 30.0775 30.029 45.0029 45.0029 45.0029 45.0000 54.988 59.970 69.9965 74.9965 74.9969 89.970 89.970 89.970 89.970	0686 818 0344 1.7917 2.3781 2.201 3.449 3.449 3.449 3.449 3.449 3.449 3.7381 2.996 1.589 1.768 3996 089

L.E. radius: 0.579 Slope of radius through L.E.: 0.084

NACA 64-208

[Stations and ordinates given in percent of airfoil chord]

Upper S	Surface	Lower S	Surface
Station	Ordinate	Station	Ordinate
0 .688 1.480 2.421 4.912 7.490 119.925 29.946 139.974 44.988 50.027 75.032 85.002 90.031 75.030 90.001 100.000	0 .8640 991 2286 975 44 4 5 5 5 4 4 4 4 5 5 5 4 4 4 4 5 5 5 4 4 4 5 5 5 2 2 2 2	0 5552 12.5798 12.579890 10.0876 25.0886 25.0559 25.05	0 606 722 896 -1. 177 -1. 557 -2. 0555 -2. 395 -2. 640 -2. 912 -2. 949 -2. 921 -2. 788 -2. 581 -2. 316 -2. 010 -1. 673 -1. 319 -608 -033 -110

L.E. radius: 0.455 Slope of radius through L.E.: 0.084

NACA 64-210

[Stations and ordinates given in percent of airfoil chord]

	,		
Station	Ordinate	Station	Ordinate
0 4313 4163 114987 114987 114988 114988 1199	0 86776 1.38865446 1.38865486 1.38865486 1.38865486 1.3886588 1.3886 1.3	0 .8697 1.3599 5.1103 10.113 15.106 25.081 30.032 45.005 54.987 59.975 64.962 74.968 89.977 84.988 89.977 94.988	0 767 -1.9140 -1.5124 -2.0400 -2.7168 -3.748 -3.748 -3.748 -3.748 -3.748 -3.748 -3.748 -3.748 -3.748 -3.748 -3.748 -3.748 -3.7415 -2.858 -1.556 -1.556 -1.568 -1.56

L.E. radius: 0.720 Slope of radius through L.E.: 0.084

NACA 64,-012

Stations and ordinates given in percent of airfoil chord

Station Ordinate Station Ordinate 0 0 0 0 .5 .978 .5 978 .75 1.179 .75 -1.179 1.25 1.490 1.25 -1.496 2.5 2.035 2.5 -2.031 5.0 2.810 7.5 -3.394 7.5 3.394 7.5 -3.391 10 3.871 10 -3.871 15 4.620 15 -4.620 20 5.173 20 -5.173 25 5.576 25 -5.573 30 5.844 30 -5.84 40 5.981 40 -5.978 40 5.981 40 -5.978 45 5.798 45 -5.798 50 5.056 55 -5.066 60 4.548 60 -4.548
.75
65 3.974 65 -3.974 70 3.350 70 -3.350 75 2.695 75 -2.695 80 2.029 80 -2.029 85 1.382 85 -1.382 90 .786 90786 95 .288 95 -288 100 0 100 0

NACA 641-212

[Stations and ordinates given in percent of airfoil chord]

Upper Surface				-
0 0 0 0 0 0 0 0 0 0 0 0 0 0 0 0 0 0 0	Upper	Surface	Lower	Surface
118	Station	Ordinate	Station	Ordinate
	.659 1.142 1.382 1.382 1.382 1.382 1.382 1.982 1	55,383,56180582331942054304 024,5212183805885194205430 050,885160358056 050,885160358056 050,885160358054	5815382467999988111535267770515050505050505050505050505050505050	-1.38491725687480149697494780073899973589749478007494780073674947800736998

L.E. radius: 1.040 Slope of radius through L.E.: 0.084

NACA 64,-112

[Stations and ordinates given in percent of airfoil chord]

Upper S	Surface	Lower S	Surface
Station	Ordinate	Station	Ordinate
0 .459 .704 1.198 2.441 4.934 7.932 14.936 19.936 19.936 19.951 29.991 39.991 50.000 55.000 70.002 70.002 80.002 85.019 99.007 100.000	0 1.025 1.5267 1.5267 1.5266 1	0 541 7902 2 5599 5 0668 10 0649 25 0049 30 0299 45 0099 54 980 69 9776 84 983 94 990 100 000	0 -1952 -1.475 -1.475 -1.475 -1.475 -1.477 -5.1612 -4.771 -5.445 -5.445 -5.445 -5.445 -5.445 -5.445 -4.5012 -2.8647 -1.6847 -1
L.B. radio	is: 1.040		

L.E. radius: 1.040 Slope of radius through L.E.: 0.042

NACA 64-412

[Stations and ordinates given in percent of airfoil chord]

Upper
Station
0 3569544 3509273275252233 122777894888233 124778949996650 1249889996650 124989996650 1250999999999999999999999999999999999999

L.E. radius: 1.040 Slope of radius through L.E.: 0.168

NACA 642-015

Stations and ordinates given in percent of airfoil chord

Upper Surface		Lower	Surface
Station	Ordinate	Station	Ordinate
0 5725 5725 10 12 57 10 10 10 10 10 10 10 10 10 10 10 10 10	0 1.1.2.5.4.4.5.6.6.7.7.7.6.6.5.4.4.5.2.1 0 1.1.2.5.4.4.5.6.6.7.7.7.6.6.5.4.4.5.2.1 0 1.1.2.5.4.4.5.6.6.7.7.7.6.6.5.4.4.5.2.1 0 1.1.2.5.4.4.5.6.6.7.7.7.6.6.5.4.4.5.2.1	0 125705 125705 12570505050505050505050505050505050505050	0 -1.208 -1.4562 -1.8524 -1.5249 -4.812 -5.985 -6.985 -7.473 -6.820 -4.813 -5.246 -5.346 -5.346

L.E. radius: 1.590

NACA 642-415

Stations and ordinates given in percent of airfoil chord

Upper Surface		Lower Surface	
Station	Ordinate	Station	Ordinate
0 2926673226 2926732261668145633544400022662145928889950000001115926621419498899500000000000000000000000000000000	0 1.291 1.5758833 14.5758842 12.666 1.26661 1.	0 .701 -9704	0 -1.091 -1.299 -1.610 -2.1399 -2.8579 -3.7796 -4.882 -5.191 -5.3721 -5.4333(4) -4.076 -3.4374 -4.076 -3.4374 -4.504 -3.288 -3.288

L.E. radius: 1.590 Slope of radius through L.E.: 0.168

NACA 642-215

[Stations and ordinates given in percent of airfoil chord]

Upper Surface		Lower	Surface
Station	Ordinate	Station	Ordinate
0 3997223361 1238335110781 123838889999700000000000000000000000000000	0115941666644902449341662 252596666644902449334662 252596666649002449331466	0 .663 .868 .37647 .516690 .10.163 .20.1122 .30.0230 .25.10.0948 .50.9804 .50.9804 .50.9804 .50.9804 .50.9804 .50.9804 .50.9804 .50.9804 .50.9804 .50.9804 .50.9804 .50.9804 .50.9804 .50.9804 .50.9804 .50.9804 .50.9804 .50.9804	0 154 -1.382 -1.7738 -2.3814 -3.8145 -4.3210 -5.682 -6.089 -6.402 -6.402 -6.402 -5.171 -4.865 -3.141 -1.675 -1.003 -1.003 -1.003

L.E. radius: 1.590 Slope of radius through L.E.: 0.084

NACA 643-018

Stations and ordinates given in percent of airfoil chord

Upper	Surface	Lower	Surface
Station	Ordinate	Station	Ordinate
0 12.570 12.570 1505	0 1.428 1.7207566 1.2100566 1.2100566 1.2100566 1.2100566 1.2100566 1.2100566 1.2100666 1.21006666 1.2100666666 1.21006666666666666666666666666666666666	0 .5755 57.255 10 150 25 0 5 0 5 0 5 0 5 0 5 0 5 0 5 0 5 0	0 11.75666322 1.710866322 1.710897899920 1.75567789720 1.4582268 1.4582268 1.4582268 1.14582268 1.14582268 1.14582268 1.14582268 1.14582268 1.14582268 1.14582268 1.14582268

NACA 643-418

[Stations and ordinates given in percent of airfoil chord]

			_
Upper	Surface	Lower	Surface
Station	Ordinate	Station	Ordinate
0 .2636 .4860 .2152 .4509 .21509 .7095,7763 .7095,7763 .7007 .1916,7763 .3918 .885,100 .1311 .700 .1311 .700 .1311 .700 .700 .700 .700 .700 .700 .700 .7	0 1.508 1.840 2.3757 4.908 8.277 4.908 8.2776 10.176 10.320 10.325 10.32	7440815553337775503446953233 70584915553332775503446953233 2057105322571550494949949 11225770522235544555494949949	0 -1.59436225552266443622555226644362555526665989498555512664449255552666444

L.E. radius: 2.208 Slope of radius through L.E.: 0.168

NACA 643-218

[Stations and ordinates given in percent of airfoil chord]

Upper	Surface	Lower	Surface
Station	Ordinate	Station	Ordinate
0 .380 1.092547 1.092547 1.79988 1.948.8531 1.948.8531 1.944.8912 1.95658 1.95668 1.95688 1.95	0 1.473 1.7859 1.47859 2.186 4.4966 1.52850 1.	0 .620 .883 .4075 .5193 .10.197 .10.203 .10.197 .10.058 .45.0076 .47.994 .45.0076 .47.994 .49.981 .49.981 .49.981 .49.981 .49.981	011-22-34-56-64-56-94-56-66-22-88-56-94-58-98-35-7-7-7-7-7-7-7-7-7-7-7-7-7-7-7-7-7-7-

L.E. radius: 2.208 Slope of radius through L.E.: 0.084

NACA 643-618

[Stations and ordinates given in percent of airfoil chord]

Upper	Surface	Lower	Surface
Station	Ordinate	Station	Ordinate
0 .1559 .80827 .89827 .89827 .89827 .99827 .4986 .99827 .4986 .7827 .70827 .9092 .1963 .19	0 1.84528 1.84528 1.84518 1.84	0 8511 16918 35514 105805374 1058054 1	0 -1 450 23450 -1 4810 -2 4927 -1 7220 -1 7220

L.E. radius: 2.208 Slope of radius through L.E.: 0.253

NACA 644-021

[Stations and ordinates given in percent of airfoil chord]

Upper Surface		Lower	Surface
Station	Ordinate	Station	Ordinate
0 .1.2.5.5 0 .1.2.5.5 1.2.5.7 .1.2.5.0.5 1.2.5.7 .1.2.5.0.5 1.2.5.	0 1.95.48 9.75 9.8 9.95.48 9.95.48 9.95.88 9.95.89 9.95.89 9.95.40 9.95.40 9.95.40 9.95.40 9.95.40 9.95.40 9.95.40 9.95.40 9.95.40 9.95.40 9.95.40 9.95.40 9.9	0 .57.55 0 .57.55 12.57.0 .5 12.57.0 .5 15.0 .	0 -1.646 -1.9587 -2.548715 -2.548715 -5.7698 -9.8079 -10.4311 -10.4311 -10.4311 -10.4314 -2.449 -3.2213 -1.2449 0

L.E. radius: 2.884

NACA 644-421

Stations and ordinates given in percent of airfoil chord

Upper Surface		Lower	Surface
Station	Ordinate	Station	Ordinate
0 2477536 54588 379773445 6 7778 9 360 5 9 9 1 1 1 1 1 2 8 7 1 2 9	0 1.723 2.101 2.707 3.834 5.484 6.744 7.786 9.448 10.678 11.591 12.209 12.572 12.572 12.220 12.572 12.610 10.797 9.8198 7.491 6.203 4.876 2.276 1.079	0	0 -1.5231 -2.8279 -3.0900 -4.2188 -5.77594 -6.74594 -8.3219 -8.3219 -8.4199 -7.4538 -7.4538 -7.4538 -7.4538 -1.56022 -1.8692 -1.8694 -1.8508 -1.8508

L.E. radius: 2.884 Slope of radius through L.E.: 0.168

NACA 644-221

[Stations and ordinates given in percent of airfoil chord]

		The state of the s	
Upper Surface		Lower	Surface
Station	Ordinate	Station	Ordinate
0 3696577243669991 1027774366939600705655773149889396007000000000000000000000000000000000	0 1.049 2.618 3.6652 4.72828 9.7240 11.502 11.502 11.502 11.502 11.502 11.502 11.502 11.502 11.77 6.521 6.885 1.77 6.521 6.885 1.77 6.521 6.885 6.77 6.521 6.885 6.77 6.77 6.77 6.77 6.77	0 .94238 -94238 -9472286 -9472286 -9472281 -9472281 -9472281 -9472291 -9472291 -947291	0 -1.590 -1.590 -2.904 -3.293 -4.586 -6.248 -7.432 -8.291 -9.360 -9.360 -9.360 -7.552 -4.572 -1.593 -1.533 -1.533 -1.533 -1.5337 -1.5337 -1.5337

L.E. radius: 2.884
Slope of radius through L.E.: 0.084

NACA 65,3-018
[Stations and ordinates given in percent of airfoil chord]

Upper Surface		Lower	Surface
Station	Ordinate	Station	Ordinate
0 1.25.05 1.25	0 112 248 112 148 148 148 148 148 148 148 148 148 148	0 5725 5725 10 150 5 12.57 10 150 150 150 150 150 150 150 150 150	0 -1-29948 -1-299481

L.E. radius: 1.92

NACA 65,3-618
[Stations and ordinates given in percent of airfoil chord]

Upper Surface		Lower Surface	
Station	Ordinate	Station	Ordinate
0 17670 13843076 145076	0 1.434 1.767 2.2845 3.2445 9.866 10.767 11.950 12.201 12.201 12.330 10.5339 7.7734 12.3368 1.435	0 824 1.113 1.659 2.970 5.560 10.566 15.561 25.421 25.421 30.3262 40.174 45.085 54.923 59.858 69.778 74.776 84.808 94.932 100.000	0 -1.1347 -1.2471 -2.18496 -3.8496 -3.845230 -5.845230 -5.87775 -5.57775 -5.2760 -4.13566 -1.35665 -1.35665 -1.35666 -1.35666 -1.35666 -1.35666 -1.35666

NACA 65,3-418 a= 0.8

[Stations and ordinates given in percent of airfoil chord]

2			
Upper	Surface	Lower S	Burface
Station	Ordinate	Station	Ordinate
0 246711 24775118374582100555299010000000000000000000000000000	0 1.416 1.736 2.224 3.133 4.542 5.62 6.617 9.319 10.233 10.939 11.600 11.600 11.602 11.307 10.751 9.906 6.51 5.289 3.818 2.289 9.30	0 112 37999 2776 288 2476 288 2777 28 25 27 27 28 27 27 28 27 27 28 27 27 28 27 27 28 27 27 28 28 28 28 28 28 28 28 28 28 28 28 28	0 -1.4122348 -1.477277883777-207883777-207883777-207883777-207883777-207883777-207883777-2078787878787878787878787878787878787878

L.E. radius: 1.92 Slope of radius through L.E.: 0.194

NACA 65 (216)-415

Stations and ordinates given in percent of airfoil chord]

Upper	Surface	Lower	Surface
Station	Ordinate	Station	Ordinate
0 244 4690 2156440 2156440 2156689 2156667 21560	0 1.4947 24947 24947 24947 2507 2507 2507 2507 2507 2507 2507 250	0 75310 75310 2 193560 10 15 13 15 15 15 15 15 15 15 15 15 15 15 15 15	0960 -1.110 -1.359 -1.801 -2.411 -2.832 -3.169 -3.673 -4.267 -4.267 -4.507 -4.507 -4.507 -4.507 -4.507 -4.507 -7.521 -2.909 -1.848 -1.278 -2.905 -0.030

L.E. radius: 1.498 Slope of radius through L.E.: 0.233

NACA 65-006

[Stations and ordinates given in percent of airfoil chord]

Upper	Surface	Lower	Surface
Station	Ordinate	Station	Ordinate
0 125705 12570505050505050505050505050505050505050	0 .4747 .57476 .57476 .57589472 .1589972 .111222222222222222222222222222222222	0 12570505050505050505050505050505050505050	0 - 4764 - 7717 - 9556 - 1,589 - 1,824 - 2,197 - 2,482 - 2,697 - 2,9852 - 2,988 - 2,988 - 2,985 - 1,594 - 1,595 - 1,59

L.B. radius: 0.240

NACA 65-009

[Stations and ordinates given in percent of airfoil chord]

Upper	Surface	Lower	Surface
Station	Ordinate	Station.	Ordinate
0 125705 572505 1257050505050505050505050	0 1112235744444455522111 0	0 1.25.70 5 5.7250 5 1.25.70 12050 50 50 50 50 50 50 50 50 50 50 50 50	0 700 -1.058 -1.19683 -2.7729 -2.7729 -4.287 -4.4969 -4.4969 -4.4969 -4.4969 -4.4969 -4.4969 -4.4969 -4.4969 -4.7728 -2.88562 -1.2638 -1.2638 -1.2638 -1.2638 -1.2638 -1.2638 -1.2638 -1.2638

L.E. radius: 0.552

NACA 65-206

[Stations and ordinates given in percent of airfoil chord]

Upper	Surface	Lower	Surface
Station	Ordinate	Station	Ordinate
0 .460 .7700 1.49397 79.9456 14.9339.9562 14.999781 19.9990 50.0096 650.016 650.0096 670.028 90.0096 90.0096 90.0096 90.0099 90.0099	0 .6422 6422 6422 6422 6422 6422 6422 6422	0 57900 1.355661 2.556661 70.0001 1.556661 2.556661 2.556661 2.556661 2.55661 2.55661 2.55661 2.5661	0 - 121 - 502 - 608 - 768 - 768 - 768 - 1523 - 1685 - 1.880 - 1.922 - 1.880 - 1.922 - 1.846 - 1.1447 - 1.216 - 963 - 699 - 1437 - 192 - 007

L.E. radius: 0.240 Slope of radius through L.E.: 0.084

NACA 65-209

[Stations and ordinates given in percent of airfoil chord]

, p			
Upper	Surface	Lower	Surface
Station	Ordinate	Station	Ordinate
0	0	0 .559 816 1.5595 5092 7.5995 10.0996 15.0892 25.0071 30.009 45.0000 549.961 779.961 779.961 779.961 94.969 94.969 94.969	0 - 6482 - 7948333-1-69577-2-2-69354 -1-69577-2-2-69354 -3-3-4901-3-3-3937331-2-2-2-3-3-2-2-2-2-2-2-2-2-2-2-2-2-2-

L.E. radius: 0.552 Slope of radius through L.E.: 0.084

NACA 65-210

[Stations and ordinates given in percent of airfoil chord]

Upper Surface		Lower	Surface
Station	Ordinate	Station	Ordinate
0	0 11233744578 892779995588 92779995588 92779995588 92779995772 96227228 9727995772 972222 97222 97222 97222 97222 97222 97222 97222 97222 972222 97222 97222 97222 97222 97222 97222 97222 97222 972222 97222 97222 97222 97222 97222 97222 97222 97222 972222 97222 97222 97222 97222 97222 97222 97222 97222 972222 97222 97222 97222 97222 97222 97222 97222 97222 9722	0 .565 .8331 2.5922 5.1006 10.1006 15.1011 25.0791 35.0499 45.0000 54.9863 45.0000 54.99575 74.9956 66.99575 84.986 100.000	0 - 1999

NACA 65₁ -012

[Stations and ordinates given in percent of airfoil chord]

oppor	Surface	Lower	Surface
Station	Ordinate	Station	Ordinate
0 -5755 -1.2.57.05 1.2.57.05	0 1112534455555555443321 0 11125344555555555443321 0 111264725662794722313595076	0 .57.55 5.7.25 10 .50 .5 10 .50 .5 10 .50 .5 10 .50 .5 10 .	0 -11387662 -1138762 -113

NACA 65-410

[Stations and ordinates given in percent of airfoil chord]

NACA 651-212

Stations and ordinates given in percent of airfoil chord

Station
0 1.23 4.1514 2.879 1.9.879 1.9.906 2.9.901 1.9.906 2.9.901 1.9.900 2.9.901 1.9.900 2.9.901 1.9.900 2.9.901 1.9.900 2.9.901 1.9.900 2.9.901 1.9.900 2.9.901 1.9.900 2.9.901 1.9.900 2.

NACA 65₁-212 a = 0.6

Stations and ordinates given in percent of airfoil chord

Upper S	Surface	Lower S	Surface
Station	Ordinate	Station	Ordinate
0 3998 1.35567277388349941 1.3537297388849941 1.958834999834999883499988999889998899989998	0 982 1.5190 3.71920 3.71920 4.5208 5.6619 5.68483 5.6	0 601 8366 1.544 5.1671 7.671 10.1167 20.131 30.1069 45.0017 45.901 45.901 45.901 45.901 45.901 45.901 45.901 88.80 74.901 89.901 89.901	0

L.E. radius: 1.000 Slope of radius through L.E.: 0.110

NACA 652 -015

Stations and ordinates given in percent of airfoil chord

Upper	Surface	Lower	Surface
Station	Ordinate	Station	Ordinate
0 12.500 57.2500 10.5000 10.500 10.500 10.500 10.500 10.500 10.500 10.500 10.500 10.5000 10.500 10.500 10.500 10.500 10.500 10.500 10.500 10.500 10.5000 10.500 10.500 10.500 10.500 10.500 10.500 10.500 10.500 10.5000 10.500 10.500 10.500 10.500 10.500 10.500 10.500 10.500 10.5000 10.500 10.500 10.500 10.500 10.500 10.500 10.500 10.500 10.5000 10.500 10.500 10.500 10.500 10.500 10.500 10.500 10.500 10.5000 10.500 10.500 10.500 10.500 10.500 10.500 10.500 10.500 10.5000 10.500 10.500 10.500 10.500 10.500 10.500 10.500 10.500 10.5000 10.500 10.500 10.500 10.500 10.500 10.500 10.500 10.500 10.5000 10.500 10.500 10.500 10.500 10.500 10.500 10.500 10.500 10.5000 10.500 10.500 10.500 10.500 10.500 10.500 10.500 10.500 10.5000 10.500 10.500 10.500 10.500 10.500 10.500 10.500 10.500 10.5000 10.500 10.500 10.500 10.500 10.500 10.500 10.500 10.500 10.5000 10.500 10.500 10.500 10.500 10.500 10.500 10.500 10.500 10.5000 10.500 10.500 10.500 10.500 10.500 10.500 10.500 10.500 10.5000 10.500 10.500 10.500 10.500 10.500 10.500 10.500 10.500 10.5	0 1.3752 4592 11.3702 12.3702	0 • 12.5000 12	0 -1.124 -1.356 -1.7524 -2.2459 -3.2459 -4.5555 -5.225 -6.7652 -7.498 -7.498 -7.428 -5.404 -7.428 -1.428

NACA 651 -412

[Stations and ordinates given in percent of airfoil chord]

Upper Surface		Lower	Surface
Station	Ordinate	Station	Ordinate
0 .585937 70.285937 70.2857 70.7851 10.2857 70.7851 10.2857 10.0861 10.0863 10.0866 10	01.06988447002112.23.4447.0212.23.4447.0212.23.44	0	0 810 - 956 -1.160 -1.1995 -2.3604 -3.3673 -3.773 -3.222 -2.801 -2.7551 -3.222 -2.320 -1.267 -2.751 -2.751 -2.751 -2.751 -2.751 -2.751 -2.751 -2.751

L.E. radius: 1.000 Slope of radius through L.R.: 0.168

NACA 652-215

Stations and ordinates given in percent of airfoil chord

Upper Surface		Lower	Surface
Station	Ordinate	Station	Ordinate
0 46452558442118884472269349999999999999999999999999999999999	0 1.42566 1.480567095889588958895889588888888888888888888	0 .845.88 .528 .55.62 .55.88 .	0 -1.070 -1.282 -1.591 -2.134 -2.125 -3.532 -4.035 -5.126 -6.179 -6.366 -6.1427 -6.368 -6.1427 -4.373 -3.628 -2.848 -2.061 -1.303 -626 -1.120

L.E. radius: 1.505 Slope of radius through L.E.: 0.084

NACA 652-415

Stations and ordinates given in percent of airfoil chord

Upper Surface		Tower	Surface
Station	Ordinate	Station	Ordinate
0 3146117 502367882 102367862677635 10247794155500057966 10247794157555005 10247794157555005 10247794157555005 10247794157555005 10247794157555005 10247794157555005 10247794157555005 10247794157555005 10247794157555005 10247794157555005 10247794157555005 10247794157555005 10247794157555005 10247794157555005 10247794157555005 10247794157555005 10247794157555005 10247794157555005 10247794157555005 1024779415755005 1024779415755005 102477941575005 1024779475005 10247794005 10247794005 10247795 10247795 10247795 10247795 10247775 10247775	0 1.4800 2080 1.49080 2080 2080 2080 2080 2080 2080 2080	0	0 008 -1.008 -1.472 -1.95998 -3.5150 -4.9705 -5.3555 -5.3555 -4.5705 -3.55576 -4.5706 -3.55576 -4.5706 -3.55576 -4.5706 -3.6544 -1.206

L.E. radius: 1.505 Slope of radius through L.E.: 0.168

NACA 653-018

Stations and ordinates given in percent of airfoil chord

Upper Surface		Lower	Surface
Station	Ordinate	Station	Ordinate
0 .725 -725 -725 -70 -70 -70 -70 -70 -70 -70 -70 -70 -70	0 1.601416 7.756633776663774566472956647295664729566877566472956888888888888888888888888888888888888	0 .5755 57255 10 .5755 10 .575	0 -1-2-378635766 3778637786377863778637786377863774647956 990188774564795688756267943332319

L.E. radius: 1.96

NACA 652 -415 a = 0.5

[Stations and ordinates given in percent of airfoil chord]

Upper	Surface	Lower	Surface	
Station	Ordinate	Station	Ordinate	
0 2454 4926 4926 4705 21575 4926 4705 5611 2496 7705 2496 1916 2949 2949 2949 2949 2949 2949 2949 294	0 11.596.52.59.59.59.59.59.59.59.59.59.59.59.59.59.	0 7556734266 11.5756754266 11.5756754266 11.5756754266 11.5756754266 11.575675426 11.5756754 11	0 -1-37765 -1-3776556 -2-377656 -2-37765 -3-3768 -3-3768 -3-3-3-3-3-3-3-3-3-3-3-3-3-3-3-3-3-3-3	
T.R. redi	I. R. redinge 1.505			

L.E. radius: 1.505 Slope of radius through L.E.: 0.233

NACA 653-218

[Stations and ordinates given in percent of airfoil chord]

Upper	Upper Surface		Surface	
Station	Ordinate	Station	Ordinate	
0 388 625 1.110 2.349 7.311 9.8819 7.811 9.835 24.858 29.942 39.9	0 1.382 1.6776 2.9328 45.15376 2.9328 45.15776 9.92666 9.926666 10.079	0 .612 .875 .390 .2.660 5.181 .7.689 10.191 15.182 .25.142 .30.1165 .25.142 .30.1165 .25.142 .30.927 .74.923 .77.926 .84.937 .74.923 .77.926 .84.937 .79.926 .84.937 .79.926	0 -1.282 -1.5332 -2.5646 -3.5956 -4.9370 -4.9370 -7.622 -7.806 -7.806 -7.806 -7.806 -7.906 -6.1365 -4.5500 -4.5500 -1.801 -1.801 -1.801	

L.E. radius: 1.96 Slope of radius through L.E.: 0.084

NACA 653-418

[Stations and ordinates given in percent of airfoil chord]

Upper Surface		Lower	Surface
Station	Ordinate	Station	Ordinate
0 2783 2793 218323 218323 218323 218323 21932 21	0 1.418 1.7299 2.1041 1.48668 7.9061 4.54782 1.09149 11.149149 11.	0 7227 72277 1.81377 10.5814 150.52814 255.288	0 218 -1.4491 -2.4507 -2.52170 -4.1250 -5.8140 -6.8564 -6.8564 -6.8564 -6.8564 -6.8564 -6.8564 -6.8564 -6.8564 -6.8564 -6.8564 -7.5812

L.E. radius: 1.96 Slope of radius through L.E.: 0.168

NACA 653-618

[Stations and ordinates given in percent of airfoil chord]

Upper S	Surface	Lower	Surface
Station	Ordinate	Station	Ordinate
0 172 8859 2.0462 6.935 2.4456 9.4451 19.565 24.56738 39.991 50.007 50.0141	0 1.446 1.776 2.293 3.268 4.776 5.971 6.978 8.602 9.848 10.803 11.504 11.972 12.210 12.186 11.877 11.293 10.479	0 828 1.1661 2.974 5.584 10.569 15.494 25.426 30.174 45.085 50.000 54.923 59.859 64.811	0 -1.356 -1.651 -2.152 -2.880 -3.426 -5.4672 -5.7784 -5.7792 -5.7792 -5.2593 -4.7259
65.189 70.219 75.230 80.220 85.189 90.138 95.068 100.000	9.482 8.338 7.075 5.719 4.306 2.863 1.433	64.811 69.781 74.770 79.780 84.811 89.862 94.932	-3.302 -2.506 -1.705 943 268 .463

L.E. radius: 1.96 Slope of radius through L.E.: 0.253

NACA 653 -418 a = 0.5

[Stations and ordinates given in percent of airfoil chord]

	Surface		I
Station	Ordinate	Station	Ordinate
0	0	0	0
.197	1.440	1.089	-1.164
.411	1.766 2.271	1.632	-1.683
2.057	3-233	2.943	-2.197
4.493	4.715	5.507 8.034	-2.951 -3.515
6.966	4.715 5.891 6.882	10.541	-3.978
9.459	8.482	15.519	-4.690 -5.213
19.533	9.709	25.396	-5.595 -5.853
29.691	11.325	30.309 35.211	-5.853
列·789 39·899	11.770	40.101	-5.998 -6.026
15.022	11.897	44.978	-5.905
50.182	11.506	49.818	-5.626 -5.216
55.313	9.820	59.636	-4.696
65.372	8.674	64.628	-3.433
70.347 75.298	7.397 6.038	69.653	-2.734
80.232	4.636	79.768	-2.024
85.159 90.089	3.247	89.911	-1.331
95.030	.777	94.970	201
100.000	0	100.000	0

L.E. radius: 1.96 Slope of radius through L.E.: 0.233

NACA 653 -618 a = 0.5

[Stations and ordinates given in percent of airfoil chord]

Upper Surface		Cace Lower Surface	
Station	Ordinate	Station	Ordinate
0	0	0	0
0569686450 0569486450 0568420 074588494565 074723 074588494565 074588495 074588495 074588495 075885 07788 077885 077885 077885 077885 077885 077885 077885 077885 07788 077885 077885 07788 077	1.469 1.821 2.375 3.449 5.415 6.445 10.893 12.687 13.459 12.179 9.375 12.179 9.375 12.220 0	941 1.8154 2.806 1.75946 10.8779 25.6993 30.1516 20.5903 340.1516 49.455 54.454 69.455 69.455 69.455 69.455 69.455 69.455 69.455 69.455 69.455 69.455 69.455 69.455 69.455 69.455 69.455 69.456 69.455	-1.055 -1.293 -1.895 -2.8969 -2.8196 -2.82196 -4.3277 -4.455407 -4.455407 -4.455407 -4.455407 -4.455407 -4.455407 -4.455407 -4.455407 -2.48368 -3.84916 -3.84916 -3.84916

L.E. radius: 1.96 Slope of radius through L.E.: 0.349

NACA 654 -021

[Stations and ordinates given in percent of airfoil chord]

Upper Surface		Lower	Surface
Station	Ordinate	Station	Ordinate
0 •5755 •125705 12570505050505050505050505050505050505050	0 118301428 22880144788 231147	0	0 -1 - 2 - 2 - 2 - 2 - 2 - 2 - 2 - 2 - 2

NACA 654-421

[Stations and ordinates given in percent of airfoil chord]

Upper Surface		Lower	Surface
Station	Ordinate	Station	Ordinate
0 2468 93522 470557566 2458622776629 19358227796576629 1946835522 1946835756629 194683576629 194683576629 194683576629 194683576629 194683576629 194683576629 194683576629 194683576629 194683576629 194683576629 194683576629 194683576629 194683576629 194683576629 19468357629 1946837629 194687	0 1.601 1.956 2.4953 3.505 5.085 6.329 7.371 10.304 11.271 12.430 12.158 11.457 10.531 9.166 6.5388 3.595 10.531 9.166 6.5388 3.5176	0 75327 75327 10 56657 12 44284 10 44283 11 54283 11 54283 12 13 56 12 13 56 14 50 949 15 14 88 57 16 14 88 57 16 14 88 57 17 9 8 9 8 9 9 9 100 100 100 100 100 100 100 100 100 100	0

L.E. radius: 2.50 Slope of radius through L.E.: 0.168

NACA 654-221

[Stations and ordinates given in percent of airfoil chord]

Upper S	Surface	Lower	Burface
Station	Ordinate	Station	Ordinate
0	0 1.567 1.902 2.402 3.335 4.7835 5.918 6.865 9.5714 10.381 11.007 11.404 11.570 11.404 11.055 10.372 9.461 8.390 7.195 5.918 4.925 8.620 7.195 5.925 8.620 7.195 8.620 8.620 7.195 8.620 8.620 8.620 8.620 7.195 8.620 8 8 8 8 8 8 8 8 8 8 8 8 8 8 8 8 8 8 8	0 .628 .892 1.110 2.681 5.209 10.222 15.213 20.192 25.166 30.135 40.068 45.033 50.000 51.974 69.916 64.916 74.912 84.928 89.948 89.948	0

NACA 654 -421 a = 0.5

Stations and ordinates given in percent of airfoil chord

Upper	Surface	Lower	Surface
Station	Ordinate	Station	Ordinate
0 155 3633 1992 4.814 6.880 9.3795 19.4538 29.7542 24.7538 29.7542 450.211 55.362 60.421 60.421 60.421 60.398 70.394 80.100 95.034 100.000	0 1.620 1.991 2.5531 5.631 5.631 5.7772 10.951 12.000 12.765 13.4362 13.4362 12.954 13.4362 12.954 13.636 10.954 13.636 10.954 13.636 10.954 1	0 845 1.157 2.088 5.586 10.629 10.629 10.629 120.5461 20.5461	0 -1.696511590 -1.6965517690 -2.74529366 -7.7.7.7.65 -6.7.7.7.7.65 -6.7.7.7.65 -6.7.7.7.65 -6.7.7.7.65 -6.7.7.7.65 -6.7.7.7.65 -6.7.7.7.65 -6.7.7.7.65 -6.7.7.7.65 -6.7.7.7.65 -6.7.7.7.7.65 -6.7.7.7.7.65 -6.7.7.7.7.7.7.7.7.7.7.7.7.7.7.7.7.7.7.7

L.E. radius: 2.50 Slope of radius through L.E.: 0.233

NACA 65(215)-114

[Stations and ordinates given in percent of airfoil chord]

Upper S	Surface	Lower	Surface
Station	Ordinate	Station	Ordinate
0 .4561 .71957.4.9226 .1.1957.9.9226 .1.9.9326 .1.9.9326 .1.9.9326 .2.9.9326 .2.9.9326 .2.9.9326 .0.010 .0.025 .0.025 .0.025 .0.000 .0.000	0 1.3646 0 1.36466 1.36466 1.36466 1.4766 1.4766 1.4766 1.4776 1.	0 544 77995 1.566774 1.570774 1.00774 1.00764 1.00	0 02304 -1.2304 -2.077822 -2.98010 -5.18659 -6.13888 -6.172144 -5.1728 -3.8016 -2.269 -1.509 -1.509

L.E. radius: 1.311 Slope of radius through L.E.: 0.042

NACA 65(421)-420

[Stations and ordinates given in percent of airfoil chord]

Upper S	Surface	Lower	Surface
Station	Ordinate	Station	Ordinate
0 2480 2582 24950 2450 25796 4477 25796 4457 2668 2677 2677 2677 2677 2677 2677 267	0 1.8774 1.8774 2.3758 4.0666 7.06655 10.815 11.4939 12.0572 11.0126 9.8661 11.0126 9.77.5660 9.8661 11.150 12.0572 11.0126 9.77.5600 12.0572 11.0126 9.8661 0.5203 11.150	0 742 1.0508 1.5508 2.848 5.7917 10.4204 25.3516 25.3516 25.3516 25.3516 25.3516 25.3516 26.3016 27.3518 27.35	0 -1.584 -1.584 -1.584 -2.614 -3.602 -4.370 -4.992 -5.973 -7.819 -7.8819 -7.8676 -7.8676 -7.8676 -7.8983 -2.983 -2.983 -2.983 -2.983 -1.121

L.E. radius: 2.27 Slope of radius through L.E.: 0.168

NACA 66,1-212

[Stations and ordinates given in percent of airfoil chord]

-FP	Burface	Lower	Surface
Station	Ordinate	Station	Ordinate
0 124 6667 2 3879 4 3879 4 8895 24 9905 24 9905 24 9905 25 0036 70 0665 85 065 85 065 85 0000	0 114986 114986 114986 114986 114986 114986 114986 114986 114986 115986	0	0 -847 -1003345 -1.653-1.653-2.59639 -2.59639 -2.59639 -3.3822 -4.5756 -4.869 -4.7423 -4.57563-2.1667 -4.160

Slope of radius through L.E.: 0.084

NACA 66(215)-016

[Stations and ordinates given in percent of airfoil chord]

Upper	Surface	Lower	Surface
Station	Ordinate	Station	Ordinate
0 • 72505 • 12505 • 12505 • 120505 • 12	0 1.147578 24.147578 25.2927 25.2927 27.777.778.2927 27.777.778.2927 27.777.778.2927 21.5927 2	0 1.555 7.25 10 150 50 50 50 50 50 50 50 50 50 50 50 50 5	0 -1.44 -1.4758 -1.4758 -3.2927 -4.62652 -5.63650 -7.37995 -7.79957 -7.74 -7.74 -5.98766 -5.987669 -2.75897

L.E. radius: 1.575

NACA 66(215)-216 a = 0.6

[Stations and ordinates given in percent of airfoil chord]

Upper	Surface	Lower	Surface
Station	Ordinate	Station	Ordinate
0 37071744418181886622276883976933311988188692976833311988189661198818966119899999999999	0 1.586 2421 1.586 615 1.586 617 1.536 8.068 9.996 1.428 8.068 9.9999 8.8895 1.286 1	0 629 1,4886 1,4886 1,2716 10,1212 20,11688 35,1064 20,1777 54,8896 49,9777 54,8896 64,8896	0 -1.112 -1.508 -2.1608 -2.1869 -3.141 -3.934 -4.702 -5.7180 -6.312 -6.312 -6.3548 -6.357 -6.3548 -1.177 -1.1255 -1.1275 -1.1255

L.B. radius: 1.575 Slope of radius through L.E.: 0.110

NACA 66 (215)-216

Stations and ordinates given in percent of airfoil chord

Upper	Burface	Lower S	Surface
Station	Ordinate	Station	Ordinate
0 4010 1.1282 4.3483 4.3483 14.8840 2.4.8949 2.4.8970 3.4.8970 3.4.99970 3.4.99970 3.4.99970 3.6.9070	0 111850 48 50 48 50 48 50 48 50 48 50 48 50 48 50 50 50 50 50 50 50 50 50 50 50 50 50	0	0 -1.304 -1.344 -2.188 -2.580 -4.964 -4.964 -6.676 -6.676 -6.676 -6.838

L.E. radius: 1.575 Slope of radius through L.E.: 0.084

NACA 66(215)-416

[Stations and ordinates given in percent of airfoil chord]

Upper	Surface	Lower	Surface
Station	Ordinate	Station	Ordinate
0 -303 1,008 2,225 4,691 9,677 14,691 19,720 24,757 29,898 44,000 55,050 60,135 70,161 75,170 85,150 90,000	812403928 6812403928 69732444436650730612 25973245767899737701167692 89774062 100998776542 10	0 .697 .992 2.7775 57.820 25.243 150.280 25.243 150.280 25.245 30.1952 450.000 544.9504 450.000 544.9504 8859 74.8859 894.9000	0 -1.25-9964-71 -1.55-9964-71 -2.55-9964-71 -2.55-9964-71 -2.55-996-71 -2.55-71 -5-55-75-75-75-75-75-75-75-75-75-75-75-7

L.E. radius: 1.575 Slope of radius through L.E.: 0.168

NACA 66-006

[Stations and ordinates given in percent of airfoil chord]

Upper	Surface	Lower	Surface
Station	Ordinate	Station	Ordinate
0 12570505050505050505050505050505050505050	0 .4614 .6943 .9187 .9187 1.5752 2.14018 2.26182 2.29700 2.26151 2.3163 1.9543 1.1075 2.2662	0 125705 125705 12570505050505050505050505050505050505050	0 - 461 - 594 - 993 - 918 - 1.257 - 1.752 - 2.119 - 2.618 - 2.7899 - 2.925 - 2.985 - 2.925 - 2.611 - 2.513 - 2.611 - 2.662

L.B. radius: 0.223

NACA 66-206
[Stations and ordinates given in percent of airfoil chord]

Upper	Surface	Lower	Surface
Station	Ordinate	Station	Ordinate
0 1617 17022 17022 19419 19954 19954 19954 19952 19962 19900 190000 1900	0 5022 6792 1.102 1.5948 1.5749 1.5749 1.5772 1.577	0 -72959591 12-5555618 7-29555618 12-5555618 12-5555618 12-55618 12-55618 12-5619 12-5619 12-5619 13-6	0

L.E. radius: 0.223 Slope of radius through L.E.: 0.084

NACA 66-009

[Stations and ordinates given in percent of airfoil chord]

Station	Ordinate 0687824 -1.030 -1.368 -1.880 -2.283 -2.626
0	0 687 821 -1.030 -1.368 -1.880 -2.283 -2.626
0 •75 1.25 2.50 7.5	687 824 -1.030 -1.368 -1.880 -2.283 -2.626
• 12.5.7.0 • 12.5.7.0	-5.178 -5.6017 -4.17457 -4.1457 -4.1457 -4.1458 -4.1458 -4.1611 -5.12611 -2.2611 -3.774
	85 90 95

L.E. radius: 0.530

NACA 66-209

[Stations and ordinates given in percent of airfoil chord]

Upper Surface		Lower	Surface
Station	Ordinate	Station	ordinate
0	0 .81559451061588486552021 739252451061588486552021683799352145555555554455555556445555555644555555644555555	0 554411 12558891 12558891 10.08879 25.08879 25.001000 25.001000 25.001000 25.001000 25.001000 25.001000 25.001000 25.001000 25.001000 25.001000	0 - 635 - 752 - 752 - 1180 - 1 562 - 1 857 - 2 107 - 2 504 - 3 031 - 3 386 - 3 404 - 3 386 - 3 187 - 3 286 - 3 186 - 3

L.E. radius: 0.530 Slope of radius through L.E.: 0.084

NACA 66-210

Stations and ordinates given in percent of airfoil chord

Upper Surface		Lower	Surface
Station	Ordinate	Station	Ordinate
0 136 1679 1.171 2.1412 1.9029 7.929 14.903 15.903 16.003 16	0 895991882 944957882445556862455919951445557044557028457702845704	0 .564 .8219 .2.5888 5.0901 10.1027 .2.088 .25.076 .30.048 .25.076 .30.0316	0 7060 -18451 -1.7610 -2.3896 -2.38964 -3.4664 -3.8805 -3.8662 -3.8662 -3.9668 -3.968 -3.5275 -2.8281 -2.6976 -1.6996 -2.6996

L.E. radius: 0.662 Slope of radius through L.E.: 0.084

NACA 66₁ -012

[Stations and ordinates given in percent of airfoil chord]

Upper	Upper Surface		Surface
Station	Ordinate	Station	Ordinate
0 125705 12570505050505050505050505050505050505050	0 1112 53 44 555 556 555 543 221 0	0 125705 125705 12570505050505050505050505050505050505050	0 -1-2-5-8-9-6-6-8-8-9-7-6-9-8-8-9-7-6-9-8-8-9-7-6-9-8-8-9-7-6-9-8-9-8-9-7-9-8-9-8-9-7-9-8-9-8-9-8-9-8

L.B. radius: 0.952

NACA 661 -212

[Stations and ordinates given in percent of airfoil chord]

Upper Surface		Lower	Surface
Station	Ordinate	Station	Ordinate
0 1.2666 1.2666 1.398798 1.398798 1.9988 1.9999 1.9	0 9534919 9534911 11,4991 21,4	0 .5344 2.605,7 .621 10.122 10.122 10.106 25.092 36.0098 10.00	0 853 -1.0419 -1.2419 -2.1717 -2.9759 -4.5776 -4.5776 -4.5776 -4.5776 -4.5179 -4.5179 -4.5179 -4.5179 -4.5179 -4.5179 -2.2179 -1.409 -1.157

L.E. radius: 0.952 Slope of radius through L.E.: 0.084

NACA 662-015

[Stations and ordinates given in percent of airfoil chord]

Upper Surface		Lower	Surface
Station	Ordinate	Station	Ordinate
0 1257 1505 1257 1505 1257 1505 1505 1505 1505 1505 1505 1505 15	0 1.367550 1.247550 1.367250 1	0 • • • • • • • • • • • • • • • • • • •	0 -1.3475500 1223 -1.621757500 134755500 134755500 1347555300 1347500

L.E. radius: 1.435

NACA 662-215

[Stations and ordinates given in percent of airfoil chord]

Upper Surface		Lower	Surface
Station	Ordinate	Station	Ordinate
0 12.855988966666666666666666666666666666666	0 1.409 1.409 1.77417 3.4192 2.4192 2.4193 2.777 2.928 2.595 2.992	0	0 -1.269451 -1.56451 -2.7858145 -2.78586118 -5.6922590 -6.18882 -5.60736076 -2.8571 -2.8561 -2.8561 -2.8561 -2.8561 -2.8561

L.E. radius: 1.435 Slope of radius through L.E.: 0.084

NACA 663-018

[Stations and ordinates given in percent of airfoil chord]

Upper Surface		Lower	Surface
Station	Ordinate	Station	Ordinate
0 • 1-2-50-5 57-2-50-5 1-2-50-5 1-2-50-5 1-2-50-50-50-50-50-50-50-50-50-50-50-50-50-	01.579.640130 3712.66013033888615.233888615.233888618888887.559.5716429.7164446	0 1250 5 57250 5 1250 5	0 323 -1.5752 -2.5699 -3.66913 -4.52133 -7.848 -7.848 -8.7101 -8.7101 -8.7133 -7.84998 -8.7328 -8.7328 -6.55971 -4.234 -4.234 -6.5914 -6.5914 -6.9146

NACA 662-415

[Stations and ordinates given in percent of airfoil chord]

**		Town	Surface
Upper Surface		Tower.	Surrace
Station	Ordinate	Station	Ordinate
0 .5449 1.2411 1.24719 .241719 .24719 .29736 .7736 .79736 .79736 .79736 .9950 .0926 .09	0 1.187928 20677328 20677328 20677328 20677328 20677328 2077856 207786 2077856 20778	0 .6866 9581 972891 12.72891 10.222184 15.222184 15.0048 15.00	0 -1.006 -1.1445 -1.1445 -1.8454 -2.4549 -2.3313 -3.9327 -4.749 -5.189 -5.189 -5.287 -4.3630 -4.3630 -4.3630 -4.3630 -2.8393 -4.3630 -2.8393 -2.003 -1.180 -1.180

L.E. radius: 1.435 Slope of radius through L.E.: 0.168

NACA 663-218

[Stations and ordinates given in percent of airfoil chord]

Upper Surface		Domer	Surface
Station	Ordinate	Station	Ordinate
0 3828 611342708 1138	0 1.6354 1.6354 1.2.828 1.2.828 1.2.828 1.2.828 1.2.828 1.2.828 1.2.828 1.2.828 1.2.964 1.2.96	0 .611 .8785 2.654 5.173 7.680 10.182 15.1759 25.1157 30.058 45.0058 45.000 54.972 59.9946 64.921 74.995 79.995 89.999	0 -1.268 -1.496 -1.840 -2.456 -3.370 -4.690 -5.658 -6.390 -7.8767 -7.903 -7.838 -7.838 -7.8550 -5.5524 -4.555 -3.409 -1.196

L.E. radius: 1.955 Slope of radius through L.E.: 0.084

NACA 663-418
[Stations and ordinates given in percent of airfoil chord]

Upper Surface		Lower	Surface
Station	Ordinate	Station	Ordinate
0 .280 .5981 .194 .656 .6361 .19.653 .24.726 .29.729 .39.885 .44.940 .55.056 .60.178 .70.178 .70.191 .80.185	0 1.405 1.692 2.147 3.000 4.3347 7.6673 9.633 10.2759 11.188 10.923 11.188 10.923 11.188 10.923 11.188 10.923 11.188 10.923 11.188 10.923 11.188 10.923 11.188 11.198 11.1	0 720 9919 1.5804 10.33497 25.2271 25.2271 25.2271 25.2271 25.2271 25.2271 25.2271 25.2271 25.2271 25.2271 25.2271 25.2271 25.2271 25.2271 25.2271 25.2271 25.2271 26.2271 27.	0 -1.41296 -1.47256 -3.6451 -3.6451 -4.97893 -6.76836 -6.75836 -6.75836 -6.75836 -6.75836 -6.75836 -6.75836 -6.75836 -6.75836 -7.

L.E. radius: 1.955 Slope of radius through L.E.: 0.168

NACA 664-021 Stations and ordinates given in percent of airfoil chord

Upper Surface		Lower	Surface
Station	Ordinate	Station	Ordinate
0 125705 572505 125705 12257050505050505050505050505050505050505	0 1.525 1.8240 2.045 4.2233 4.2233 4.2233 6.052 7.3376 9.153 9.153 9.153 10.186 9.735 10.186 9.735 10.186 9.735 10.186 9.735 10.186 9.735 10.186 10.1	0 12505 572505 12505 105050505050505050505050505050505050	0 -1.825 -1.8240 -2.045 -2.045 -4.520 -5.03666 -9.7354 -9.7354 -10.4070 -10.4866 -9.6793 -10.4866 -9.6793 -10.4970 -10.4

L.E. radius: 2.550

NACA 664-221

Stations and ordinates given in percent of airfoil chord

Upper Surface		Lower	Surface
Station	Ordinate	Station	Ordinate
0 .3720 .6015 .2.3800	0 1.570 1.869 2.342 3.226 4.5653 6.5655 9.170 10.7093 11.4783 11.5381 11.5381 11.5381 11.5381 11.5381 11.5381 11.5381 11.5381 11.5381 11.5396 11.032	0 628 8900 1 4905 2 6777 5 200 90 10 212 15 20 185 20 185	0 -1.470 -1.7298 -2.8548 -3.94805 -7.5258 -7.5258 -7.5258 -7.5258 -7.5258 -9.3351 -7.5258 -9.3351 -7.5258 -9.3351 -7.5258 -7.5259 -1.4400 0

L.E. radius: 2.550 Slope of radius through L.E.: 0.084

NACA 67, 1-215
[Stations and ordinates given in percent of airfoil chord]

Upper	Surface	Lower	Surface
Station	Ordinate	Station	Ordinate
0 .102 .6128 .6128 .61361 .738414 .7384859 .94889 .9597 .000 .000 .000 .000 .000 .000 .000 .0	01112544456778888888776555973	0	0 -1.3655 -1.3

NACA 747A415

Stations and ordinates given in percent of airfoil chord

Upper	Surface	Lower	Surface
Station	Ordinate	Station	Ordinate
0 18982177261888846477443344766 1899455998891344443341106 1945558991344445211106375 000000000000000000000000000000000000	8226611880777766145798887655459	0 11.695138 41.792 02 810489338 41.792 02 810489518 41.792 02 81048938 41.792 02 81050495 81.792 81.	0 -1.1606 -1.1606 -1.1822 -2.70581 -2.70581 -3.5015 -4.4968 -3.5015 -3

NACA 747A315

[Stations and ordinates given in percent of airfoil chord]

Upper
Station
0 24919 24919 24919 2479 25598 25598 25746 25746 25746 25746 25746 25746 25746 25746 25746 25746 25746 25746 25746 25746 25746 25746 25756 25766

L.E. radius: 1.544 Slope of radius through L.E.: 0.232

IV - PREDICTED CRITICAL MACH NUMBERS

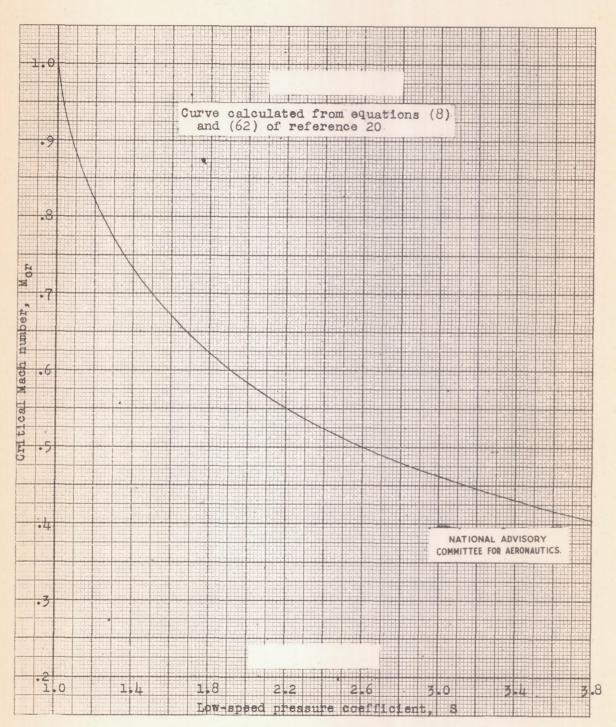
IV - PREDICTED CRITICAL MACH NUMBERS

Critical Mach number chart	s83
Variation of critical Mach number with low-speed section lift coefficient for the NACA 0006, 0009, and 0012 airfoil sections	584
Variation of critical Mach number with low-speed section lift coefficient for several NACA 14-series airfoil sections of various thicknesses	s85
Variation of critical Mach number with low-speed section lift coefficient for several 24-series airfoil sections of various thicknesses	s86
Variation of critical Mach number with low-speed section lift coefficient for several NACA 44-series airfoil sections of various thicknesses	s87
Variation of critical Mach number with low-speed section lift coefficient for several NACA 230-series airfoil sections of various thicknesses	s88
Variation of critical Mach number with low-speed section lift coefficient for several NACA 63-series airfoil sections of various thicknesses, cambered for various design lift coefficients	s89
Variation of critical Mach number with low-speed section lift coefficient for several NACA 63-series symmetrical airfoil sections of various thicknesses	S90
Variation of critical Mach number with low-speed section lift coefficient for several NACA 63-series airfoil sections of various thicknesses, cambered for a design lift coefficient of 0.2	591
Variation of critical Mach number with low-speed section lift coefficient for several NACA 63-series airfoil sections of various thicknesses, cambered for a design	
lift coefficient of 0.4	S92

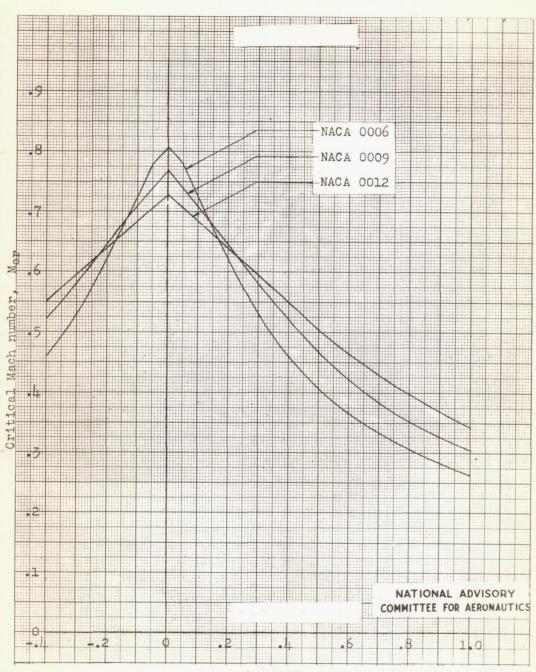
Variation of critical Mach number with low-speed section lift coefficient for two NACA 63-series airfoil sections of different thicknesses, cambered for a design lift coefficient of 0.6	. S93
Variation of critical Mach number with low-speed section lift coefficient for several NACA 64-series symmetrical airfoil sections of various thicknesses	. 594
Variation of critical Mach number with low-speed section lift coefficient for several NACA 64-series airfoil sections of various thicknesses, cambered for a design lift coefficient of 0.1	. S94a
Variation of critical Mach number with low-speed section lift coefficient for several NACA 64-series airfoil sections of various thicknesses, cambered for a design lift coefficient of 0.2	. S95
Variation of critical Mach number with low-speed section lift coefficient for several NACA 64-series airfoil sections of various thicknesses, cambered for a design lift coefficient of 0.4	. s96
Variation of critical Mach number with low-speed section lift coefficient for two NACA 64-series airfoil sections of different thicknesses, cambered for a design lift coefficient of 0.6	. S97
Variation of critical Mach number with low-speed section lift coefficient for several NACA 65-series symmetrical airfoil sections of various thicknesses	. s98
Variation of critical Mach number with low-speed section lift coefficient for several NACA 65-series airfoil sections with a thickness ratio of 0.18 and cambered for various design lift coefficients	. S99
Variation of critical Mach number with low-speed section lift coefficient for several NACA 65-series airfoil sections of various thicknesses, cambered for a design lift coefficient of 0.2	. sloo

Variation of critical Mach number with low-speed section lift coefficient for several NACA 65-series airfoil sections of various thicknesses, cambered for a design lift coefficient of 0.4	S101
Variation of critical Mach number with low-speed section lift coefficient for several NACA 65-series airfoil sections with mean line of the type a = 0.5 and cambered for a design lift coefficient of 0.4	.S102
Variation of critical Mach number with low-speed section lift coefficient for two NACA 65-series airfoil sections of different thicknesses, cambered for a design lift coefficient of 0.6	S103
Variation of critical Mach number with low-speed section lift coefficient for two NACA 65-series airfoil sections with mean line of the type a = 0.5, with different thicknesses, and cambered for a design lift coefficient of 0.6	S104
Variation of critical Mach number with low-speed section lift coefficient for several NACA 66-series symmetrical airfoil sections of various thicknesses	S105
Variation of critical Mach number with low-speed section lift coefficient for several NACA 66-series airfoil sections of various thicknesses, cambered for a design lift coefficient of 0.2	s106
Variation of critical Mach number with low-speed section lift coefficient for two NACA 66-series airfoil sections of different thicknesses, cambered for a design lift coefficient of 0.4	S107
Variation of critical Mach number with low-speed section lift coefficient for several NACA 66-series airfoil sections with a thickness ratio of 0.16 and cambered for various design lift coefficients	s108
Variation of critical Mach number with low-speed section lift coefficient for several NACA 6-series airfoil sections with different positions of minimum pressure and various thicknesses, cambered for various design	
lift coefficients	S109

Variation of critical Mach number with low-speed section	
lift coefficient for two-NACA 7-series airfoil sections	
with a thickness ratio of 0.15 and cambered for different	
design lift coefficients	10

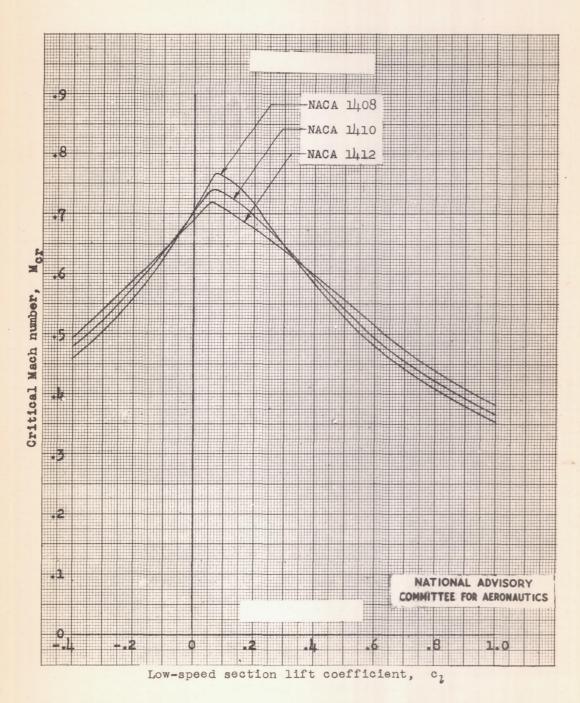


Critical Mach number chart

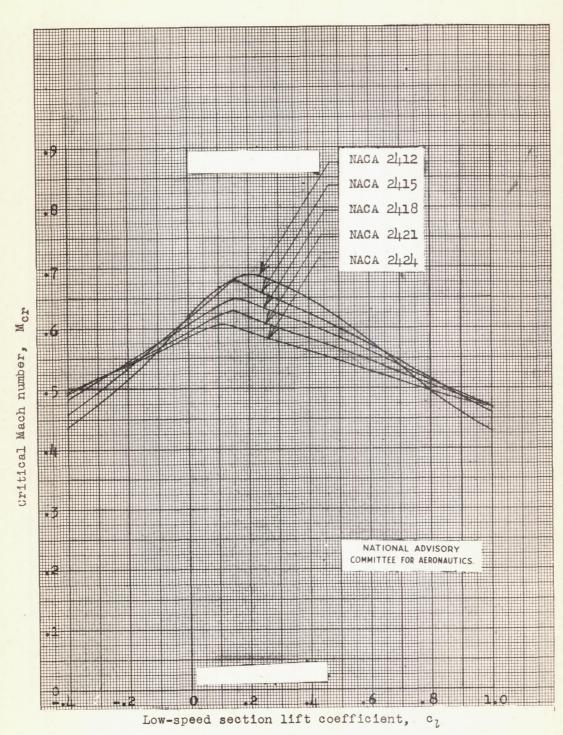


Low-speed section lift coefficient, c_l

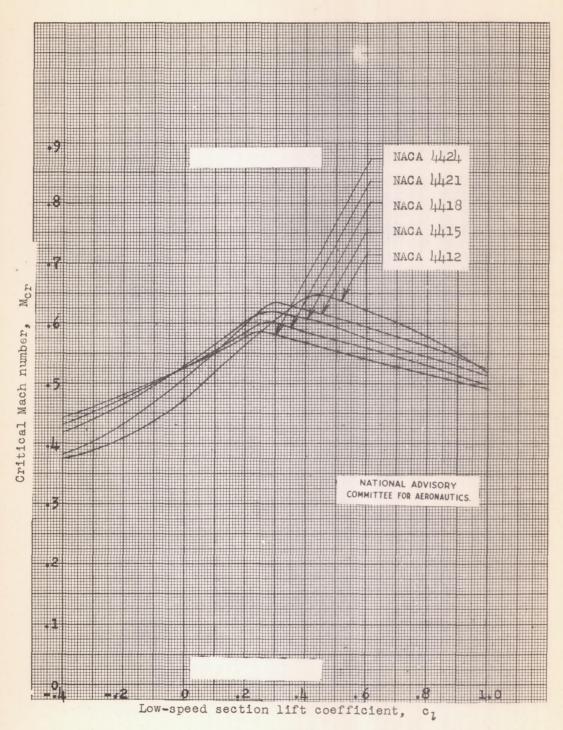
Variation of critical Mach number with low-speed section lift coefficient for the NACA 0006, 0009, and 0012 airfoil sections.



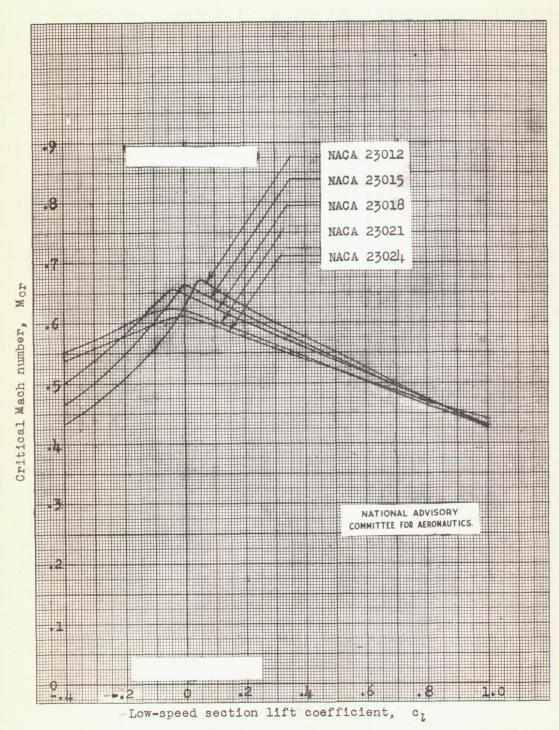
Variation of critical Mach number with low-speed section lift coefficient for several NACA lu-series airfoil sections of various thicknesses.



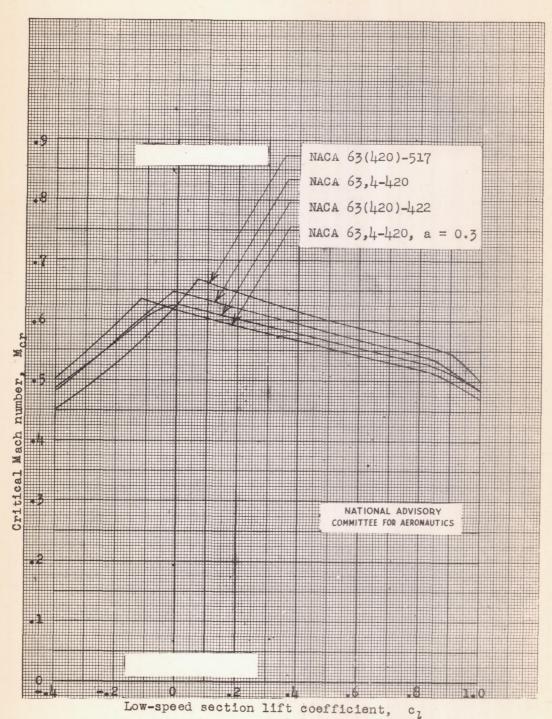
Variation of critical Mach number with low-speed section lift coefficient for several NACA 24-series airfoil sections of various thicknesses.



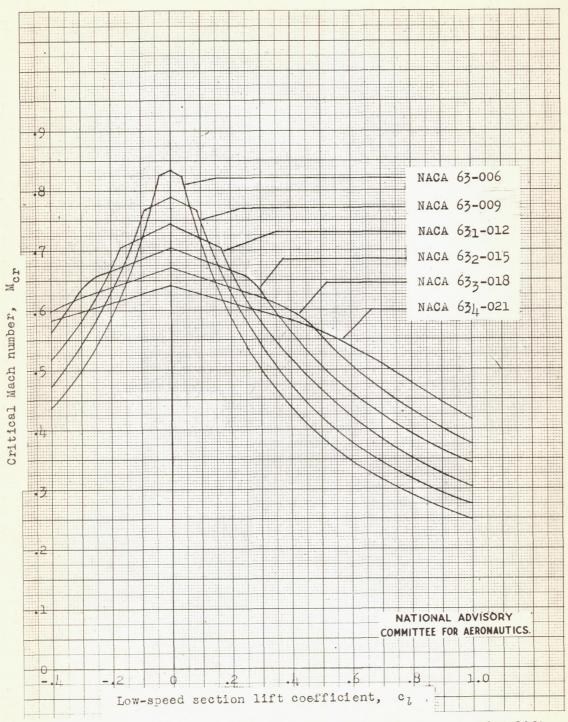
Variation of critical Mach number with low-speed section lift coefficient for several NACA 44-series airfoil sections of various thicknesses.



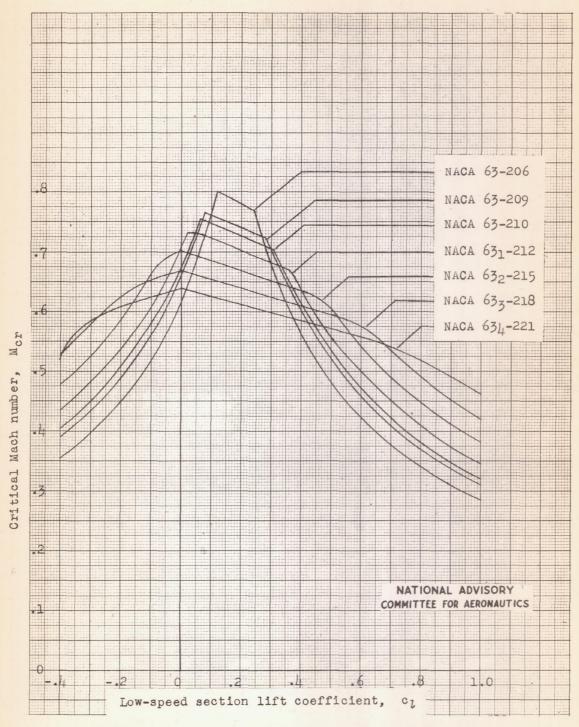
Variation of critical Mach number with low-speed section lift coefficient for several NACA 230-series airfoil sections of various thicknesses.



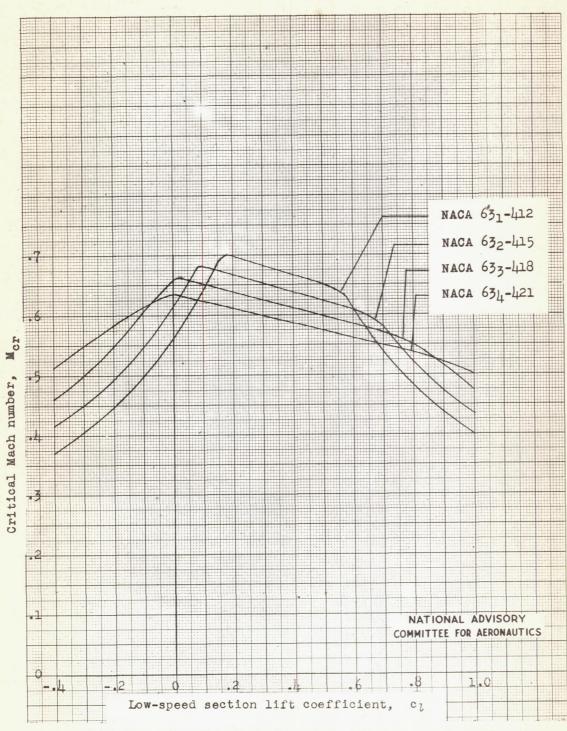
Variation of critical Mach number with low-speed section lift coefficient for several NACA 63-series airfoil sections of various thicknesses, cambered for various design lift coefficients.



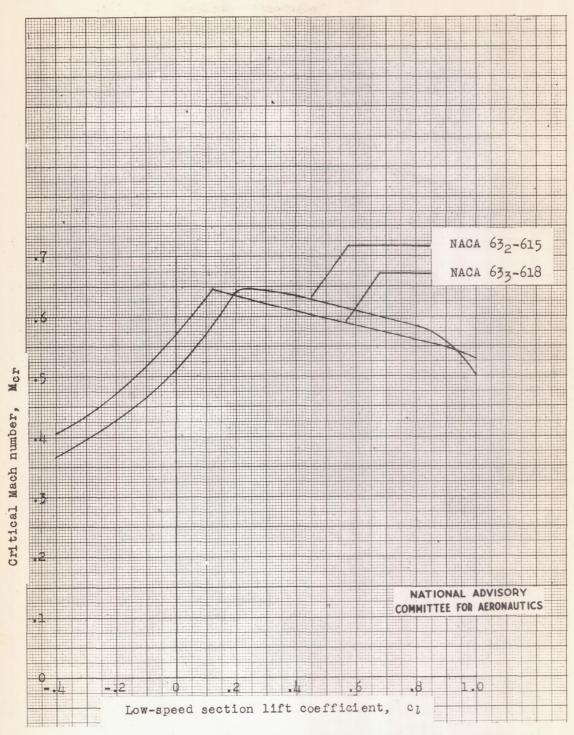
Variation of critical Mach number with low-speed section lift coefficient for several NACA 63-series symmetrical airfoil sections of various thicknesses.



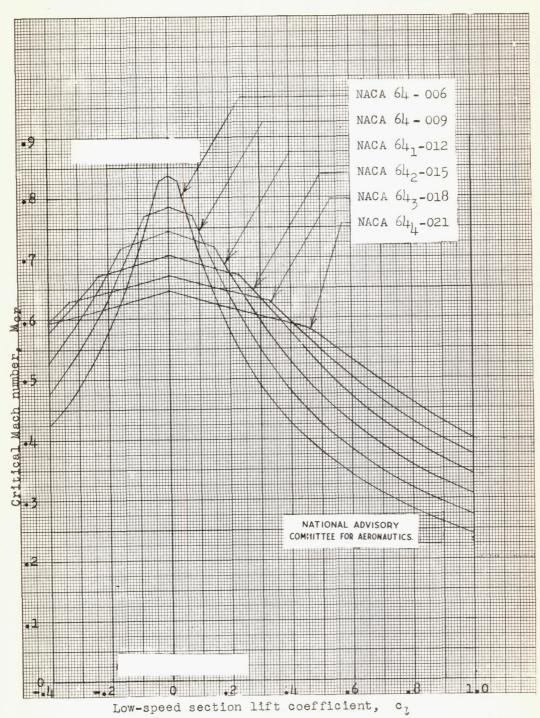
Variation of critical Mach number with low-speed section lift coefficient for several NACA 63-series airfoil sections of various thicknesses, cambered for a design lift coefficient of 0.2.



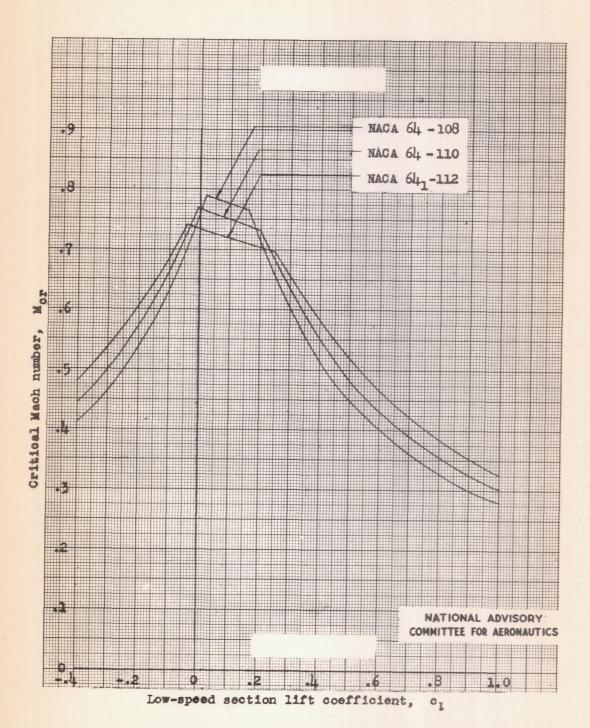
Variation of critical Mach number with low-speed section lift coefficient for several NACA 63-series airfoil sections of various thicknesses, cambered for a design lift coefficient of 0.4.



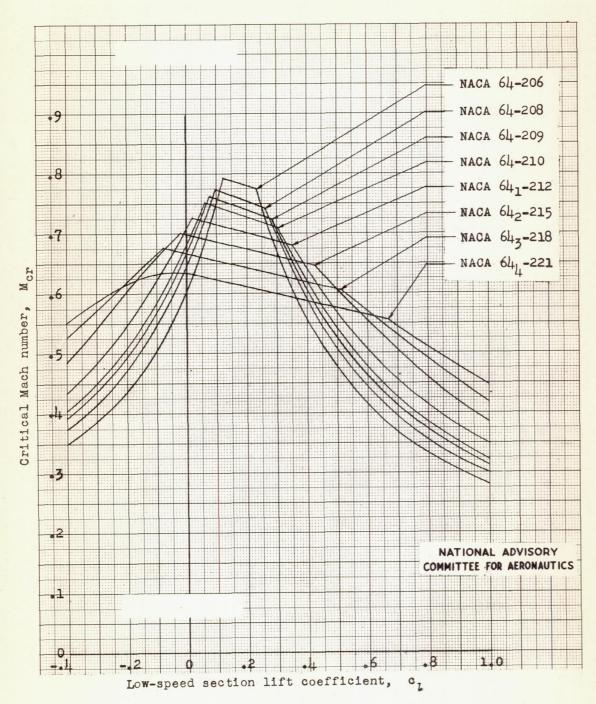
Variation of critical Mach number with low-speed section lift coefficient for two NACA 63-series airfoil sections of different thicknesses, cambered for a design lift coefficient of 0.6.



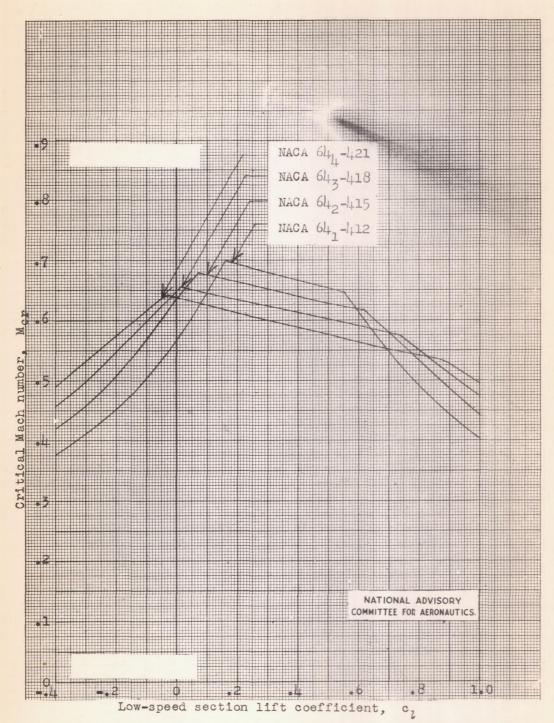
Variation of critical Mach number with low-speed section lift coefficient for several NACA 64-series symmetrical airfoil sections of various thicknesses.



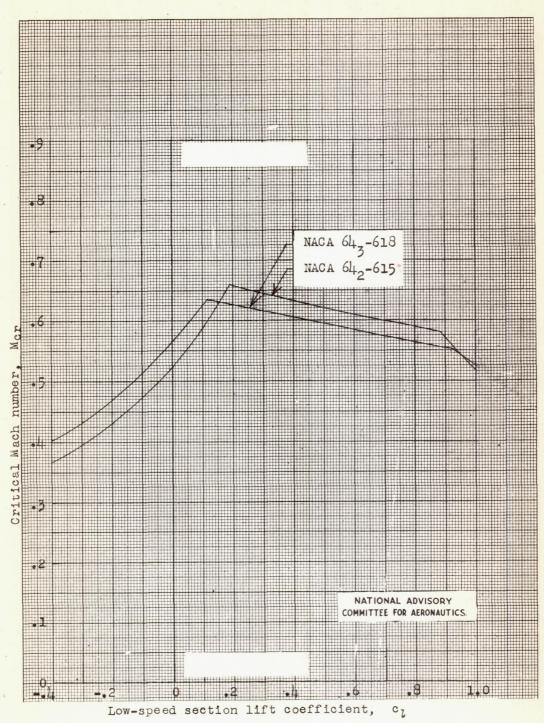
Variation of critical Mach number with low-speed section lift coefficient for several NACA 64-series airfoil sections of various thicknesses, cambered for a design lift coefficient of 0.1.



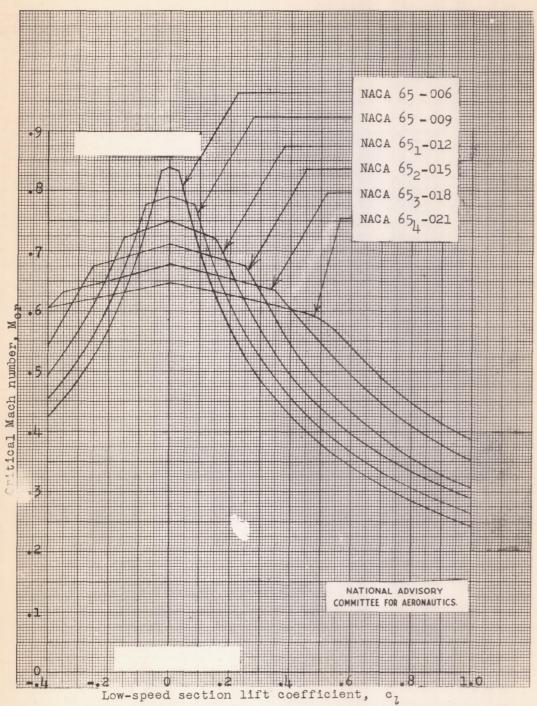
Variation of critical Mach number with low-speed section lift coefficient for several NACA 64-series airfoil sections of various thicknesses, cambered for a design lift coefficient of 0.2.



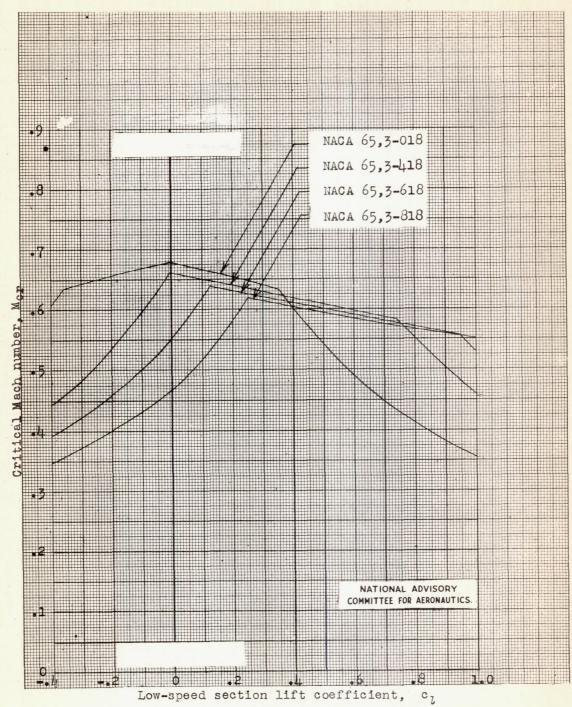
Variation of critical Mach number with low-speed section lift coefficient for several NACA 64-series airfoil sections of various thicknesses, cambered for a design lift coefficient of 0.4.



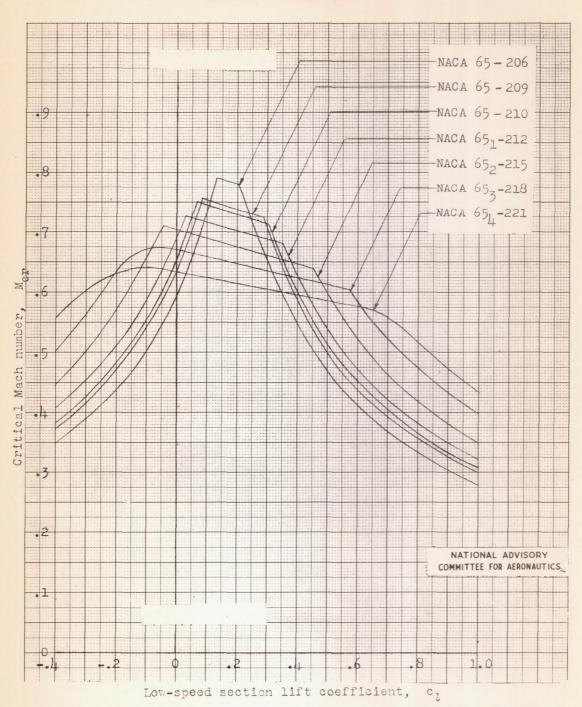
Variation of critical Mach number with low-speed section lift coefficient for two NACA 64-series airfoil sections of different thicknesses, cambered for a design lift coefficient of 0.6.



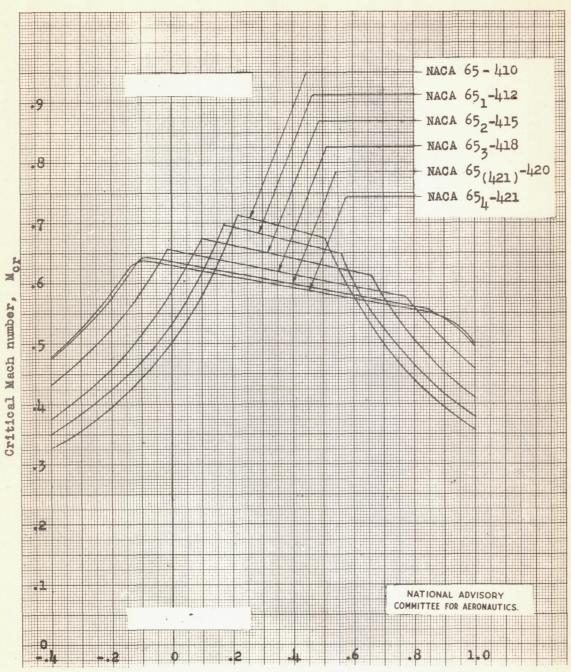
Variation of critical Mach number with low-speed section lift coefficient for several NACA 65-series symmetrical airfoil sections of various thicknesses.



Variation of critical Mach number with low-speed section lift coefficient for several NACA 65-series airfoil sections with a thickness ratio of 0.18 and cambered for various design lift coefficients.

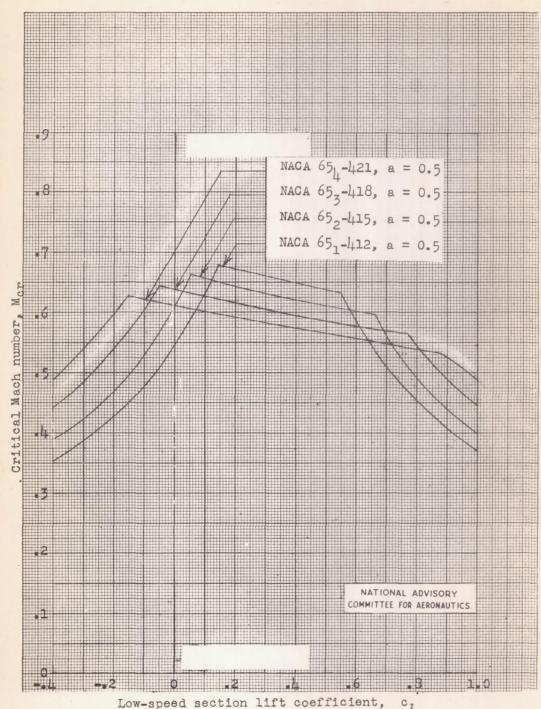


Variation of critical Mach number with low-speed section lift coefficient for several NACA 65-series airfoil sections of various thicknesses, cambered for a design lift coefficient of 0.2.

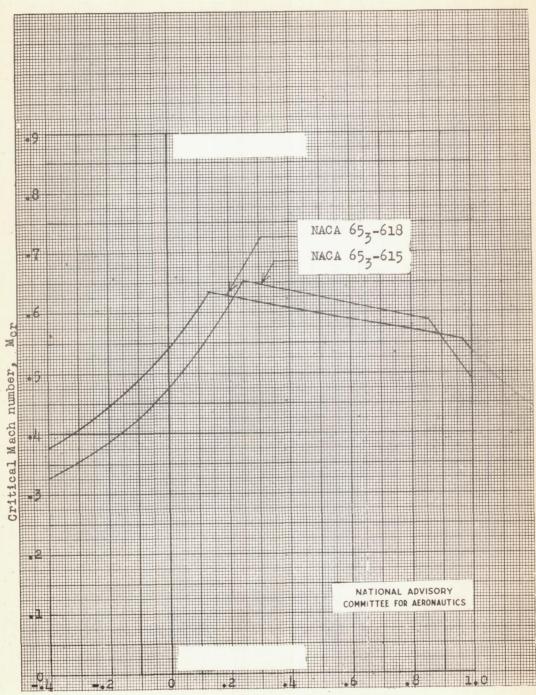


Low-speed section lift coefficient, c1

Variation of critical Mach number with low-speed section lift coefficient for several NACA 65-series airfoil sections of various thicknesses, cambered for a design lift coefficient of 0.4.

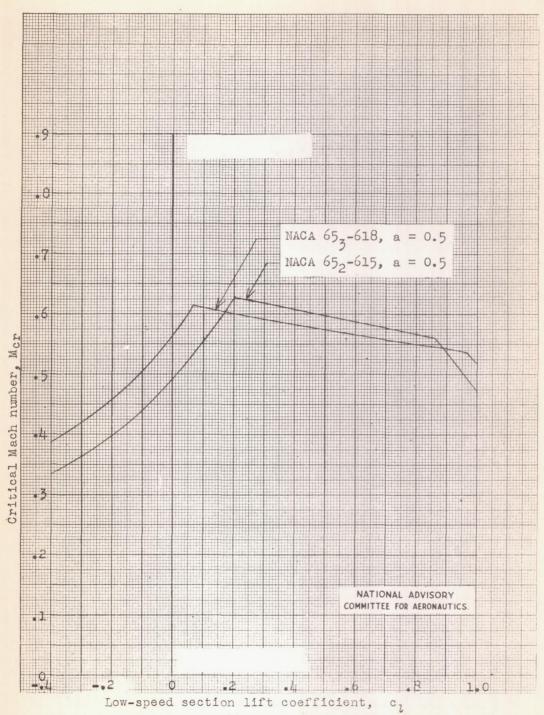


Variation of critical Mach number with low-speed section lift coefficient for several NACA 65-series airfoil sections with mean line of the type a = 0.5 and cambered for a design lift coefficient of 0.4.

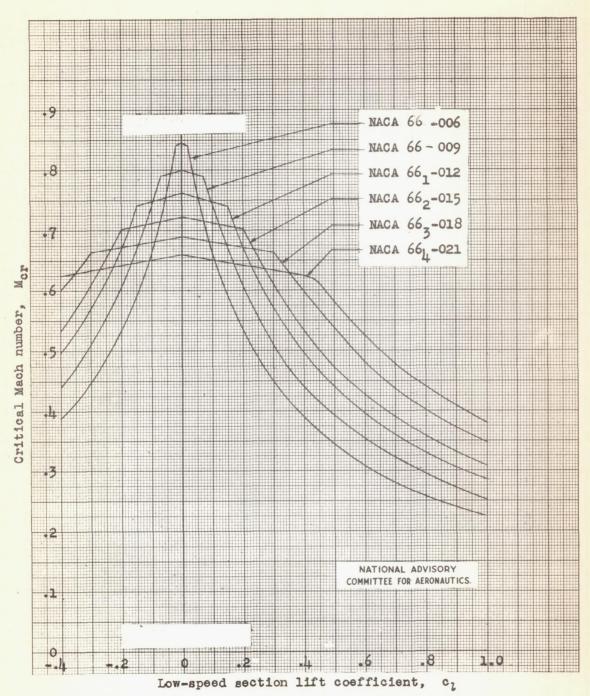


Low-speed section lift coefficient, c_1

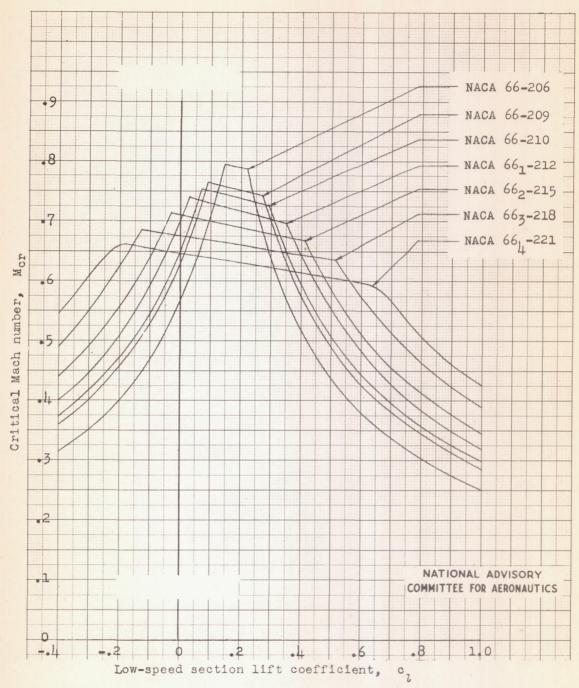
Variation of critical Mach number with low-speed section lift coefficient for two NACA 65-series airfoil sections of different thicknesses, cambered for a design lift coefficient of 0.6.



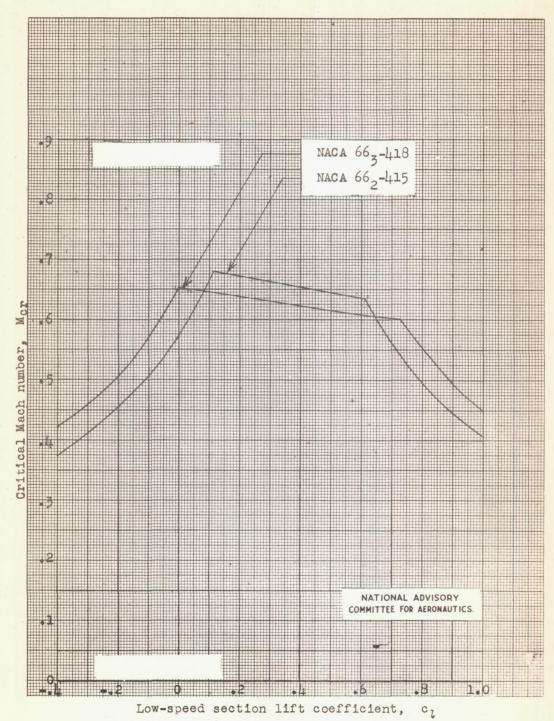
Variation of critical Mach number with low-speed section lift coefficient for two NACA 65-series airfoil sections with mean line of the type a = 0.5, with different thicknesses, and cambered for a design lift coefficient of 0.6.



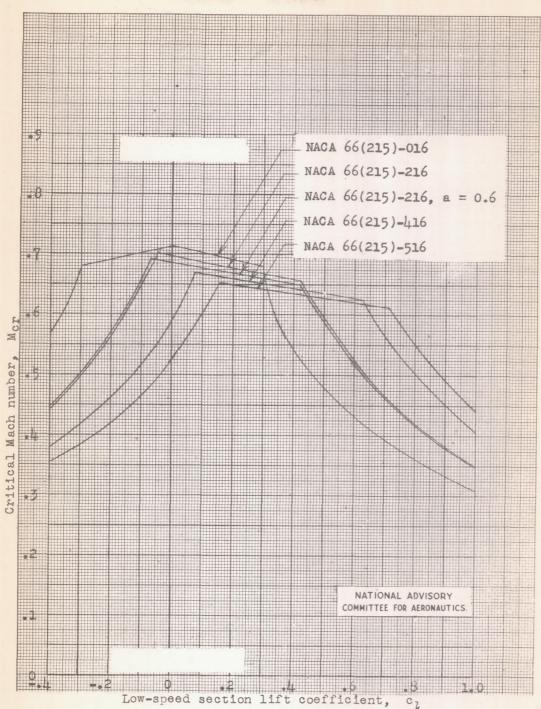
Variation of critical Mach number with low-speed section lift coefficient for several NACA 66-series symmetrical airfoil sections of various thicknesses.



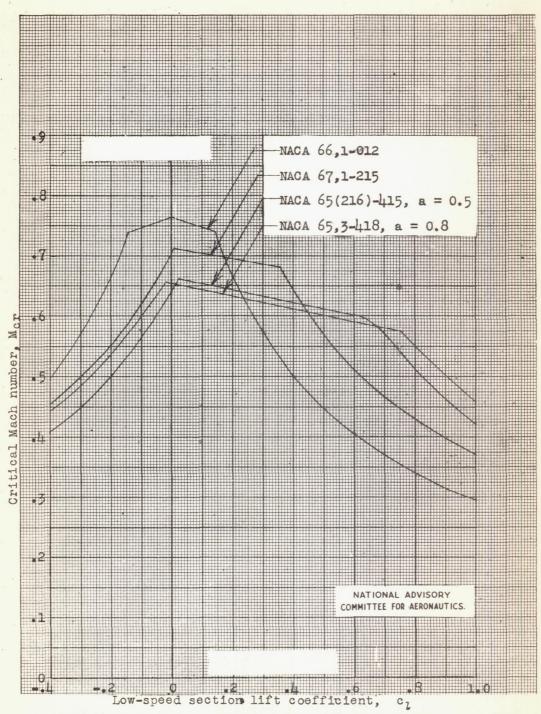
Variation of critical Mach number with low-speed section lift coefficient for several NACA 66-series airfoil sections of various thicknesses, cambered for a design lift coefficient of 0.2.



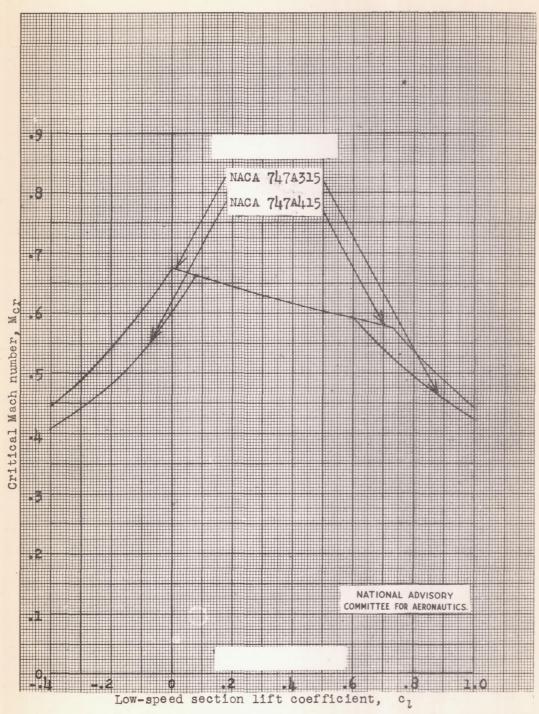
Variation of critical Mach number with low-speed section lift coefficient for two NACA 66-series airfoil sections of different thicknesses, cambered for a design lift coefficient of 0.4.



Variation of critical Mach number with low-speed section lift coefficient for several NACA 66-series airfoil sections with a thickness ratio of 0.16 and cambered for various design lift coefficients.



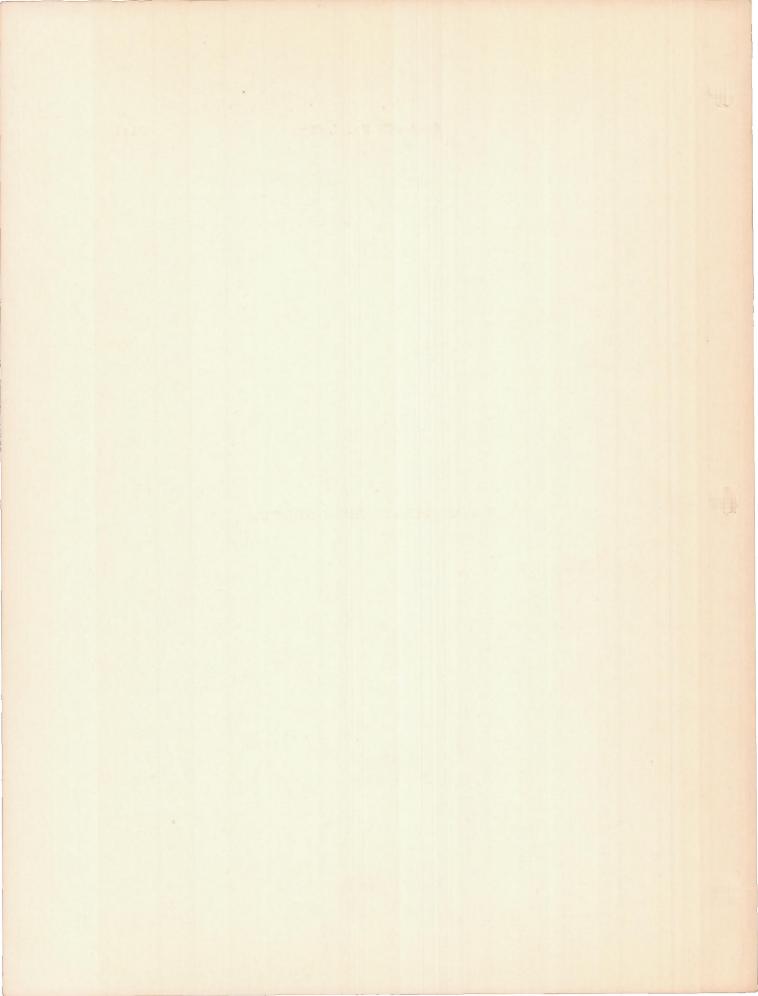
Variation of critical Mach number with low-speed section lift coefficient for several NACA 6-series airfoil sections with different positions of minimum pressure and various thicknesses, cambered for various design lift coefficients.



Variation of critical Mach number with low-speed section lift coefficient for two NACA 7-series airfoil sections with a thickness ratio of 0.15 and cambered for different design lift coefficients.



V - AERODYNAMIC CHARACTERISTICS



V - AERODYNAMIC CHARACTERISTICS

Aerodynamic characteristics of	P the	2							
NACA 0006 airfoil section									S115a
Aerodynamic characteristics of NACA 0009 airfoil section									S115t
Aerodynamic characteristics of NACA 1408 airfoil section .									S115c
Aerodynamic characteristics of NACA 1410 airfoil section .									S115d
Aerodynamic characteristics of NACA 1412 airfoil section .									S115e
Aerodynamic characteristics of NACA 2412 airfoil section .	the								S116
Aerodynamic characteristics of NACA 2415 airfoil section .	the								S117
Aerodynamic characteristics of NACA 2418 airfoil section .									S118
Aerodynamic characteristics of NACA 2421 airfoil section .	the · ·								S119
Aerodynamic characteristics of NACA 2424 airfoil section .	the								S120
Aerodynamic characteristics of NACA 4412 airfoil section .	the · ·								S121
Aerodynamic characteristics of NACA 4415 airfoil section .	the								S122
Aerodynamic characteristics of NACA 4418 airfoil section .	the · ·								S123
Aerodynamic characteristics of NACA 4421 airfoil section .	the								
Aerodynamic characteristics of NACA 4424 airfoil section .	the								

NACA ACR No. L5C05		Sll	3
Aerodynamic characteristics of the NACA 23012 airfoil section		Sl26	5
Aerodynamic characteristics of the NACA 23015 airfoil section		S127	7
Aerodynamic characteristics of the NACA 23018 airfoil section		s128	8
Aerodynamic characteristics of the NACA 23021 airfoil section		S129	9
Aerodynamic characteristics of the NACA 23024 airfoil section		S130)
Aerodynamic characteristics of the NACA 63,4-420 airfoil section		S131	l
NACA 63,4-420 airfoil section with 0.25c slotted flap (a) Configuration		S132	2
location 1	• .	Sl33	3
location 2		S13 ¹	+
Aerodynamic characteristics of the NACA 63,4-420, a = 0.3 airfoil section		Sl35	5
Aerodynamic characteristics of the NACA 63(420)-422 airfoil section		S136	5
Aerodynamic characteristics of the NACA 63(420)-517 airfoil section		S136	£
Aerodynamic characteristics of the NACA 63-006 airfoil section		s1361	0
Aerodynamic characteristics of the NACA 63-009 airfoil section		s136	3
Aerodynamic characteristics of the NACA 63-206 airfoil section		s136a	i
Aerodynamic characteristics of the NACA 63-209 airfoil section		S136	Э
Aerodynamic characteristics of the NACA 63-210 airfoil section		s1361	e

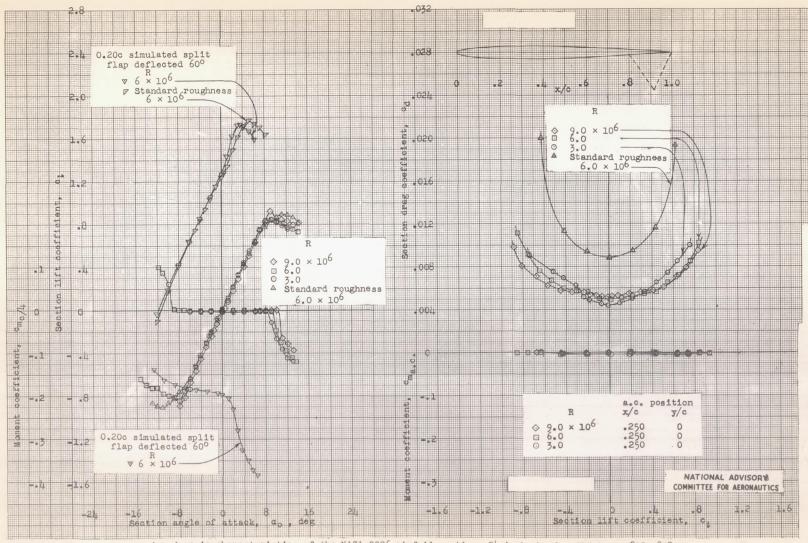
Aerodynamic characteristics of the NACA 631-012 sirfoil section	36g
Aerodynamic characteristics of the NACA 631-212 airfoil section	36h
Aerodynamic characteristics of the NACA 631-412 airfoil section	
Aerodynamic characteristics of the NACA 632-015 airfoil section	36j
Aerodynamic characteristics of the NACA 632-215 airfoil section	6k
Aerodynamic characteristics of the NACA 632-415 airfoil section	
Aerodynamic characteristics of the NACA 632-615 airfoil section	6m
Aerodynamic characteristics of the NACA 633-018 airfoll section	6n
Aerodynamic characteristics of the NACA 633-218 airfoil section	60
Aerodynamic characteristics of the NACA 633-418 airfoil section	6p
Aerodynamic characteristics of the NACA 633-618 airfoil section	6q
Aerodynamic characteristics of the NACA 634-021 airfoil section	6r
Aerodynamic characteristics of the NACA 634-221 airfoil section	бз
Aerodynamic characteristics of the NACA 634-421 airfoil section	5t
Aerodynamic characteristics of the NACA 64-006 airfoil section	37
Aerodynamic characteristics of the NACA 64-009 airfoil section	7a
Aerodynamic characteristics of the NACA 64-108 airfoil section	

NACA ACR No. L5CO5	Sll4a
Aerodynamic characteristics of the NACA 64-110 airfoil section	S137c
Aerodynamic characteristics of the NACA 64-206 airfoil section	
Aerodynamic characteristics of the NACA 64-208 airfoil section	S137e
Aerodynamic characteristics of the NACA 64-209 airfoil section	
Aerodynamic characteristics of the NACA 64-210 airfoil section	
Aerodynamic characteristics of the NACA 641-012 airfoil section	S137h
Aerodynamic characteristics of the NACA 641-112 airfoil section	S137i
Aerodynamic characteristics of the NACA 641-212 airfoil section	S137j
Aerodynamic characteristics of the NACA 641-412 airfoil section	s138
Aerodynamic characteristics of the NACA 642-015 airfoil section	S1.38a
Aerodynamic characteristics of the NACA 642-215 airfoil section	S1.38b
Aerodynamic characteristics of the NACA 642-415 airfoil section	S139
Aerodynamic characteristics of the NACA 643-018 airfoil section	S1.39a
Aerodynamic characteristics of the NACA 643-218 airfoil section	
Aerodynamic characteristics of the NACA 643-418 airfoil section	S140
Aerodynamic characteristics of the NACA 643-618 airfoil section	S1.40a
Aerodynamic characteristics of the NACA 644-021 airfoil section	S1.40b

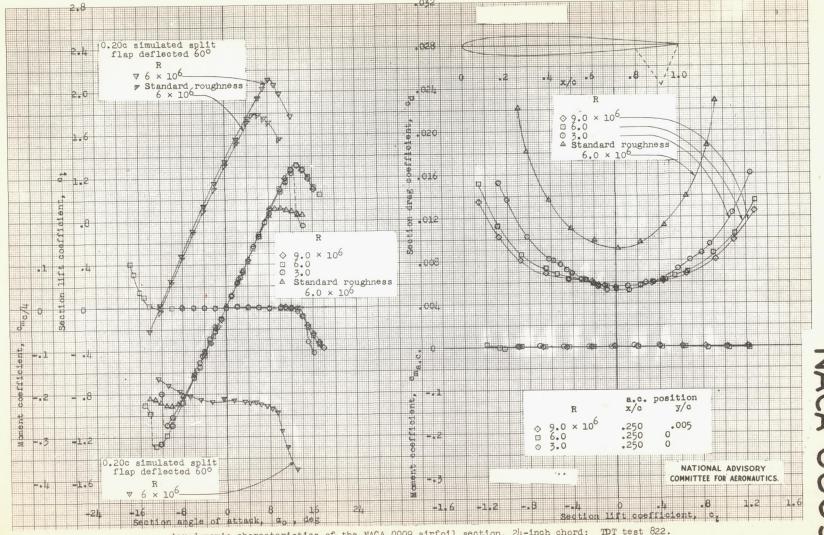
Aerodynamic characteristics of the NACA 644-221 airfoil section	 . S140c
Aerodynamic characteristics of the NACA 644-421 airfoil section	 S141
Aerodynamic characteristics of the NACA 65,3-018 airfoil section	 S142
Aerodynamic characteristics of the NACA 65,3-418, a = 0.8 airfoil section	 S143
Aerodynamic characteristics of the NACA 65,3-618 airfoil section	 S144
Aerodynamic characteristics of the NACA 65,3-618 airfoil section with 0.20c sealed plain flap	 S145
Aerodynamic characteristics of the NACA 65(216)-415, a = 0.5 airfoil section	 S146
Aerodynamic characteristics of the NACA 65-006 airfoil section	 S146a
Aerodynamic characteristics of the NACA 65-009 airfoil section	 S146b
Aerodynamic characteristics of the NACA 65-206 airfoil section	 S146c
Aerodynamic characteristics of the NACA 65-209 airfoil section	
Aerodynamic characteristics of the	S147
Aerodynamic characteristics of the NACA 65-410 airfoil section	
Aerodynamic characteristics of the NACA 651-012 airfoil section	
Aerodynamic characteristics of the NACA 651-212 airfoil section	
Lift and moment characteristics of the NACA 651-212 airfoil section with 0.20c split flap	
Aerodynamic characteristics of the NACA 651-212, a = 0.6 airfoil section	
	22470

Aerodynamic characteristics of the NACA 65(215)-114 airfoil section	S158a
Aerodynamic characteristics of the NACA 65(421)-420 airfoil section	S159
Aerodynamic characteristics of the NACA 66,1-212 airfoil section	S160
Lift and moment characteristics of the NACA 66,1-212 airfoil section with 0.20c split flap	si61
Aerodynamic characteristics of the NACA 66(215)-016 airfoil section	S162
Aerodynamic characteristics of the NACA 66(215)-216 airfoil section	S163
Aerodynamic characteristics of the NACA 66(215)-216 airfoil section with 0.20c sealed plain flap	S164
Lift and moment characteristics of the NACA 66(215)-216 airfoil section with 0.20c split flap	S165
Aerodynamic characteristics of the NACA 66(215)-216 a = 0.6 airfoil section	S166
NACA 66(215)-216, a = 0.6 airfoil section with 0.30c slotted and 0.10c plain flap: (a) Airfoil-flap configuration (b) Flap configuration (c) Aerodynamic characteristics. Slotted flap retracted (d) Lift and moment characteristics. Slotted flap deflected 22° (e) Lift and moment characteristics. Slotted flap deflected 27° (f) Lift and moment characteristics. Slotted flap deflected 32° (g) Lift and moment characteristics. Slotted flap deflected 37° (g) Lift and moment characteristics. Slotted flap deflected 37°	S172
Aerodynamic characteristics of the NACA 66(215)-416 airfoil section	S174
Aerodynamic characteristics of the NACA 66-006 airfoil section	S174a
Aerodynamic characteristics of the NACA 66-009 airfoil section	5174b

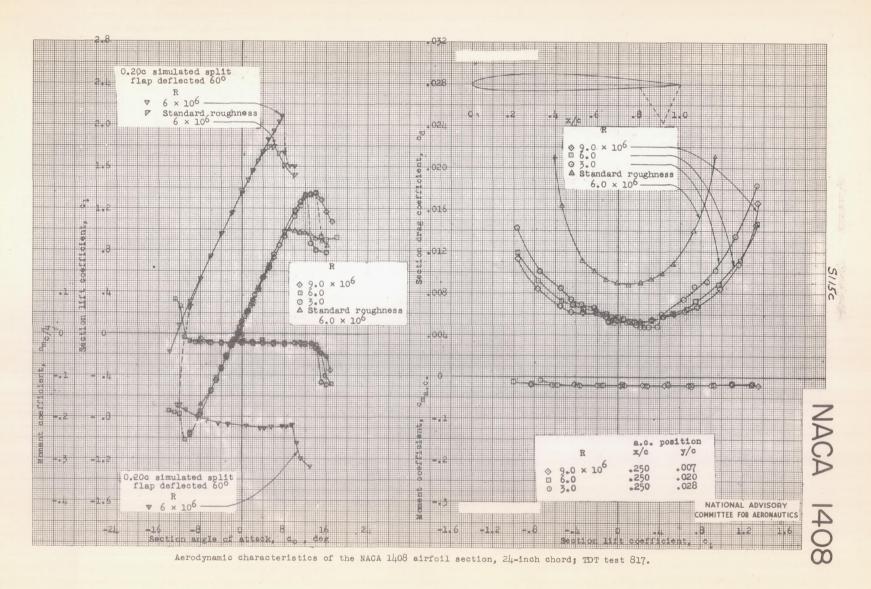
NACA ACR No. L5005	SIIS
Aerodynamic characteristics of the NACA 66-206 airfoil section	3174c
Aerodynamic characteristics of the NACA 66-209 airfoil section	3174d
Aerodynamic characteristics of the NACA 66-210 airfoil section	S175
Aerodynamic characteristics of the NACA 661-012 airfoil section	S176
Aerodynamic characteristics of the NACA 661-212 airfoil section	
Aerodynamic characteristics of the NACA 662-015 airfoil section	s178
Aerodynamic characteristics of the NACA 662-215 airfoil section	S179
Aerodynamic characteristics of the NACA 662-415 airfoil section	
Aerodynamic characteristics of the NACA 663-018 airfoil section	5181
Aerodynamic characteristics of the NACA 663-218 airfoil section	5182
Aerodynamic characteristics of the NACA 663-418 airfoil section	s183
Aerodynamic characteristics of the NACA 664-021 airfoil section	5184
Aerodynamic characteristics of the NACA 664-221 airfoil section	S185
Aerodynamic characteristics of the NACA 67,1-215 airfoil section	s186
Aerodynamic characteristics of the NACA 747A315 airfoil section	s187
Aerodynamic characteristics of the NACA 747A415 airfoil section	s188

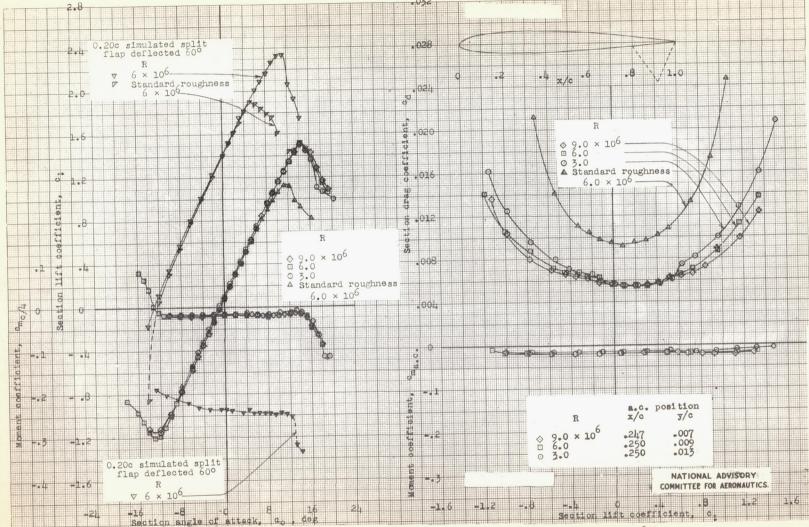


Aerodynamic characteristics of the NACA 0006 airfoil section, 24-inch chord; TDT tests 812, 878.

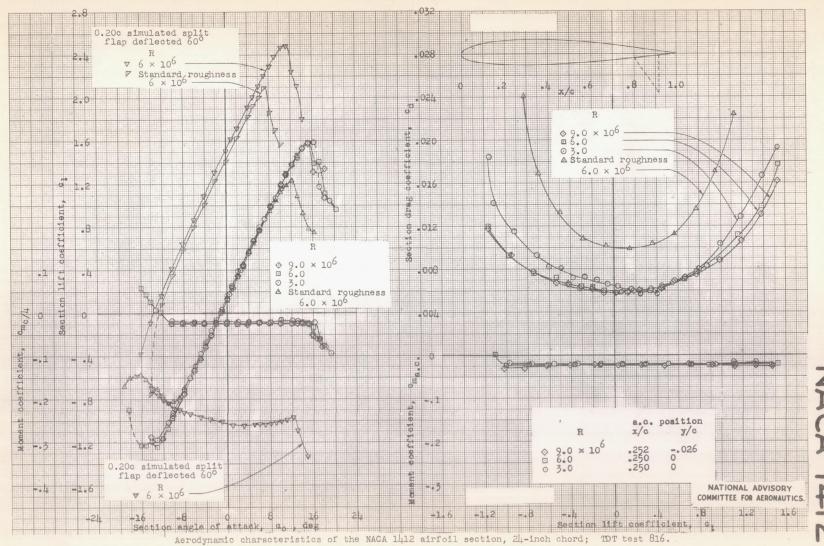


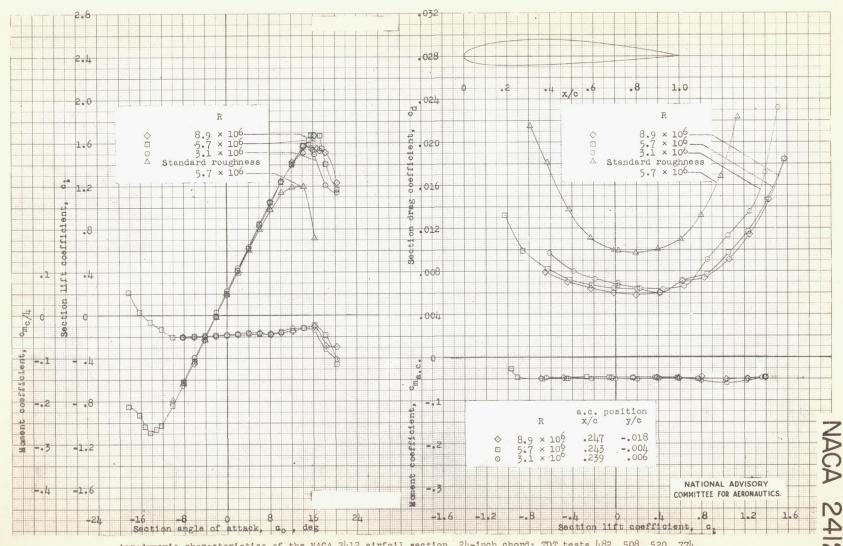
Aerodynamic characteristics of the NACA 0009 airfoil section, 24-inch chord; TDT test 822.



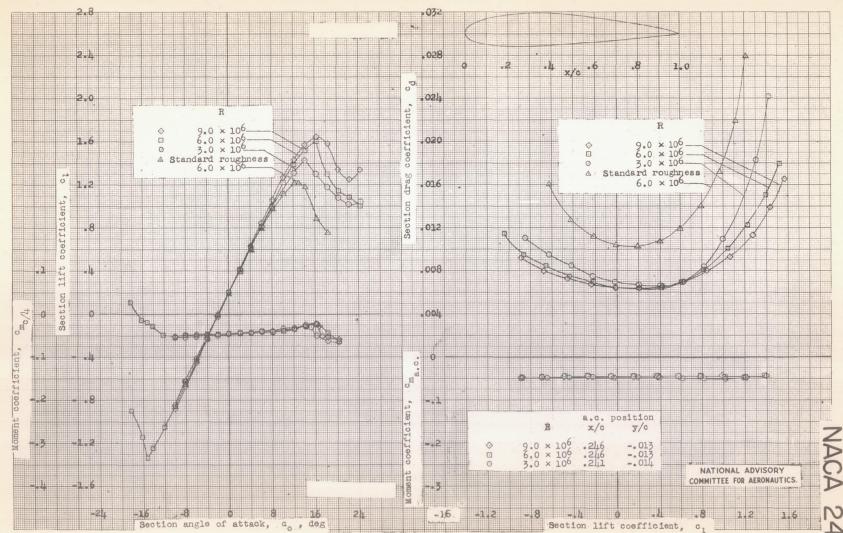


Aerodynamic characteristics of the NACA 1410 airfoil section, 24-inch chord; TDT test 820.

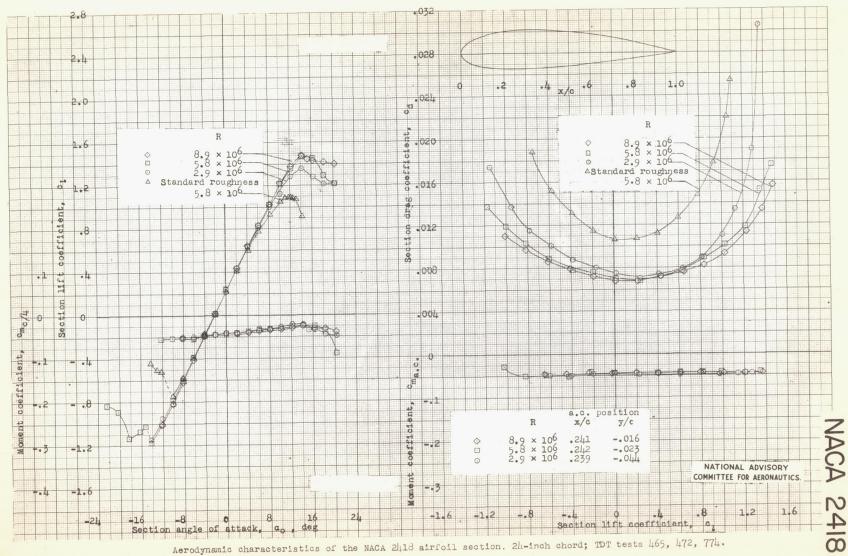




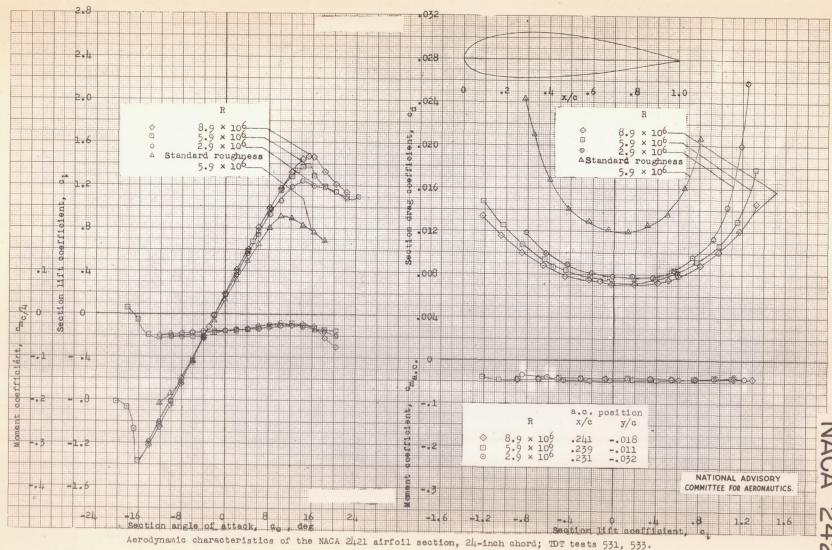
Aerodynamic characteristics of the NACA 2412 airfoil section, 24-inch chord; TDT tests 482, 508, 520, 774.

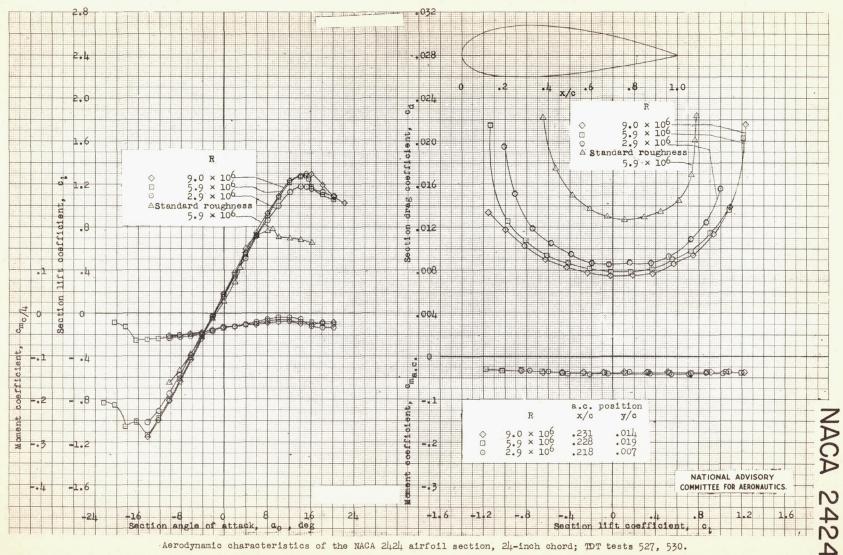


Aerodynamic characteristics of the NACA 2415 airfoil section, 24-inch chord; TDT tests 464, 498, 506, 767.

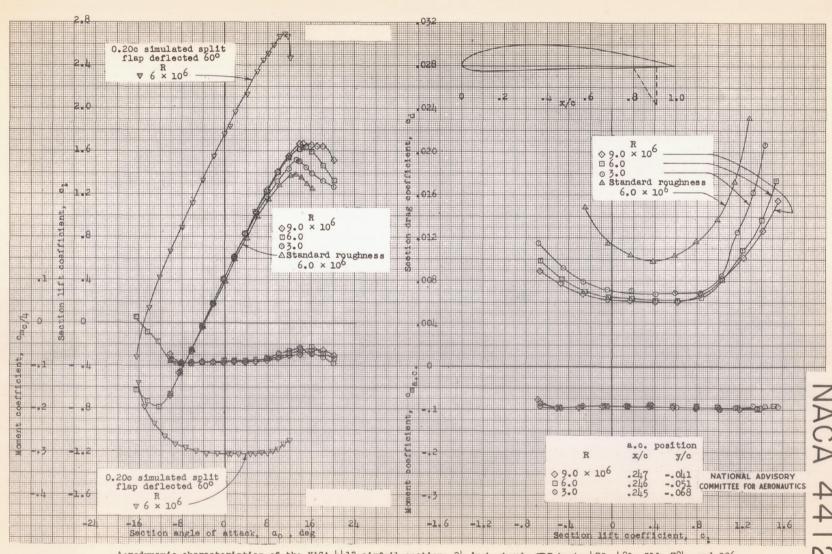


Aerodynamic characteristics of the NACA 2418 airfoil section. 24-inch chord; TDT tests 465, 472, 774.

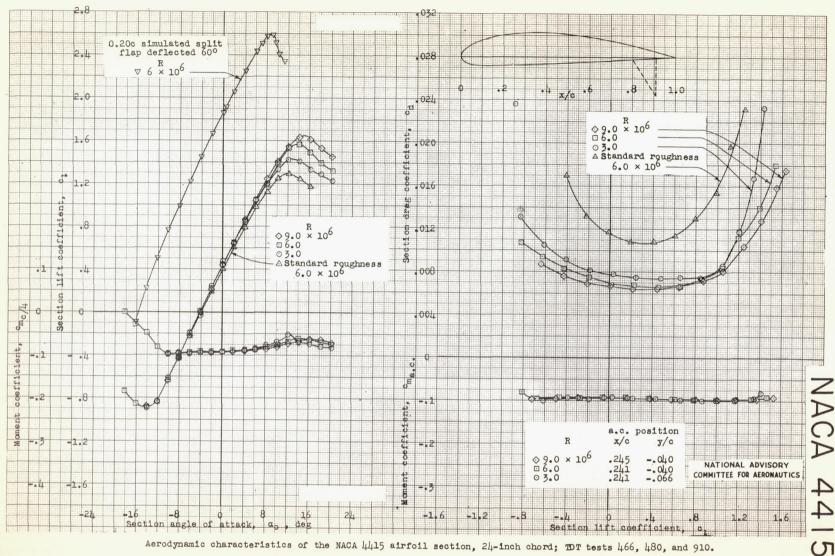




Aerodynamic characteristics of the NACA 2424 airfoil section, 24-inch chord; TDT tests 527, 530.

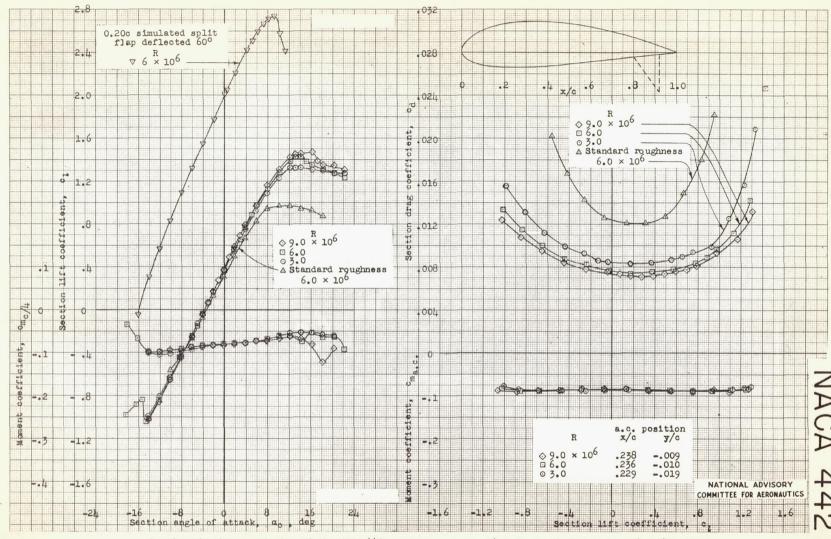


Aerodynamic characteristics of the NACA 4412 airfoil section, 24-inch chord; TDT tests 470, 481, 511, 784, and 906.

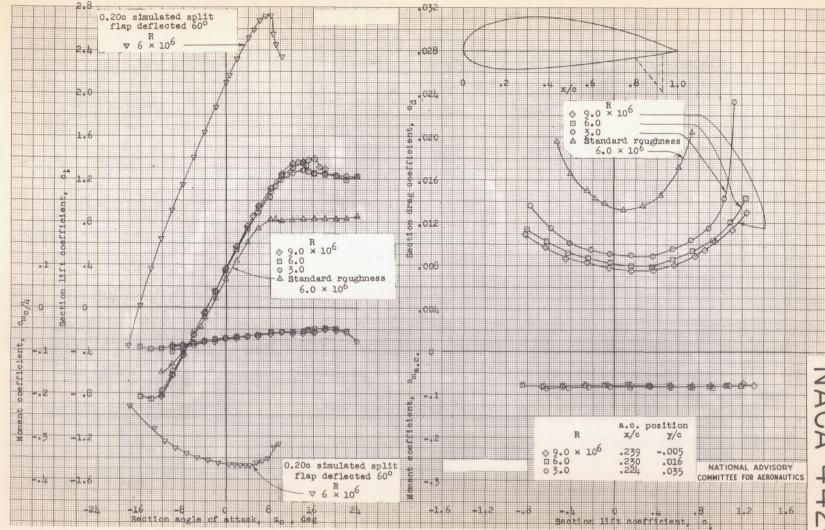


Aerodynamic characteristics of the NACA 4415 airfoil section, 24-inch chord; TDT tests 466, 480, and 910.

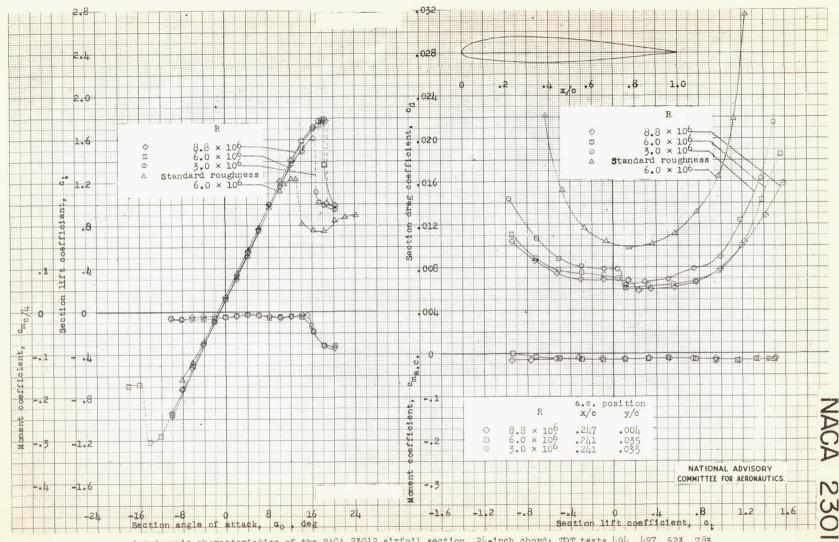
S123



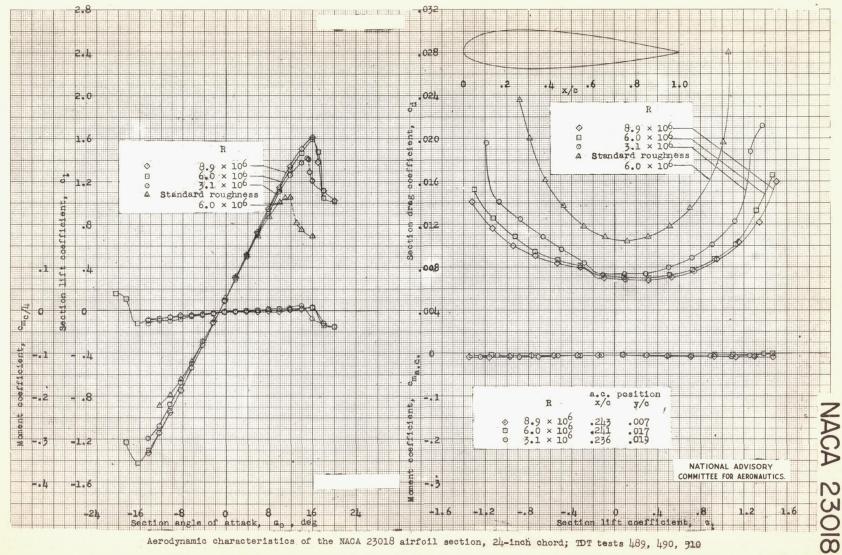
Aerodynamic characteristics of the NACA 4421 airfoil section, 24-inch chord; TDT tests 526, 528, and 909.



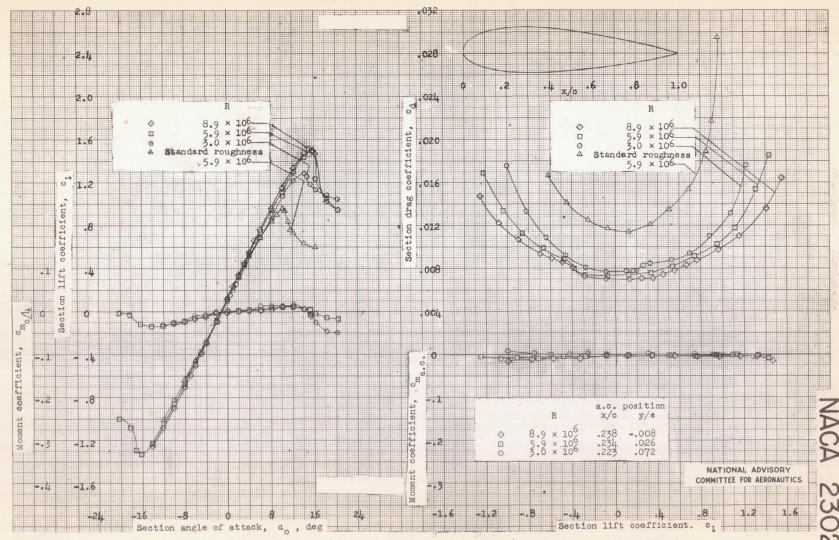
Aerodynamic characteristics of the NACA 4424 airfoil section, 24-inch chord; TDT tests 529, 532, and 908.



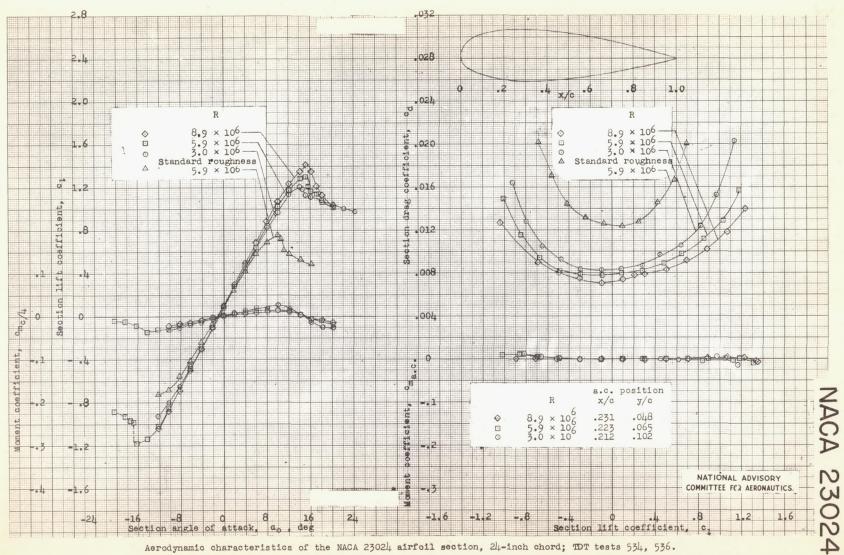
Aerodynamic characteristics of the NACA 23012 airfoil section, 24-inch chord; TDT tests 494, 497, 523, 783.



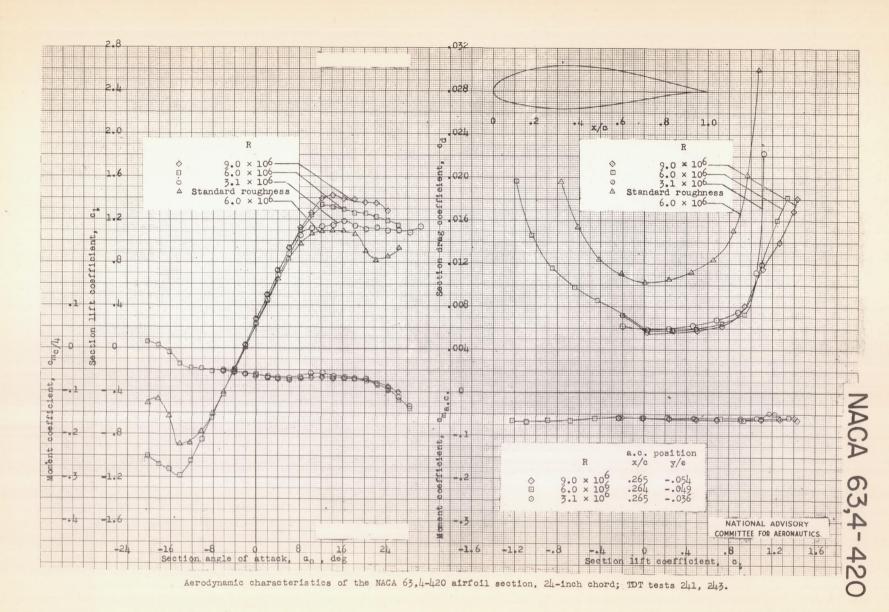
Aerodynamic characteristics of the NACA 23018 airfoil section, 24-inch chord; TDT tests 489, 490, 910

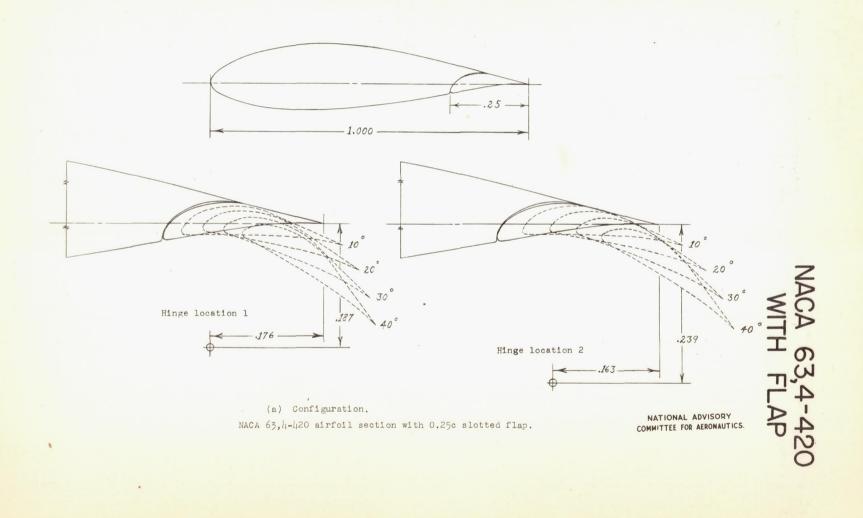


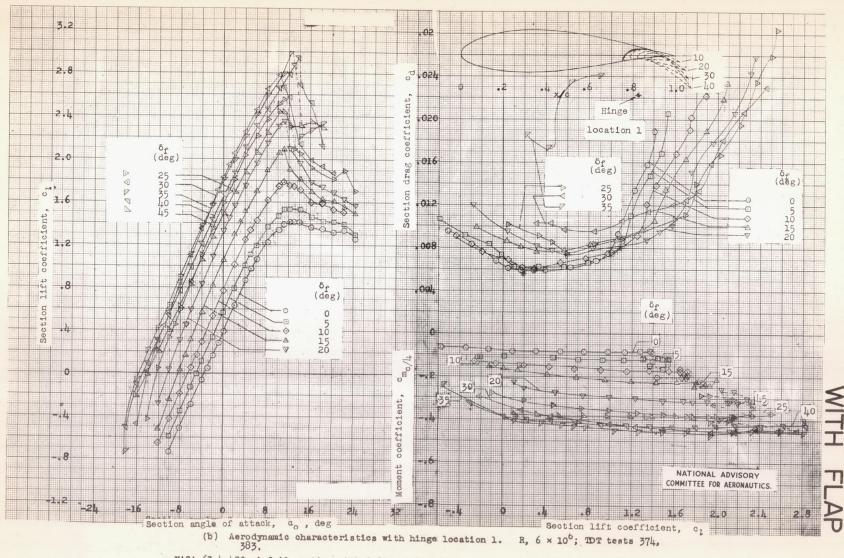
Aerodynamic characteristics of the NACA 23021 airfoil section, 24-inch chord; TDT tests 548, 549.



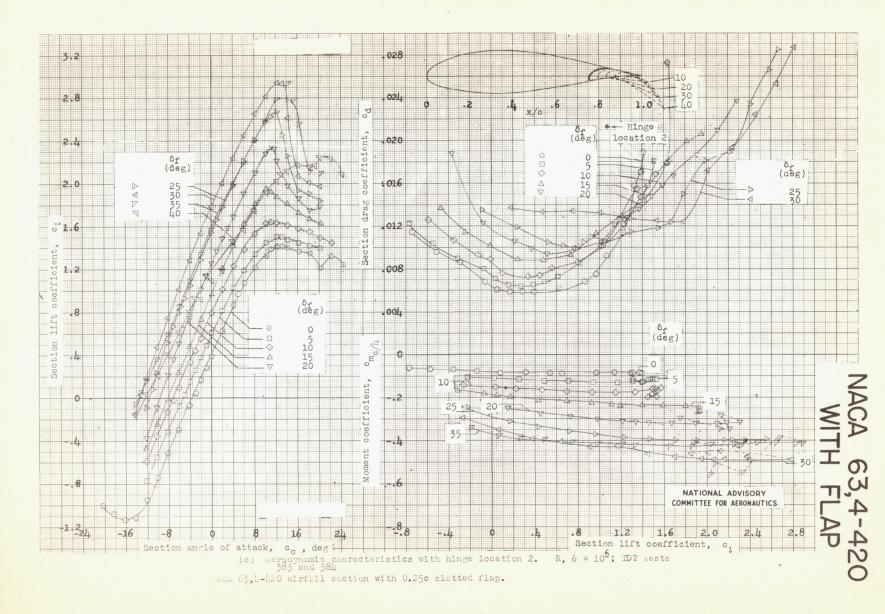
Aerodynamic characteristics of the NACA 23024 airfoil section, 24-inch chord; TDT tests 534, 536.

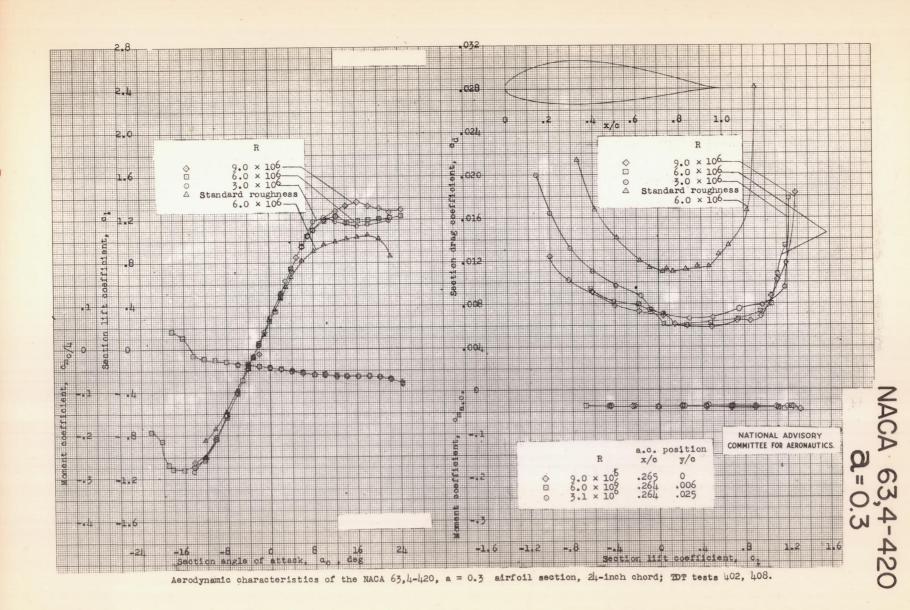


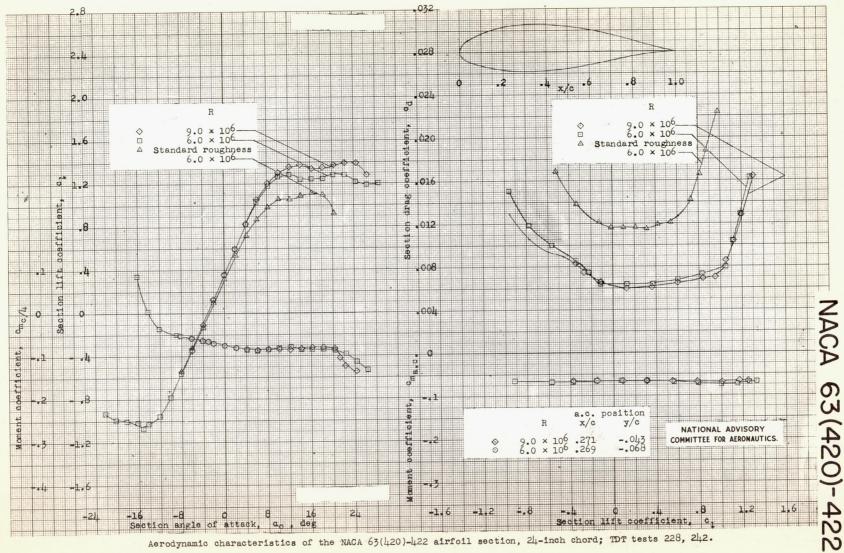




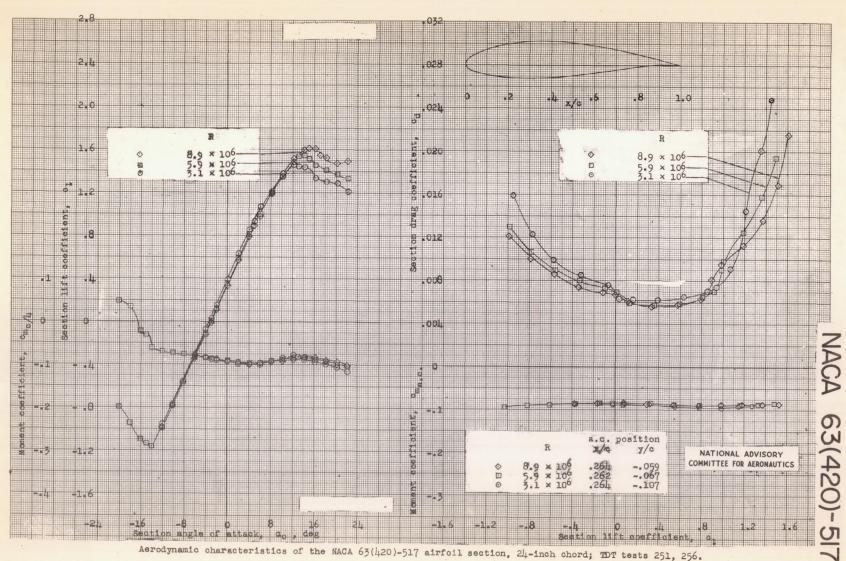
NACA 63,4-420 airfoil section with 0.25c slotted flap.



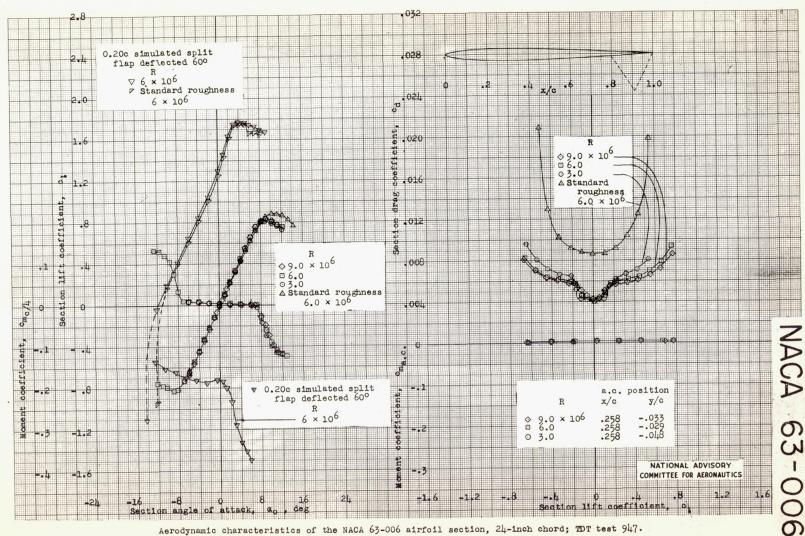




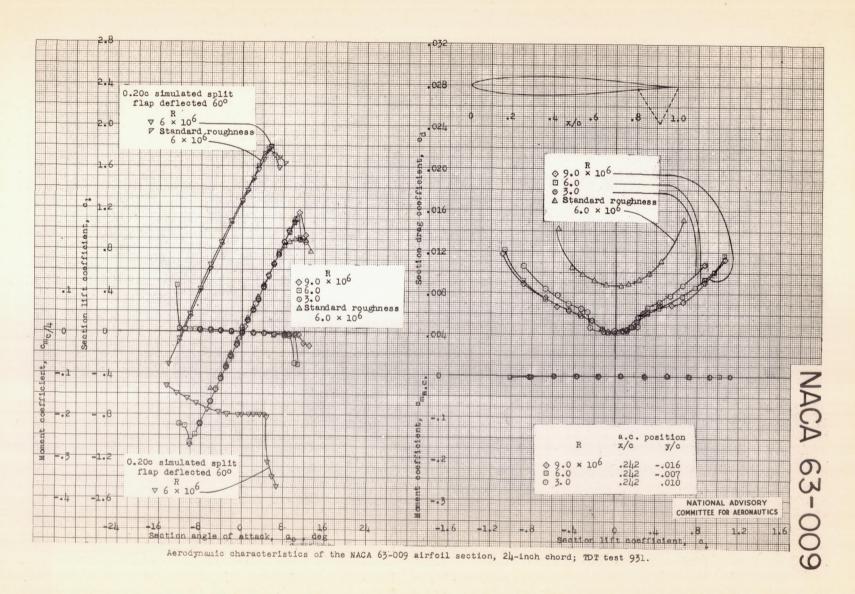
Aerodynamic characteristics of the NACA 63(420)-422 airfoil section, 24-inch chord; TDT tests 228, 242.

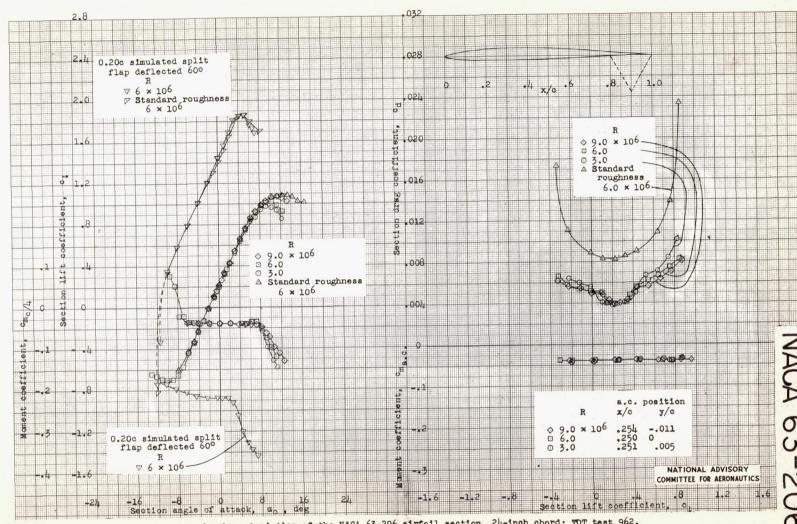


Aerodynamic characteristics of the NACA 63(420)-517 airfoil section, 24-inch chord; TDT tests 251, 256.

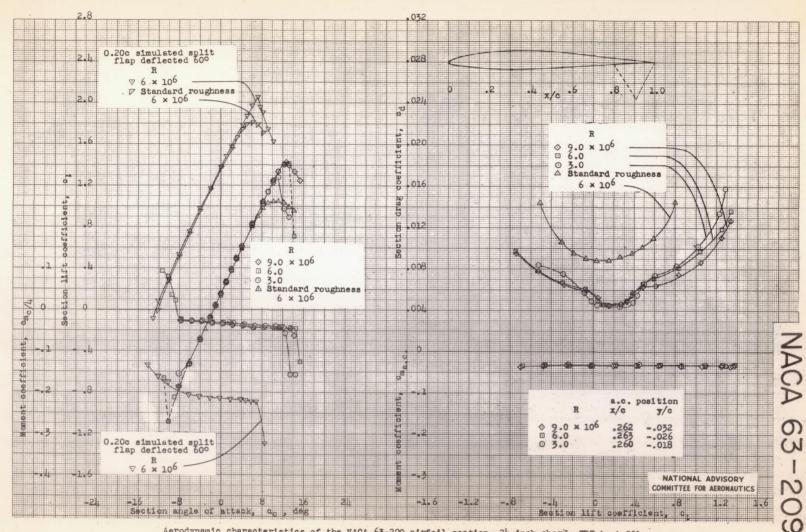


Aerodynamic characteristics of the NACA 63-006 airfoil section, 24-inch chord; TDT test 947.

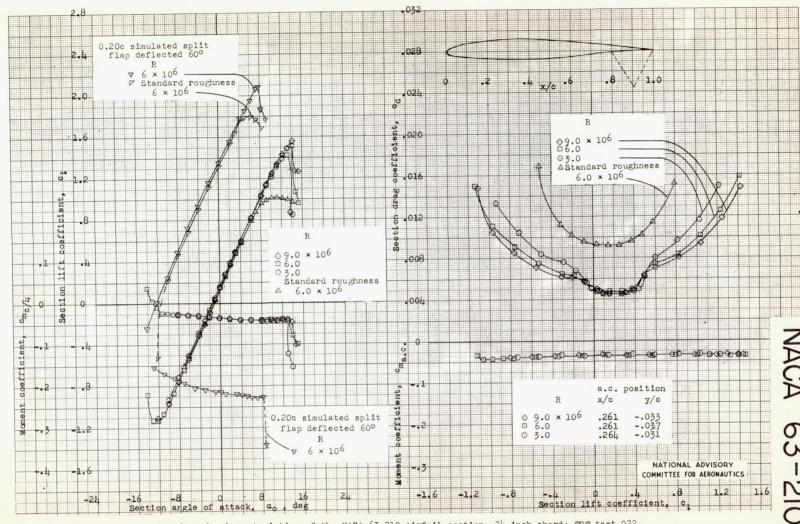




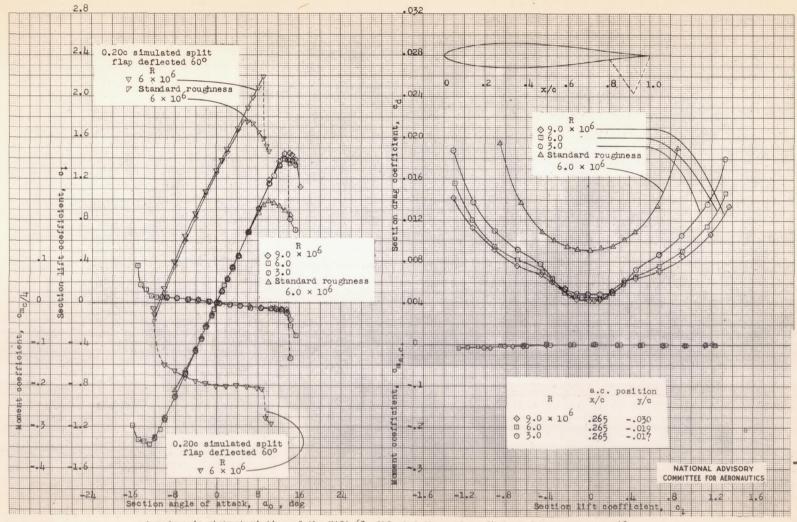
Aerodynamic characteristics of the NACA 63-206 airfoil section, 24-inch chord; TDT test 962.



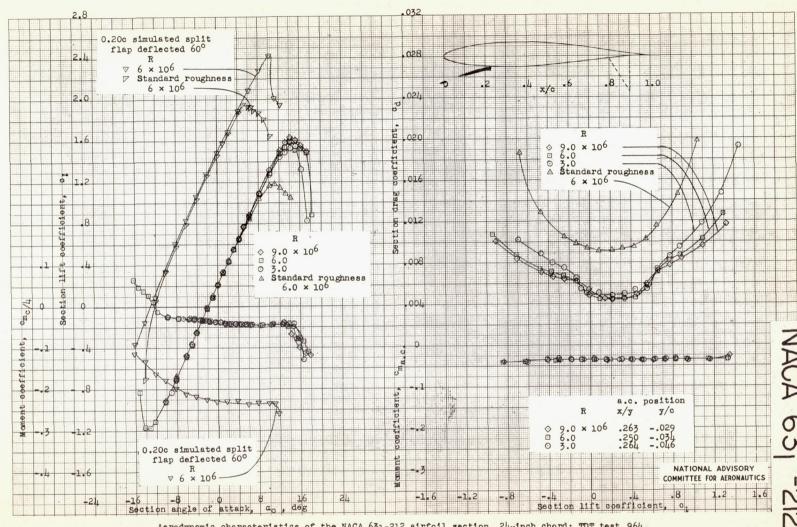
Aerodynamic characteristics of the NACA 63-209 airfoil section, 24-inch chord; TDT test 951.



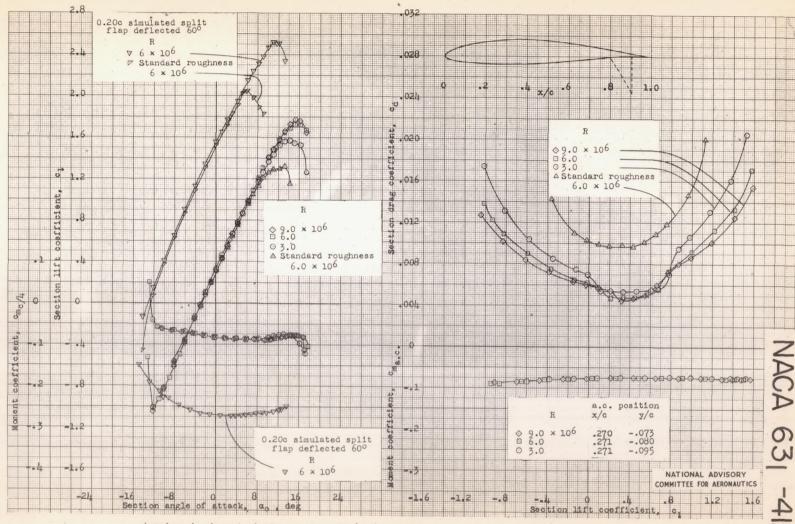
Aerodynamic characteristics of the NACA 63-210 airfoil section, 24-inch chord; TDT test 922.



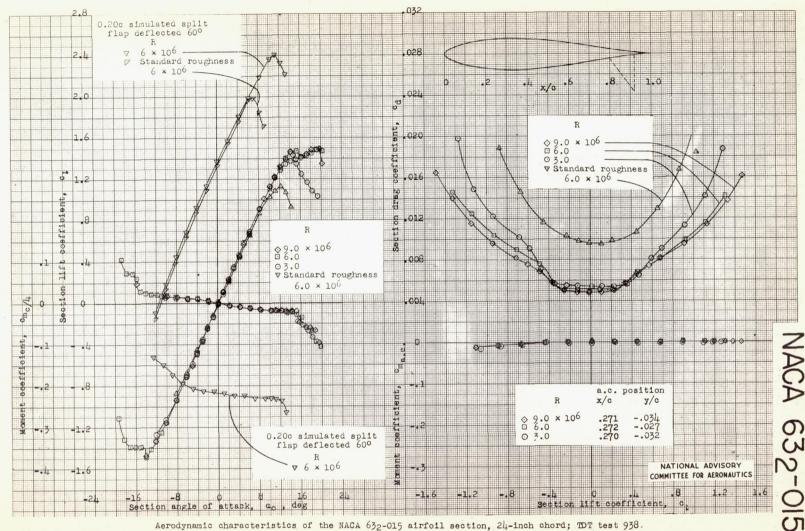
Aerodynamic characteristics of the NACA 631-012 airfoil section, 24-inch chord; TDT test 948.



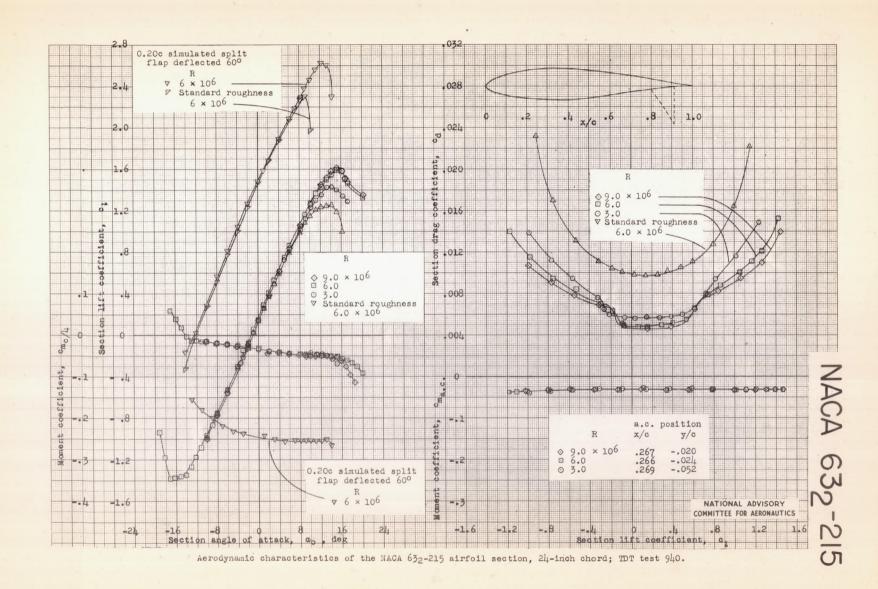
Aerodynamic characteristics of the NACA 631-212 airfoil section, 24-inch chord; TDT test 964.

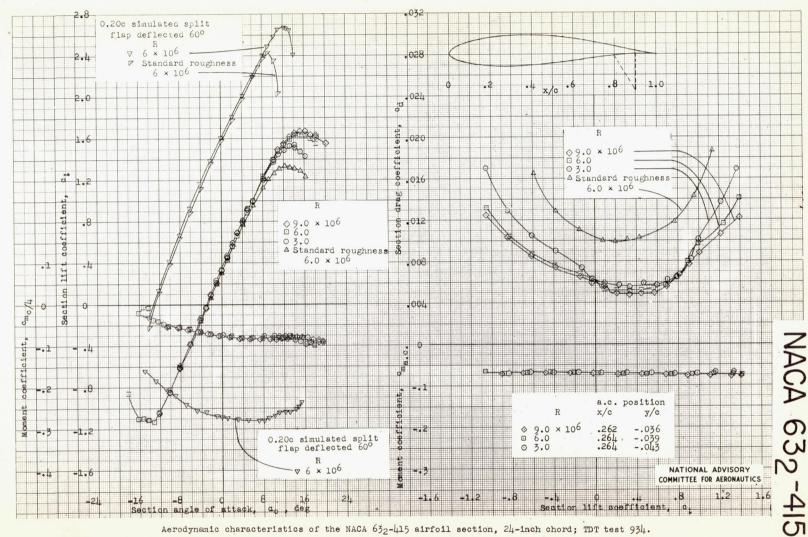


Aerodynamic characteristics of the NACA 631-412 airfoil section, 24-inch chord; TDT test 917.

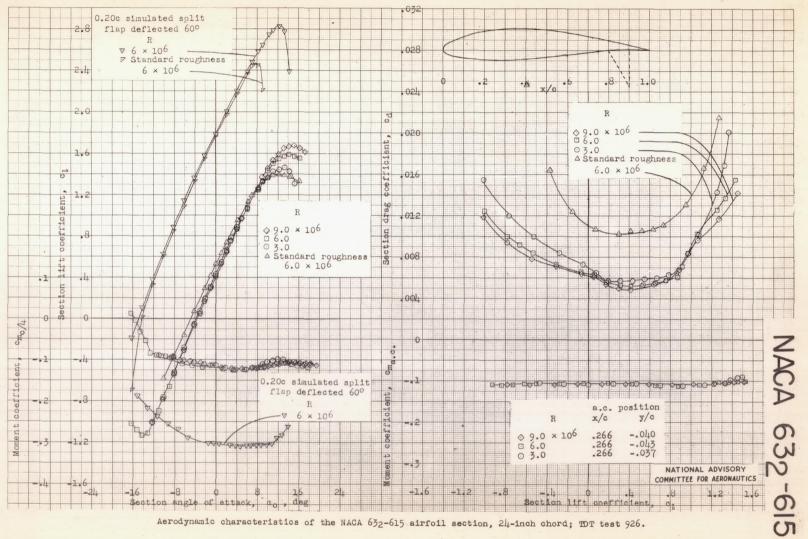


Aerodynamic characteristics of the NACA 632-015 airfoil section, 24-inch chord; TDT test 938.

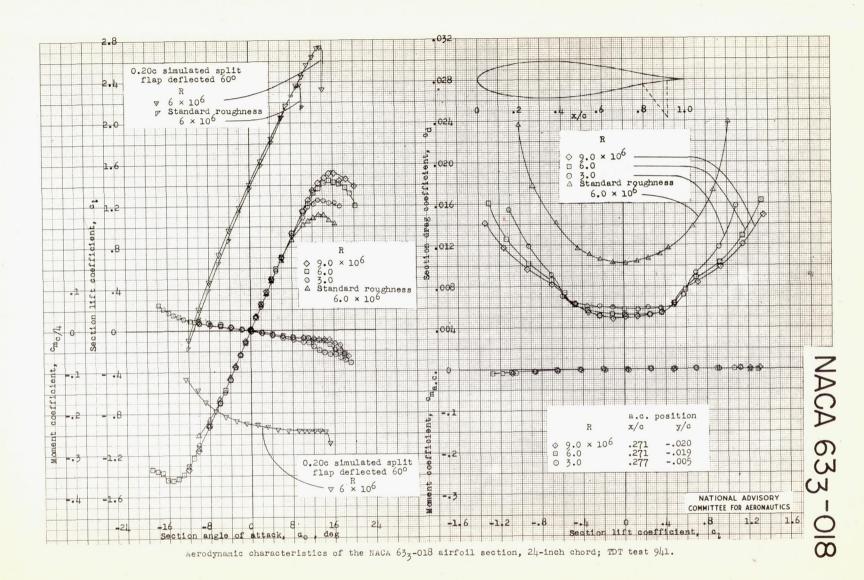


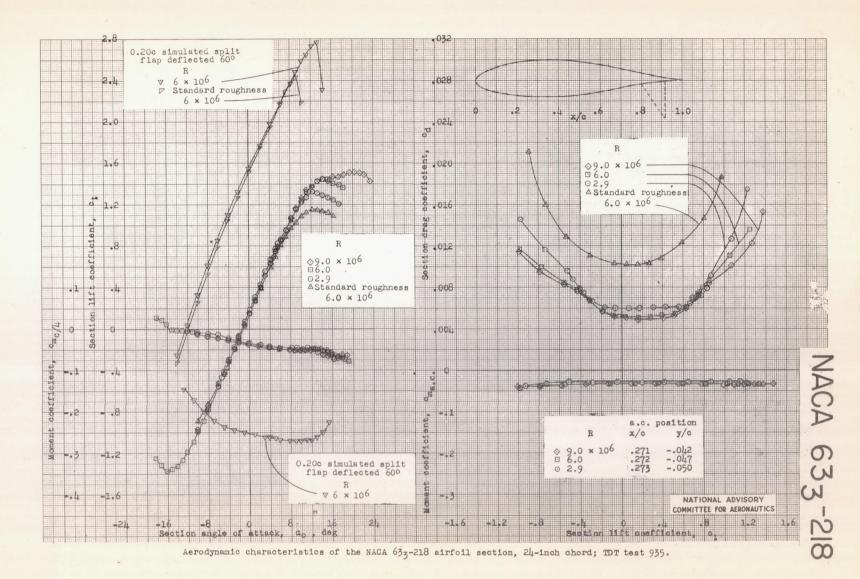


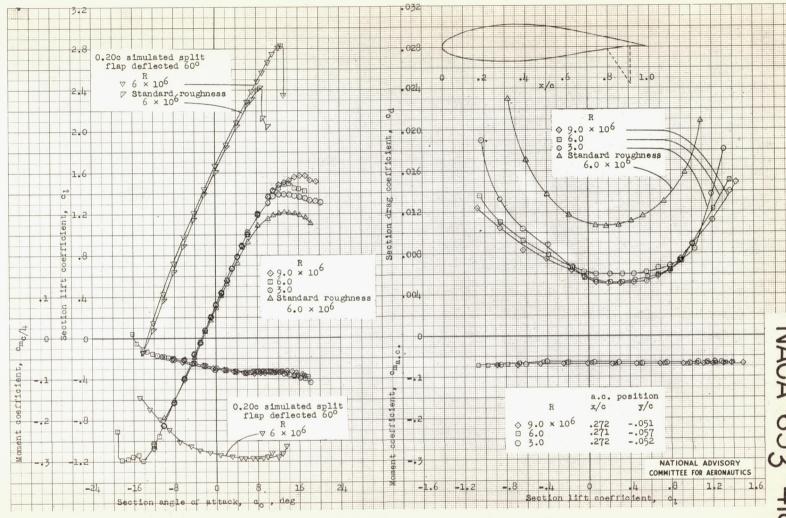
Aerodynamic characteristics of the NACA 632-415 airfoil section, 24-inch chord; TDT test 934.



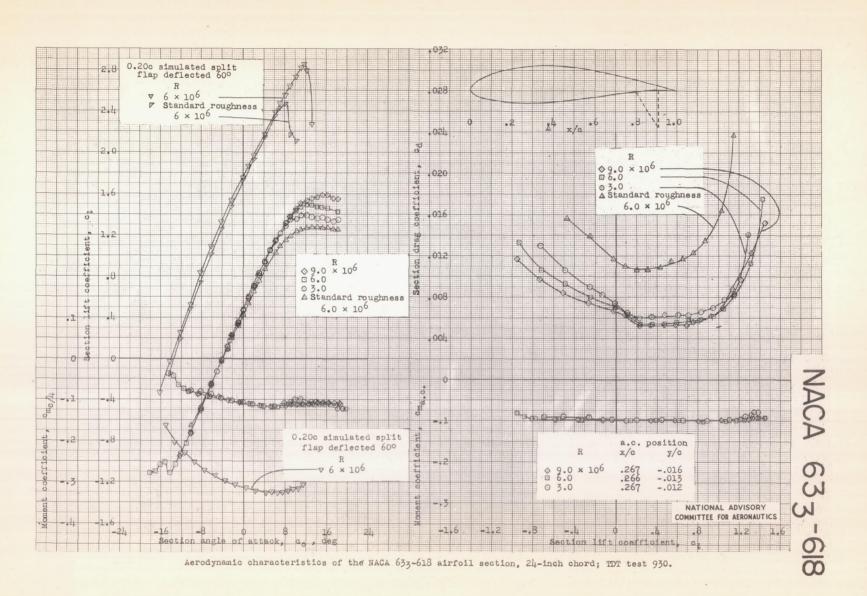
Aerodynamic characteristics of the NACA 632-615 airfoil section, 24-inch chord; TDT test 926.

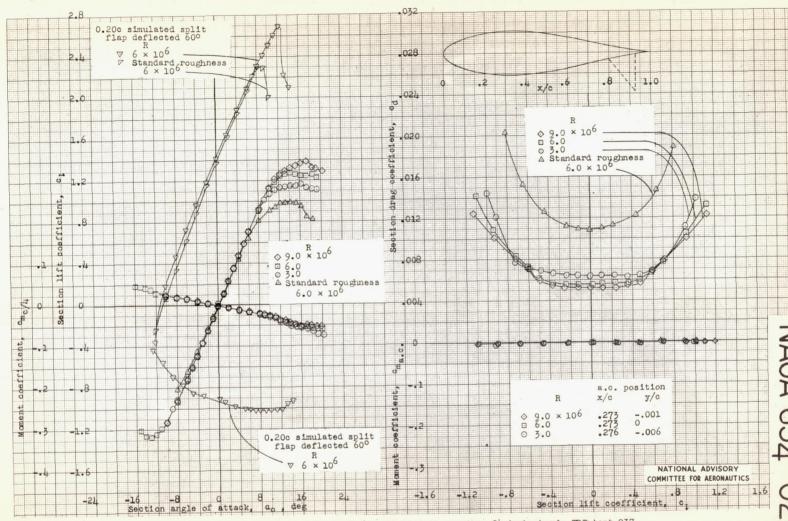




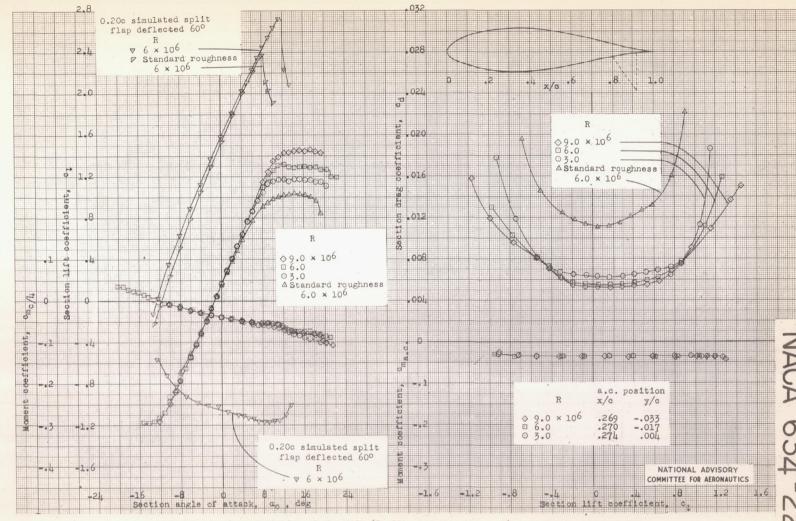


Aerodynamic characteristics of the NACA 633-418 airfoil section, 24-inch chord; TDT test 925.

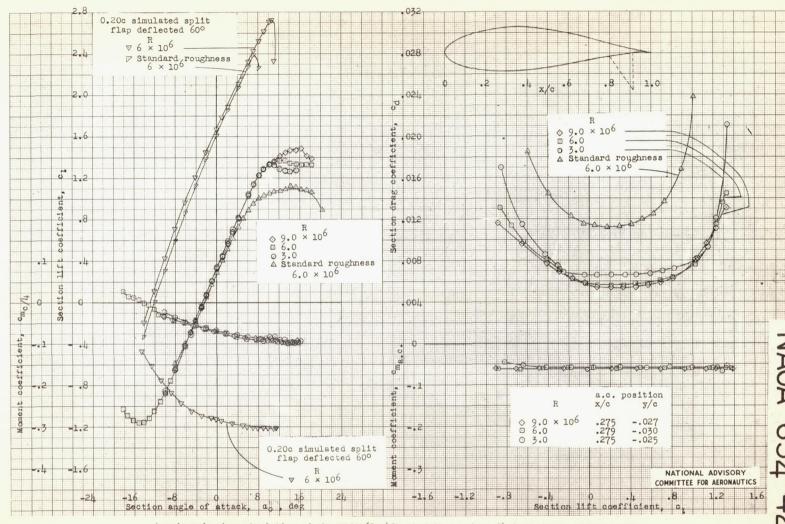




Aerodynamic characteristics of the NACA 634-021 airfoil section, 24-inch chord; TDT test 937.

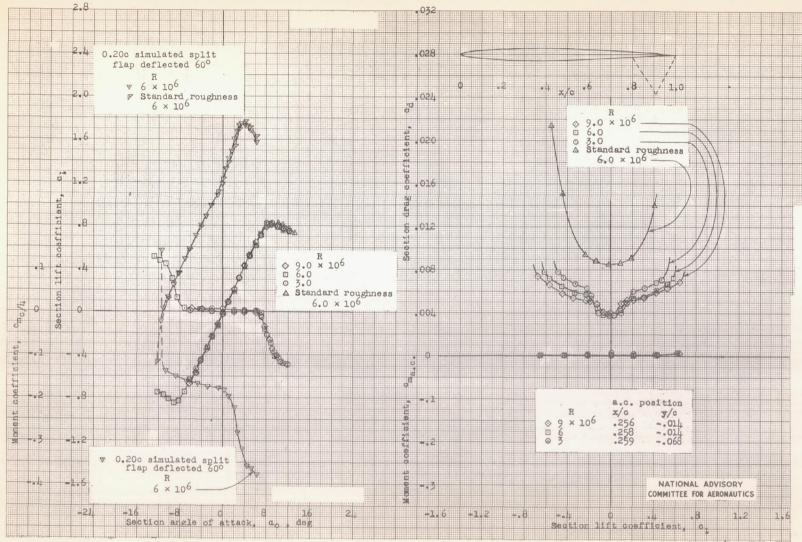


Aerodynamic characteristics of the NACA 6311-221 airfoil section, 24-inch chord; TDT test 939.

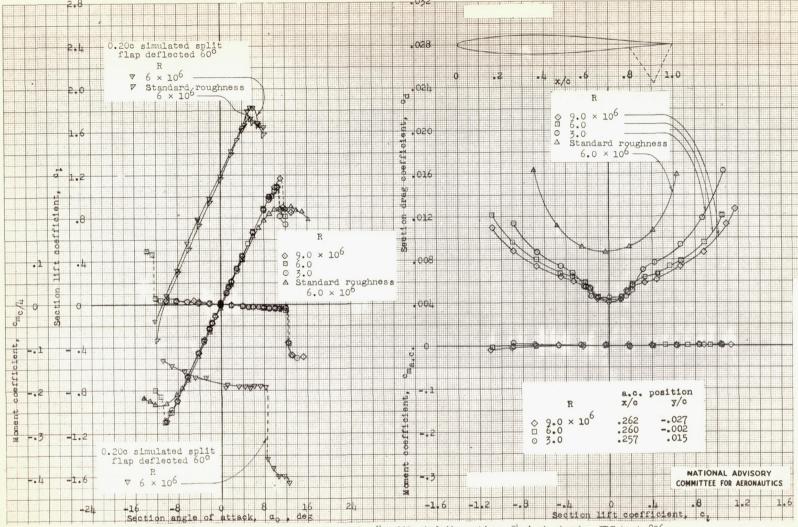


Aerodynamic characteristics of the NACA 634-421 airfoil section, 24-inch chord; TDT test 923.

O1 ~2

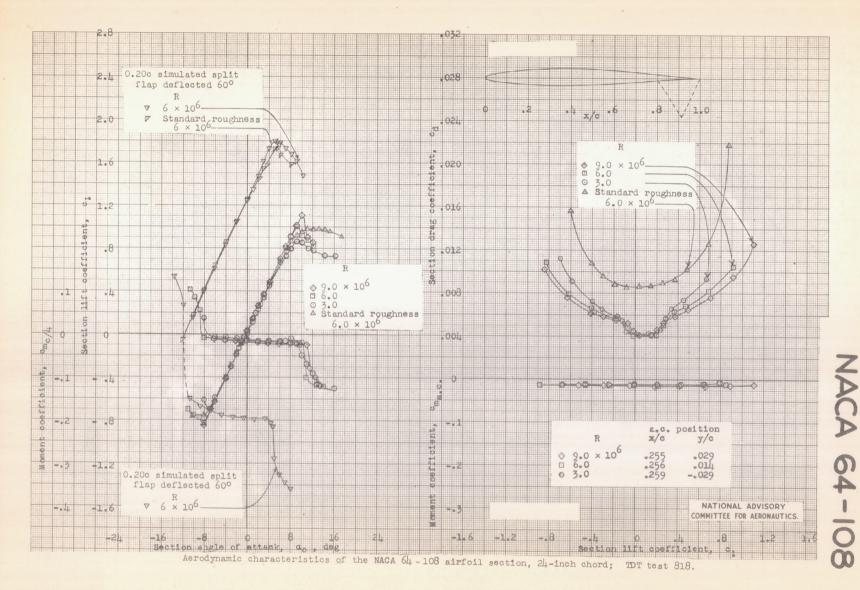


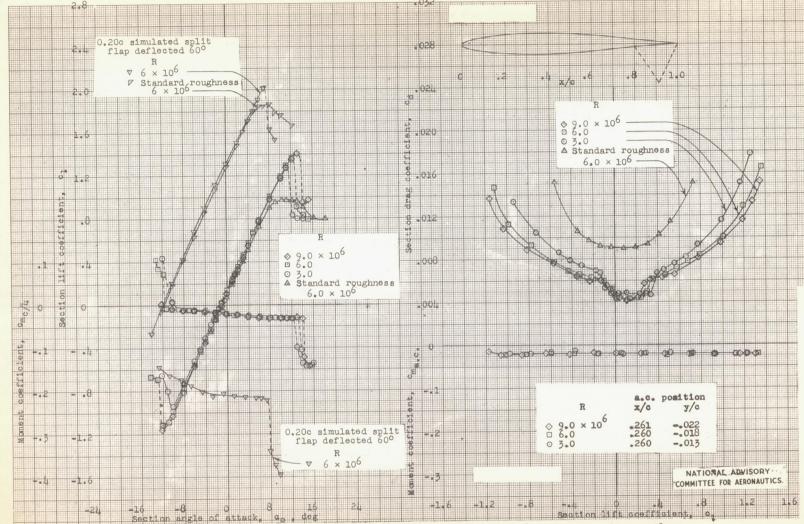
Aerodynamic characteristics of the NACA 64-006 airfoil section, 24-inch chord; TDT test 884.



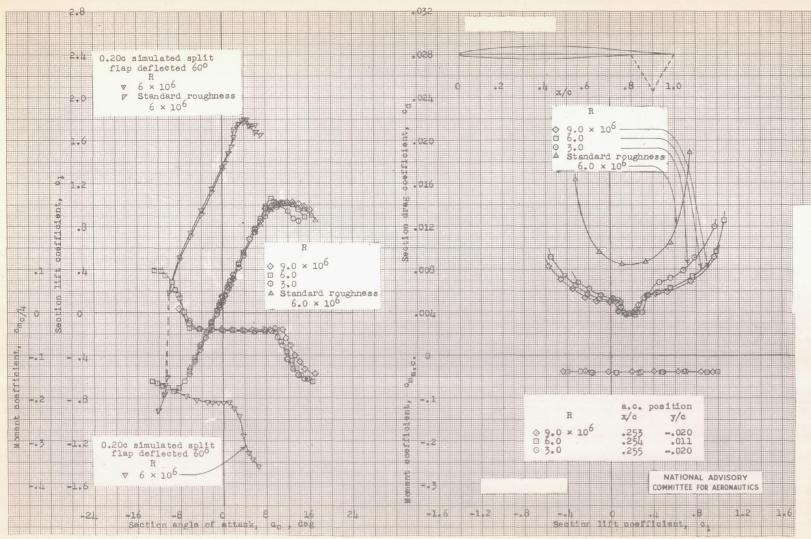
Aerodynamic characteristics of the NACA 64 - 009 airfoil section, 24-inch chord; TDT test 826.

S

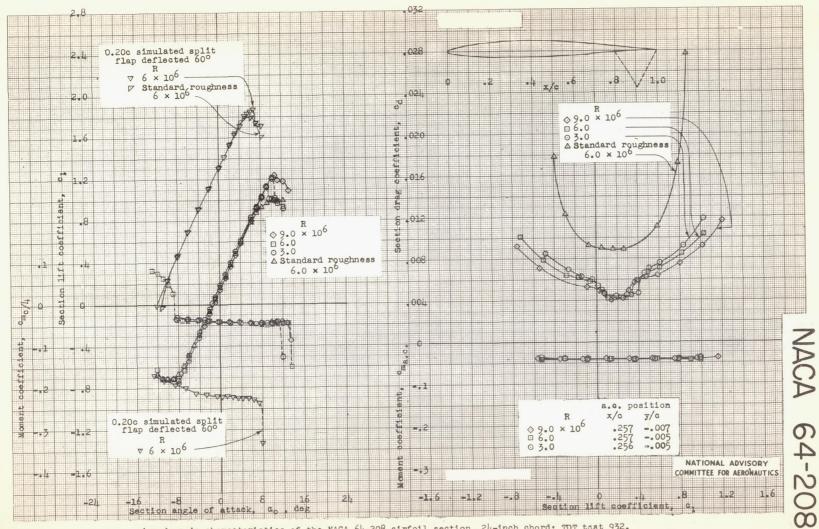




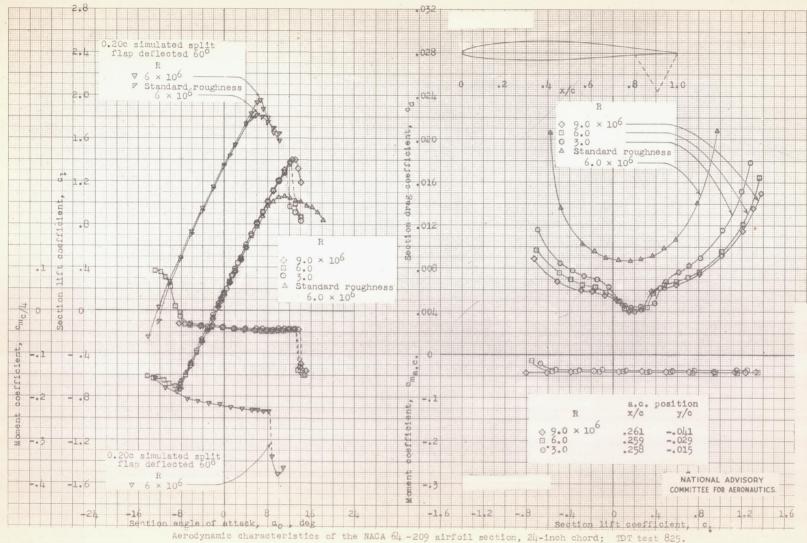
Aerodynamic characteristics of the NACA 64 110 airfoil section, 24-inch chord; TDT test 821.



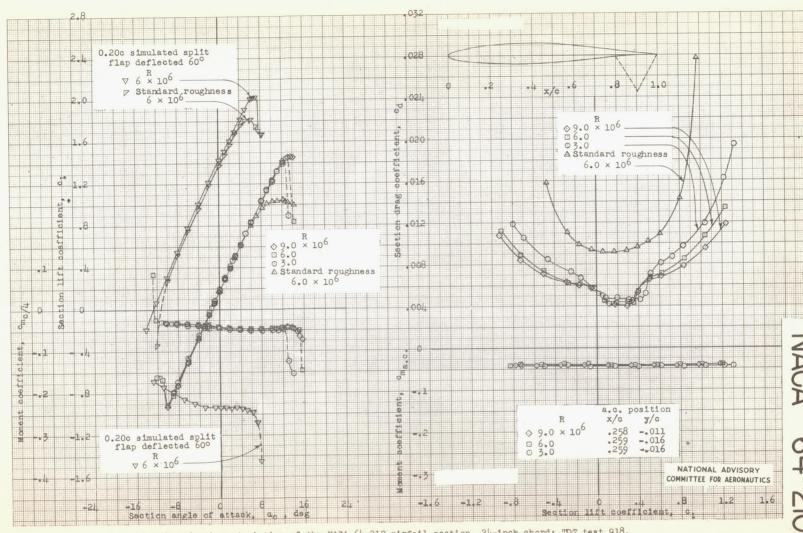
Aerodynamic characteristics of the NACA 64-206 airfoil section, 24-inch chord; TDT tests 834, 889.



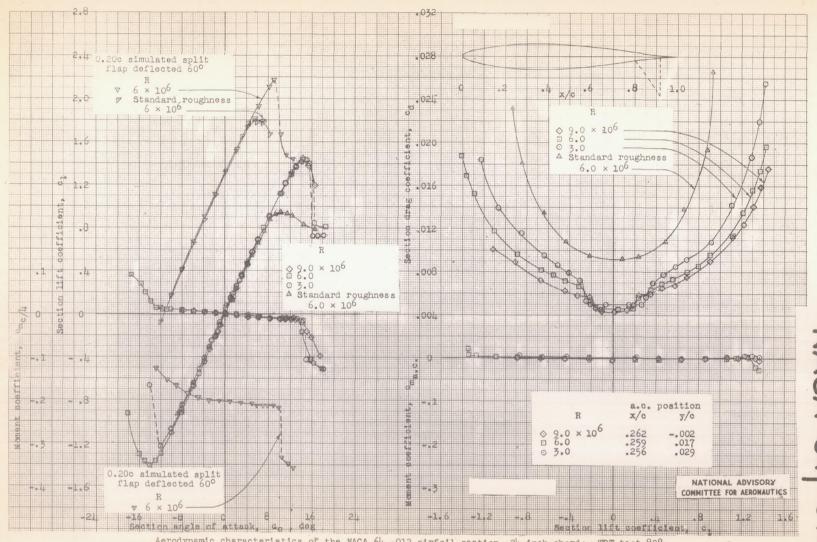
Aerodynamic characteristics of the NACA 64-208 airfoil section, 24-inch chord; TDT tost 932.



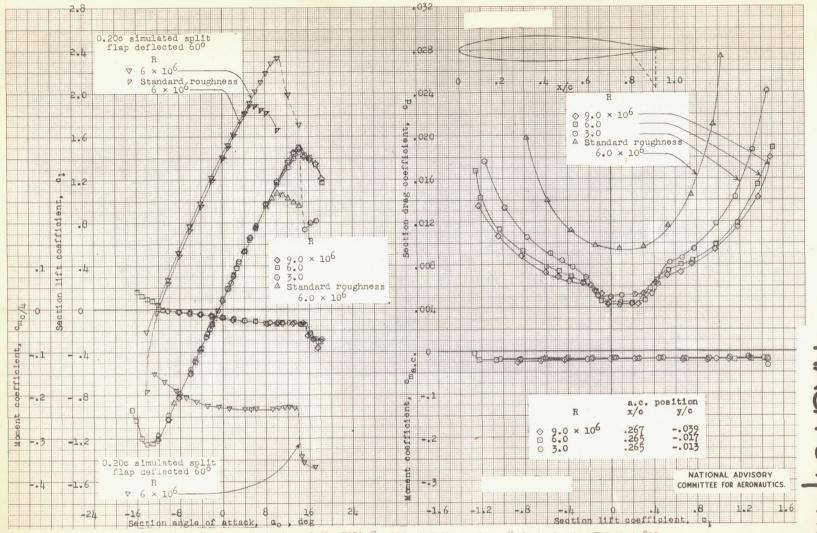
ACA 64-20



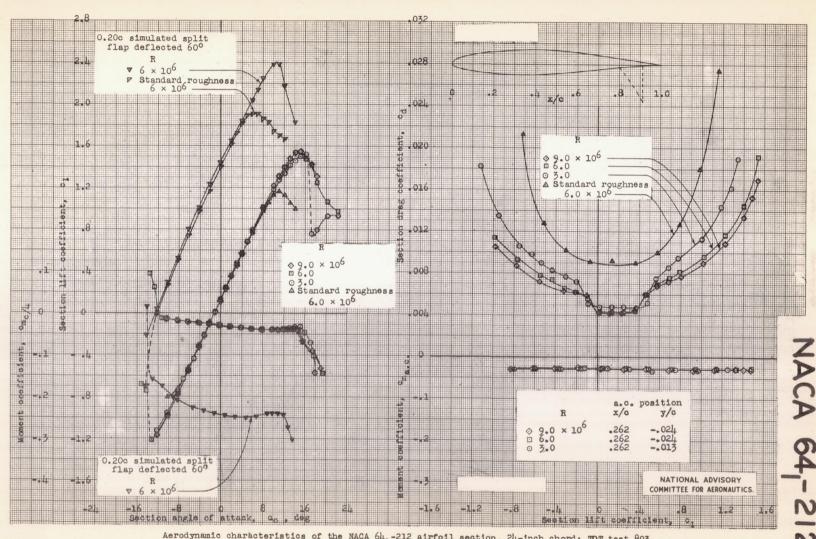
Aerodynamic characteristics of the NACA 64-210 airfoil section, 24-inch chord; TDT test 918.



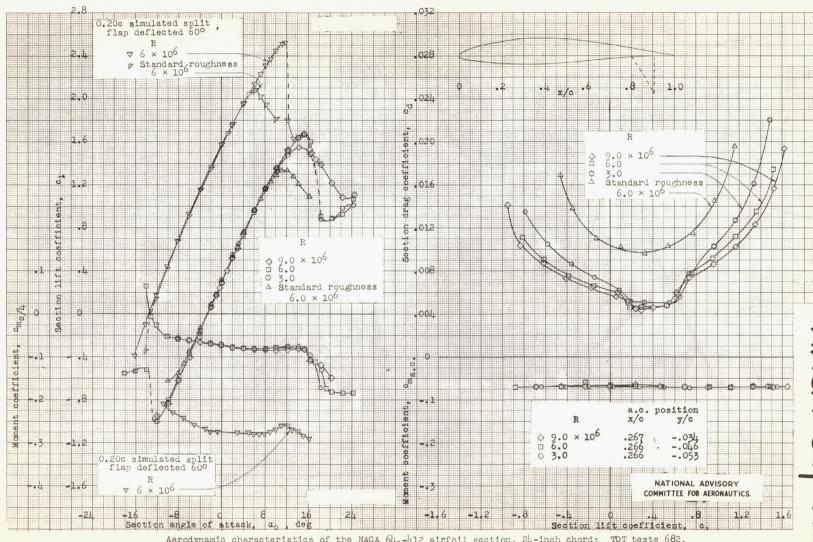
Aerodynamic characteristics of the NACA 647-012 airfoil section, 24-inch chord; TDT test 808.



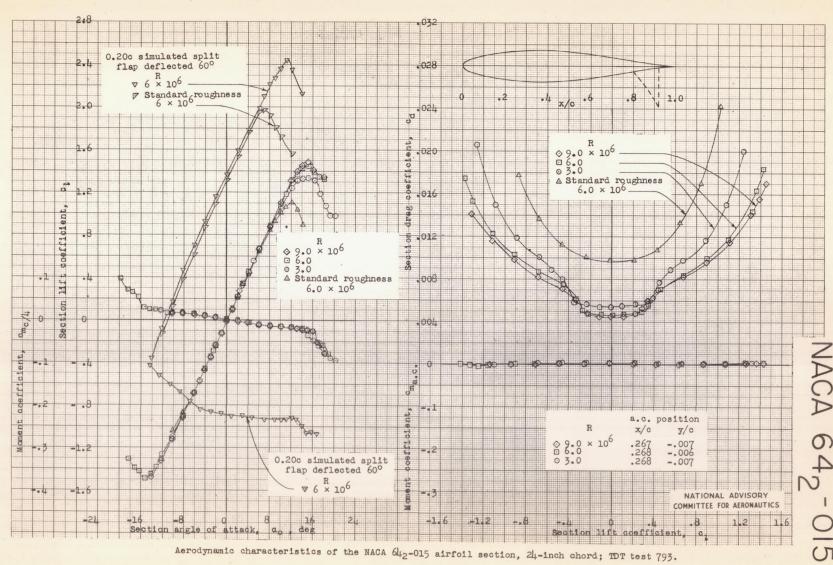
Aerodynamic characteristics of the NACA 647-112 airfoil section, 24-inch chord; TDT test 819.

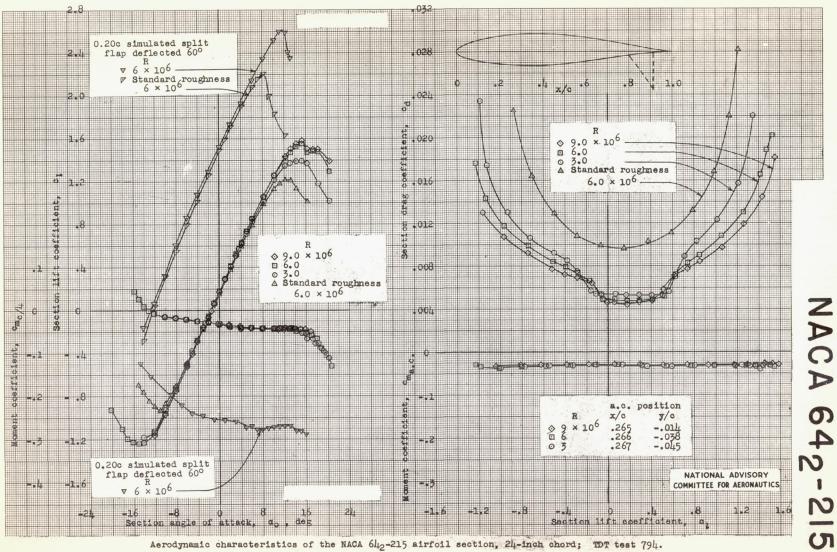


Aerodynamic characteristics of the NACA 641-212 airfoil section, 24-inch chord; TDT test 803.

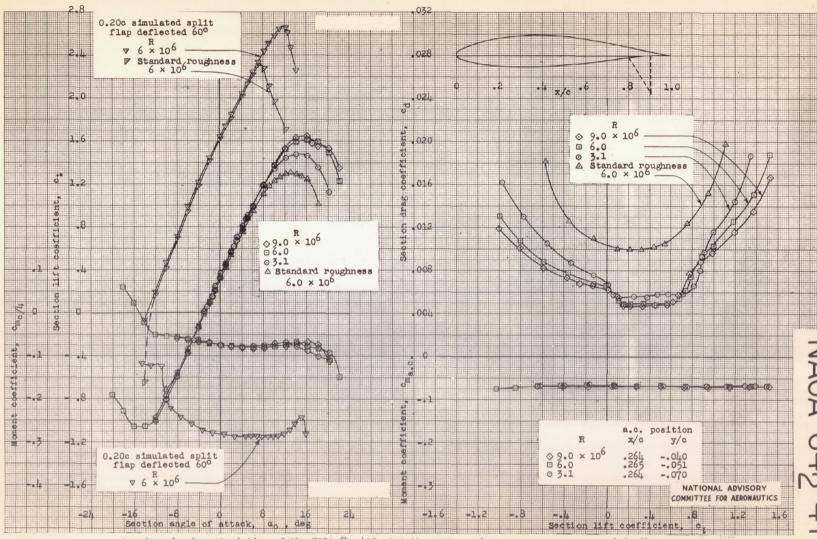


Aerodynamic characteristics of the NACA 641-412 airfoil section, 24-inch chord; TDT tests 682, 686, 831.

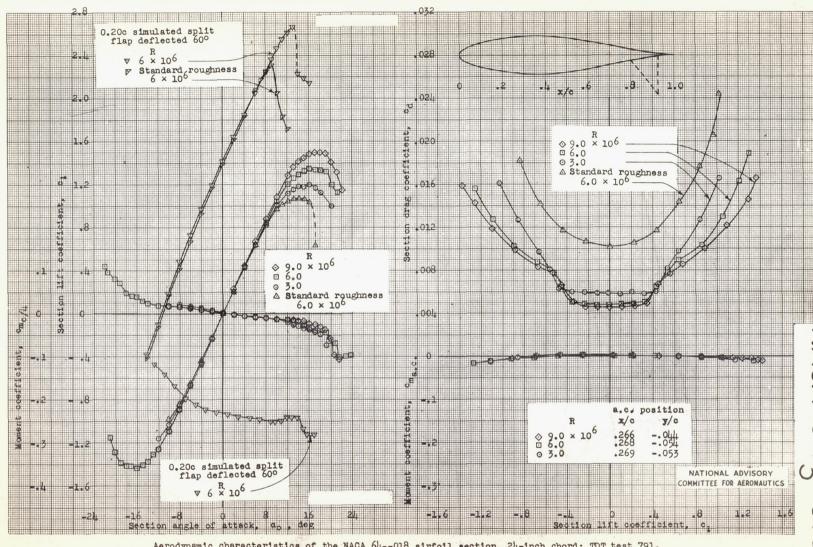




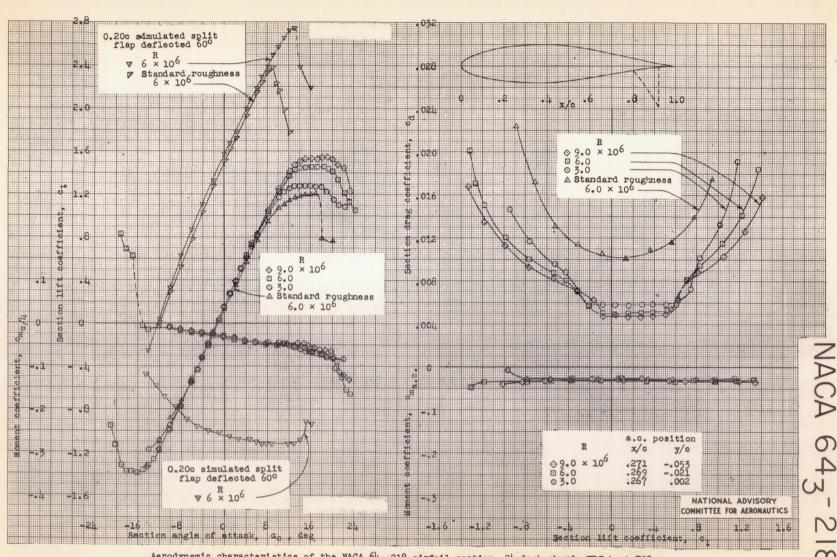
Aerodynamic characteristics of the NACA 642-215 airfoil section, 24-inch chord; TDT test 794.



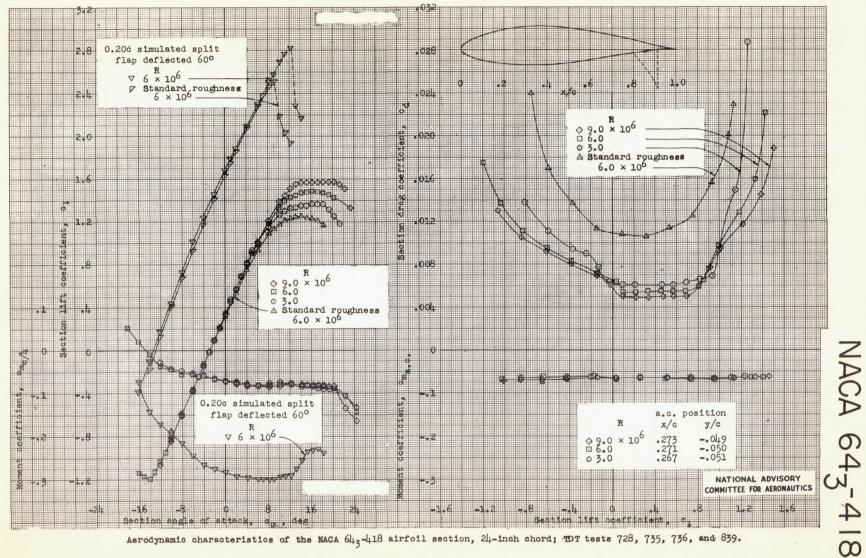
Aerodynamic characteristics of the NACA 642-415 airfoil section, 24-inch chord; TDT tests 656, 683, 733, and 843.



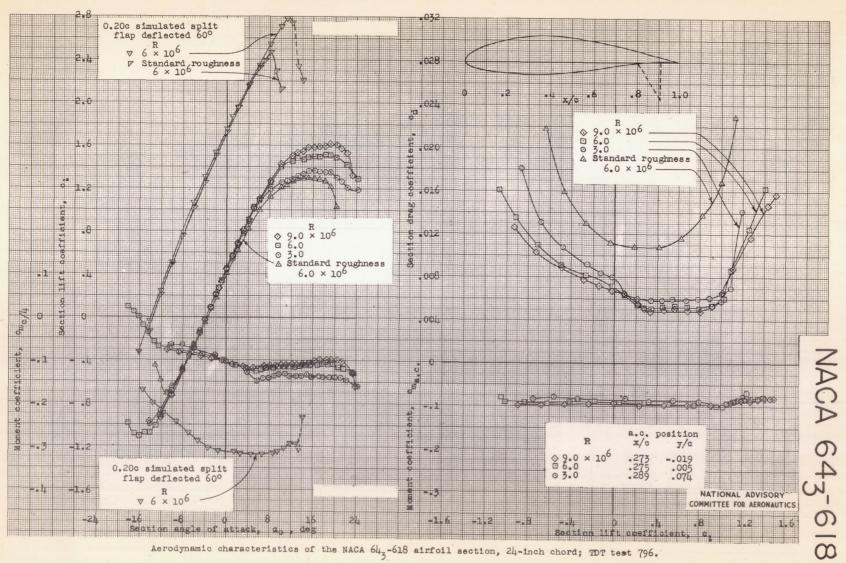
Aerodynamic characteristics of the NACA 643-018 airfoil section, 24-inch chord; TDT test 791.

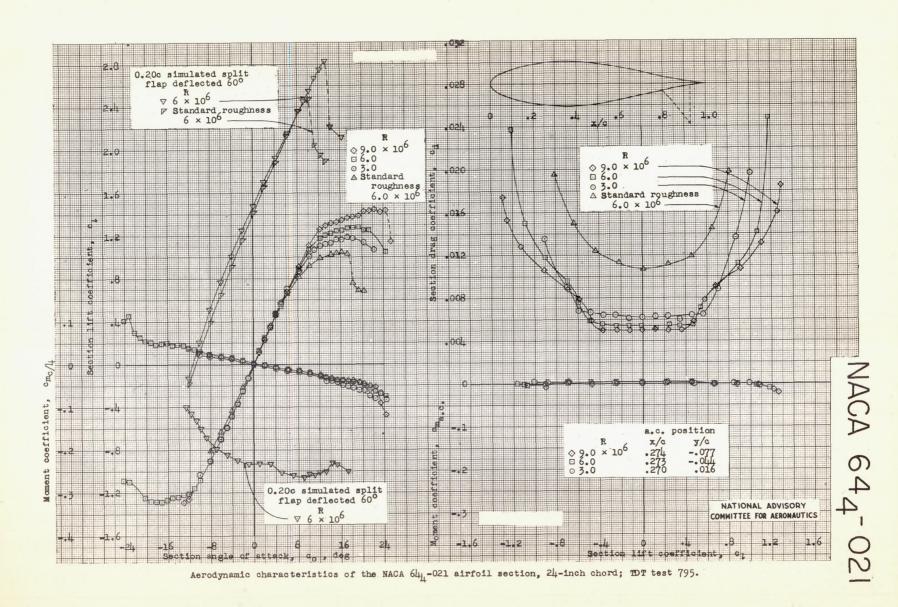


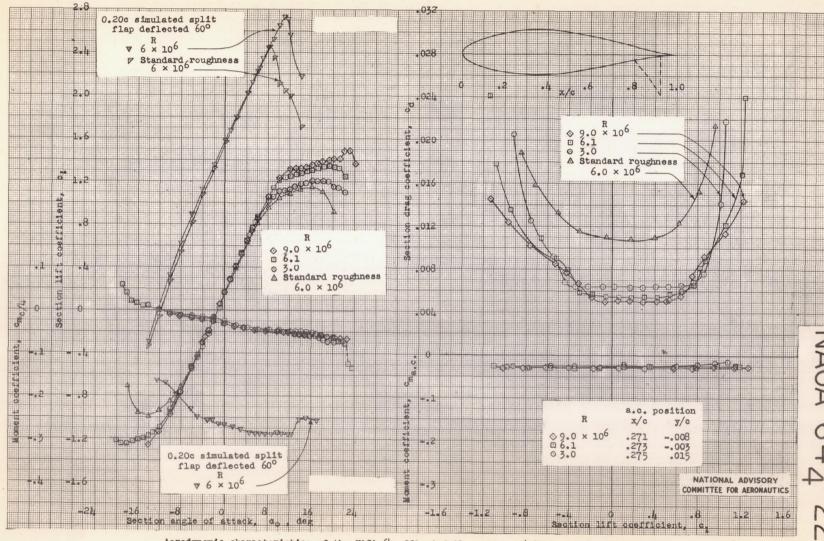
Aerodynamic characteristics of the NACA 643-218 airfoil section, 24-inch chord; TDT test 792.



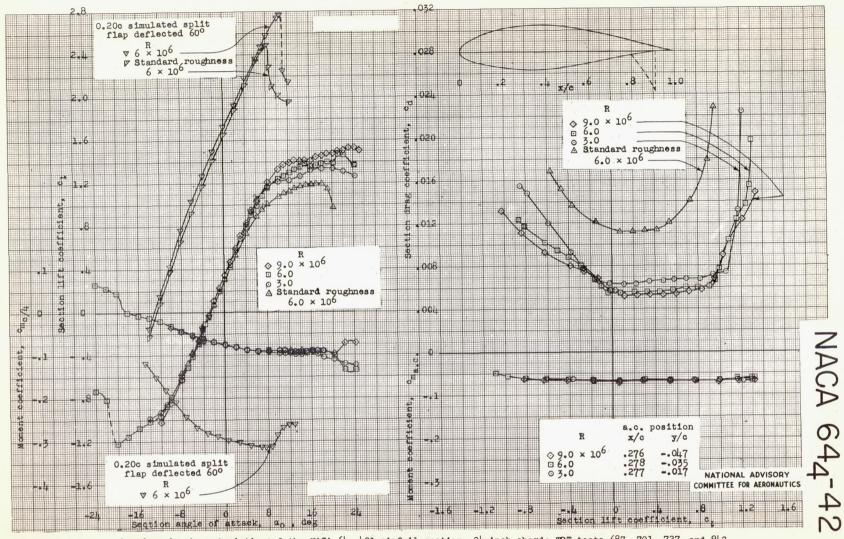
Aerodynamic characteristics of the NACA 643-418 airfoil section, 24-inch chord; TDT tests 728, 735, 736, and 839.





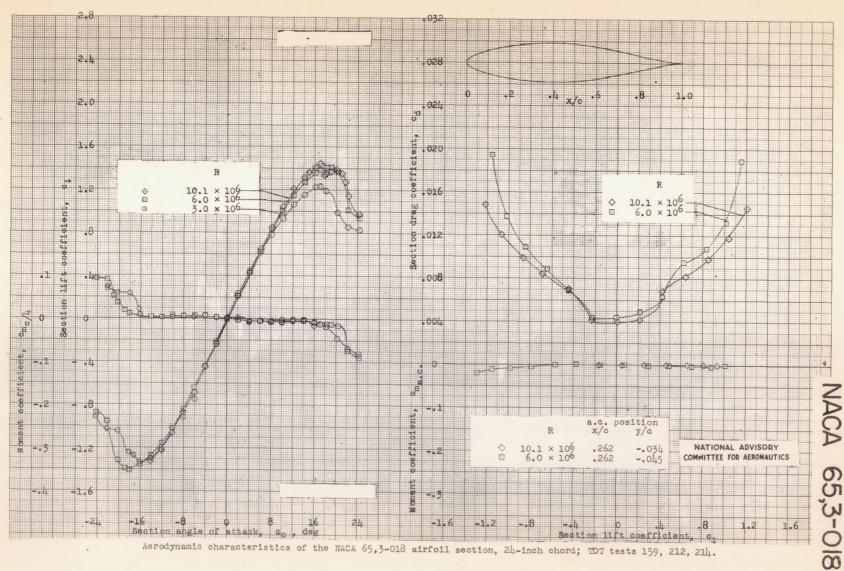


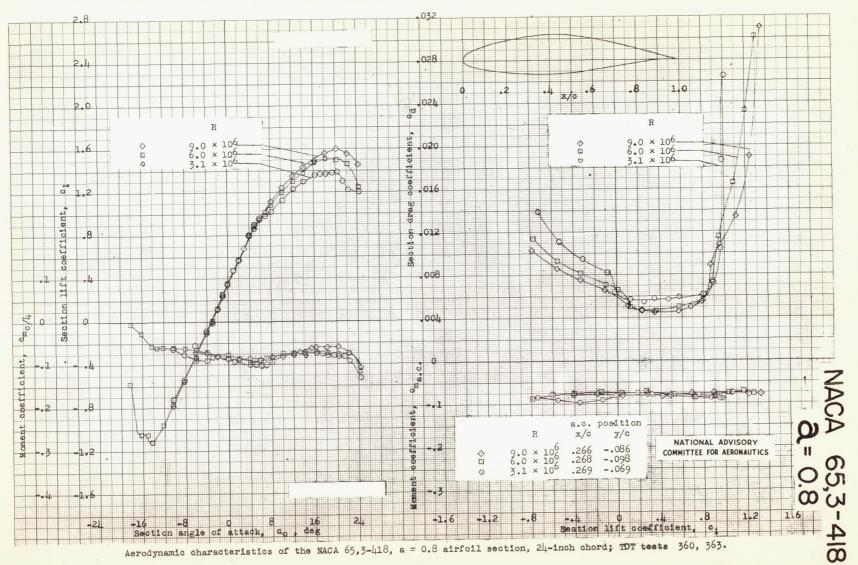
Aerodynamic characteristics of the NACA 644-221 airfoil section, 24-inch chord; TDT test 790.

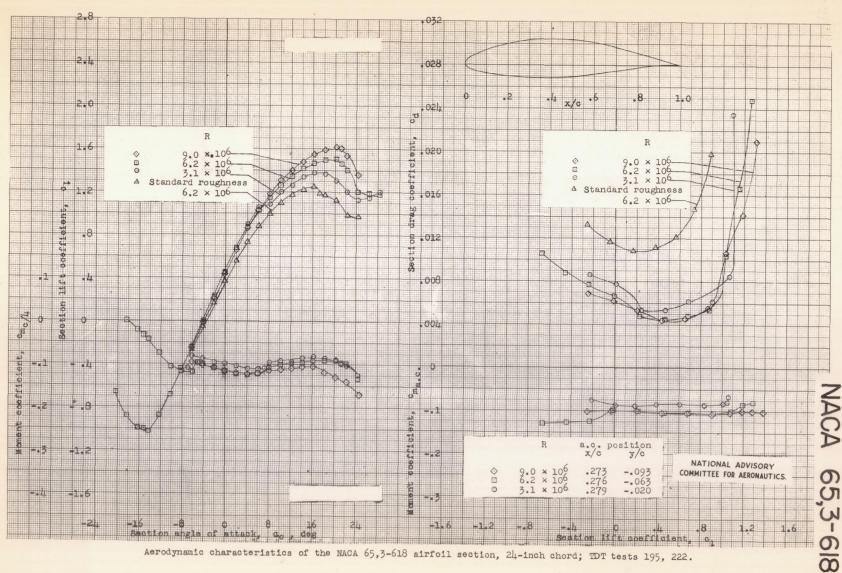


Aerodynamic characteristics of the NACA 644-421 airfoil section, 24-inch chord; TDT tests 687, 791, 727, and 842.

June

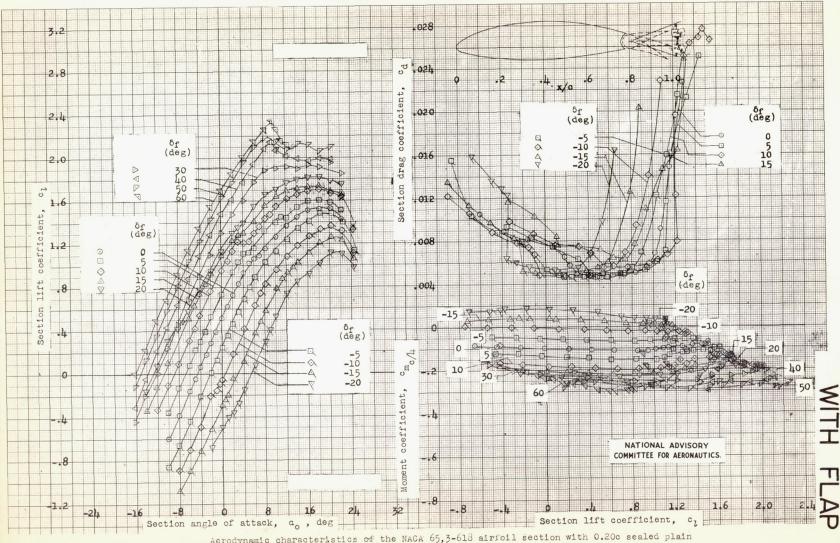




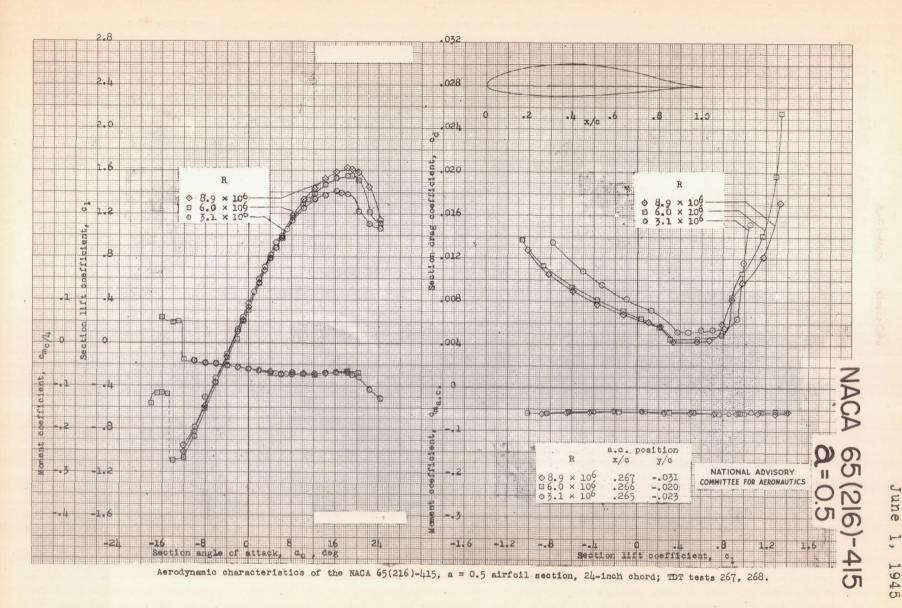


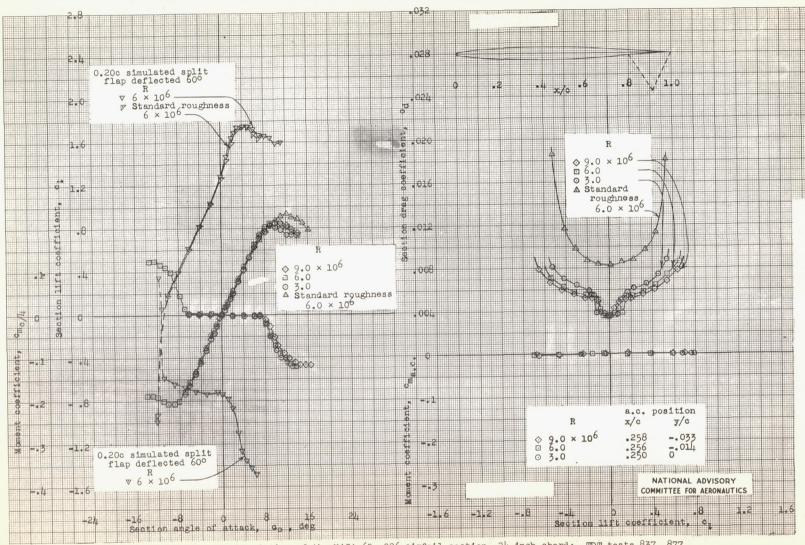
Aerodynamic characteristics of the NACA 65,3-618 airfoil section, 24-inch chord; TDT tests 195, 222.

June

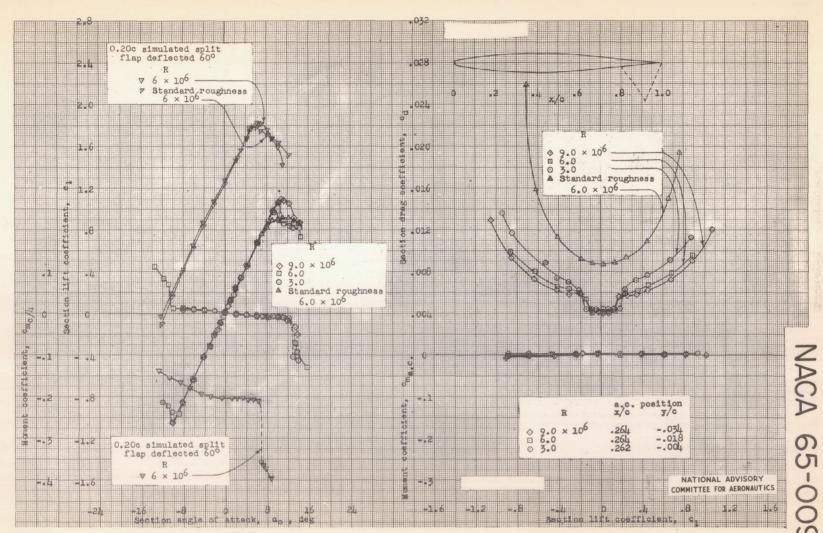


Aerodynamic characteristics of the NACA 65,3-618 airfoil section with 0.20c sealed plain flap. R, 6×10^6 ; TDT tests 343, 345, and 347.

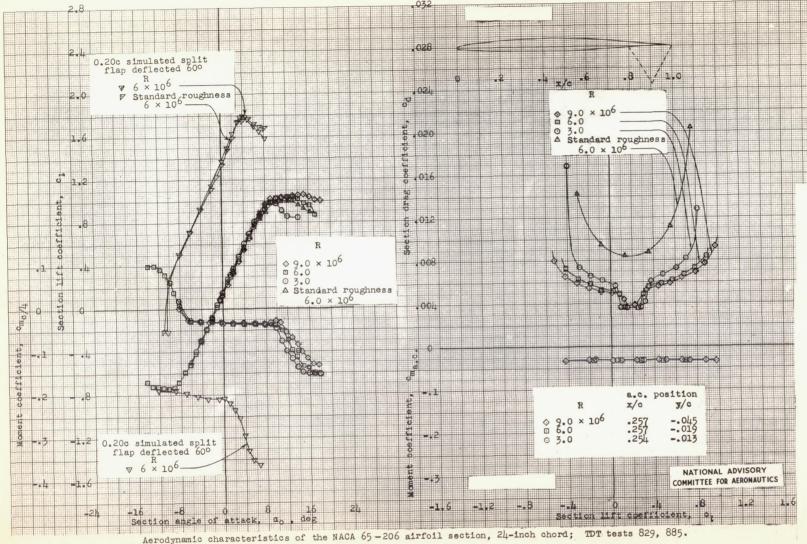




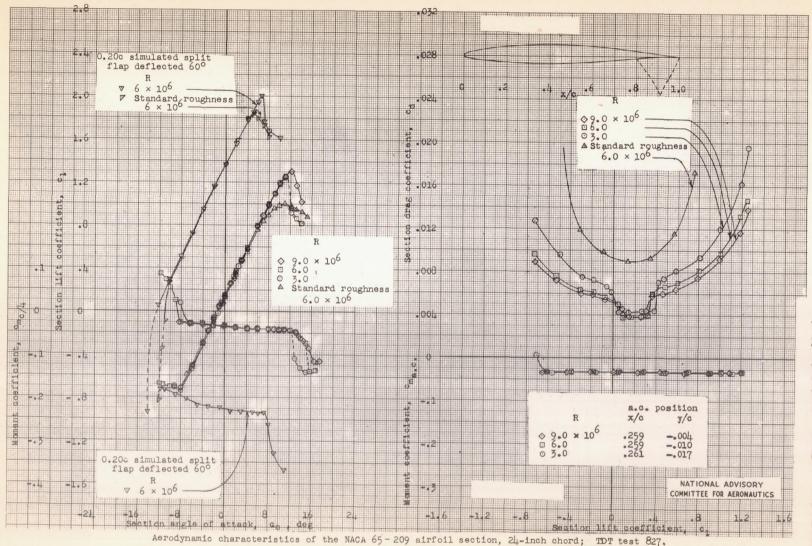
Aerodynamic characteristics of the NACA 65 - 006 airfoil section, 24-inch chord; TDT tests 837, 877.



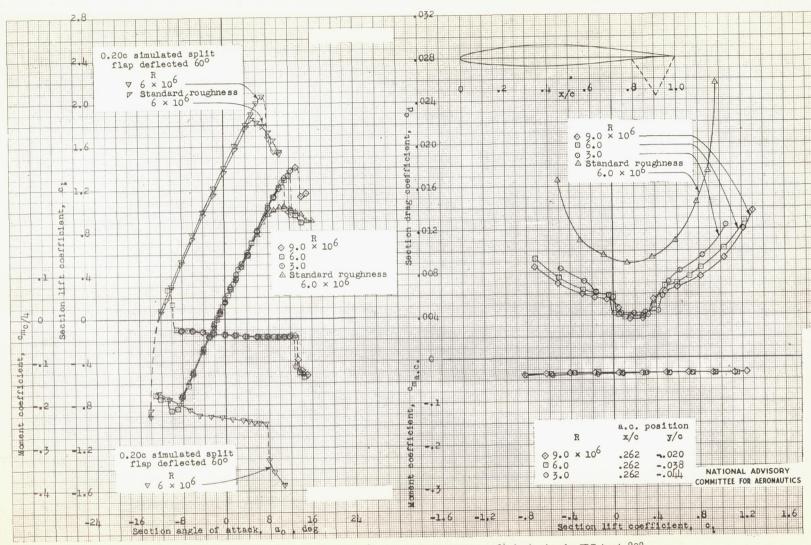
Aerodynamic characteristics of the NACA 65-009 airfoil section, 24-inch chord; TDT test 838.



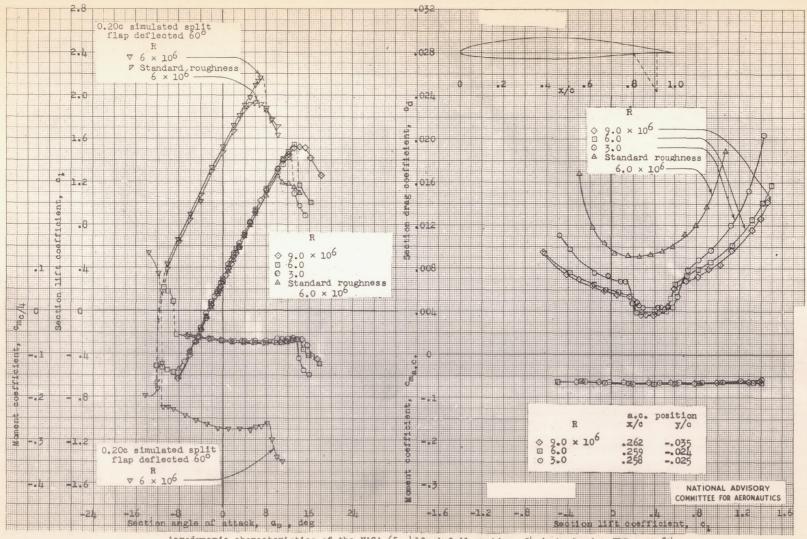
ACA 65-206



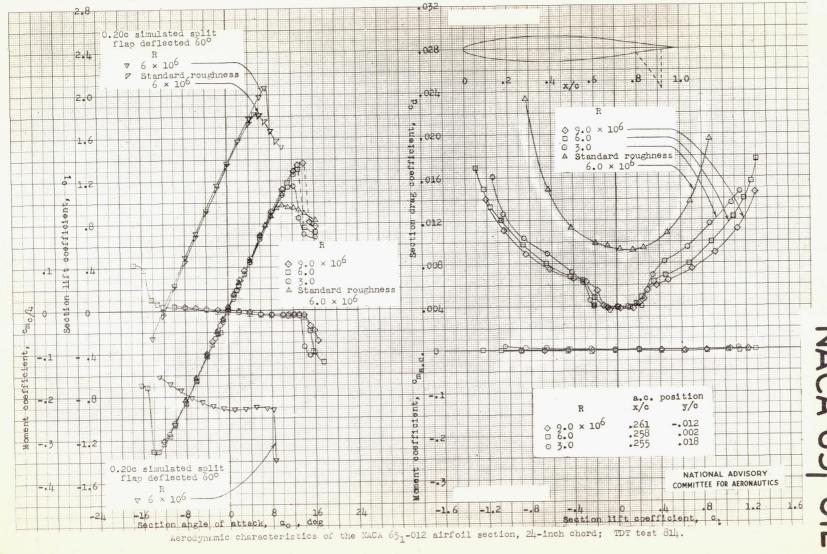
ACA 65-20

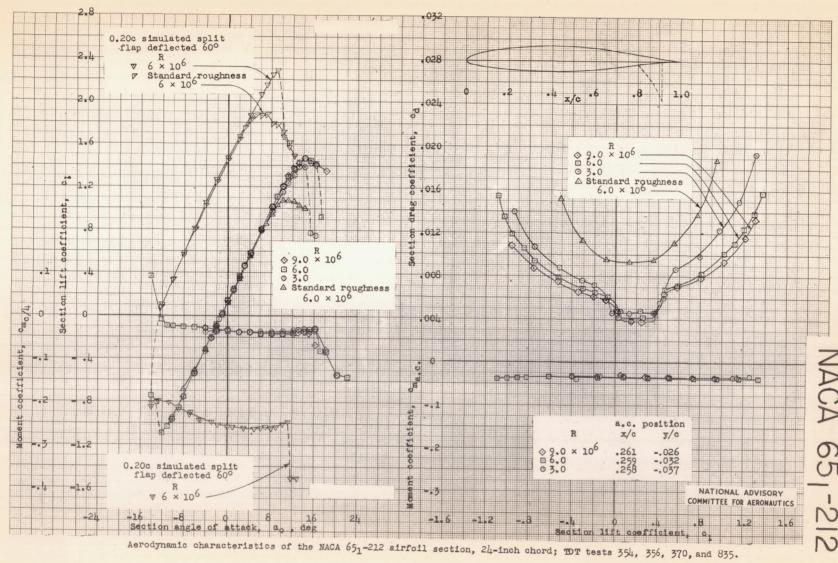


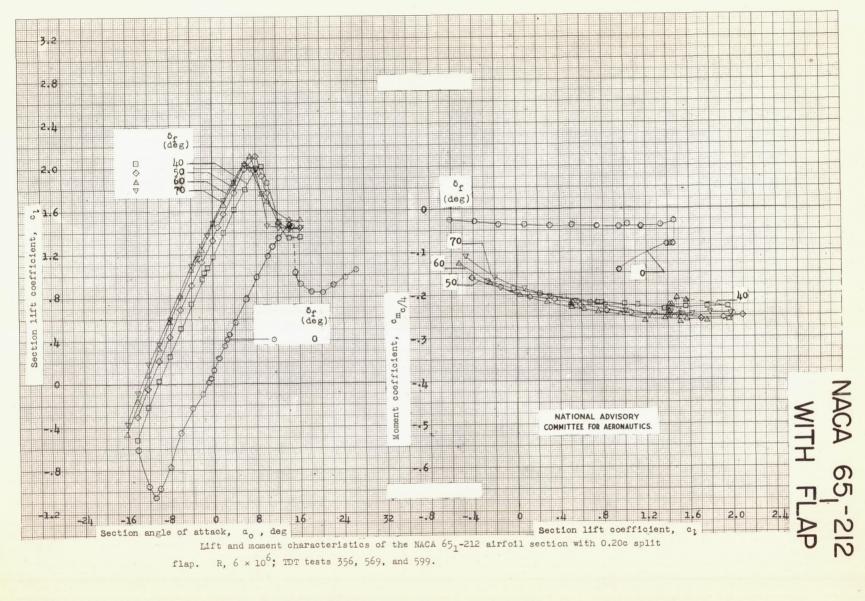
Aerodynamic characteristics of the NACA 65-210 airfoil section, 24-inch chord; TDT test 828.

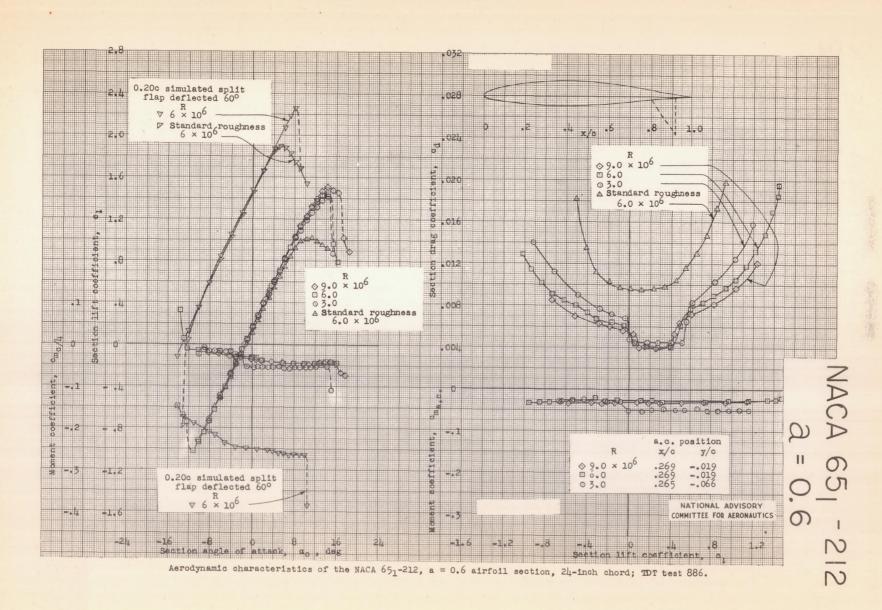


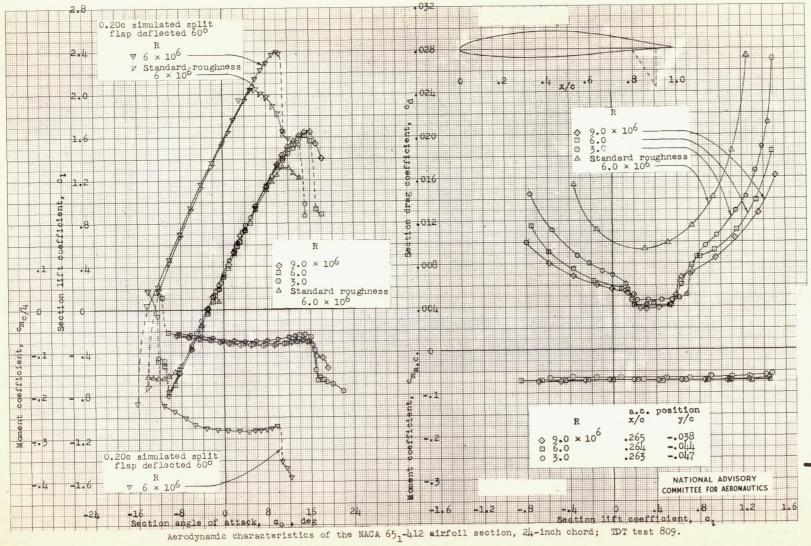
Aerodynamic characteristics of the NACA 65-410 airfoil section, 24-inch chord; TDT test 824.



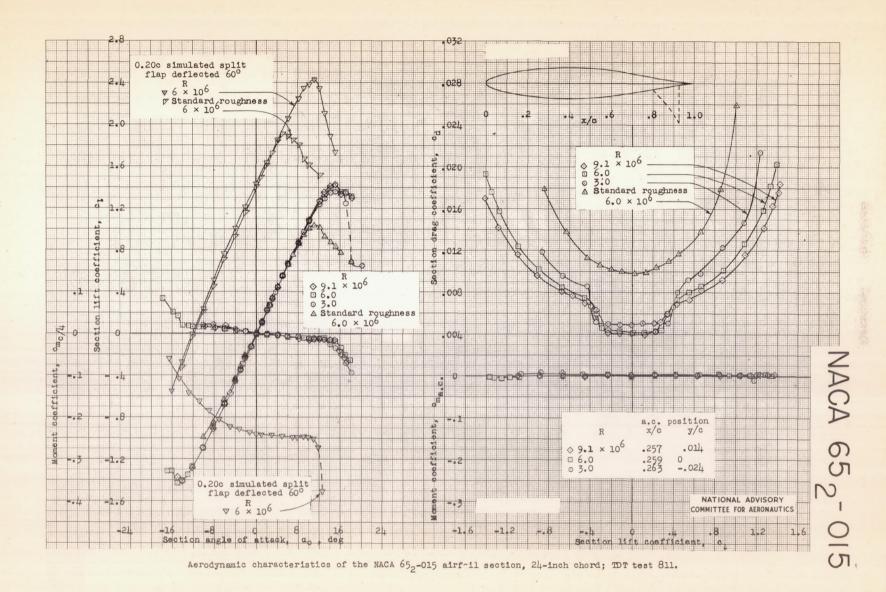


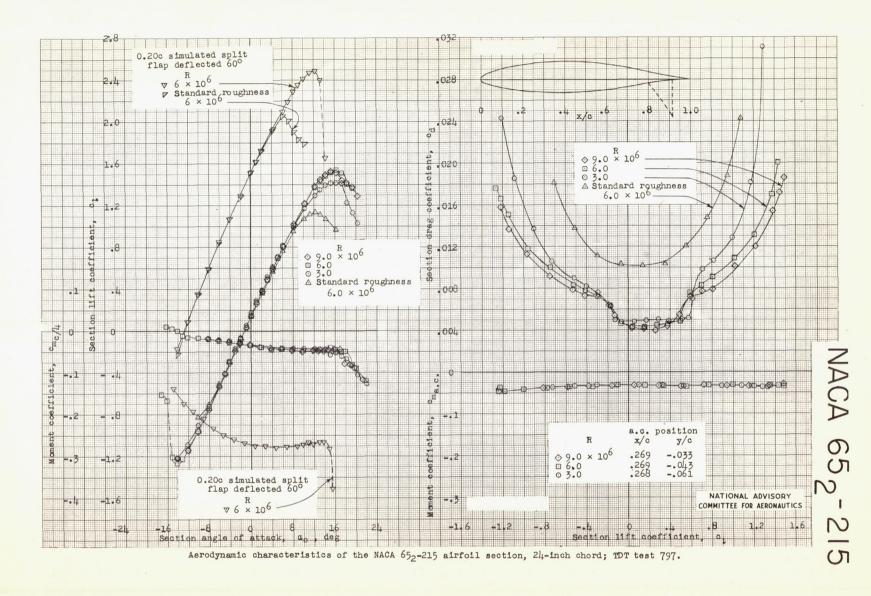


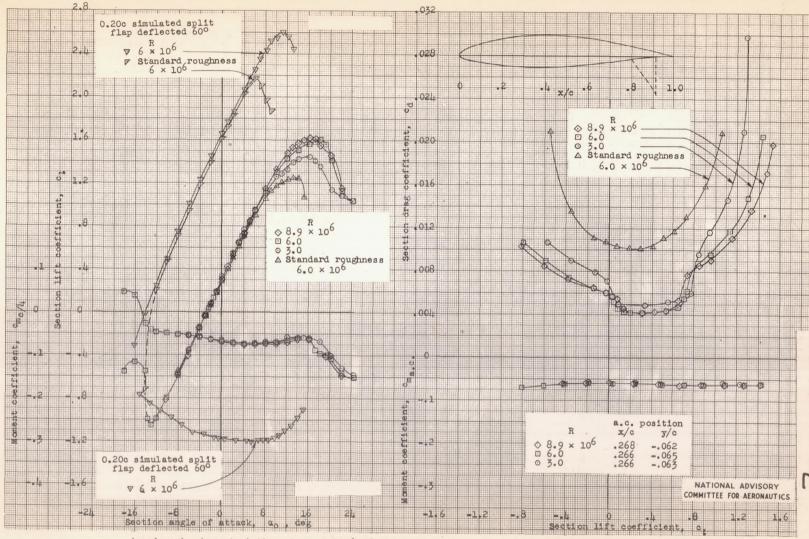




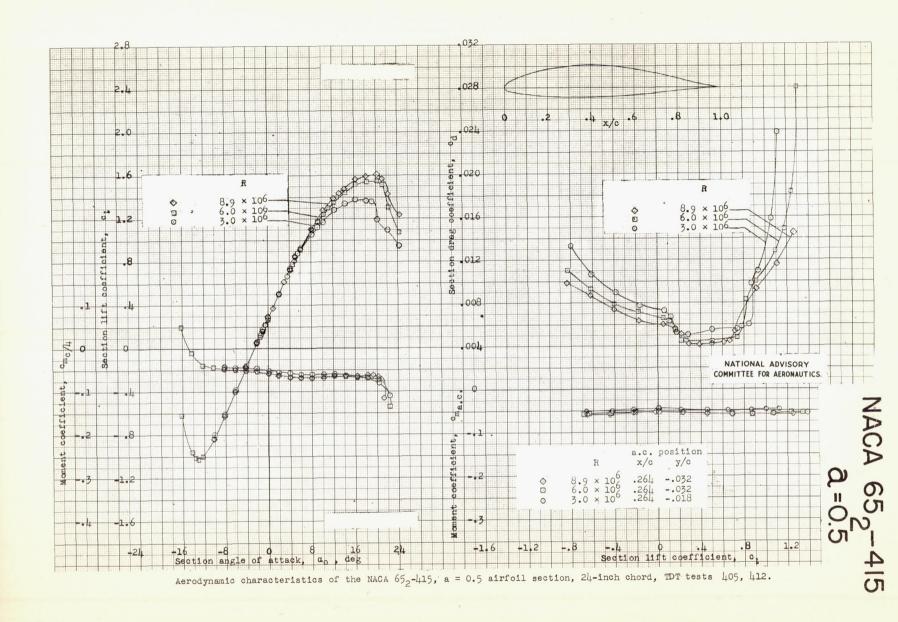
CA 65₁-41;

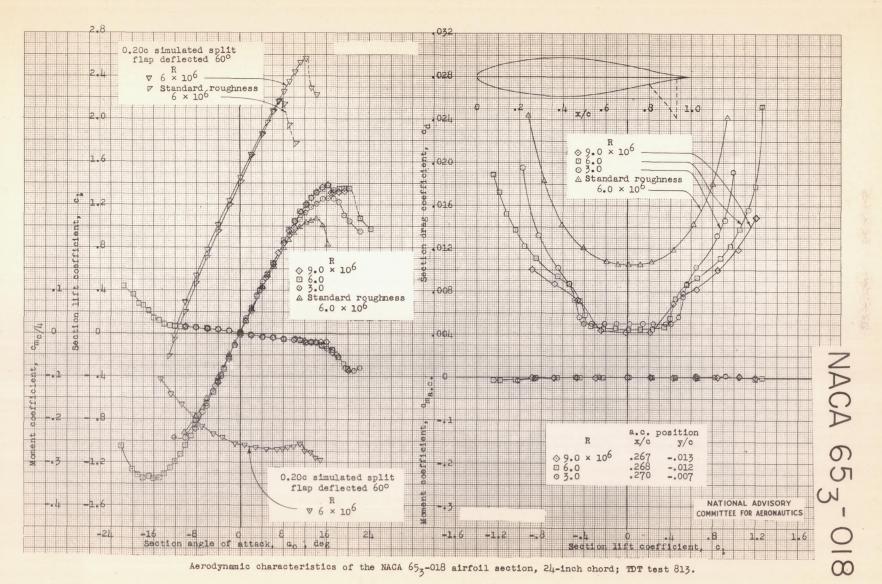


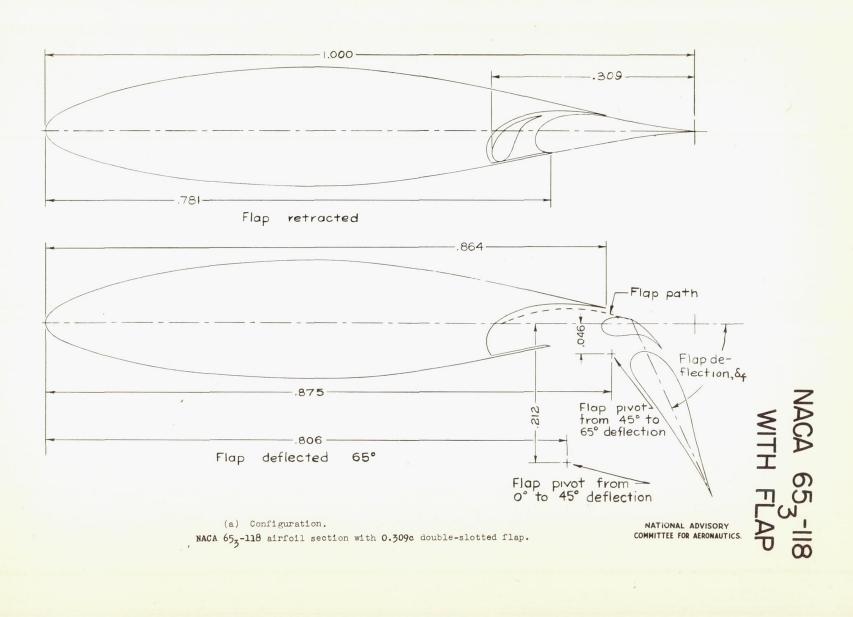


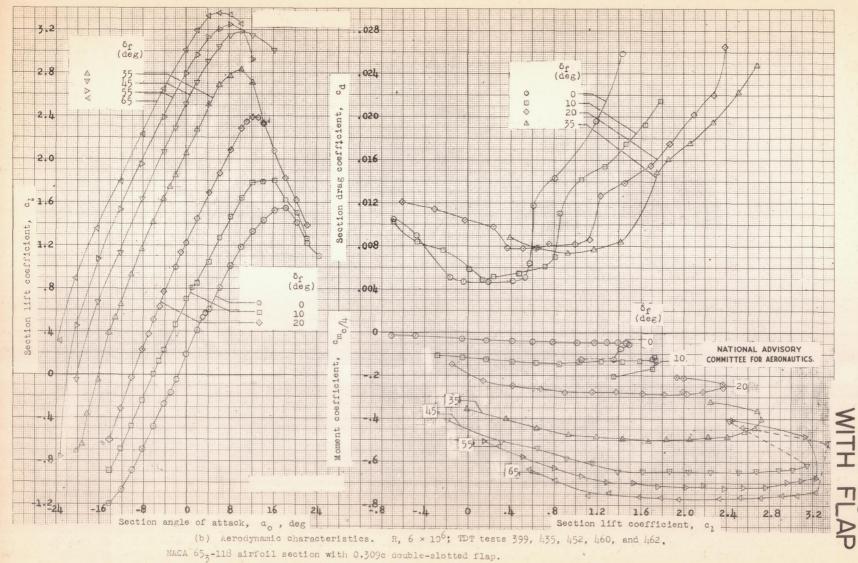


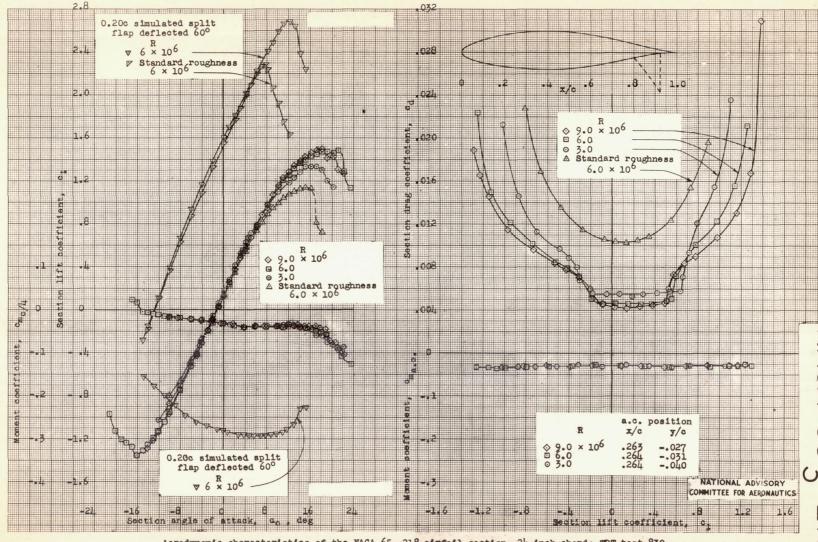
Aerodynamic characteristics of the NACA 652-415 airfoil section, 24-inch chord; TDT tests 313, 318, and 916.



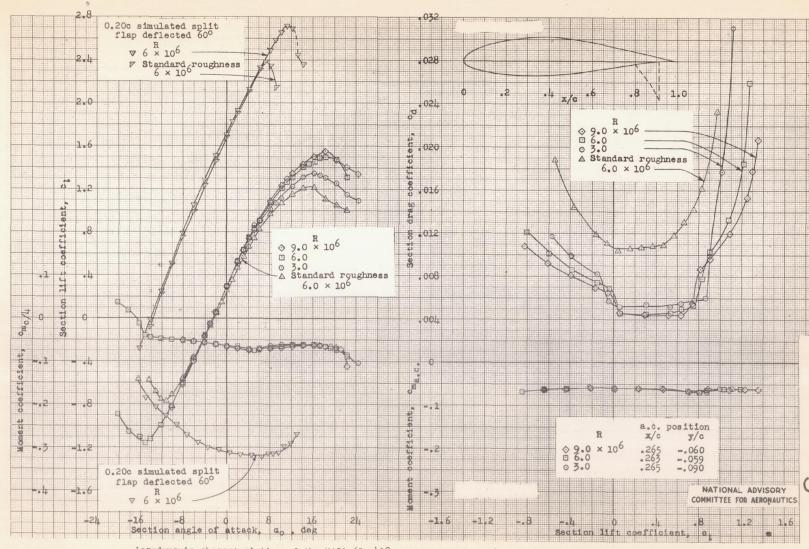




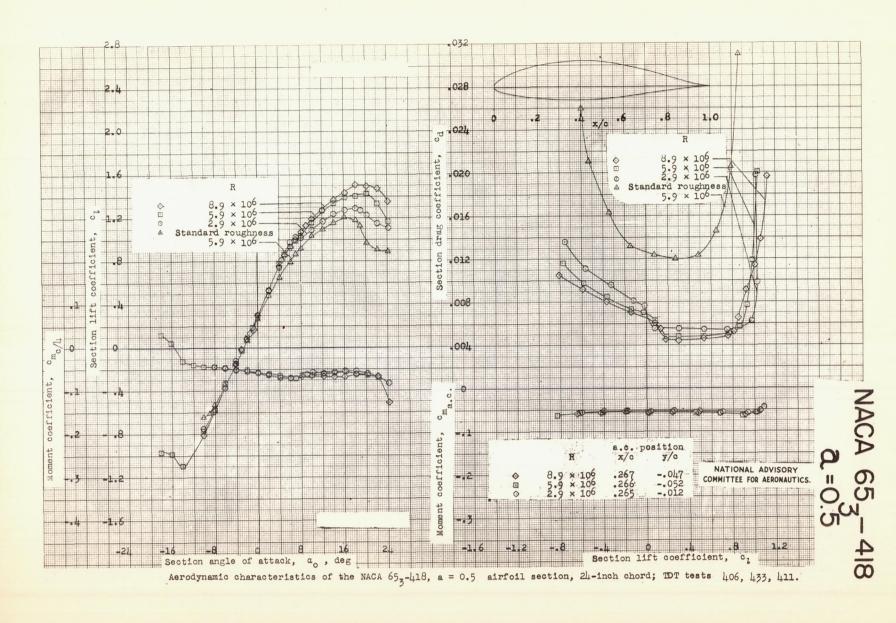


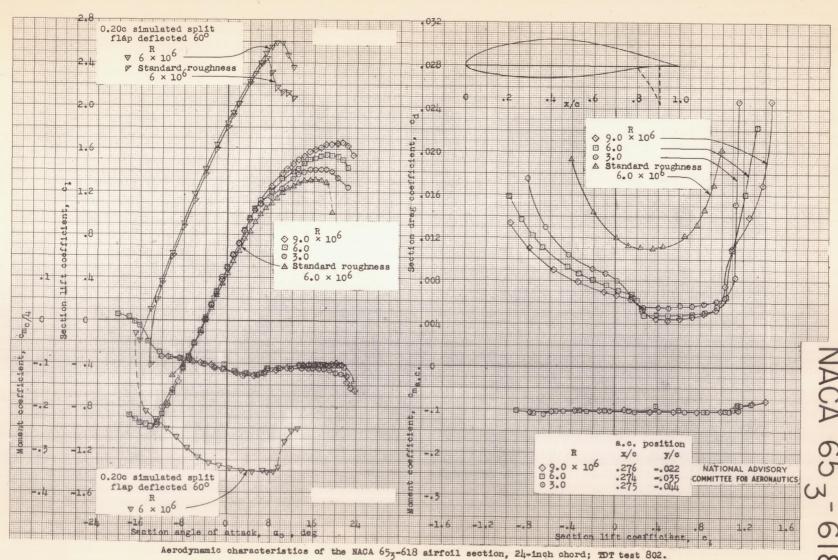


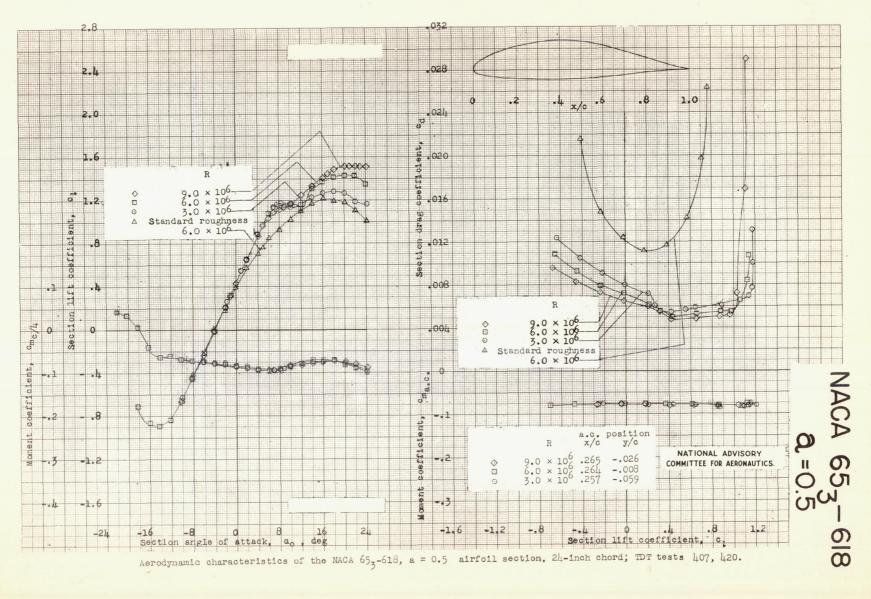
Aerodynamic characteristics of the NACA 65x-218 airfoil section, 24-inch chord; TDT test 830.

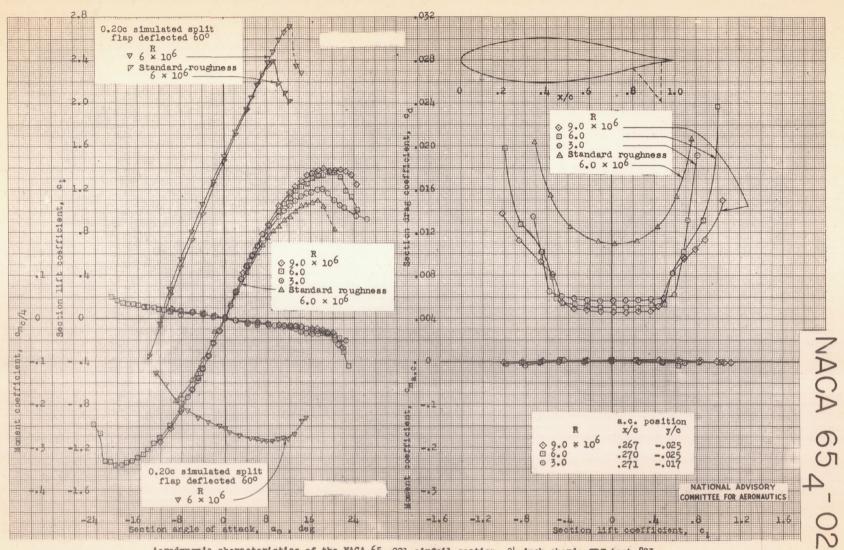


Aerodynamic characteristics of the NACA 653-418 airfoil section, 24-inch chord; TDT tests 314, 320, and 891.

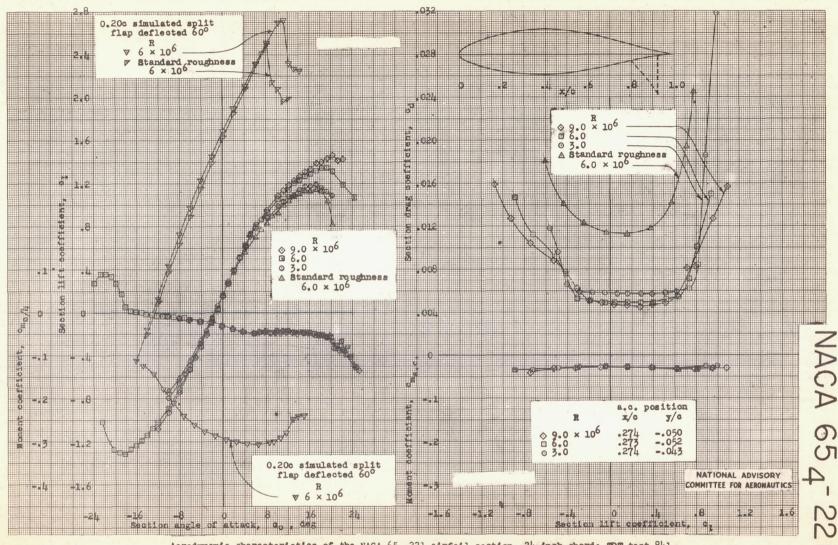




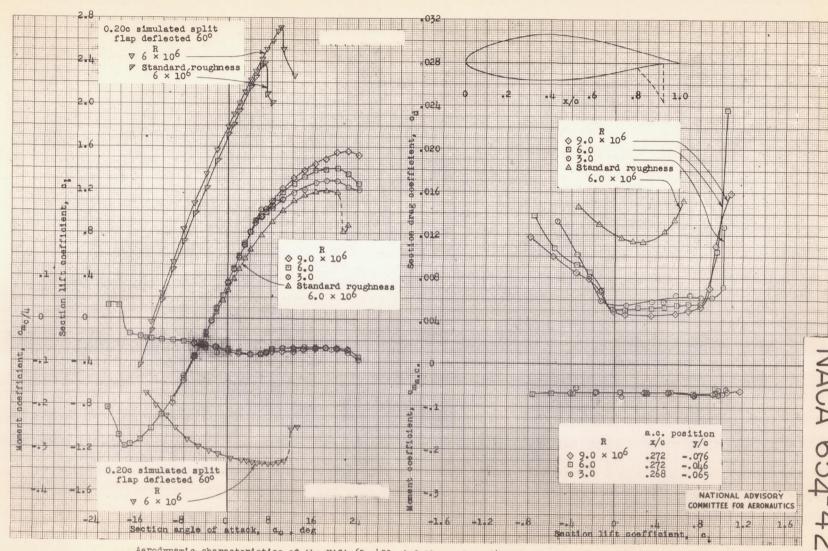




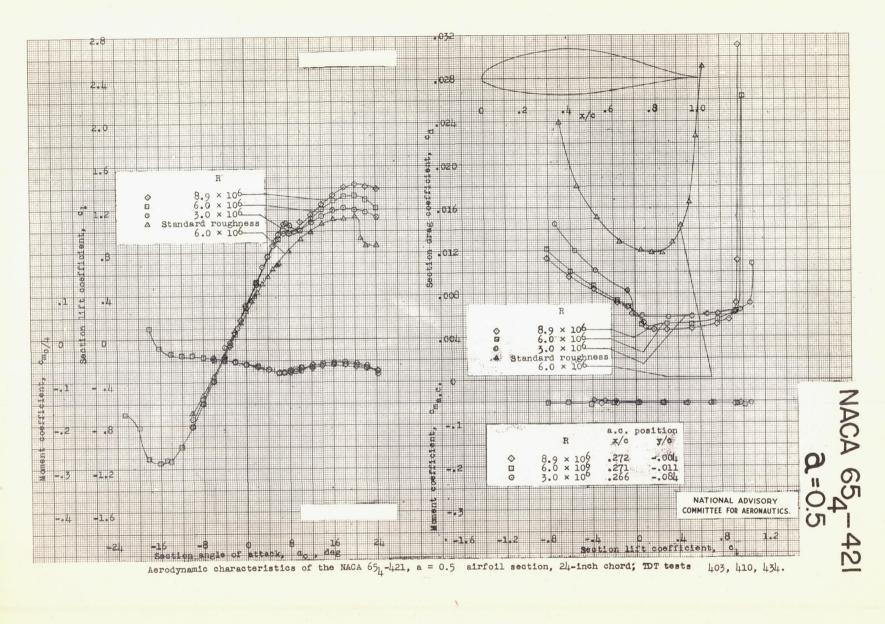
Aerodynamic characteristics of the NACA 654-021 airfoil section, 24-inch chord; TDT test 823.

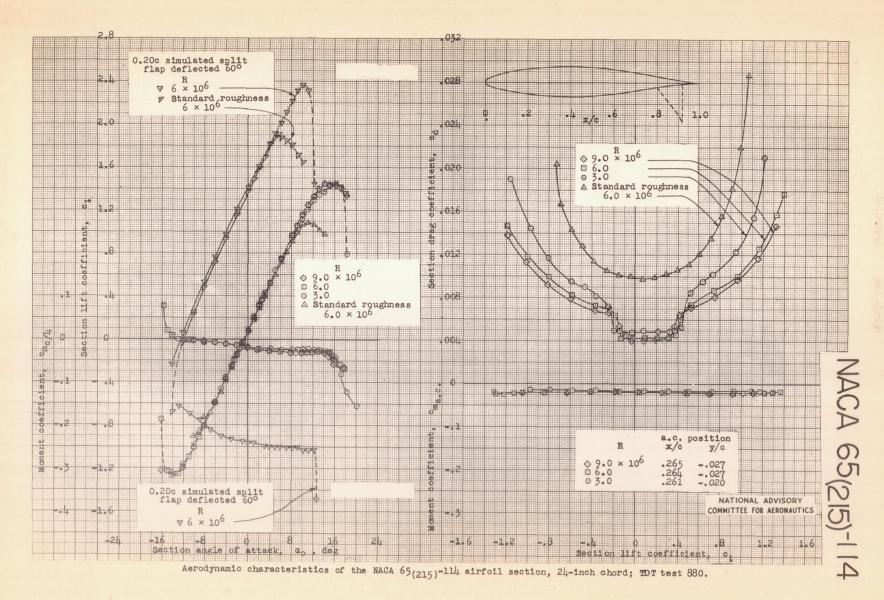


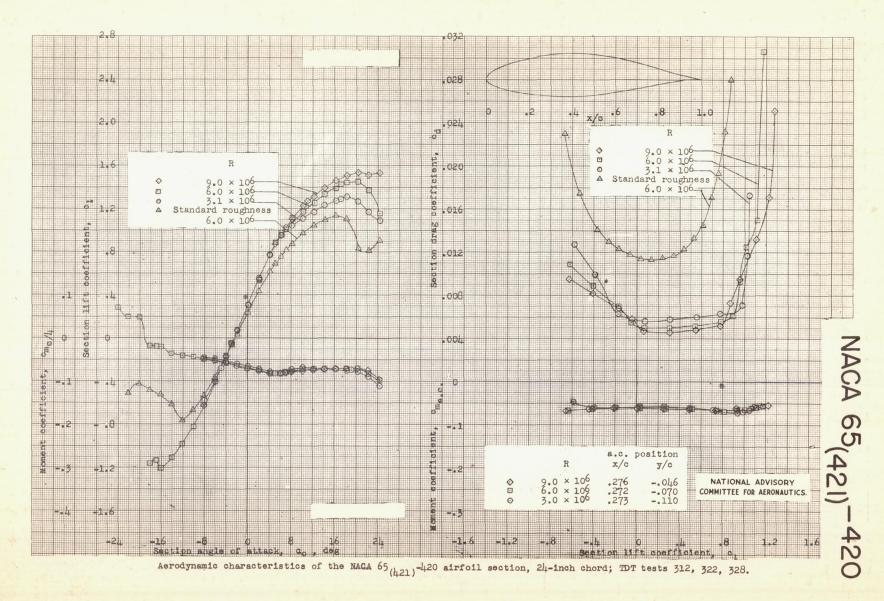
Aerodynamic characteristics of the NACA 65 1-221 airfoil section, 24-inch chord; TDT test 841.

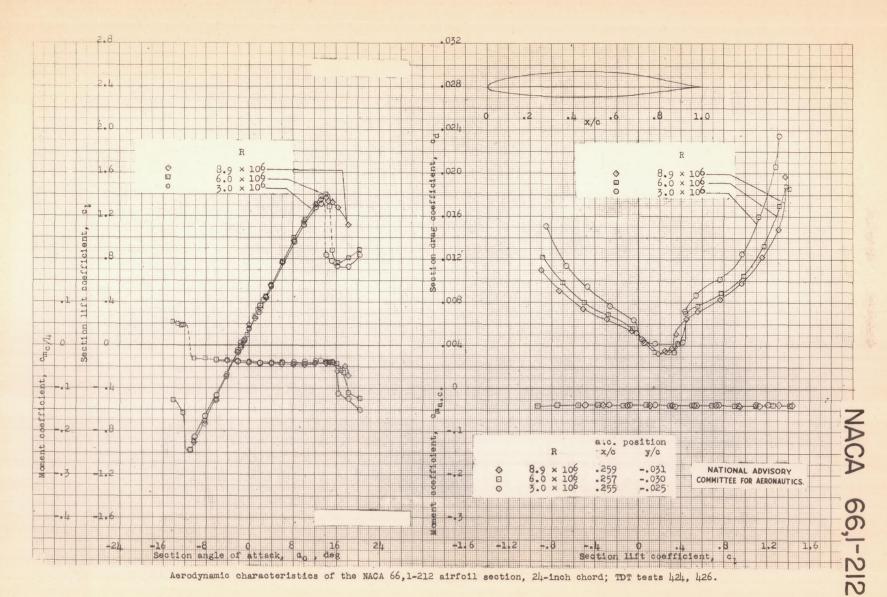


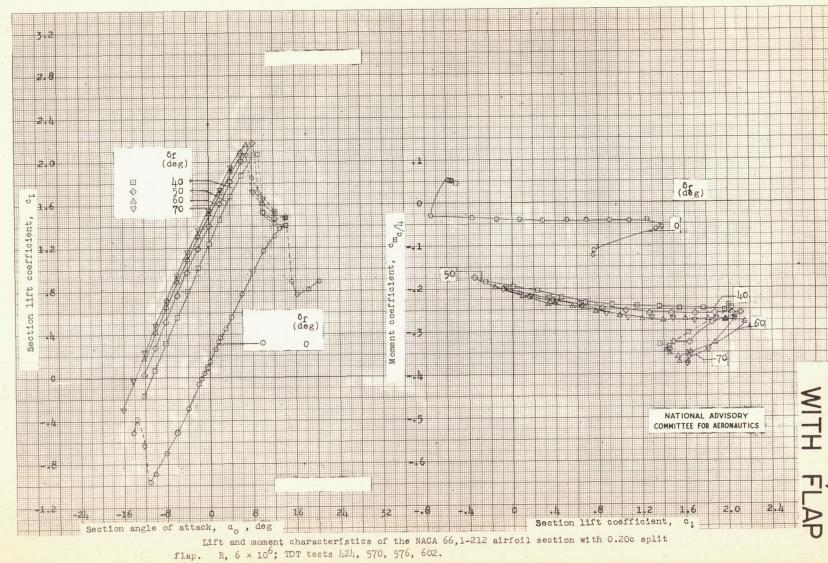
Aerodynamic characteristics of the NACA 654-421 airfoil section, 24-inch chord; TDT tests 316, 321 and 875.





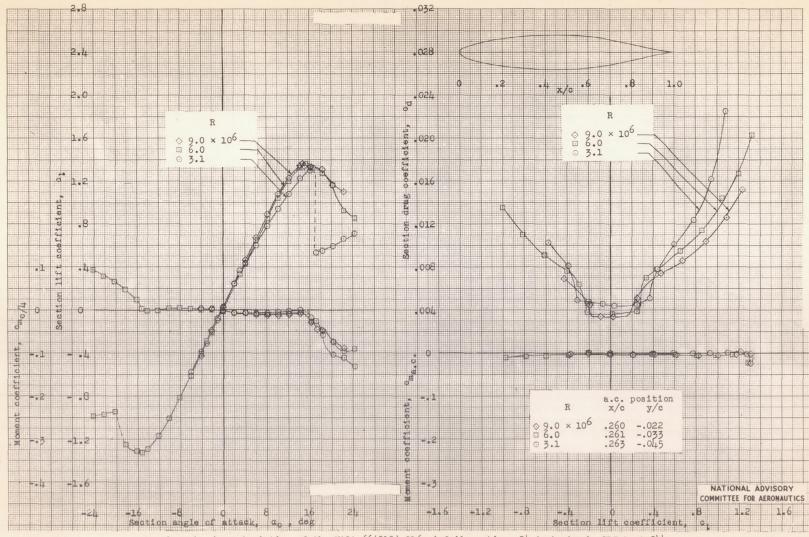




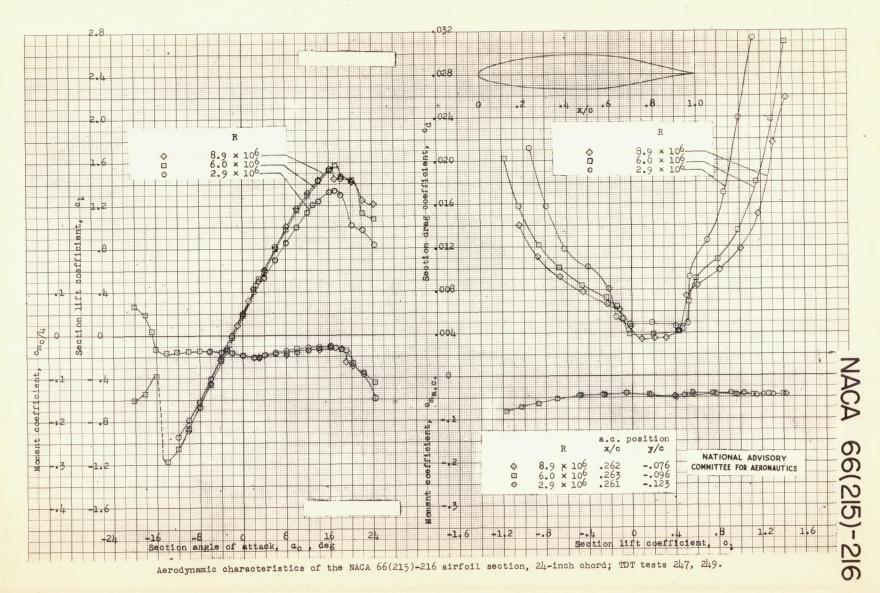


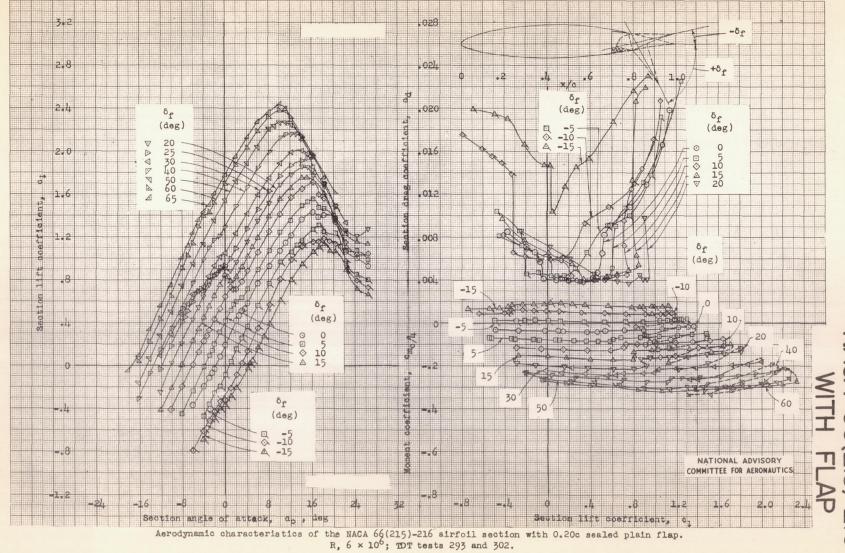
00

Apri

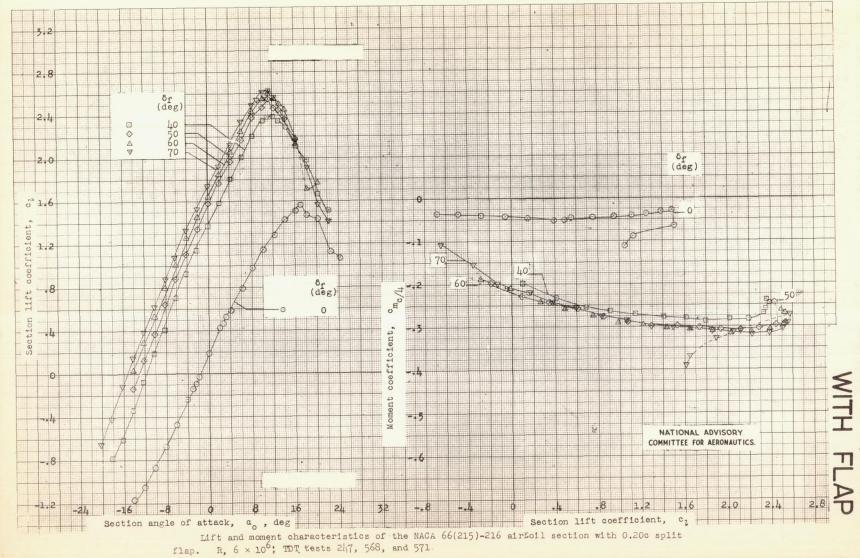


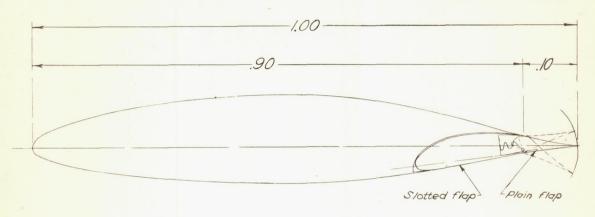
Aerodynamic characteristics of the NACA 66(215)-016 airfoil section, 24-inch chord; TDT test 244.



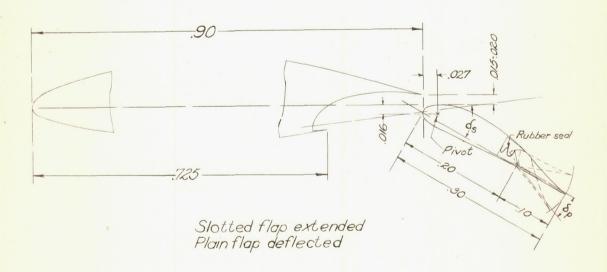


S164





Slotted flap retracted Plain flap deflected

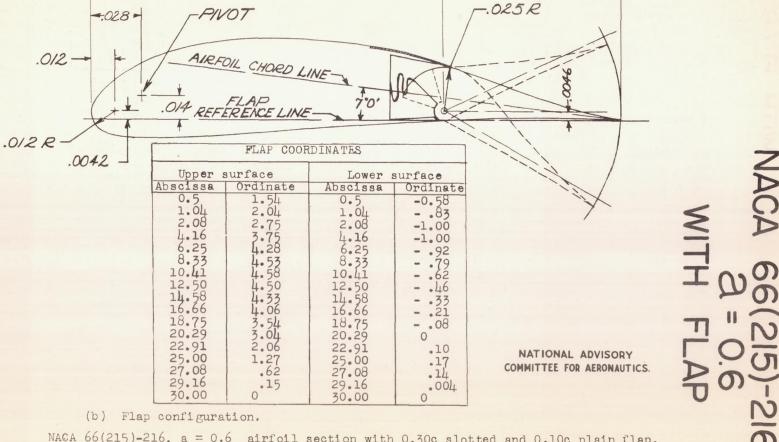


NATIONAL ADVISORY COMMITTEE FOR AERONAUTICS.

(a) Airfoil-flap configuration.

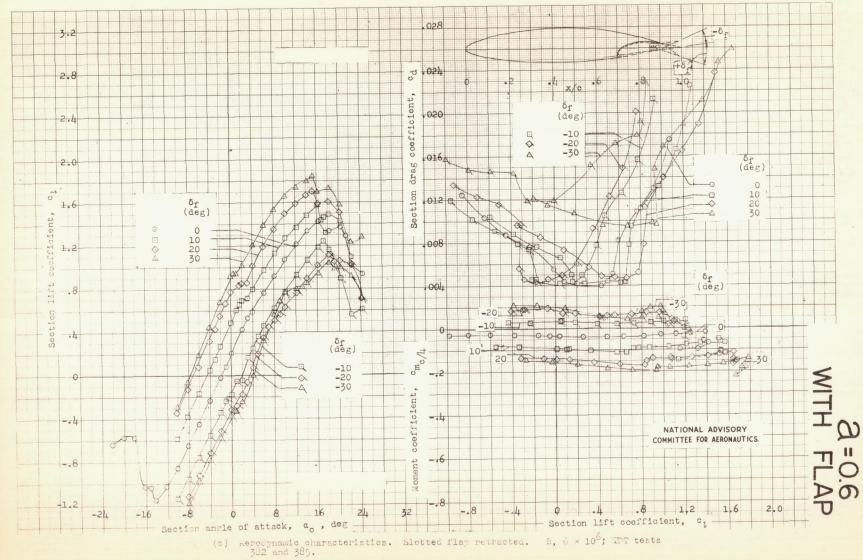
NACA 66 (215)-216, a = 0.6 airfoil section with 0.30c

slotted and 0.10 c plain flap.

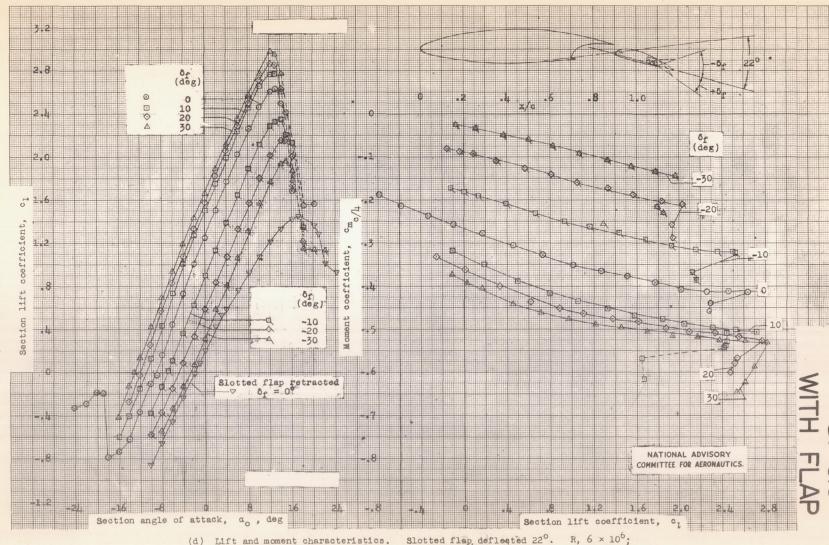


NACA 66(215)-216, a=0.6 airfoil section with 0.30c slotted and 0.10c plain flap.

.30

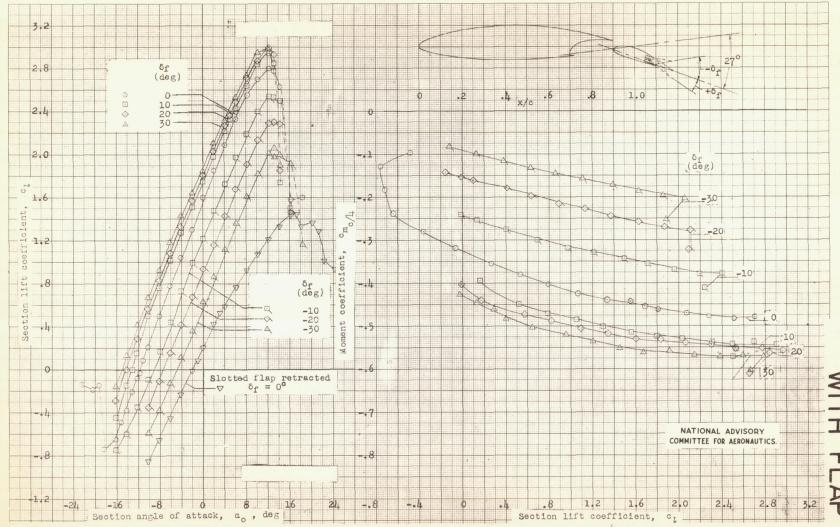


MAC. $\delta\delta(215)$ -216, a = 0.6 airfoil section with 0.30c slotted and 0.10c plain flap.

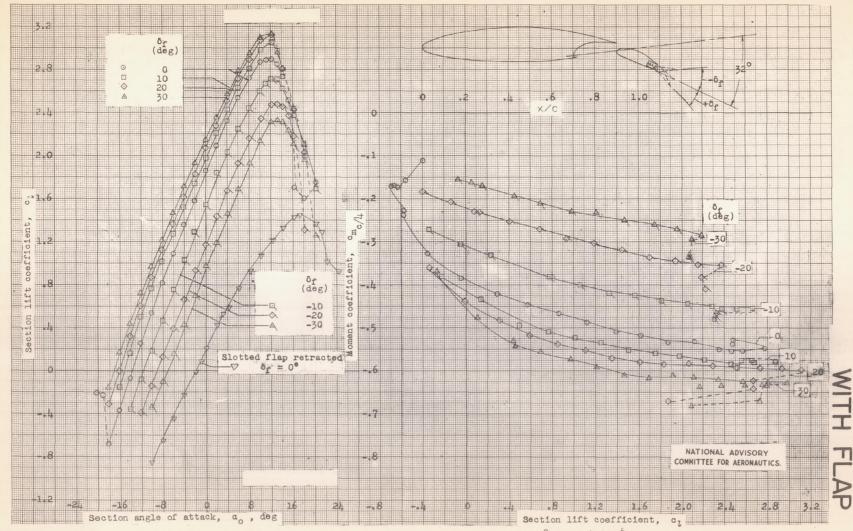


Slotted flap deflected 22°. R, 6 × 106; (d) Lift and moment characteristics. TDT tests 236, 352, and 382.

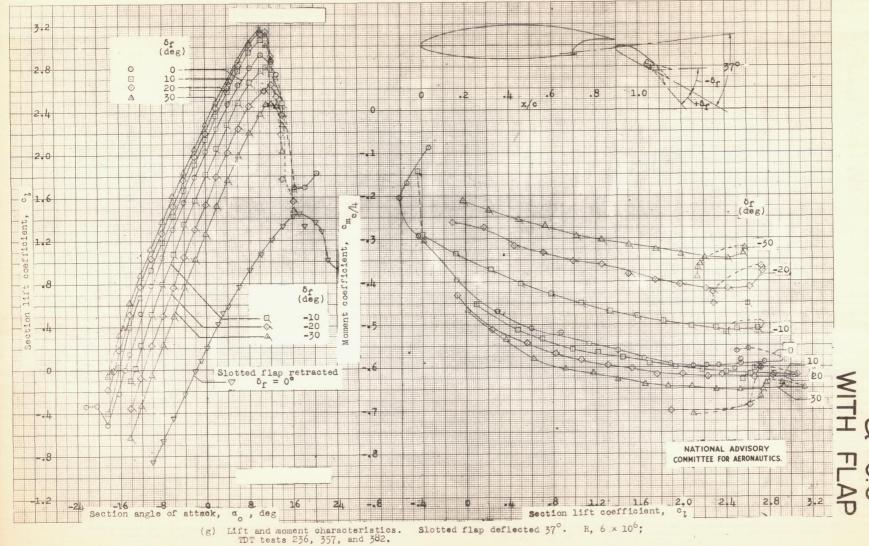
NACA 66(215)-216, a = 0.6 airfoil section with 0.30c slotted and 0.10c plain flap.



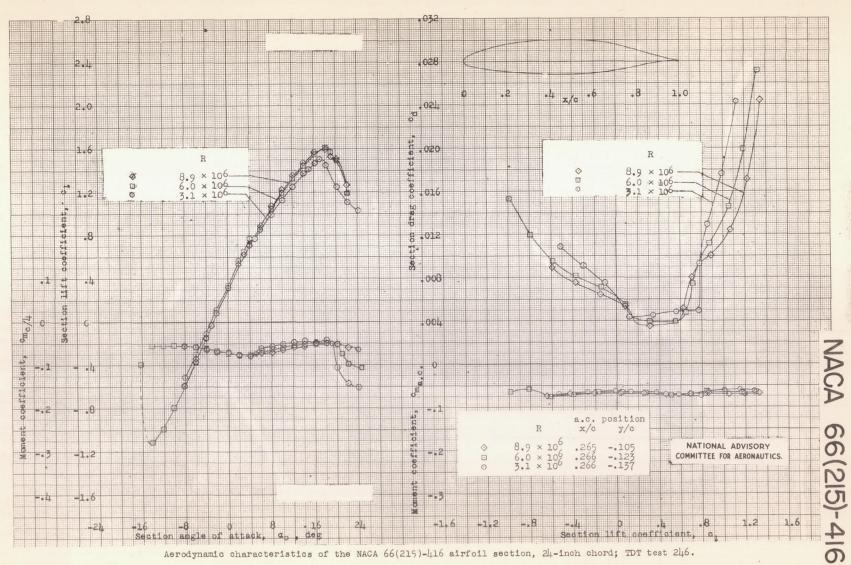
(e) Lift and moment characteristics. Slotted flap deflected 27°. R, 6×10^6 ; TDT tests 236, 352, and 382. NACA 66(215)-216, a = 0.6 airfoil section with 0.30c slotted and 0.10c plain flap.



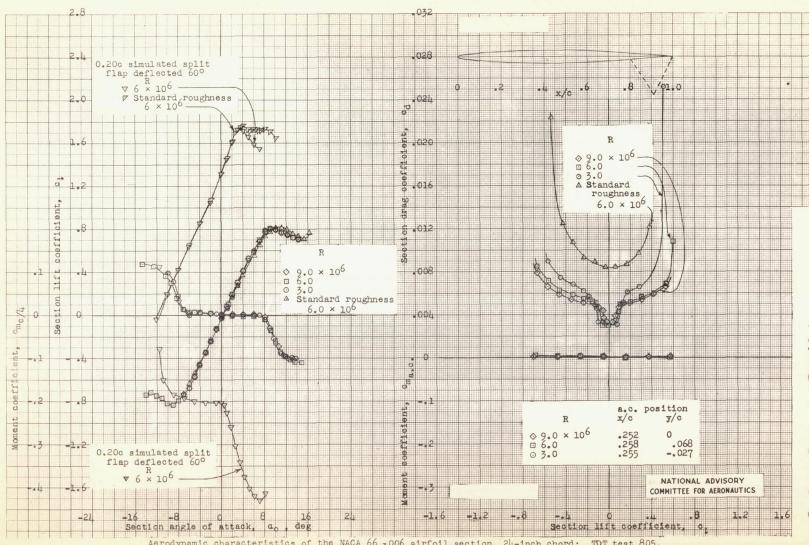
(f) Lift and moment characteristics. Slotted flap deflected 32° . R, 6×10^{6} ; TDT tests 352, 357, 359, and 382. NACA 66(215)-216, a = 0.6 airfoil section with 0.30c slotted and 0.10c plain flap.



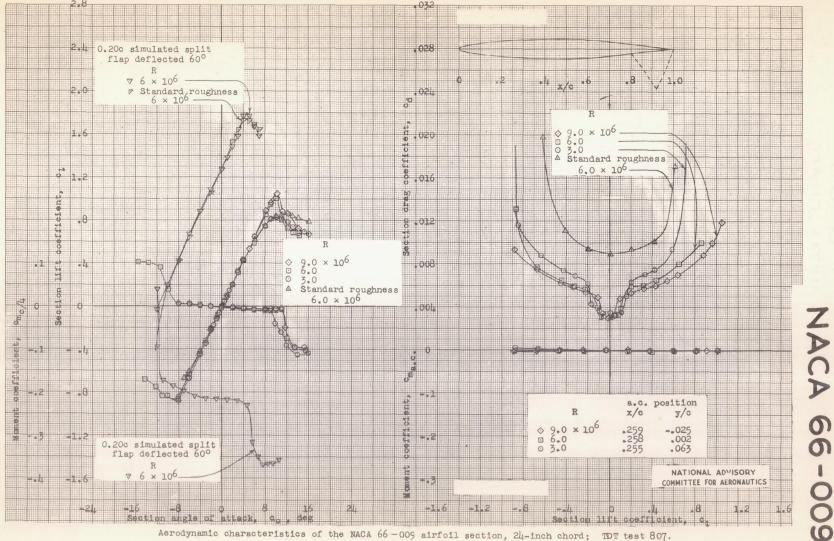
NACA 66(215)-216, a = 0.6 airfoil section with 0.30c slotted and 0.10c plain flap.



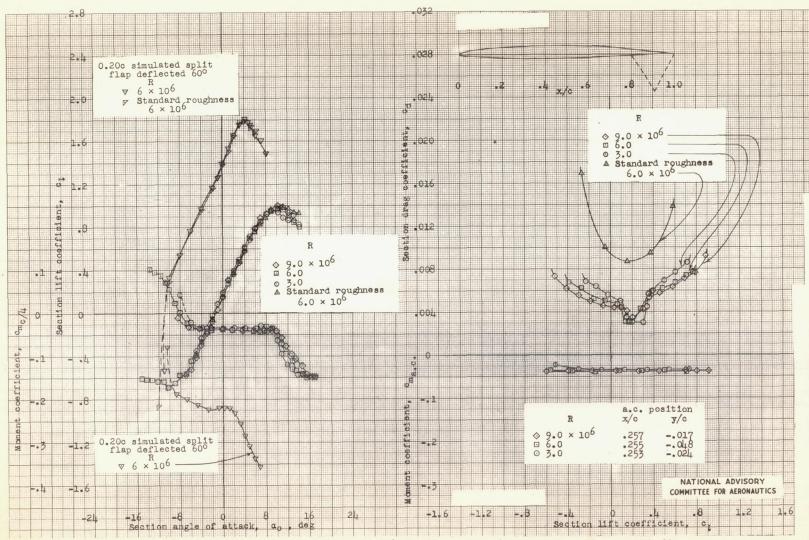
Aerodynamic characteristics of the NACA 66(215)-416 airfoil section, 24-inch chord; TDT test 246.



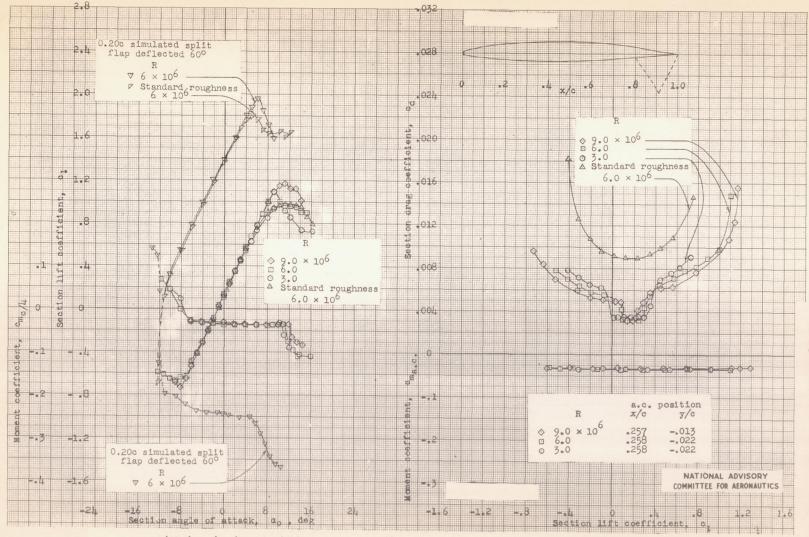
Aerodynamic characteristics of the NACA 66 - 006 airfoil section, 24-inch chord; TDT test 805.



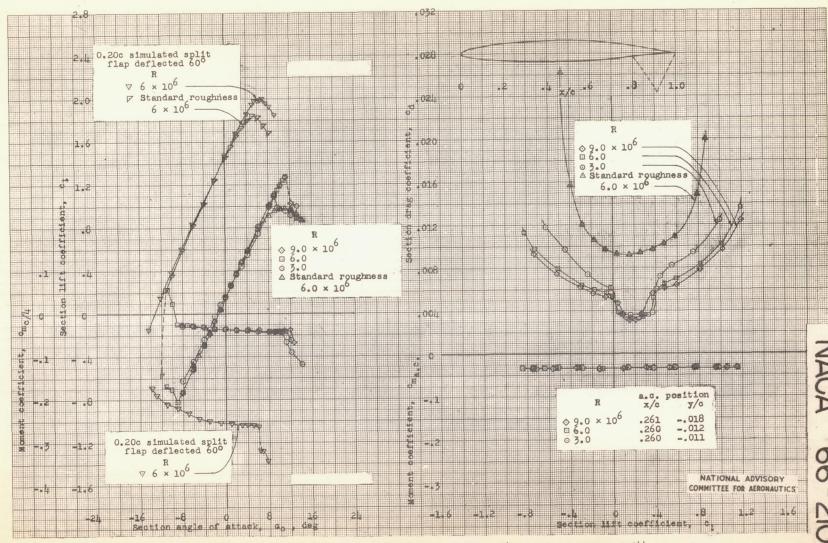
Aerodynamic characteristics of the NACA 66-009 airfoil section, 24-inch chord; TDT test 807.



Aerodynamic characteristics of the NACA 66 - 206 airfoil section, 24-inch chord; TDT tests 806, 887.

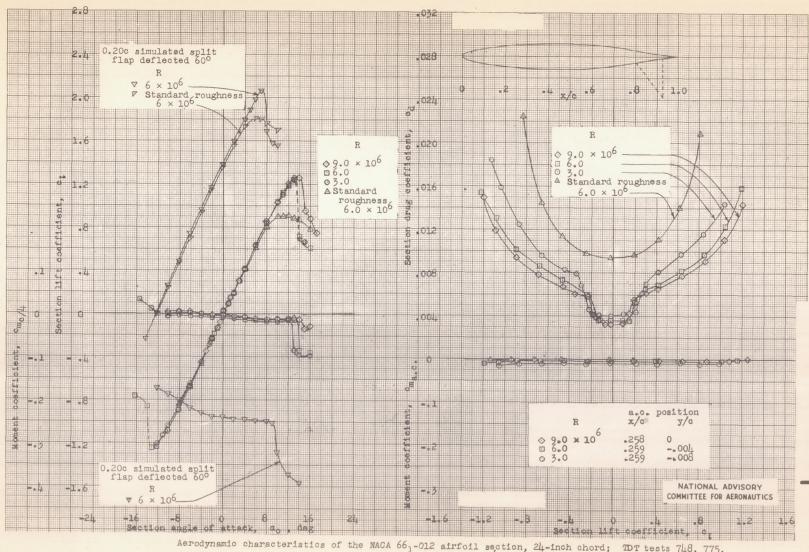


Aerodynamic characteristics of the NACA 66-209 airfoil section, 24-inch chord; TDT test 810.

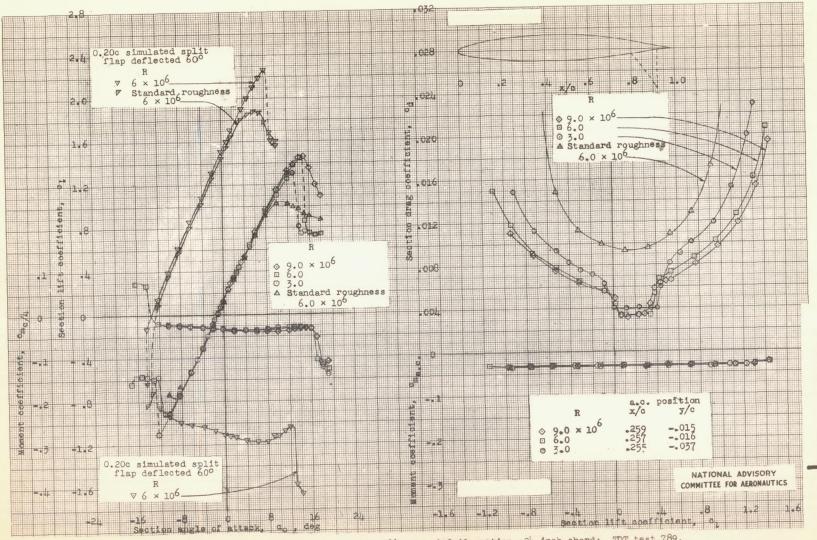


Aerodynamic characteristics of the NACA 66-210 airfoil section, 24-inch chord; TDT test 944.

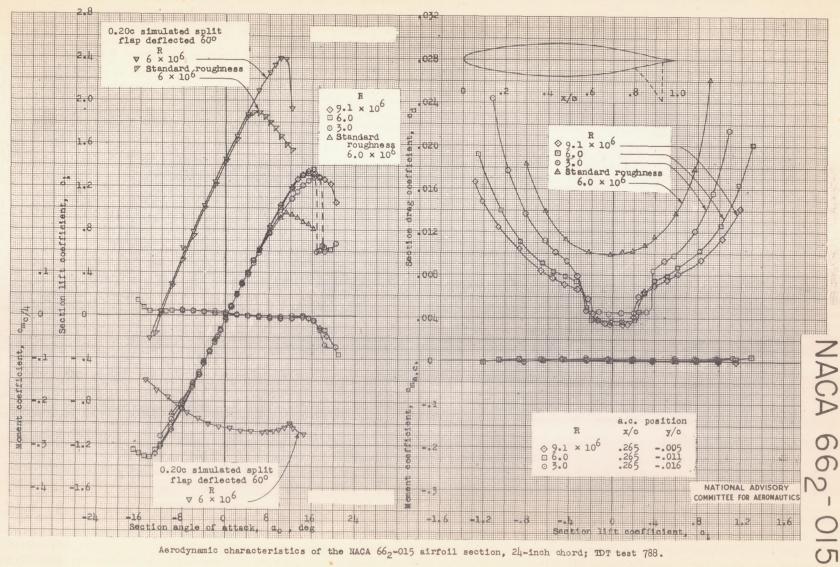
0 4 CI



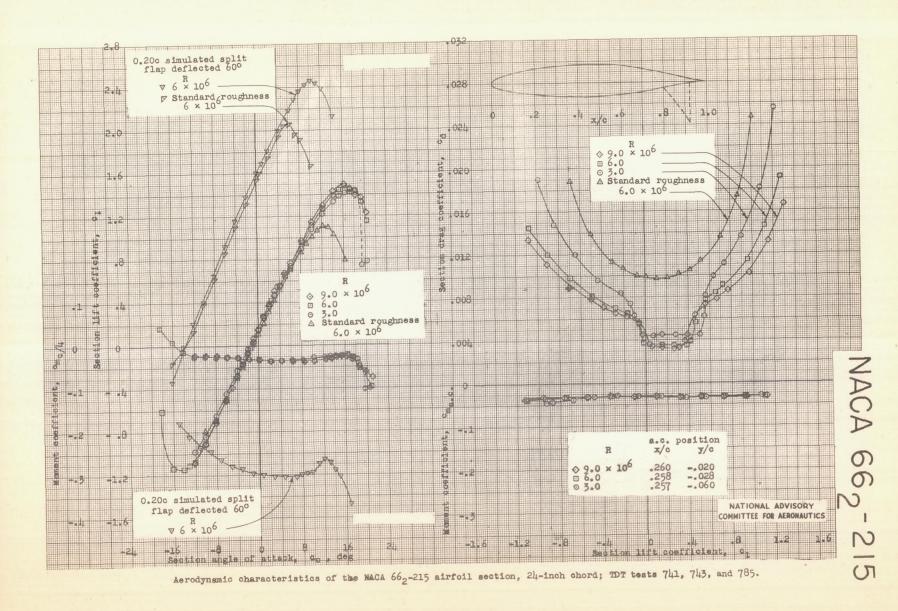
Aerodynamic characteristics of the NACA 661-012 airfoil section, 24-inch chord; TDT tests 748, 775, 776. 836.

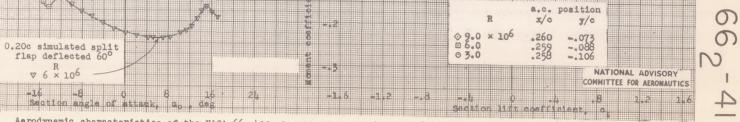


Aerodynamic characteristics of the NACA 661-212 airfoil section, 24-inch chord; TDT test 789.



Aerodynamic characteristics of the NACA 662-015 airfoil section, 24-inch chord; TDT test 788.





Aerodynamic characteristics of the NACA 662-415 airfoil section, 24-inch chord; TDT tests 746, 752, 770, and 772.

ರ

JJ. 016

R 9.0 × 10⁶ 6.0 3.0 Standard roughness 6.0 × 10⁶

000

. 020 5

.008

004

0.20c simulated split flap deflected 60° R V 6 × 106

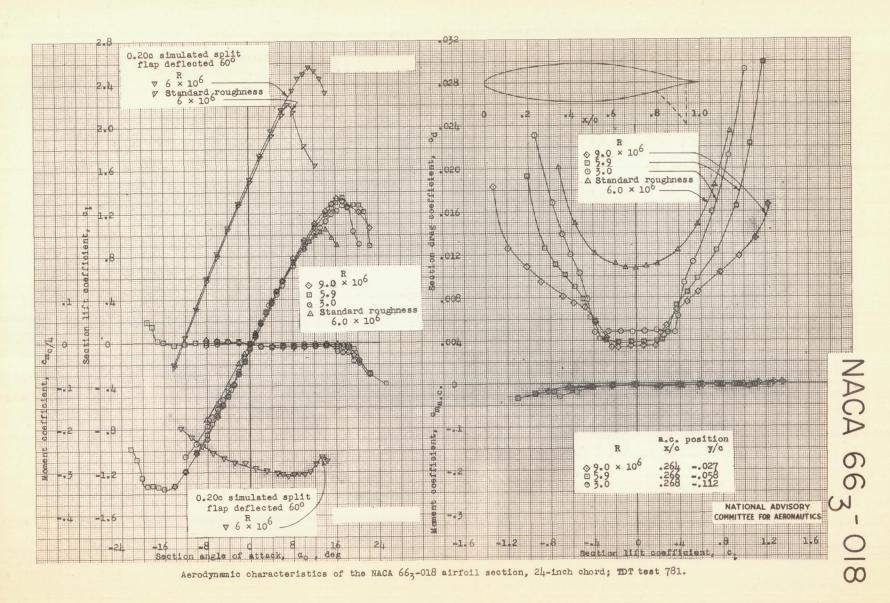
Standard roughness 6 × 10

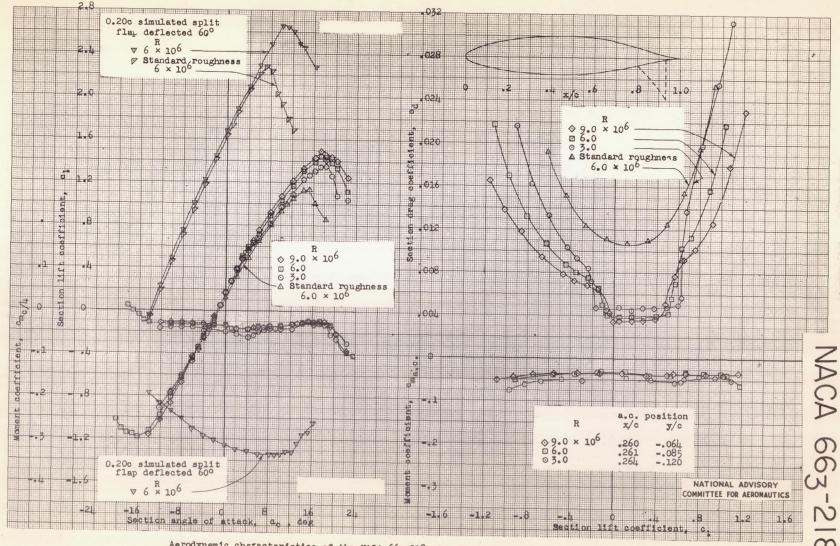
2.4

.l

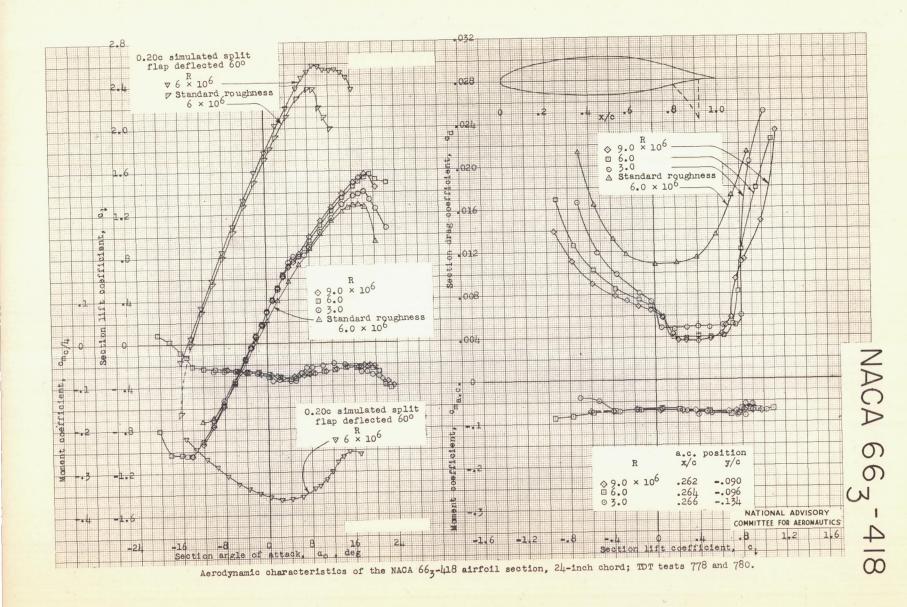
-.1

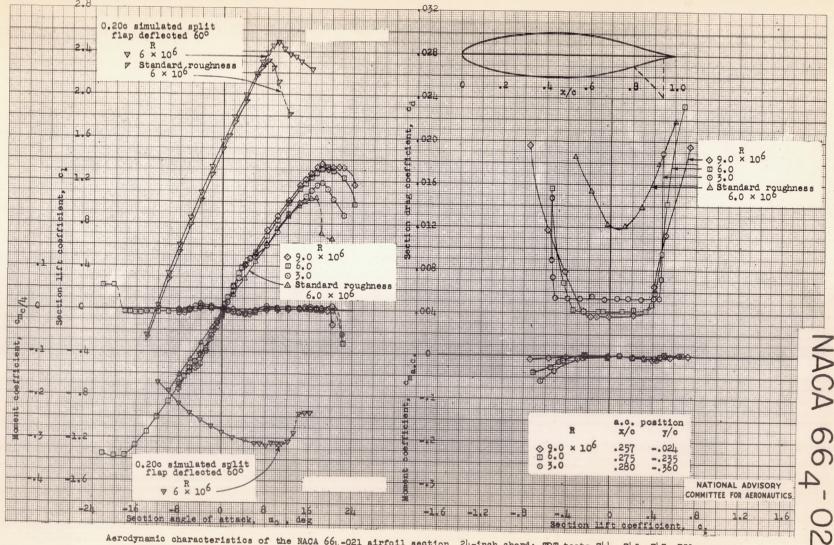
-1.2



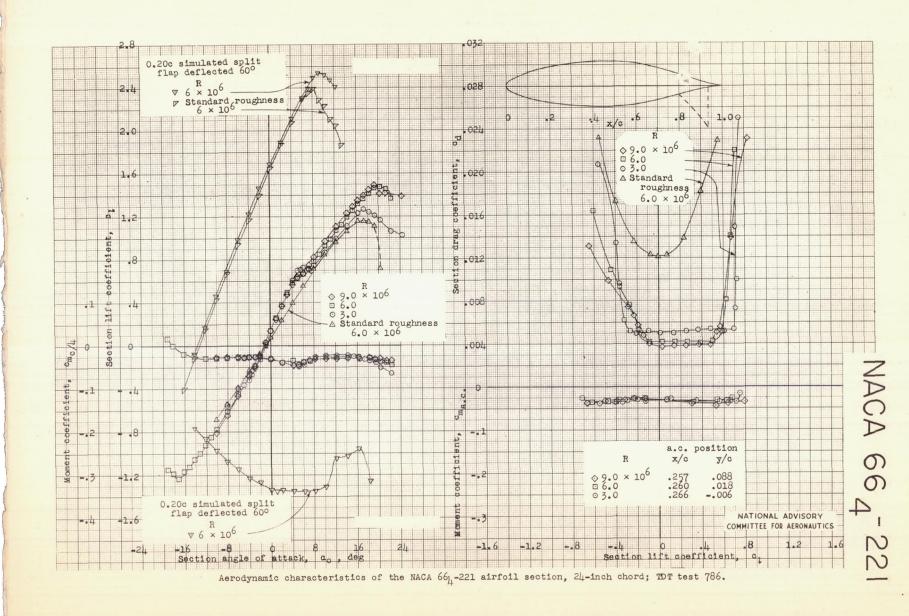


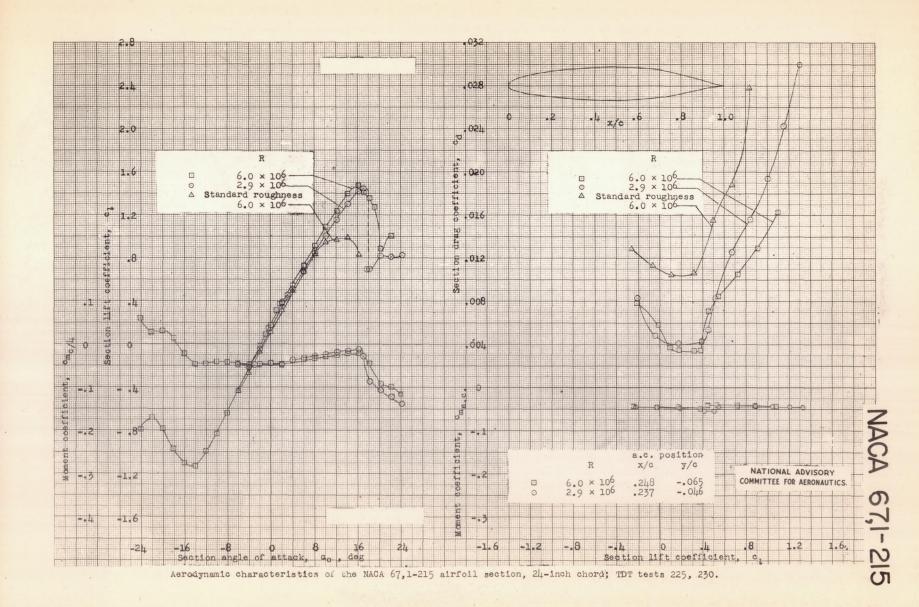
Aerodynamic characteristics of the NACA 663-218 airfoil section, 24-inch chord; TDT test 787.

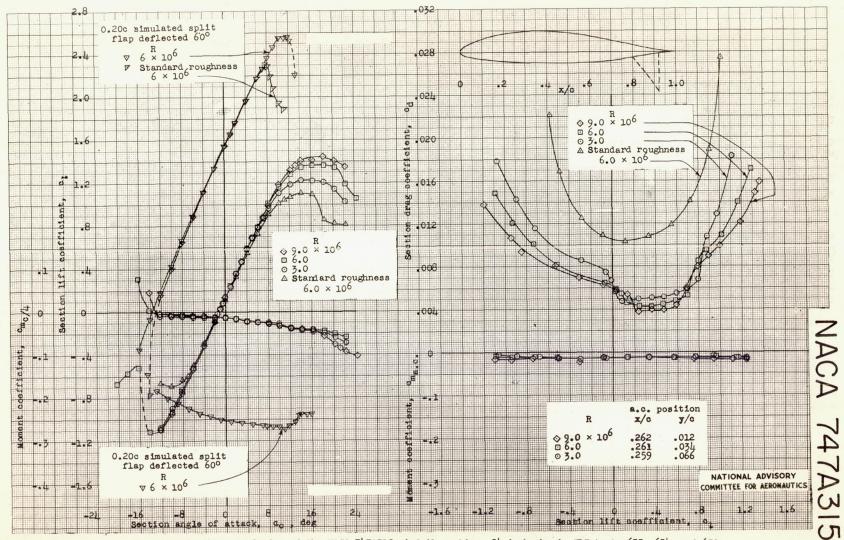




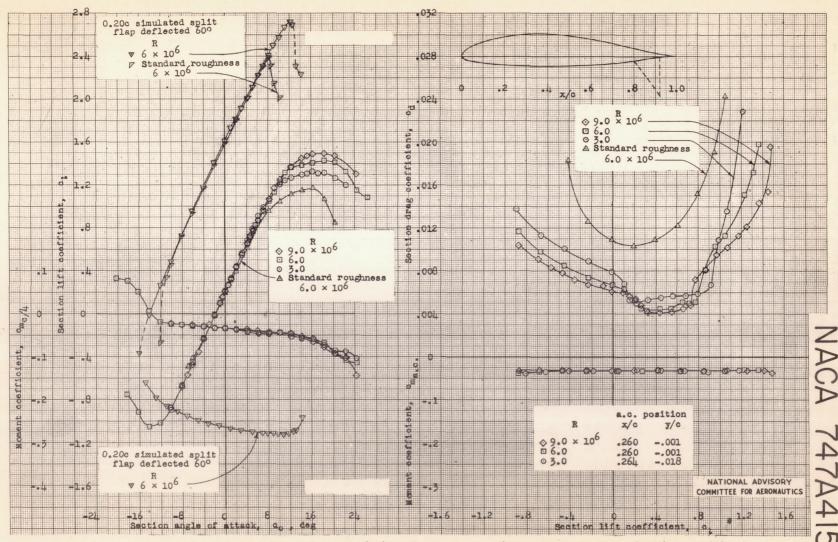
Aerodynamic characteristics of the NACA 664-021 airfoil section, 24-inch chord; TDT tests 744, 745, 747, 751, and 777.







Aerodynamic characteristics of the NACA 747A315 airfoil section, 24-inch chord; TDT tests 633, 634, and 639.



Aerodynamic characteristics of the NACA 747A415 airfoil section, 24-inch chord; TOT tests 635, 637, and 638.

